DEPARTMENT OF TRANSPORTATION

Pavement Design: Performance of Base versus Subbase

Erol Tutumluer, Principal Investigator
Department of Civil and Environmental Engineering
University of Illinois Urbana-Champaign

August 2025

Research Project
Final Report 2025-43

To get this document in an alternative format or language, please call 651-366-4720 (711 or 1-800-627-3529 for MN Relay). You can also email your request to ADArequest.dot@state.mn.us. Please make your request at least two weeks before you need the document.

Technical Report Documentation Page

1. Report No.	2.	3. Recipients Accession No.
MN 2025-43		

4. Title and Subtitle	5. Report Date
Pavement Design: Performance of Base versus Subbase	August 2025
	6.

7. Author(s)	8. Performing Organization Report No.
Erol Tutumluer, Yongsung Koh, Yujia Lu, Issam I.A. Qamhia, Halil Ceylan, and Sunghwan Kim	

9. Performing Organization Name and Address	10. Project/Task/Work Unit No.
Civil and Environmental Engineering Grainger College of Engineering University of Illinois Urbana-Champaign 506 S. Wright Street, Urbana, Illinois 61801	11. Contract (C) or Grant (G) No. 1036341

12. Sponsoring Organization Name and Address	13. Type of Report and Period Covered
Minnesota Department of Transportation Office of Research & Innovation 395 John Ireland Boulevard, MS 330 St. Paul, Minnesota 55155-1899	Final Report 14. Sponsoring Agency Code

15. Supplementary Notes
http://mdl.mndot.gov/

16. Abstract (Limit: 250 words)
The limited availability of high-quality aggregates and rising transportation costs present ongoing challenges for pavement construction and maintenance in Minnesota. To address this, local agencies are increasingly exploring the use of lower-quality, locally available materials in pavement foundation layers. This study evaluates the performance and cost-effectiveness of aggregate base and subbase layers with varying material qualities and thicknesses to develop optimized pavement designs. A comprehensive aggregate index property (AIP) database is updated to include more than 1,100 aggregate sources and used to develop predictive models for resilient modulus and shear strength using both multiple linear regression analyses and artificial neural networks. Aggregates are categorized into low-, medium-, and high-quality categories and incorporated into MnPAVE simulations under a range of traffic levels, asphalt layer thicknesses, subgrade stiffnesses, and climatic conditions. In parallel, cost-benefit analyses based on historical MnDOT bid data are conducted to identify optimal-quality thickness combinations. A flowchart-based design framework is also introduced to iteratively determine the required aggregate base and subbase thicknesses corresponding to aggregate quality levels that meet fatigue and rutting life targets. The findings offer practical guidance for the efficient use of regional materials, supporting the development of resilient and economically optimized pavement infrastructure across Minnesota.

17. Document Analysis/Descriptors	18. Availability Statement
Aggregate Quality, Pavement Design Optimization, Base, Subbase, Granular Equivalency, Cost-Benefit Analysis, Artificial Neural Network	No restrictions. Document available from: National Technical Information Services, Alexandria, Virginia 22312

19. Security Class (this report)	20. Security Class (this page)	21. No. of Pages	22. Price
Unclassified	Unclassified	39	

Pavement Design: Performance of Base versus Subbase

Final Report

Prepared by:

Erol Tutumluer, Yongsung Koh, Yujia Lu, Issam I.A. Qamhia
Department of Civil and Environmental Engineering
University of Illinois Urbana-Champaign, Urbana, Illinois

Halil Ceylan, Sunghwan Kim
Department of Civil, Construction, and Environmental Engineering
Iowa State University, Ames, Iowa

August 2025

Published by:

Minnesota Department of Transportation
Office of Research & Innovation
395 John Ireland Boulevard, MS 330
St. Paul, Minnesota 55155-1899

Acknowledgements

The authors gratefully acknowledge the sponsorship of this project by the Minnesota Local Road Research Board (LRRB).

The project's Technical Advisory Panel (TAP) members, Jackie Jiran (project coordinator), Raul Velasquez (technical liaison), Andrew Stolba, Ceren Aydin, Chad DeMenge, Eddie Johnson, Haluk Sinan Coban, Kent Exner, Michael Flaagan, Scott Holmes, Terrence Beaudry, and Timothy Andersen, are gratefully acknowledged for their guidance, support, and direction throughout the research.

The authors also would like to express their appreciation to the faculty and staff of the Department of Civil and Environmental Engineering at the University of Illinois Urbana-Champaign (UIUC) and of the Department of Civil, Construction, and Environmental Engineering at Iowa State University (ISU) for their support in the successful execution of this research project. The valuable contributions of colleagues and students at both institutions are likewise acknowledged.

Special thanks are extended to Mr. Bruce Tanquist for his development of the MnPAVE batch-run scripts, which greatly supported the analytical tasks of this project.

Contents

List of Figures

List of Tables

Executive Summary

This study addresses the critical challenge of developing cost-effective and durable flexible pavement designs in Minnesota, where the availability of high-quality aggregate materials is increasingly constrained. Sponsored by the Minnesota Department of Transportation (MnDOT) and the Local Road Research Board (LRRB), the research integrates an updated aggregate index property (AIP) database, predictive modeling, mechanistic-empirical pavement performance analysis, and cost-benefit assessments to support sustainable pavement foundation design using locally available materials.

The research began with the development of a comprehensive AIP database by merging and refining MnDOT's aggregate source information system (ASIS) and laboratory information management system (LIMS) datasets. This database includes gradation, strength, and durability properties for more than 1,100 aggregate sources across the state, providing a robust foundation for performance-based material evaluation. To establish predictive relationships between aggregate properties and key pavement design inputs, such as resilient modulus and shear strength, the study developed and refined both multiple linear regression (MLR) and artificial neural network (ANN) models. The ANN model significantly improved prediction accuracy, particularly for nonlinear resilient modulus (M_R) characterization model parameters, making the M_R models more practical for implementation.

Using the aggregate property inputs, a comprehensive set of simulations was conducted in MnPAVE across varying traffic levels (0.2 to 6 million equivalent single axle loads (ESALs)), asphalt layer thicknesses (4 to 8 inches), subgrade stiffness values (2 to 10 ksi), and Minnesota's representative climatic zones. The analyses demonstrate that low-quality aggregates can achieve acceptable performance for low-volume roads, provided that sufficient aggregate layer thickness is used. For higher traffic volumes, higher aggregate base layer quality or thicker asphalt layers are necessary to meet fatigue life expectations, while subbase quality has a more pronounced effect on rutting resistance. Granular equivalency (GE) factors were calculated based on modulus- and thickness-based responses, enabling a more rational approach to determining the structural contributions of different aggregate materials and layer thicknesses. These GE factors, combined with the performance data, were used to guide design optimizations that reduce overdesign while ensuring reliability.

To assess economic feasibility, the study conducted a cost-benefit analysis using MnDOT's historical bid price data. By comparing performance outcomes and material costs across more than 40,000 design scenarios, the research identified optimal quality for aggregate base and subbase thickness combinations for various design conditions. A flowchart-based, decision-making process was introduced to help practitioners iteratively adjust aggregate base and subbase thicknesses to meet fatigue and rutting life requirements while minimizing cost. The findings suggest that many flexible pavements, particularly those serving traffic levels below 1.5 million ESALs, can be effectively constructed using low- to medium-quality aggregate materials with properly optimized thicknesses, offering a substantial opportunity to reduce construction costs and reliance on premium aggregate sources.

The significance of this research lies in its ability to bridge performance modeling, material characterization, and economic analysis into implementable pavement design guidance. The database,

predictive models, and design optimization procedures developed through this study provide MnDOT and local agencies with the means to make more informed, performance-driven decisions that promote the efficient use of regional aggregate resources. Future studies such as field validation of optimized designs, expanded mechanical property testing for underrepresented materials, advanced nonlinear mechanistic modeling, integration of predictive models into MnPAVE, and consideration of stabilized or reinforced unbound layers could further refine and enhance pavement design practices in Minnesota.

Chapter 1: Introduction

1.1 Background

Pavement foundations comprising aggregate base and subbase layers are critical to the structural integrity and long-term performance of both flexible and rigid pavements. In pavement engineering, aggregate base and subbase layers play a vital role in distributing vehicular loads, enhancing structural support, and ensuring the durability of surface layers. Typically, aggregate base layers, positioned directly beneath the asphalt or concrete surface, are constructed using high-quality aggregates due to their load-carrying function. Subbase layers, placed below the aggregate base or directly under the surface course (in the absence of a base), serve to further distribute loads and improve drainage and frost resistance. The combined performance of these unbound granular layers significantly influences the longevity, serviceability, and maintenance demands of pavement systems.

Minnesota, like many other states, faces a growing challenge in sourcing high-quality aggregate materials near construction sites. Depletion of local aggregate reserves, rising transportation costs, and supply-chain variability have increased interest in using lower-quality or marginal materials in greater thicknesses to achieve comparable structural performance. The engineering viability of such alternatives hinges on a clear understanding of how aggregate quality indicators, e.g., size distribution, angularity, shape, plasticity, permeability, freeze-thaw durability, strength, and resilient modulus, relate to pavement performance metrics like fatigue cracking, rutting, pumping, and faulting.

The Minnesota Department of Transportation (MnDOT) and the Local Road Research Board (LRRB) have sponsored several past and ongoing research efforts to investigate the performance of various granular materials and their suitability in pavement foundation layers. Notably, prior studies by Xiao & Tutumluer (2012), Tutumluer et al. (2015), and Jibon et al. (2024) have laid the groundwork for evaluating material cost-effectiveness and refining design parameters such as granular equivalency (GE) factors. GE factors are used by local agencies to convert various granular materials into equivalent thicknesses of a standard Class 5 base aggregate, allowing for consistent and comparative pavement designs. Despite these advancements, a gap remains in how existing GE factors account for variations in material properties and layer configurations, especially in scenarios where designers must choose between a high-quality but thinner aggregate base and a thicker, lower-quality subbase.

This research project, therefore, seeks to build on previous findings and extend the current knowledge base by systematically analyzing the relationships between aggregate quality, layer thickness, and pavement performance. It emphasizes the importance of local material utilization, cost-effective structural configurations, and sustainable pavement design in line with MnDOT's strategic goals for innovation, environmental responsibility, and life-cycle asset management. By integrating field and laboratory data, mechanistic-empirical analysis results, and life-cycle cost assessments, the project aims to produce implementable design guidance that supports statewide transportation infrastructure resilience.

1.2 Research Objectives

The primary objective of this research is to evaluate the performance and cost-effectiveness of aggregate base versus subbase aggregate layers in pavement structures, particularly under scenarios where high-quality aggregates are limited or unavailable. The specific goals include:

- Identify key aggregate quality indicators and their influence on pavement design and long-term performance.
- Establish a comprehensive database of locally available aggregate materials across Minnesota, including index properties, resilient modulus, strength characteristics, and cost information.
- Evaluate multiple pavement design alternatives by varying base and subbase layer thicknesses and material qualities, using mechanistic-empirical tools such as MnPAVE.
- Quantify the impact of aggregate properties on GE factors and pavement performance outcomes.
- Conduct life-cycle cost analyses of each design scenario to recommend the most cost-effective option that satisfies pavement performance criteria.
- Provide implementable design guidance and recommendations for MnDOT and local agencies to support the efficient and sustainable use of aggregate resources in future pavement designs.

To achieve these objectives, this project provides improved predictive models that more accurately relate aggregate properties to pavement design inputs, along with technical guidance to assist practitioners in optimizing pavement foundation layers using locally available aggregates. This will ultimately improve performance, reduce costs, and support economically efficient pavement design and maintenance across the state.

1.3 Organization of the Report

This report is organized into eight chapters, each structured to address the research objectives and methodology developed for evaluating the performance of aggregate base and subbase with varying layer thicknesses and material qualities in pavement design:

- Chapter 1 presents the background and objectives of the study, highlighting the need for cost-effective pavement foundation designs using locally available aggregates and the motivation for revisiting Minnesota's aggregate selection practices.
- Chapter 2 provides a comprehensive literature review, summarizing national and international research on aggregate quality indicators and their impact on pavement performance. This chapter covers foundational topics such as pavement design needs, mechanical behavior of unbound materials, drainage, frost protection, and state-of-the-practice design methods.

- Chapter 3 documents the process of developing an updated aggregate index property (AIP) database by integrating MnDOT's aggregate source information system (ASIS) and laboratory information management system (LIMS) datasets.

- Chapter 4 establishes linkages between aggregate properties and pavement design inputs such as resilient modulus and strength. It introduces regression and artificial neural network (ANN) models to predict mechanical properties based on AIP data and classifies aggregate materials into quality levels to support subsequent performance analyses.

- Chapter 5 evaluates various pavement design alternatives through a large-scale sensitivity analysis using MnPAVE software. This chapter quantifies the impacts of aggregate base and subbase quality, layer thickness, traffic levels, climate conditions, and subgrade support on pavement fatigue and rutting performance. It also establishes GE factors for different aggregate combinations.

- Chapter 6 presents a cost-benefit analysis of selected design alternatives. By combining predicted performance and historical cost data, the chapter identifies optimal combinations of aggregate material quality and layer thickness for varying traffic and subgrade conditions. A flowchart-based framework is introduced for practitioners to guide design decisions based on fatigue and rutting performance thresholds.

- Chapter 7 discusses the research benefits and outlines potential implementation steps. It provides insights on how MnDOT and local agencies can apply the findings in material selection, pavement design practice, specification development, and pavement asset management.

- Chapter 8 summarizes the study's conclusions and provides recommendations for future research. It highlights key contributions of the project, suggests potential refinements to pavement design methodologies, and identifies areas where additional data collection or model enhancements could further support the implementation of cost-effective pavement foundation solutions.

Chapter 2: Literature Review

This chapter provides a comprehensive literature review for identifying and evaluating available data on aggregate quality and pavement performance. The research team summarizes national and international research study findings on aggregate quality indicators for aggregate base and subbase layers and how they influence pavement design and performance. The literature review covers the following topics: (1) pavement foundation needs for flexible and rigid pavements; (2) factors affecting modulus, strength, permanent deformation behavior, and efficient drainage capacity of unbound aggregate materials; (3) aggregate properties and quality indicators, with a focus on how they are linked to pavement performance indicators such as fatigue cracking and rutting of flexible pavements, and cracking, pumping, and faulting of rigid pavements; (4) pavement design methods and essential input aggregate properties for flexible and rigid pavements; (5) long-life flexible and rigid pavement design considerations, particularly drainability, stability, and reliability requirements; and (6) past related research conducted in Minnesota for the effects of varying thicknesses of aggregate bases and subbases on structural integrity, improving drainage, and mitigating freeze-thaw effects. In particular, the literature review focuses on different pavement design strategies, and how pavement aggregate base-subbase combinations help protect the underlying subgrade.

2.1 Pavement Foundation Needs

Pavement foundation layers include aggregate base course, subbase course, and engineered subgrade (i.e., compacted, or stabilized subgrade) from top to bottom. According to Saeed (2008), unbound aggregate base/subbase layers for flexible and rigid pavements generally provide (1) a construction platform, (2) structural layers for the pavement system, (3) drainage layers, (4) frost-free layers, and (5) “select fill” materials (sometimes as part of the pavement working platform). These purposes require pavement foundations to provide high enough load-supporting capacity, good permeability and drainage, good frost protection and pumping prevention. Generally, the following factors have been identified as primarily affecting unbound aggregate layer performance trends: (1) aggregate mineralogy, (2) gradation, (3) fines content (material passing 0.075 mm or No. 200 sieve), (4) type of fines (plastic or nonplastic), (5) particle shape, including texture and angularity, (6) degree of compaction, and (7) moisture content (Tutumluer et al., 2018).

2.1.1 Load-Carrying Capacity and Constructability

The load-carrying capacity of pavement foundations refers to the ability to withstand and distribute loading under construction activities and traffic. This is commonly characterized by a layer’s strength, stiffness, and permanent deformation.

For working platforms, unbound aggregate layers are often constructed on soft, engineered or soft, in situ subgrade soils to provide sufficient stability and adequate immediate support for equipment mobility and paving operations without developing excessive rutting. Kazmee et al. (2019) found that using granular layers with higher shear strength as working platforms leads to lower accumulations of

permanent deformations. By using a thicker working platform, weaker materials can achieve the same deflection as stronger materials (Tanyu et al., 2004). Figure 1 shows the basic concept of load distributions in flexible and rigid pavements.

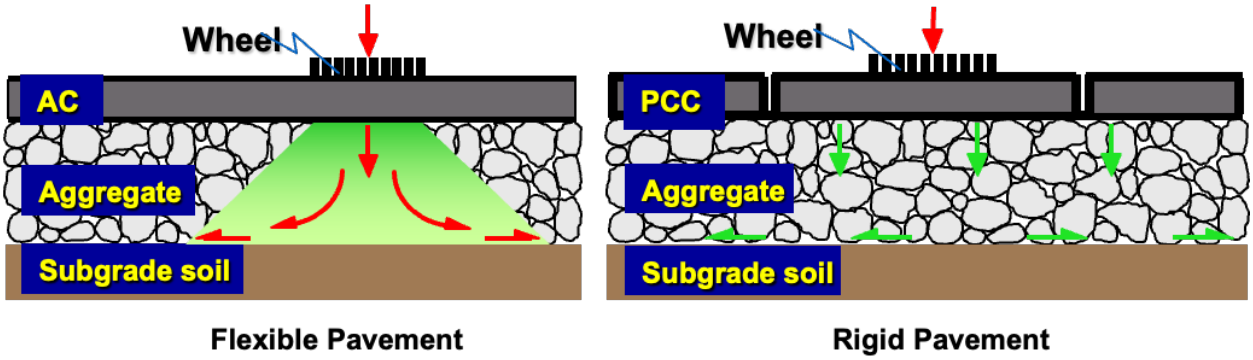

Figure 1. Load distribution in flexible and rigid pavements

Further, pavement foundation layers need to sustain repetitive traffic loading. Figure 1 illustrates the load distributions within aggregate base/subbase layers under wheel loading in flexible [asphalt concrete (AC)] and rigid [Portland cement concrete (PCC)] pavements. In flexible pavements, the aggregate base/subbase layers serve as major structural components to provide load distribution, i.e., dissipation of high wheel load stresses with depth, and ensure adequate support and stability for the asphalt surfacing. In contrast, the aggregate base/subbase layers used in rigid pavement structures primarily provide uniform support conditions to the concrete slabs; the structural contribution of such layers is often not the primary design aspect. Previous studies have shown that non-uniform foundation layers under concrete pavements, e.g., having non-uniform stiffness, would amplify critical responses such as stresses, strains, and deflections (Chavan, 2012; Roesler et al., 2016), which may lead to premature failures.

2.1.2 Permeability and Drainage

Excessive moisture in pavement foundations causes reduced strength, increased rutting accumulation, and reduced resilient modulus for the unbound layers (Haider et al., 2014; Nazarian & Yuan, 2008). Pavement distresses such as cracking, stripping, and pumping are linked to the permeability of pavement foundations (Rokade et al., 2012; Saeed, 2008; Saeed et al., 2001). For some regions with problematic expansive subgrade and cold winter climates, the impact of poor drainage may need to be investigated in further detail.

Soil water characteristic curves (SWCC) and hydraulic conductivity can be used to characterize moisture-suction behavior and permeability of pavement foundations, respectively. AASHTO recommended two design standards for the time-to-drain method, i.e., percent drained area (50%) and percent saturation (85%). Tutumluer et al. (2015) suggested using both SWCC and hydraulic conductivity to control the moisture regime in pavement foundation layers, and the two factors should be considered together to find an optimum combination of aggregate base and subbase materials. In addition, using subsurface

drainage designs such as permeable base layers and edge drains are efficient strategies recommended by some agencies (Caltrans, 2020; MnDOT, 2019a).

2.1.3 Frost Protection

Freeze action occurs in frost-susceptible soils when freezing front penetrates pavement structures and turns existing moisture into ice, as shown in Figure 2. The formation and expansion of ice lenses cause frost heaving in the upper layers, thus leading to non-uniform pavement support (Bilodeau et al., 2017; Khawaja & Tanveer, 2018). Capillary tension can bring additional water to form ice when the ground water table is close to the frost zone. When ice lenses start to melt in warmer seasons, large voids will form, which will weaken the pavement structure, reduce the load-carrying capacity, and cause excessive deflections or failures under traffic loading (Simonsen & Isacsson, 1999).

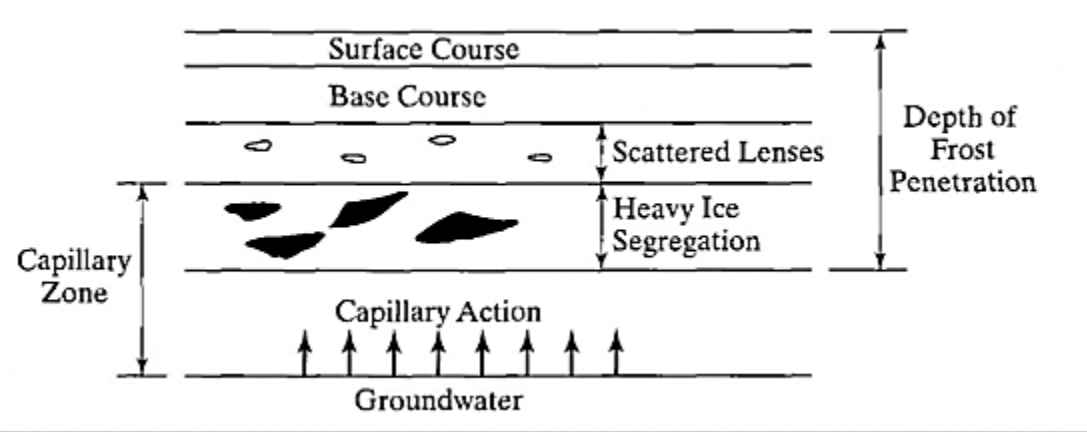

Figure 2. Mechanism of Frost Heave (Jameel & Yousif, 2021)

In Minnesota and other cold areas where pavement foundations experience one or more freeze-thaw cycles during a year, frost protection is necessary. The primary factors influencing freeze-thaw are: (1) presence of a frost-susceptible soil, (2) ambient/pavement temperature and the freezing point of the soil, and (3) presence of moisture (Johnson, 2012; Mahedi et al., 2022; Zhang et al., 2018). Rajaei and Baladi (2015) developed a frost depth prediction model using the data collected from Minnesota. The factors considered in the model included (1) material type, (2) soil thermal properties, (3) moisture content, (4) temperature, (5) wind speed, (6) precipitation, and (7) solar radiation. According to the 14 frost-monitoring sites located across Minnesota in the year 2014, all sections obtained more than 30-in. frost depth, and the maximal frost depth reached 96 in. in Otter Tail County (Oman et al., 2018). The required minimal thicknesses are 36 in. and 22 in. for flexible and rigid pavement in Minnesota for high-volume roads when unbound aggregate bases are applied (MnDOT, 2019a). Attention needs to be paid to cold regions with high frost depth.

2.1.4 Pumping Prevention

Pumping is a major distress in rigid pavements. Figure 3 shows the mechanism of pumping due to shear-induced erosion and hydraulic erosion. In Figure 3 (a), deflection-induced shear at the interface of the

concrete slab and subbase layer produces fines. The fines under the right slab will migrate to the bottom of the left slab due to suction under wheel loading (Jung & Zollinger, 2011). In the case of hydraulic erosion presented in Figure 3 (b), initial gaps between slabs lead to water accumulation under slabs. Then water is ejected with fines under wheel loading (Chen & Lytton, 2019). Pumping with material loss causes differential pavement settlement, non-uniform support under the pavement surface course, and joint faulting. To prevent pumping and maintain a uniform support under concrete slabs, erosion-resistant aggregate base/subbase materials need to be used. Degradation or abrasion resistance of aggregate courses can be evaluated and quantified using Los Angeles, Micro-Deval, and Nordic abrasion tests. Additionally, expediting water drainage can help mitigate pumping (Galinmoghadam et al., 2022).

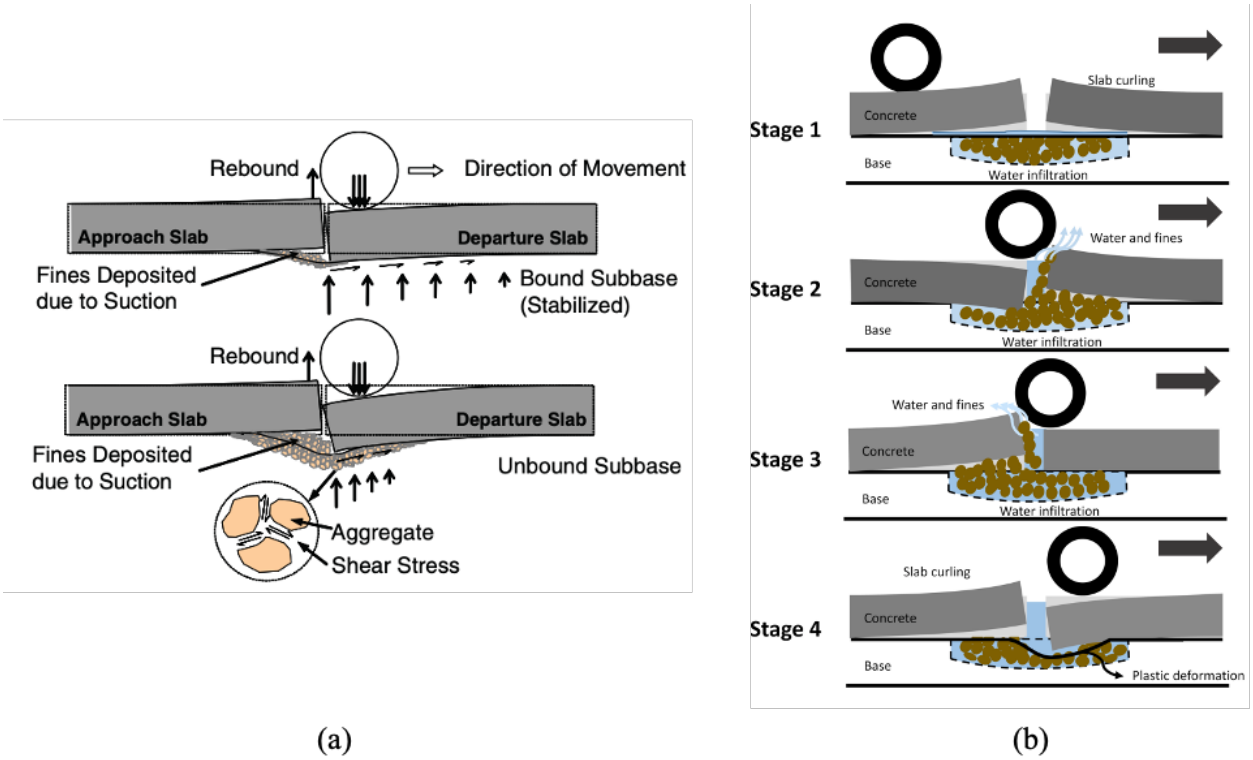

Figure 3. Development of pumping in rigid pavement due to (a) shear-induced erosion and (b) hydraulic erosion (Jung & Zollinger, 2011)

2.2 Aggregate Quality Affecting Pavement Performance

Physical characteristics of aggregates that govern load dissipation and particle-interlocking aspects differentiate “good” and “poor” quality aggregates with respect to their suitability for unbound aggregate base/subbase course applications in pavements. Moreover, the chemical properties of the aggregates governing their durability and soundness are critical to ensuring long-lasting pavement structures. A review of technical literature was conducted to identify the most important aggregate quality indicators and their linkages to pavement distresses.

2.2.1 Aggregate Quality Indicators

Aggregate quality checks are needed to ensure the satisfactory performance of aggregates in various pavement layer applications. Saeed et al. (2001) summarized the most fundamental factors related to aggregate properties contributing to pavement distresses. These are (1) shear strength, (2) density, (3) gradation, (4) fines content, (5) moisture level, (6) particle angularity and surface texture, (7) degradation during construction, and (8) drainability. In this section, the quality indicators and the importance of shear strength and stiffness are discussed first. Then, the quality indicators for mineralogy, percentages and types of fines, particle shape/morphology, resistance to degradation, degree of compaction, moisture content, and permeability are presented along with their effects on strength, permanent deformation, and resilient modulus.

2.2.1.1 Shear Strength and Stiffness

Shear strength and stiffness of unbound aggregate layers are the most important properties dominating the performance of flexible and rigid pavements (Saeed et al., 2001). Shear strength of soil and unbound materials are commonly characterized with (1) peak shear stress values from static triaxial shear tests and direct shear tests, (2) cohesion and angle of internal friction from triaxial shear tests, (3) accumulated plastic strain under repeated load triaxial tests, (4) California Bearing Ratio (CBR) (Saeed, 2008). The stiffness is commonly measured by resilient moduli obtained from conducting repeated load triaxial tests (Alavi et al., 1997).

The pavement critical responses such as stress and strain values under wheel loading are fundamental inputs for predicting pavement long-term behavior trends under mechanistic distresses such as cracking, rutting and fatigue in Pavement ME models (Jung & Zollinger, 2011; Khazanovich et al., 2006; Velasquez et al., 2009). Note that the resilient modulus is a major factor affecting these responses. By increasing the resilient modulus of aggregate base/subbase layers, the bending stresses within a concrete slab were reduced, so the service life could be extended with less appearance of cracks (Shaban et al., 2020). The permanent deformation of aggregate base layers was drastically reduced by using geogrids as stiffness enhancement in aggregate base layers (Kwon & Tutumluer, 2009). Chow et al. (2014b) developed a rutting model for unbound aggregate base/subbase materials. The model used shear stress ratio, defined as the ratio between applied shear stress and shear strength. Figure 4 illustrates how the developed rutting model matched the experimental results with high coefficients of determination, and the permanent strain was highly affected by the shear stress ratio and shear strength.

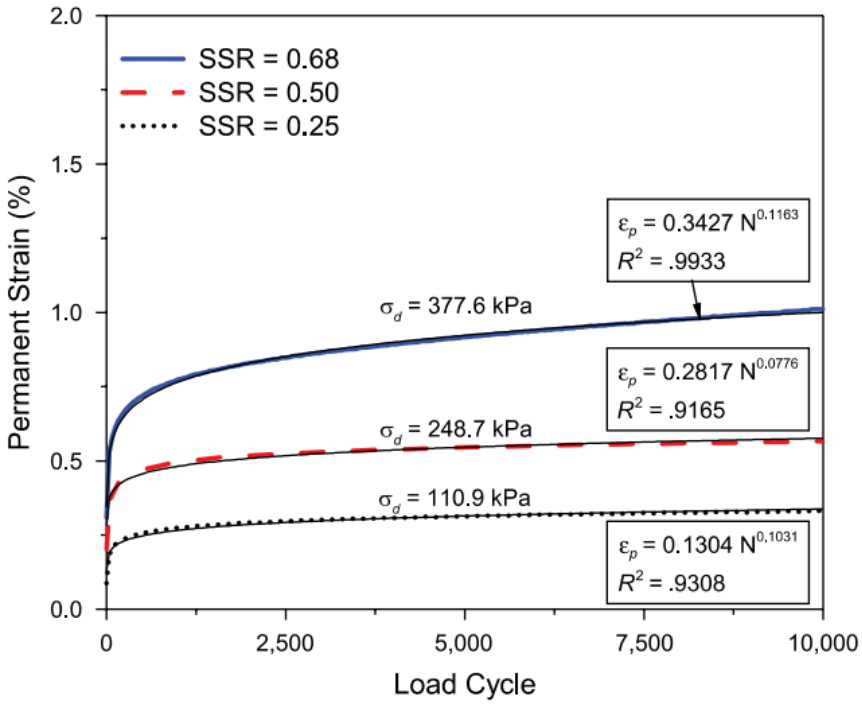

Figure 4. Effect of shear strength and shear stress ratio on permanent deformation (Chow et al., 2014b)

2.2.1.2 Mineralogy

Mineral composition of aggregates has a significant effect on the physical and chemical characteristics that ultimately govern the performance of unbound aggregate base or subbase layers under loading. This is particularly true as far as degradation and polishing due to inter-particle friction are concerned. Calcareous aggregates like limestone and dolomite show significantly lower resistance to particle degradation and polishing compared to igneous and metamorphic rocks. Therefore, unbound aggregate base/subbase layers constructed using calcareous aggregates are likely to undergo more changes in gradation during compaction and subsequently under traffic loading (Tutumluer et al., 2013). Note that not many research studies have directly evaluated the effects of aggregate mineralogy on unbound aggregate base/subbase performance. Rather, more research studies have focused on evaluating the effects of aggregate physical characteristics influenced by mineralogy on performance. Woolf (1953) presented extensive data on the results from physical tests on road building aggregates. From his data, the effects of aggregate mineralogy on physical characteristics are clearly apparent. For example, the average reported loss by abrasion for granite was 4.3%, whereas the corresponding values for limestone and dolomite were 5.7% and 5.5%, respectively.

2.2.1.3 Percentage and Type of Fines

The percentage of fines (i.e., materials passing the No. 200 sieve or smaller than 0.075 mm) and the Atterberg limits including shrinkage limit (SL), plastic limit (PL) and liquid limit (LL) are commonly used to quantify the percent and type (i.e., plastic vs. nonplastic) of fines, respectively. Increasing the percentage of fines in a mix increases permanent deformation (Barksdale, 1972; Barksdale et al., 1992;

Thom & Brown, 1988). The type of fines in an aggregate layer has also been found to significantly affect performance.

Tutumluer et al. (2009) investigated the effect of the plasticity of fines on the performance of three types of unbound aggregates (crushed limestone, crushed dolomite, and uncrushed gravel) under repeated loading using resilient modulus and permanent deformation tests, and the effect of the plasticity of fines on moisture susceptibility and strength. The study found that

1. The presence of low amounts of nonplastic fines in an aggregate layer may not adversely affect the pavement performance. For plastic fines, however, the immediate bearing value showed rapid decrease with moisture contents even at low fines contents, thus indicating increased moisture sensitivity.
2. Increasing the amount of fines did not result in significant decreases in aggregate modulus and strength behavior in the case of nonplastic fines but had a drastic effect in the case of plastic fines.
3. Plasticity of fines (i.e., PI > 10) is the second most important property that affecting aggregate behavior after particle angularity. High amounts of plastic fines at wet of optimum moisture contents adversely affect the aggregate load transfer matrix and result in excessive permanent deformation.
4. For low percentages of nonplastic fines, moisture content did not have a significant effect on aggregate performance, while aggregate type or angularity was often the governing factor. However, for aggregates with plastic fines, moisture becomes the most influential factor for aggregate behavior (Tutumluer et al. 2009).

2.2.1.4 Particle Morphology

The morphological or shape properties of aggregate particles significantly affect the performance of unbound/bound layers used in highway pavements. Figure 5 illustrates the key physical shape properties of an aggregate particle. At a macro level, angularity is generally defined as a measure of crushed faces and sharpness of the corners in an aggregate particle. In general, using aggregate sources with equidimensional (cubical) and angular particle shapes is preferred in comparison to flat, thin, or elongated particles (Barksdale et al., 1992). Roughness or irregularities at the micro level on the surface of the aggregate is termed surface texture. This aggregate property is the main factor that controls the magnitude of inter-particle frictional resistance (Dunford, 2013). The dimensional ratio of an aggregate particle is generally referred to as the flat and elongated (F&E) ratio or form property.

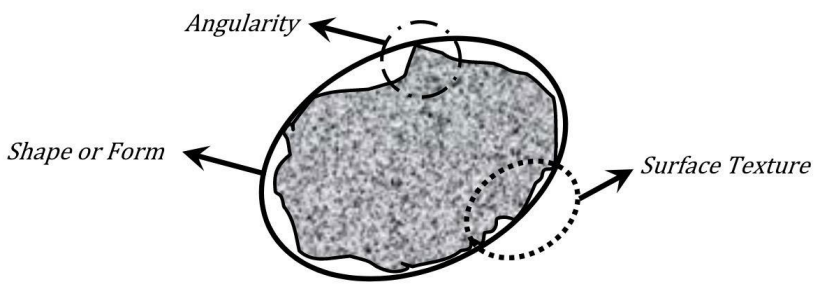

Figure 5. Key physical shape properties of an aggregate particle

Currently there are only a few standard testing procedures to measure aggregate morphological properties. ASTM D3398, "Index of Aggregate Particle Shape and Texture," provides a combined assessment of particle shape and texture. In this testing method, voids in aggregate layers compacted at different levels of compaction energy are used as an indirect indicator of angularity and/or roughness of particles. ASTM D4791 "Flat or Elongated Particles in Coarse Aggregates" is used to determine the percentage by mass of coarse aggregates that have a maximum to minimum dimension ratio greater than five. In this method, a standard caliper device is used to measure the dimensional ratio of particles. On the other hand, some image-based aggregate shape analysis systems were developed. Figure 6 shows the field evaluations of shape properties of riprap materials using state-of-art imaging segmentation algorithms to determine particle size and flat and elongated ratio.

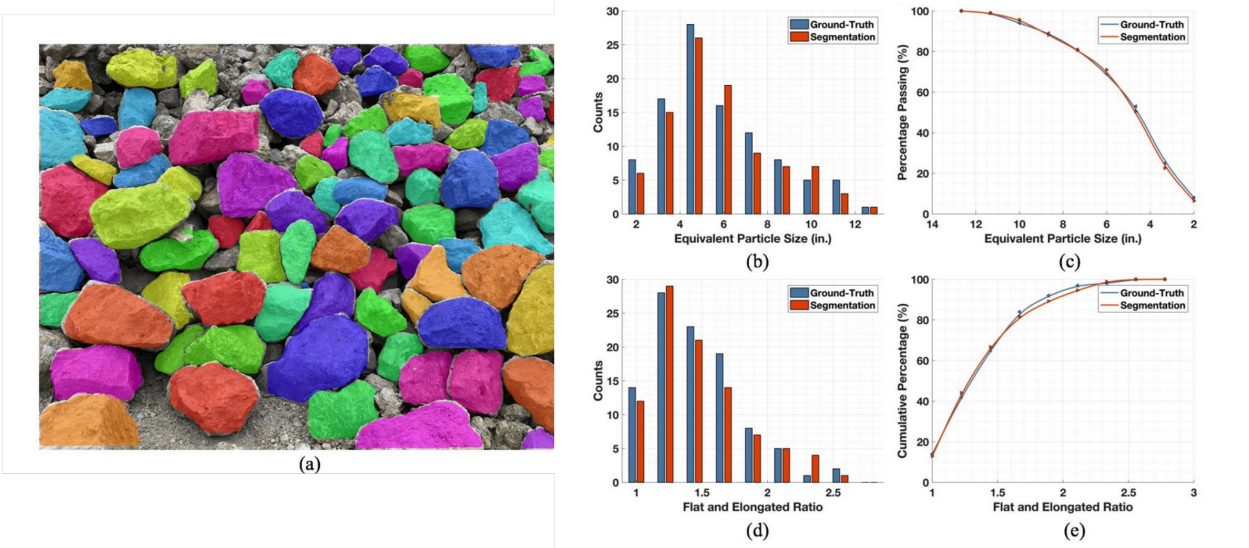

Figure 6. Field evaluations of shape properties of riprap materials using state-of-art imaging segmentation algorithms: (a) particle segmentation on field image, and validations with ground truths of (b) particle size and (c) flat and elongated ratio (Huang et al., 2020)

Table 1 summarizes the advanced imaging systems in laboratory setups, along with the measured shape property and indicators (Masad, 2007; Moaveni, 2015). Note that most of these devices need to scan one particle at a time, and some devices require stringent light conditions.

Recently, Huang et al. (2020) developed a computer-vision-based software, I-RIPRAP, for field evaluations of large-sized riprap materials. By applying state-of-the-art computer vision algorithms as shown in Figure 6, it simplified the evaluation process, benefiting from the capability of segmenting each particle within an image without compromising accuracy. In the second phase of this project, Huang et al. (2022) expanded the application to 3D space by implementing 3D reconstruction, completion, and segmentation algorithms to obtain more profound morphological information as shown in Figure 7.

Luo et al. (2023) designed and field tested a ballast scanning vehicle dedicated to the detection of railway ballast aggregate degradation/fouling.

Table 1. Imaging systems for aggregate shape analysis (Masad, 2007)

Name of Imaging System	Measured Aggregate Shape Property	Indicator
VDG - 40 Videograder (Browne et al., 2001)	Form / Size	Grain size distribution, Flatness, Slenderness ratio
Computer Particle Analyzer (Tyler, 2001)	Form / Size	Diameter, Maximum chord, Maximum length, Maximum width
Micromeritics Optimize (Browne et al., 2001)	Form / Size	Grain size distribution
Buffalo Wire Works (Browne et al., 2001)	Form / Size	Grain size distribution
Capsize (Masad, 2007)	Form / Size Angularity	Grain size distribution, Convexity-based angularity index
Whipsnade (Maerz & Zhou, 1999)	Form / Size Angularity	Grain size distribution, Minimum average curve radius (angularity)
University of Illinois Aggregate Image Analyzer (Tutumluer et al., 2005)	Form / Size Angularity Surface Texture	Grain size distribution, Angularity index, Surface texture index, F&E ratio
Aggregate Imaging System (Masad, 2003)	Form / Size Angularity Surface Texture	Angularity index (gradient method and radius method), Sphericity, Shape factor, Wavelet transform energy (surface texture)

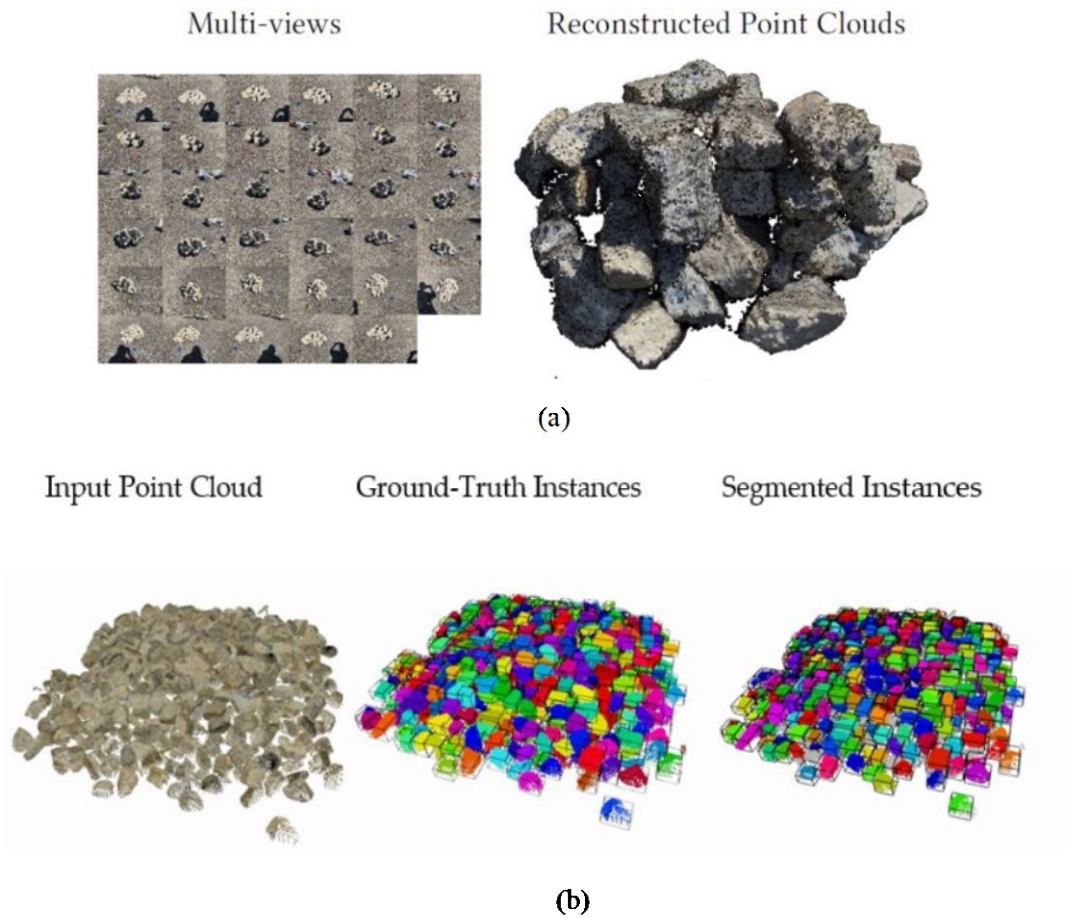

Figure 7. (a) 3D point cloud reconstruction from 2D images, (b) segmentations on 3D point cloud (Huang et al., 2022)

The impact of aggregate particle shape on the resilient modulus, shear strength, and permanent deformation behavior of unbound aggregate base/subbase layers in a pavement structure has long been realized. Allen (1973) reported that angular particles had better permanent deformation resistance due to improved particle interlock and higher angle of shear resistance between particles, as compared to rounded solid particles. Barksdale and Itani (1989) concluded that blade-shaped crushed particles are slightly more susceptible to rutting than other types of crushed aggregate. Uncrushed river gravel—typically cube-shaped, well-rounded, and with smooth surfaces—is also more susceptible to rutting than crushed aggregates. Aggregate assemblies built with uncrushed or partially crushed particles were reported to have a lower resilient modulus and higher Poisson's ratio than those with angular crushed particles (Allen & Thompson, 1974; Barksdale, 1972; Thom & Brown, 1988). This is attributed to the higher number of contact points in crushed aggregates which distribute loads better and create more friction between particles (Lekarp et al., 2000). Rao et al. (2002) conducted laboratory rapid shear triaxial tests on rounded uncrushed gravel, angular crushed stone, and a 50-50 blend of the two aggregates for which aggregate angularity index variations were quantified by imaging-based techniques. As shown in Figure 8, they observed that an increase in crushed materials beyond 50%

significantly increased friction angle as well as the resistance to permanent deformation accumulation. Cook et al. (2017) observed that unbound aggregate base materials with higher flat and elongated ratios have higher resilient modulus. The enhancement trend is more obvious for open-graded materials than dense-graded materials.

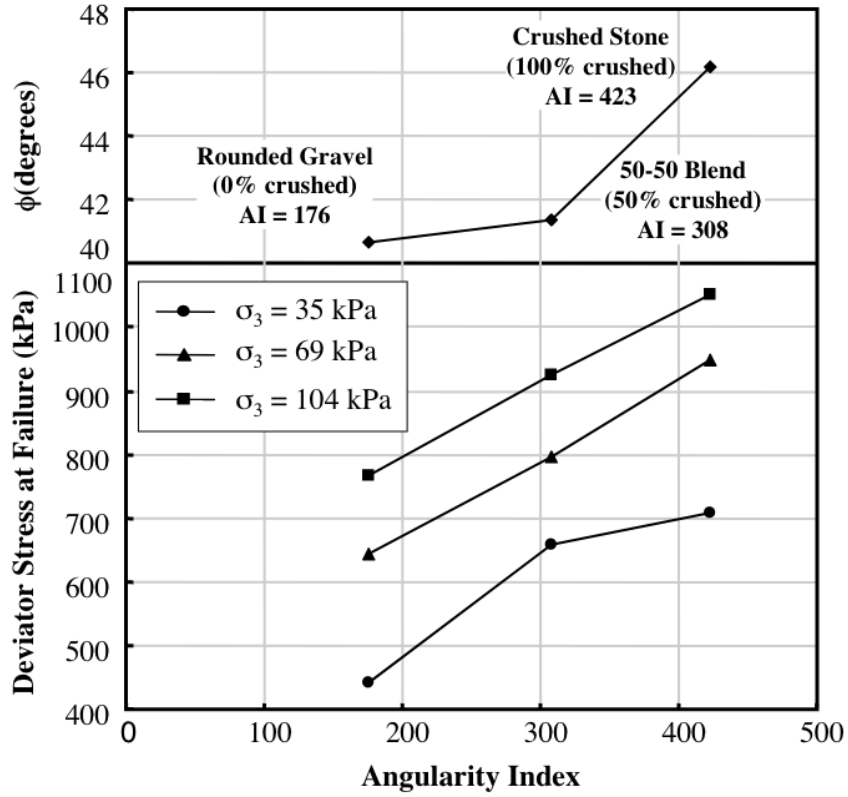

Figure 8. Effect of Particle Angularity on Strength (Rao et al., 2002)

2.2.1.5 Resistance to Degradation

The most important factors that cause in-service aggregate degradation include (1) material source properties including mineralogy and petrography, (2) shape and angularity of aggregate particles, (3) initial size distribution and arrangement of particles, (4) force concentration on particle surfaces, and (5) aggregate layer maintenance operations and environmental conditions (Tolppanen, 2001). Los Angeles abrasion (LAA) and Micro-Deval tests are commonly utilized to characterize material resistance to degradation. LAA loss (i.e., percent weight of materials passing the No. 12 sieve) and Micro-Deval loss (i.e., percent weight of materials passing No. 200 sieve) are used as quality indicators. According to MnDOT Specification 3138, MnDOT evaluates an aggregate's resistance to degradation primarily with the Los Angeles Rattler (LAR). The maximum allowable LAR losses are 40% and 35% for Class 5 and Class 6 aggregates from carbonate quarry rocks, respectively.

Saeed et al. (2001) reported in NCHRP Report 453 that LAA and Micro-Deval testing were among the most important tests that measure the performance of aggregates used in unbound pavement layers.

Several abrasion/degradation testing procedures for correlating the laboratory testing results with the field performance of asphalt pavements were compared (Wu et al., 1998). The results showed that Micro-Deval and magnesium sulfate soundness tests provide the best correlations with field performance.

Erichsen et al. (2011), on the other hand, concluded that a suitable durability test is dependent on the aggregate quality and method of degradation in the field. The LAA test correlates better with degradation by fragmentation while Micro-Deval and Nordic abrasion tests correlate better to degradation by wearing, in which a more poorly graded gradation curve is obtained after the tests. Similarly, Cooley and James (2003) tested aggregates from 72 sources in eight states with Micro-Deval and LAA and reported a poor correlation between Micro-Deval, sodium sulfate soundness, and LAA for the same aggregates, indicating that these tests are essentially measuring different properties, depending on the aggregate source.

2.2.1.6 Degree of Compaction

Before the aggregate samples are tested for strength, modulus, and deformation behavior, the first task is to compact them at the corresponding gradation to determine their moisture-density relationships. Because pavement layers in the field often are compacted to predetermined percentages of the maximum dry density (MDD) values, it is important to establish the values of MDD and optimum moisture content (OMC) for each aggregate gradation ahead of construction. Through compaction, strength can be increased, deformation tendency can be reduced in the field, bearing capacity of a granular layer can be improved, and undesirable volume changes (such as those caused by frost action, swelling, and shrinkage) may be controlled (Holtz, 1990).

The percentage of achieved density over the maximum dry density is usually used as a quality indicator to quantify the degree of compaction (DOC). The impact of density appears to be larger on the permanent deformation behavior of aggregates. Decreased density, as measured by DOC, substantially increases permanent deformation. Barksdale (1972) found that decreasing the DOC from 100% to 95% of maximum dry density increased permanent axial strain by 185% (on average). Increasing density from the standard Proctor to the modified Proctor maximum density decreased permanent deformation by 80% for crushed limestone and by 22% for gravel (Allen, 1973).

2.2.1.7 Moisture Content

Moisture has been widely recognized to adversely affect the performance of unbound aggregate layers in pavement structures and can affect aggregates in three different ways: (1) make them stronger with capillary suction, (2) make them weaker by causing lubrication between the particles, and (3) reduce the effective stress between particle contact points resulting from increasing pore water pressure, thus decreasing the strength. The moisture content is defined as a percentage of moisture in total sample by weight. AASHTO T 255 and T 265 cover the procedures to measure the moisture content using an oven-dried method. Additionally, the saturation moisture content refers to the maximum moisture content that can be contained in materials when all open pores are filled with water. The moisture content and

saturation moisture content, commonly used as quality indicators, can affect the resilient modulus and strength of aggregate layers due to the capillary and lubrification effects.

Thompson and Robnett (1979) and Dempsey (1981) found that open-graded aggregates did not develop pore pressures upon loading, but uniformly graded dense aggregates with higher fines contents did develop pore pressures that resulted in a reduction in resilient modulus values. Thom and Brown (1987) found that no noticeable pore water pressures developed below 85% saturation and that most of the reduction in resilient moduli was the result of the lubricating effect of the water. It can also be assumed that increasing the water content reduces the capillary suction between particles, thus decreasing the effective stress and the resilient moduli. Therefore, moisture can have a positive effect on unbound granular materials as long as the moisture increases the capillary suction between particles. Once the saturation reaches a point at which it reduces capillary suction, the moisture becomes a detriment to preventing residual deformation and can cause a lubricating effect.

2.2.1.8 Grain Size Distribution

One of the primary variables in any laboratory testing of aggregate materials is the grain size distribution. The grain size distribution is commonly reported in percent finer by weight on typical sieves as described in AASHTO T 27 and ASTM C136. Differences in aggregate gradations can often lead to significantly different behavior for the same aggregate type. This is the result of the different packing order and void distributions, which play a crucial role in load carrying through particle-to-particle contact in an aggregate matrix. To control the gradation of an individual aggregate sample, sieving and size separation of the aggregate materials need to be undertaken based on washed sieve analysis. Many agencies specify the grain size distribution thresholds for different material classes, and Figure 9 shows the gradation requirements for aggregate base/subbase materials by MnDOT.

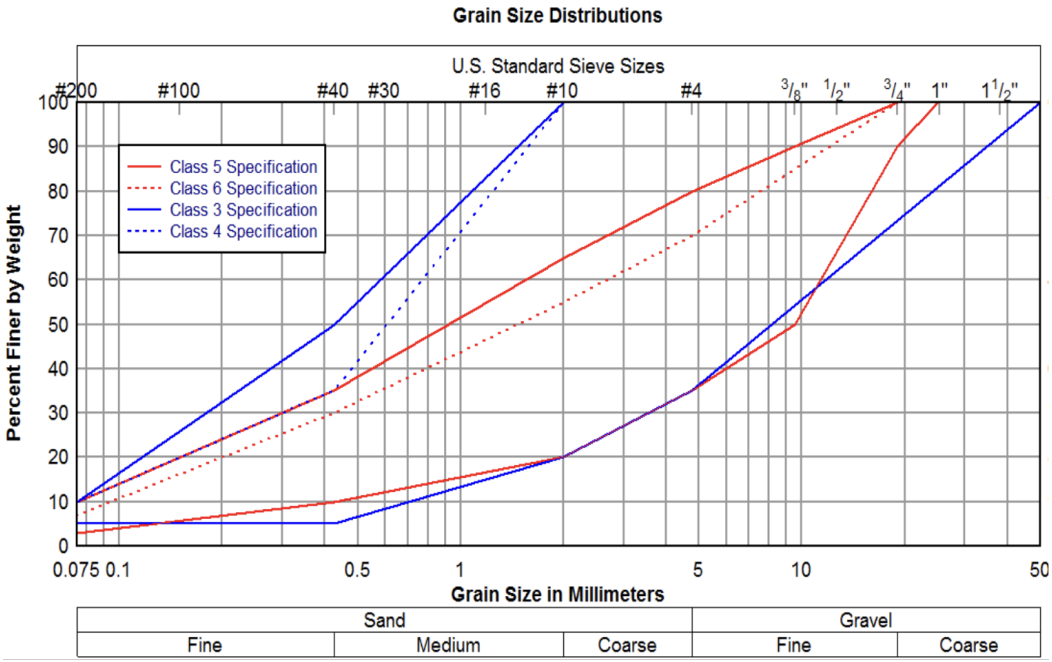

Figure 9. Gradation thresholds for MnDOT materials

Well-graded aggregates have been found to have higher resilient modulus values (Jorenby & Hicks, 1986; Kamal et al., 1993; Lekarp et al., 2000). Thom and Brown (1988) found that the effect of grading varied with the compaction level. When uncompacted, specimens with uniform grading accumulated the least permanent deformation, whereas the resistance to permanent deformation was similar for all gradations when the specimens were heavily compacted. Kamal et al. (1993) and Dawson et al. (1996) found the effect of grading to be more significant than the DOC, with the densest mix having the highest permanent deformation resistance. Brown and Chan (1996) successfully reduced rutting in granular base layers by selecting an optimum aggregate material grading that maximized compacted density. These performance characteristics were demonstrated through experiments with two types of wheel tracking and the use of repeated load triaxial tests at the University of Nottingham in the United Kingdom.

2.2.1.9 Permeability

The hydraulic conductivity (or the coefficient of permeability) is an essential quality indicator for analysis and design of the subsurface drainage systems along with other engineering properties of materials, such as the grain size distribution, packing, degree of saturation, and frost susceptibility. Laboratory determination of the coefficient of permeability is highly recommended, particularly for aggregate base, subbase, fill materials, and other drainage layers; and test methods for this purpose are quite mature. Obtaining in-situ measurements of permeability for aggregate base/subbase layers is desired from the standpoint of adequate engineering design. With the advent of portable Gas Permeameter Test devices as introduced by White et al. (2010), this becomes possible and is widely used in quality control and quality assurance (QC/QA). In cases where field measurement and laboratory testing of permeability is not possible, empirical approaches can be used with caution to estimate permeability from readily available material properties such as gradation and moisture and density conditions.

2.2.2 Linkage to Flexible Pavement Distress

Because aggregate materials constitute more than 90% of flexible pavements, they can highly influence the overall performance, load-carrying capacity, and type and rate of pavement distresses. The two common distresses for asphalt pavements are rutting and fatigue cracking, and they have been commonly considered for pavement life predictions in Pavement ME (formerly MEPDG) models. Several aggregate properties can influence the type and severity of distresses that develop in flexible pavements. Saeed (2008) studied some of the main distresses that appear in flexible pavements and the contributing factors of the unbound layer's properties. A summary of the findings is presented in Table 2 (Saeed, 2008).

Table 2. Flexible pavement distresses and the linkages to aggregate property (Saeed, 2008)

Distress	Description of distress	Unbound layer failure mechanism	Contributing factor
Fatigue Cracking	Fatigue cracking first appears as fine, longitudinal hairline cracks running parallel to one another in the wheel path and in the direction of traffic; as the distress progresses the cracks interconnect, forming many-sided, sharp-angled pieces; eventually cracks become wider and, in later stages, some spalling occurs with loose pieces prevalent. Fatigue cracking occurs only in areas subjected to repeated loadings.	Lack of base stiffness causes high deflection/strain in the HMA surface under repeated wheel loads, resulting in fatigue cracking of the HMA surface. High flexibility in the base allows excessive bending strains in the HMA surface. The same result can also be due to inadequate base thickness. Changes in base properties (e.g., moisture-induced) with time can render the base inadequate to support loads.	• Low modulus of the base layer • Low density of the base layer • Improper gradation • High fines content • High moisture level • Lack of adequate particle angularity and surface texture • Degradation
Rutting/ Corrugation	Rutting appears as a longitudinal surface depression in the wheel path and may not be noticeable except during and following rains. Pavement uplift may occur along the sides of the rut. Rutting results from a permanent deformation in one or more pavement layers or subgrade, usually caused by consolidation and/or lateral movement of the materials due to load.	Inadequate shear strength in the base allows lateral displacement of particles with applications of wheel loads and results in a decrease in the base layer thickness in the wheel path. Rutting may also result from the densification of the base due to inadequate initial density. Changes in base (mainly degradation-producing fines) can result in rutting. The base can also lose shear strength from moisture-induced damage, which will cause rutting.	• Low shear strength • Low base material density Improper gradation • High fines content • High moisture level • Lack of particle angularity and surface texture • Degradation • High moisture content coupled with traffic can contribute to stripping
Depressions	Depressions are localized low areas in the pavement surface caused by settlement of the foundation soil or consolidation in the subgrade or base/subbase layers due to improper compaction. Depressions contribute to roughness and cause hydroplaning when filled with water.	Inadequate initial compaction or nonuniform material conditions result in an additional reduction in volume with load applications. Changes in material conditions due to poor durability or frost effects may also result in localized densification with eventual fatigue failure.	• Low density of base material • Low shear strength of the base material combined with inadequate surface thickness
Frost Heave	Frost heave appears as an upward bulge in the pavement surface and may be accompanied by surface cracking, including alligator cracking with resulting potholes. Freezing of underlying layers resulting in an increased volume of material causes the upheaval. An advanced stage of the distortion mode of distress resulting from differential heave is surface cracking with random orientation and spacing.	Ice lenses are created within the base/subbase during freezing temperatures, particularly when freezing occurs slowly, as moisture is pulled from below by capillary action. During spring thaw large quantities of water are released from the frozen zone, which can include all unbound materials.	• Freezing temperatures • Source of water • Permeability of material (high enough to allow free moisture movement to the freezing zone, but low enough to also allow suction or capillary action to occur)

2.2.3 Linkage to Rigid Pavement Distress

Rigid pavements are very durable if adequately designed and high-quality materials and good construction practices are used. The effect of aggregate on PCC pavement performance has been well-documented by many researchers (Delatte, 2018). Moreover, service conditions such as temperature, humidity, and induced loads are among the factors that add complexity to the design and construction of concrete pavements. Delatte (2018) claimed the main functions of aggregate base/subbase layer in PCC pavements are: (1) providing uniform, stable and permanent support, (2) increasing the modulus of subgrade reaction, (3) minimizing the damaging effects of frost action, (4) preventing pumping, and (5) providing a working platform for construction equipment.

Poor performance of PCC pavements can often be attributed to different qualities and properties of the aggregates used to construct the PCC. Darter et al. (1979) identified that a low-quality subbase layer led to higher potentials of pumping and edge punchouts in Illinois. Similarly, Hanna (2003) summarized aggregate quality aspects closely linked to predominant distresses in PCC pavements. According to Hanna (2003), the quality indicators for aggregates that can significantly affect the performance of concrete pavements were mainly divided into five categories: (1) physical properties, (2) mechanical properties, (3) chemical and petrographic properties, (4) durability properties, and (5) others. Cracking, pumping, faulting, and roughness are the most common distresses of rigid pavements constructed with recycled aggregates, along with aggregate source properties that influence these distresses as well as the proposed quality measures to check them (Saeed, 2008). Table 3 presents major distresses of rigid pavements and corresponding contributing factors relevant to aggregate base/subbase layer properties (Saeed, 2008).

Table 3. Rigid pavement distresses and the linkages to aggregate property (Saeed, 2008)

Distress	Description of distress	Unbound layer failure mechanism	Contributing factor
Cracking	Cracks transverse to the pavement centerline, generally within the center one-third of the slab. Corner breaks and diagonal cracks appear as top-down hairline cracks across slab corners where the crack intersects the joints less than 6 ft from the corner; cracking progresses to result in several broken pieces with spalling of crack and faulting at the crack or joint up to ½ in. or more. The corner break is a crack completely through the slab (as opposed to corner spalls, which intersect the joint at an angle).	Inadequate support or loss of support from the unbound aggregate base/subbase resulting from settlement or erosion can increase tensile stresses in the slab under repeated wheel loads and result in increased transverse or corner or diagonal cracking which initiates at the bottom or top of the slab (corner cracks at the top). When a crack develops, an increased load is placed on the base, resulting in deformation within the base and surface roughness of the pavement; the crack introduces moisture to the base, resulting in further loss of support and possibly erosion and faulting thereby resulting in further deformation and roughness. Corner breaks (and associated faulting) are caused by a lack of base support from erosion and pumping of the base material and freeze-thaw softening of the base.	• Low base stiffness and shear strength • Pumping of base/subgrade fines causing loss of support • Low density in base Improper gradation • High fines content High moisture level • Lack of adequate particle angularity and surface texture • Degradation under repeated loads and freeze-thaw cycling
Pumping/ Faulting	Pumping and faulting begin as water seeping or bleeding to the surface at joints or cracks and progress to fine material being pumped to the surface; the ultimate condition is an elevation differential at the joint termed faulting. Pumping action is caused by repeated load applications that progressively eject particles of unbound material from beneath the slabs.	Pumping involves the formation of a slurry of fines from a saturated erodible base or subgrade, which is ejected through joints or cracks in the pavement under the action of repetitive wheel loads.	• Poor drainability (low permeability) • Free water in base Low base stiffness and shear strength • Highly erodible base • High fines content Degradation
Frost Heave	Differential heave during freezing and formation of ice lenses causes roughness due to uneven displacement of PCC slabs; thaw weakening results in loss of support from base and subgrade which may cause pumping and faulting and corner breaks; under heavy loads, the loss of support can result in cracking of slabs.	Ice lenses are created within the base/subbase during freezing temperatures, particularly when freezing occurs slowly, as moisture is pulled from below by capillary action and migrates toward the freezing front. During spring thaw, large quantities of water are released from the frozen zone, which can include all unbound materials.	• Freezing temperatures • Capillary source of water • Permeability of material high enough to allow free moisture movement to the freezing zone

2.3 Pavement Design Methods

Pavement design methods can be divided into three main groups: empirical, mechanistic-empirical (M-E), and mechanistic. Most pavement design methods are either empirical or mechanistic-empirical. Empirical models are data-driven, derived from historical observations and/or real-world performance data. They are straightforward and have limited predictive ability, especially in differing conditions. For mechanistic-empirical models, load and environmental-induced stresses, strains, and deflections are calculated using a mechanistic model, and then transfer functions are used to relate pavement structural behavior and performance to performance and distresses such as rutting or fatigue cracking.

2.3.1 Flexible Pavement Design Methods

2.3.1.1 AASHTO 1993

AASHTO 1993 is one of the widely adopted empirical flexible pavement design methods in the US, extending the principles of AASHTO 1972 with some changes that include using resilient modulus to characterize the subgrade instead of a soil support number, characterizing pavement materials in terms of resilient modulus, CBR and R-value, incorporating environmental factors like moisture and temperature, and replacing the previously subjective regional factor term. It also considers the impact of drainage on pavement performance by assigning a drainage coefficient (m) in the Structural Number (SN) calculation, which is in the range of 0.4 for very poor to 1.4 for best-quality drainage. The drainage coefficient is generally set to 1.0 in most states across the United States.

The guidelines have certain limitations that need to be considered. They are based on the AASHO Road test, which was conducted on only one road's specific material and soil type. Additionally, there is only an empirical relationship linking traffic to equivalent single axle loads (ESALs), and there is limited guidance on selecting structural coefficients and drainage modification factors.

2.3.1.2 AASHTOWare Pavement ME

AASHTOWare Pavement ME is a mechanistic-empirical methodology that overcomes some of the empirical limitations of the AASHTO 1993. It calculates Pavement structural responses to load via multi-layer elastic analysis. The method links pavement stresses and strains to performance indicators using a transfer function to predict the International Roughness Index (IRI) and other distresses for flexible pavements. It also employs an incremental approach to calculate responses to loads over discrete periods (months or semi-monthly). AASHTOWare operates iteratively, taking a designer's pavement configuration input and outputting damage predictions based on traffic (which is divided into classes) and climate data. The predicted damage is then compared to threshold values to assess the pavement configuration's acceptability.

Some of the limitations overcome by AASHTOWare from the earlier empirical AASHTO models and design procedures are as follows:

- Axle loads can be modeled mechanistically without conversion to ESALs, allowing for a detailed representation of the entire load spectra.
- Requires more input parameters in contrast to the empirical models, allowing designers to determine the level of detail of input based on the road's function and available information. Input parameters cover aspects like traffic composition, climate data, and material properties information such as volumetric properties, Atterberg limits, and various moduli and strengths.
- It uses the Enhanced Integrated Climatic Model (EICM), which considers moisture and temperature variations within the pavement, using detailed information such as hourly temperature, precipitation, wind speed, relative humidity, and cloud cover.

The latest AASHTOWare version incorporates updated climate discussions for Modern Era Retrospective Reanalysis (MERRA), a high-quality NASA climate database, offering continuous hourly climate estimates from 1979 onwards, along with North American Regional Reanalysis (NARR) (AASHTO, 2020).

2.3.1.3 Asphalt Institute Method

The asphalt institute design method is ME. The method is based on layered elastic analysis. It associates tensile stress at the bottom of Hot Mixed Asphalt (HMA) layer with asphalt fatigue and compressive stress at the top of the subgrade with rutting. The pavement thickness is tailored to manage these stresses to meet performance goals or design criteria. Essential inputs for this approach comprise the average annual temperature, traffic volume, the subgrade's resilient modulus, and the subbase's type and thickness.

State-wise Flexible Pavement Design Methods

Minnesota (MnPAVE Software)

MnPAVE, developed by MnDOT based on the work of the University of Minnesota, is a mechanistic-empirical pavement design software based on a multilayered elastic analysis (WESLEA). The project “Best Practices for the Design and Construction of Low Volume Roads – Revised” provides a detailed overview of the thickness design procedure with MnPAVE and the assumptions for traffic, failure criteria, reliability, and material properties (Skok et al., 2003). MnPAVE offers three design levels (i.e., basic, intermediate, and advanced) based on the amount and quality of known information about traffic data and material properties, which is like AASHTOWare Pavement ME levels 1, 2, and 3 inputs. It supports both English and S.I. units, features modifiable HMA modulus temperature adjustment equations, and provides reliability estimates through Monte Carlo simulations. MnPAVE employs elastic layered analysis (WESLEA) and Miner’s law for damage assessment, highlighting fatigue and rutting. The software factors in five seasons during design and accommodates traffic load spectra input (Tanquist, 2021).

Washington (EverPave Software)

Washington State Department of Transportation (WSDOT) employs the WESLEA to measure pavement stresses and deformations. In overlay design, it evaluates fatigue cracking and rutting as key damage parameters. Allowable ESALs are deduced from tensile strain at the bottom of the HMA layer (fatigue cracking) and vertical strain atop the subgrade (rutting). Seasonal effects are incorporated by adjusting layer moduli and recalculating for each season. Damage is assessed utilizing Miner's law.

Texas (FPS21 Software)

Texas employs FPS21, a design system for flexible pavements developed by the Texas Transportation Institute. Compared to pavement ME design, it requires fewer input parameters, non-recursive calculations, and no requirement for climatic data. It uses a Linear Elastic mechanistic model, and pavement performance is predicted using correlations between surface curvature and serviceability loss from the original AASHO Road Test. It also includes the necessary correlations for mechanistic design assessments in perpetual pavement designs, for instance, linking the maximum vertical compressive strain at the top of the subgrade to the anticipated number of ESALs before subgrade rutting occurs.

Alaska (AKFDP - 2 Software)

The Alaska Flexible Pavement Design Method is like that of EverPave, a mechanistic empirical pavement design software, and employs WESLEA to evaluate fatigue cracking and rutting as damage parameters and assesses total damage via Miner's law.

California (CalME Software)

CalME adopts Caltrans' empirical method, derived from a field test conducted by Caltrans and AASHTO, along with ME methods. It has input parameters like AASHTOWare for traffic and climatic data and performs mechanistic analysis by utilizing linear elastic Odemark's transformation and Boussinesq's equations. CalME design process operates an incremental-recursive model, analyzing the damage at each step. For reliability assessment, Monte Carlo Simulations are employed.

French Design Method

The French pavement design method is a comprehensive approach to pavement design. It is based on ME design. One of the key features is its traffic model that incorporates different axle types - single, tandem, and tridem for equivalent axle load calculations, offering a detailed understanding of traffic-induced stresses. For climate considerations, the method suggests using Miner's Law to compute equivalent temperature. Additionally, the method considers traffic volume when evaluating permanent subgrade deformation (Pereira & Pais, 2017).

2.3.2 Rigid Pavement Design Methods

2.3.2.1 Portland Cement Association

The Portland Cement Association (PCA) introduced a comprehensive thickness-design procedure for concrete highways and streets in 1984, catering to jointed plain, jointed reinforced, and continuously reinforced concrete pavements (JPCP, JRCP, and CRCP, respectively). A notable aspect of the process is incorporating erosion analysis alongside fatigue analysis. Erosion Analysis is pivotal in identifying pavement issues such as pumping, foundation erosion, and joint faulting, tying them to pavement deflections rather than flexural stresses, with critical deflection often occurring at the slab corner under a near-corner axle load.

Four pivotal factors direct the thickness design:

- The Concrete Modulus of Rupture, indicating the flexural strength of concrete, is ascertained at 28 days as per the ASTM C78 Standard Test Method for Flexural Strength of Concrete Using Simple Beam with Third Point Loading.
- Subgrade and Subbase Support: This is characterized by the modulus of subgrade reaction (k). Remarkably, the PCA method asserts that the yearly variation of k values, especially the reduced subgrade support during thaw periods, has minimal to no impact on the requisite thickness of concrete pavements.
- Design Period: The design period is generally 20 years.
- Traffic: The PCA design procedure requires detailed traffic data such as average daily truck traffic (ADTT) and axle-load distribution, focusing on trucks with six or more tires, alongside load safety factors (LSFs) to adjust the design based on varying traffic volumes and conditions across different roadway types.

2.3.2.2 AASHTO 1993

The AASHTO rigid pavement design procedure, published alongside the flexible pavement guide, draws its empirical foundation from the AASHO Road Test, refined further through theoretical insights and practical experience. Design input factors include the pavement serviceability index (PSI), traffic load, and various coefficients, an assumed slab thickness (D) validated or adjusted through design equations, slab length, and specifying the requisite slab steel content to ensure the structural integrity and performance of the pavement.

In rigid pavement design, the modulus of subgrade reaction (k) is used instead of the resilient modulus (M_R), and k varies seasonally. AASHTO provides two relationships for correlating k with M_R, one without a subbase and another with a subbase. It also provides for an effective k, representing a year-round equivalent modulus.

The design parameters specified by AASHTO for flexible pavements, encompassing time constraints, traffic, reliability, environmental impacts, serviceability, stage construction, and the assessment of swelling and frost heave, hold for rigid pavements also. In AASHTO Rigid Pavement design, crucial design

variables include the elastic modulus of concrete, determined per ASTM C469 or correlated with compressive strength. The concrete modulus of rupture is gauged as the mean value post 28 days using third point loading according to AASHTO T 97 or ASTM C78. The load transfer coefficient (J) evaluates a pavement's load transfer ability across joints and cracks, and the drainage coefficient for drainage efficacy assessment.

2.3.2.3 MEPDG and AASHTOWare Pavement ME

Concrete pavement design procedures are gradually making the transition from use of empirical methods based on field observations to mechanistic determinations where mechanical responses such as stress, strain, and deflection are computed and employed in design to predict concrete pavement performance over the design period. A nationwide mechanistic-empirical method for rigid pavement design has been developed under NCHRP 1-37A, also called the MEPDG. It currently provides comprehensive design guidelines for PCC pavements and has been extensively evaluated by state DOTs for its applicability in lieu of other existing design methods after its release. Several significant improvements made to the MEPDG include nonlinear temperature effects, bottom-up and top-down transverse cracking prediction, faulting predictions, climatic influences, steer-drive axle spacing, etc. Figure 10 illustrates the MEPDG design framework for rigid pavement, adopted by AASHTO.

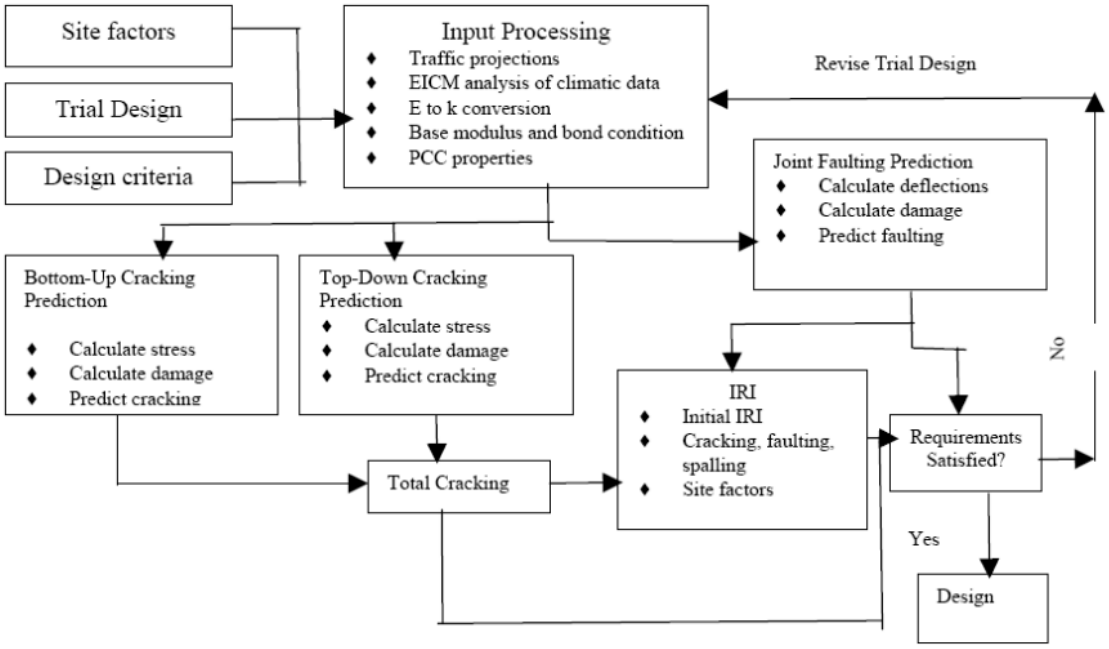

Figure 10. Design framework for JPCP in the MEPDG

AASHTOWare Pavement ME for rigid pavement design employs a detailed representation of the entire load spectra by modeling axle loads mechanistically. The input parameters cover aspects such as traffic composition, climate data, and material properties information. Additionally, it employs an incremental approach to calculate response to loads over discrete time periods and uses the EICM for the climate

model. Different from flexible pavements, a total cracking model, which includes bottom-up cracking and top-down cracking prediction models, and a joint faulting model are used to predict the pavement service life.

2.3.2.4 Long-life Concrete Pavement

As compared to concrete pavements with normal design lives (e.g., 35 years), long-life concrete pavement (LLCP) design requires addressing properly the following issues with special care:

(1) Development of an erosion model for material properties under dynamic wheel loading;
(2) Improved consideration of foundation and subdrainage models;
(3) Subdrain installation in concrete pavement construction;
(4) Feasible pavement strategies and promising features for providing long life for each type of concrete pavement selected; and
(5) Case studies of past long life concrete pavements.

To this end, a more efficiently designed aggregate base/subbase course for specific site conditions is needed to minimize erosion, moisture susceptibility, and frost penetration under traffic and environmental loadings. Also needed is a greatly improved and more comprehensive design procedure to fully consider aggregate base/subbase layer, subgrade, and drainage needs of concrete pavements with related implementation guidelines.

Technical specifications about existing LLCP foundation designs for aggregate base/subbase and/or subgrade material types, thickness design, subsurface drainage, and other special requirements are summarized in Table 4 and Table 5 for domestic and international design practices, respectively. As shown in Table 4, CRCP is mainly used in California, Illinois, and Texas for high-volume and heavy-duty roads. Any of the three common base types, i.e., cement-treated, asphalt-treated, and unbound granular bases, can be chosen for use depending on historical performance and design preferences. Good subsurface drainage was unanimously reported to reduce pumping and erosion-related premature failures due to trapped water and thus resulted in prolonged performance lives.

Table 4. Summary of Long-Life Concrete Pavement (LLCP) foundation designs in the U.S.

State	LLCP Type	Foundation Design	References
California	CRCP JPCP	(a) 4-in. cement-treated (3.5%) base over 8-in. granular; (b) Cement-treated (4%) base over A-2-4 granular subbase; (c) Using either cement- or asphalt-treated base for good drainage properties.	Rao et al. (2006)
Florida	JPCP	(a) Well performing pavements: good subbase drainage; (b) Poorly performing pavements: poor subbase drainage (causing pumping and corner cracks); (c) 4-in. asphalt- / cement-treated permeable base over a stabilized subgrade (asphalt separation layer in between for fines migration prevention); (d) 5-ft. subgrade/embankment composed of special select material meeting AASHTO A-3 soil classification; (e) An edge drain is used in all concrete pavements.	Armaghani and Schmitt (2006)
Illinois	CRCP	(a) Use the 1993 AASHTO Guide; (b) Hot mix asphalt stabilized base; (c) 12-in. aggregate subbase layer (1.5-in. and 8-in. maximum aggregate size of the top 3 in. and the bottom 9 in., respectively).	Winkelman (2006)
Iowa	JPCP	(a) Limited data available about subgrades; (b) Longitudinal cracking is one of the most common distresses for low and medium volume roads; (c) Subgrade failure can cause longitudinal cracking.	Ceylan et al. (2006)
Texas	CRCP	a) 6-in. cement-stabilized base with a 1-in. asphalt layer on top, or 4-in. asphalt-stabilized base; (b) Pumping and erosion of the base caused punchout distress.	Hossain et al. (2006)
Virgina	/	a) Blocked drains caused premature failures even for concrete and materials of high quality; (b) Good pavement condition: no clogged drains; (c) 4-in. AASHTO #57 aggregate bases over 6-in. cement treated soil (10% cement by volume); (d) 4-in. dense-graded base for shoulders; (e) Use edge drains	Hossain and Elfino (2006)

State	LLCP Type	Foundation Design	References
Washington	JPCP	(a) Joint faulting due to poor underlying conditions and lack of dowels; (b) Currently used base layer: 4-in. dense-graded HMA over 4-in. crushed stone; (c) Cemented-treated base caused severe joint faulting, pumping, and cracking; (d) Asphalt-treated base caused minimal joint faulting (which occurred due to stripping because of low asphalt content, i.e., 2.5 to 4.5%); (e) Crushed stone caused faulting (due to fines migration from base and subgrade to the top of base)	Muench et al. (2006)

Several agencies, i.e., FHWA, AASHTO, and NCHRP, sponsored a scanning study to identify design philosophies, material requirements, construction procedures, and maintenance strategies used in Europe and Canada to build long life concrete pavements. The important observations and findings made are summarized in Table 5. Open-graded permeable base layers and high-quality aggregates are used in Canada but not in the European countries visited. Dense-graded hot-mix asphalt, cement-treated base layers, and unstabilized bases are used in several countries. In Germany, an interlayer of either 0.2-in.-thick nonwoven geotextile or dense-graded hot-mix asphalt is used to separate a cement-treated base from the concrete slab. Thick foundations are used for frost protection. These systems are drainable and stable, but not open graded. Recycled materials including asphalt, concrete, and masonry from building demolition are used in the foundations. Sometimes deep, high-quality foundations are used. The unbound granular materials used for concrete pavement subbases in Europe are generally better-quality materials (better graded, better draining although not open graded, and with lower fines content) than the materials typically used as select fill and granular subbase in the United States.

Table 5. Summary of Long-Life Concrete Pavement (LLCP) foundation designs outside the U.S.

Country	LLCP Type	Foundation Design	References
Australia	CRCP JPCP	(a) Typically use CRCP and a design thickness catalog; (b) JPCP de-bonded from base layer to allow for free curling and warping of concrete slab; (c) A lean-mix concrete base with minimum compressive strength of 725 psi at 42 days (no induced joints and limited construction joints); (d) A minimum 12-in. subbase of select material with CBR > 30% after 4-day soak, PI < 12, and compressive strength of 145 psi (top 6-in. subbase is stabilized with 2% hydrated lime if soaked CBR < 30%)	Vorobieff and Moss (2006)
Austria	JPCP	(a) Typical high volume (18-40 million design axle loads) pavement: 10-in. JPCP on 2-in. bituminous interlay over 18- in. unbound base or 8-in. cement-stabilized base; (b) 18- to 20-ft. joint spacing; (c)Two-lift concrete slab with recycled/inexpensive aggregate used in the bottom 8-in. and more wear resistant aggregate in the upper 1.5 in. with an exposed aggregate surface (d) 5-ft. subgrade/embankment composed of special select material meeting AASHTO A-3 soil classification; (e) An edge drain is used in all concrete pavements.	Hall (2007)
Belgium	CRCP	a) Minimal-maintenance in-service life of 30 years and expected life span of 40 to 50 years; (b) 2.4-in. asphalt base over 7.9-in. lean-mix concrete over 7.9- to 31.5-in. sand subbase (over specially compacted 3.3- to 4.9-ft. subgrade); (c) The asphalt base prevents reflective cracking from the subbase; (d) High-strength concrete base, asphalt base course, excellent bond between asphalt layer and upper and lower concrete layers, and high-quality concrete contribute to good performance; (e) Side gutters, sufficient cross slope, thick layer of drainage sand, and drainage pipes on the edge of the shoulder lead to good drainage	Caestecker (2006)

Country	LLCP Type	Foundation Design	References
Canada	JPCP	(a) Standard design in Ontario: doweled JPCP with a 14-ft widened outside lane; (b) Use 1993 AASHTO Guide and Canadian PCA's M-E rigid design method; (c) 4-in asphalt-treated, open-graded drainage base (0.75-in. maximum aggregate size and 1.8% asphalt content); (d) Open-graded cement-treated base as an alternative; (e) JPCP over 6-in. granular base over granular subbase of varying thickness in Quebec for frost heave prevention; (e) 11-in. CRCP over open-graded cement-stabilized base as an alternative in Quebec	Hall (2007)
Germany	JPCP	(a) 8.6- to 13.8-in. JPCP over base and frost protection layers; (b) Use geotextile between concrete slab and cement stabilized bases to de-bond these two layers	Hall (2007)

2.4 Long-life Pavement Design Considerations

Flexible pavement degradation in colder regions can be divided into deterioration mechanisms for asphalt concrete materials, and deterioration mechanisms for unbound layers and subgrade soils (Zubeck & Doré, 2009). The factors affecting AC materials include thermal contraction and fracture, fatigue cracking, rutting, aging, and disintegration from water, salt, and frost. The factors affecting unbound layers and subgrade soils include differential volume change by frost heave and bearing capacity loss during spring thaw.

Zeiada et al. (2019) examinates flexible pavements' performance in colder regions and the effect of different design factors. The researchers utilized data from Long-Term Pavement Performance database for pavements with no maintenance records. Further, IRI data was used as a performance metric. The study concluded that thinner pavements without subsurface drainage exhibited an increased IRI, followed by a sudden decrease, attributed to frost-heave effects causing spikes and dips in the IRI value. Additionally, the research highlighted factors that significantly impacted pavement performance, such as the freezing index, freeze/thaw cycles, wind velocity, relative humidity, and average temperature

2.4.1 Pavement Design Consideration for Frost Impacts

Frost heave significantly contributes to concrete pavement distresses such as slabs cracking, pumping, faulting, instability, settling, non-uniform support, etc. In Minnesota and other cold regions of the world, distresses in concrete pavements associated mainly with frost heaving and thaw weakening can be commonly encountered given the presence of three factors: freezing temperatures, availability of

moisture, and presence of frost-susceptible soils. The pavement failure mechanism associated with freeze-thaw is illustrated in Figure 11 (White et al., 2004).

For flexible pavement design procedures, methods of preventing or minimizing frost damage are briefly reviewed as follows: (1) simply increasing the pavement thickness to account for the damage and loss of support caused by frost action as the AASHTO 1993 Guide implies; (2) reducing the depth of frost-impacted subgrade under the pavement (between the bottom of the pavement structure and frost depth) by extending the pavement sections well into the frost depth; (3) replacing the frost susceptible subgrade with non-frost susceptible material; (4) using an insulation layer between the pavement and subgrade; (5) preventing free water from infiltrating into pavement structures; (6) providing a capillary break in the subgrade water flow path; (7) using alternative insulation materials (saw dust, sand/tire chips mix, extruded Styrofoam) for preventing frost action; (8) using peat layer above the subgrade soils.

The U.S. Army Corps of Engineers (USACE) formulated three frost action mitigation methods: complete protection, which calculates frost penetration depth and employs frost-resistant materials accordingly; limited-subgrade-frost-penetration, which minimizes deformation by restricting frost penetration into the subgrade; and reduced-strength, which reduces the strength of the subgrade material during spring thaw to account for subgrade weakening and ensure conservative pavement designs (Andersland & Anderson, 1978).

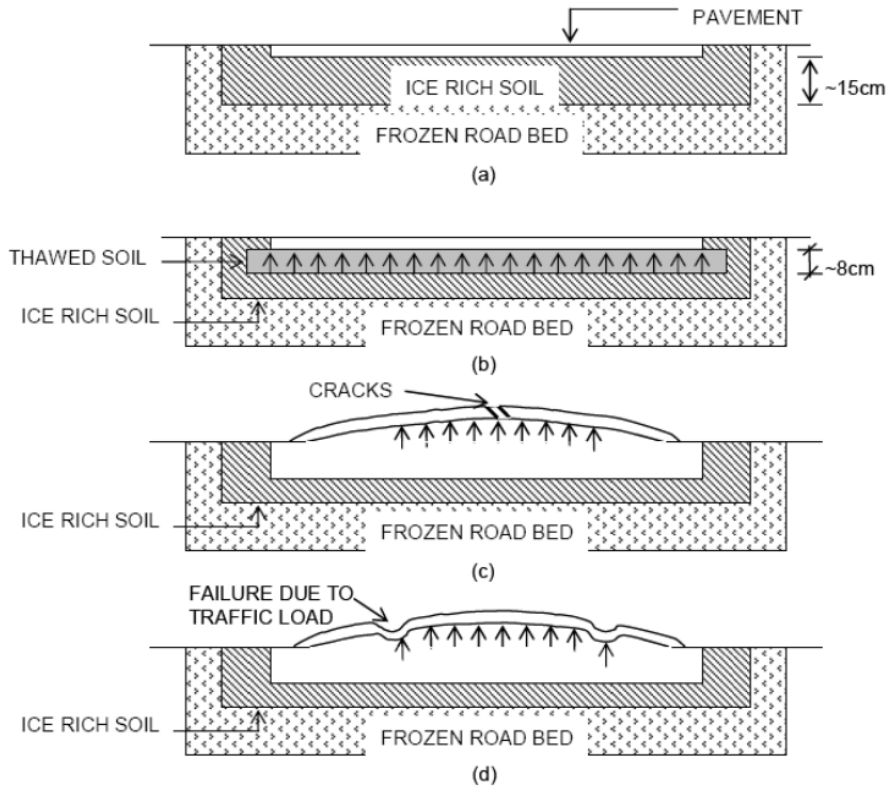

Figure 11. Failure mechanism related to freeze-thaw (White et al., 2004)

2.4.2 Pavement Design Consideration for Drainage

In colder regions such as Minnesota, poor drainage can instigate frost heave, compromising the pavement structure's stability. Huang (2004), emphasized the importance of the drainage layer's placement in a pavement structure for maintaining adequate permeability and strength, with Figure 12 illustrating two possible locations. One option is utilizing the aggregate base course as a drainage layer, meeting strength and permeability criteria. Alternatively, the drainage layer can be added atop the subgrade as an extra layer or incorporated as part of the subbase. Positioning the drainage layer directly beneath the PCC or HMA is preferable to expedite drainage and preclude pumping. Shallow underdrain pipes are highlighted for their effectiveness in enhancing subsurface drainage compared to deeper ones. Huang (2004) underscored the efficacy of merging open-graded aggregate with longitudinal edge drains and discharge pipes in pavement drainage.

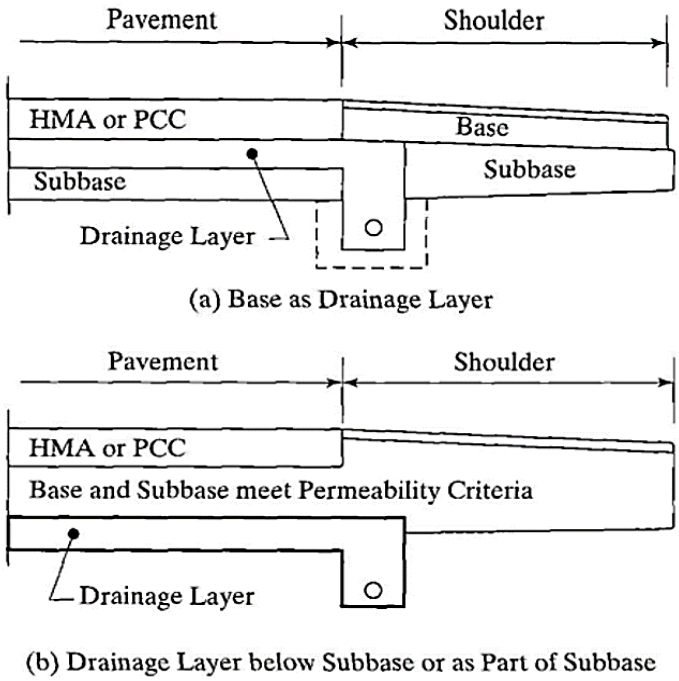

Figure 12. Possible location for drainage layer (Huang, 2004)

In order to mitigate the entry of free water into the subgrade, it is advisable to position the drainage lines at either the bottom or the center of the non-frost-susceptible layer, or alternatively, along the periphery of this layer, as per the guidelines outlined by MacKay et al. (1992). According to Smith (2006), placing the drainage layer above the base course is advisable to facilitate the quick evacuation of melted free water from the pavement structure during Spring thawing period.

2.4.2.1 Incorporating Geosynthetics

Geosynthetic materials used for pavement applications include geotextiles, geogrids, and geocomposites. They are used to improve the engineering properties and/or the constructability of a pavement section Smith (2006).

Geotextile fabrics could significantly contribute to soil stabilization and drainage. Produced from synthetic or natural materials, they separate, filter, reinforce, protect, or drain soils, thus enhancing the durability and efficacy of numerous infrastructure endeavors. Note that a concern for using a geotextile in cold regions is that free water could travel laterally through the geotextile to a freezing section and exacerbate frost damage in the affected area (Shoop & Henry, 1991; Smith, 2006). Wicking geotextiles equipped with specialized hydrophilic and hygroscopic 4DG™ fibers enable suction-driven lateral drainage, can remove water from the soil, which is particularly beneficial in cold regions like Minnesota for mitigating freeze-thaw issues (Wang et al., 2017). These geotextiles efficiently extract water from unsaturated soils in pavement structures as observed by Currey (2016), promoting an increase in soil resilient modulus and enhancing roadway performance. Testing indicates that these geotextiles can draw water from the soil even at moisture levels near optimum and help maintain soil moisture content post-rainfall close to pre-rainfall levels, showcasing an adequate distance for soil moisture reduction.

Geogrids are used for structural improvement and stabilization of aggregate base layers, and could restrain lateral movement of aggregates and alleviate the tension force caused by the swelling of expansive soils. Zornberg and Gupta (2009) investigated the effect of geogrids on mitigating longitudinal cracks caused by swelling subgrade soil. Longitudinal cracks were observed in a field test section without a geogrid after a few months, but no longitudinal cracks appeared in the geogrid-stabilized sections.

2.4.2.2 Use of Insulation Layers

An insulation layer primarily aims to mitigate the detrimental effects of freeze-thaw cycles, thus maintaining structural integrity and extending pavement life in cold regions. Using geofoam insulation could alleviate frost heave challenges and contribute to the structural preservation of roadways and airfield embankments in cold-weather regions (Esch, 1995). Laboratory and field studies in Alaska showed that extruded polystyrene geofoams perform well as insulation layers in airfield and road applications, with expected design lives exceeding 25 years on some occasions (Esch, 1995).

When using geofoams as insulation layers, engineers should mitigate the insulation in the deformation layer as well as the near-surface differential icing by adjusting pavement design. This could be achieved by increasing layer thickness or using stiffer materials above the insulation layer to minimize its deformation and stress levels. Additionally, the insulation layer inhibits the heat flow between the subgrade and the surface layer, which may make the surface of the pavement colder than adjacent sections without insulation layers, causing differential icing on adjacent roadway sections (Li & Haas, 1996). In such an instance, placing a granular layer on top of the insulation layer could reduce differential freeze by acting as a heat reservoir (ibid.).

2.5 Effect of Varying Thicknesses of Aggregate Base and Subbase on Pavement Performance

Pavement design aims to achieve optimal pavement configuration and layer thicknesses considering serviceability, sustainability, and economy. Aggregates constitute 70% to 100% by weight of all bound and unbound pavement layers in road applications and, accordingly, their types and properties significantly affect the end performance (Tutumluer et al., 2013). Using high-quality aggregates is favored to improve pavement performance. However, it brings more cost, especially in regions that lack high-quality aggregate sources.

Alternative cost-effective pavement foundation designs using lower quality aggregates have emerged in the past research. Tutumluer and Barksdale (1995), Jiang et al. (2021) and Ahmed et al. (2021) applied "inverted" pavement design by using a stiff stabilized subbase layer under an unbound aggregate base layer, and it could potentially be used to reduce AC and aggregate base layer thickness. According to observations, when AC thickness exceeds 3.2 in., the predicted number of cycles to fatigue failure are greater than 10 million if aggregate base thickness ranges from 100 mm to 150 mm (4 in. to 6 in.) (Ahmed et al., 2021). In the MnDOT project titled "Effectiveness of geotextiles/geogrids in roadway construction; determine a granular equivalent", thinner aggregate base layers stabilized with geogrids outperformed conventional flexible pavements with thicker aggregate base layers (Alimohammdi et al., 2021).

On the other hand, a reduction in the thickness of granular layers tends to adversely affect pavement performance. To find the optimal pavement designs with a balance between performance and cost, a better understanding of the effect of varying aggregate base/subbase thicknesses is fundamental. Hence, we conducted a comprehensive review of how changing the thickness of aggregate base/subbase layers affects resilient modulus, structural responses, distress and service life, drainage and frost prevention to explore the potential of utilizing alternative cost-effective designs.

2.5.1 Resilient Modulus

Resilient modulus is a key parameter to estimate the strain and stress at critical locations in a mechanistic model during pavement design. Resilient modulus of granular materials and soils is anisotropic, stress-dependent, and varies with traffic loads, layer configurations and climatic conditions. Xiao et al. (2011) and Xiao and Tutumluer (2012) utilized GT-PAVE, a nonlinear finite-element-method-based pavement analysis software, to infer the equivalent resilient modulus values for aggregate base and subbase materials when the AC layer thickness changes as shown in Figure 13. In contrast, the input resilient modulus for aggregate base/subbase materials are the same regardless of thicknesses of AC layers according to MnDOT's pavement design manual, so more accurate predictions of pavement performances can be obtained.

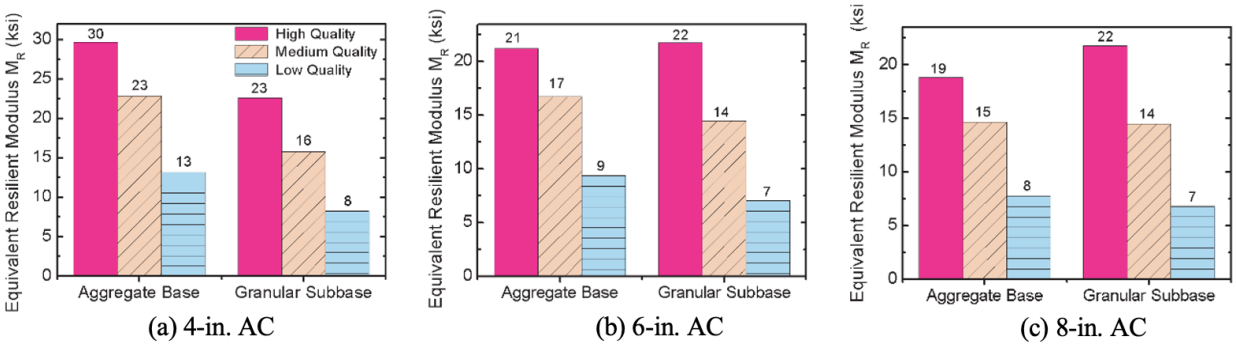

Figure 13. Equivalent resilient modulus linked to aggregate quality for different asphalt surface thicknesses (Xiao & Tutumluer, 2012)

Khazanovich et al. (2006) studied the effect of aggregate base and subbase thickness on the resilient moduli for Minnesota materials based on multi-layer elastic theory. Figure 14(a) shows that increasing aggregate base layer thickness from 10 in. to 20 in. reduces the resilient modulus of the aggregate base layer but slightly increases the resilient modulus of the subgrade layer. However, the subbase resilient modulus is not significantly influenced by aggregate base layer thickness. Figure 14(b) infers that an increase of subbase thickness does not substantially impact the aggregate base and subbase moduli but increases the subgrade modulus at a similar rate. Similar trends were observed in the field for aggregate base layers as illustrated in Figure 15 (Alimohammdi et al., 2021), which shows two unreinforced control sections, and seven test sections stabilized with different types of geogrids. The resilient moduli of the 6-in. aggregate base layers were higher than those for 10-in. aggregate base layers regardless of whether they were reinforced with geogrids.

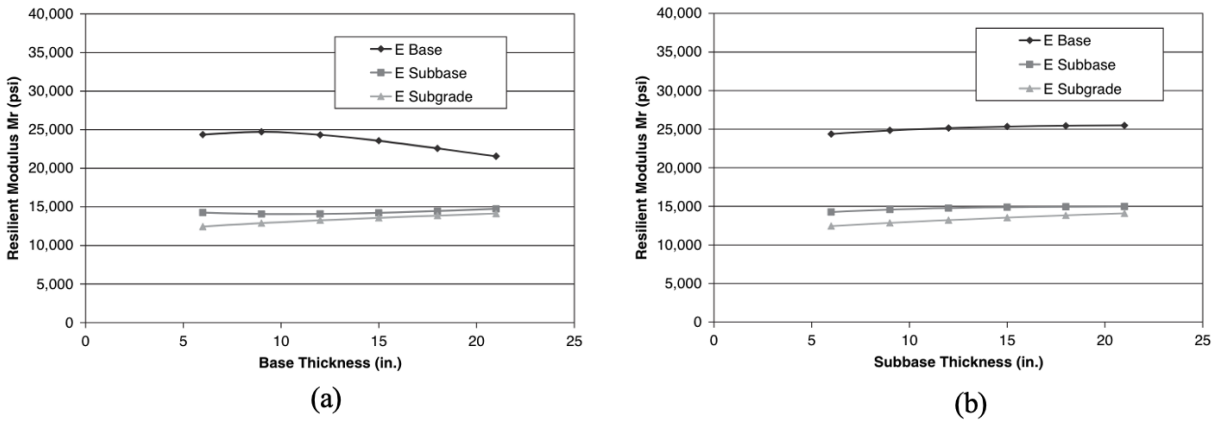

Figure 14. Effect of base and subbase thickness on resilient modulus (Khazanovich et al., 2006)

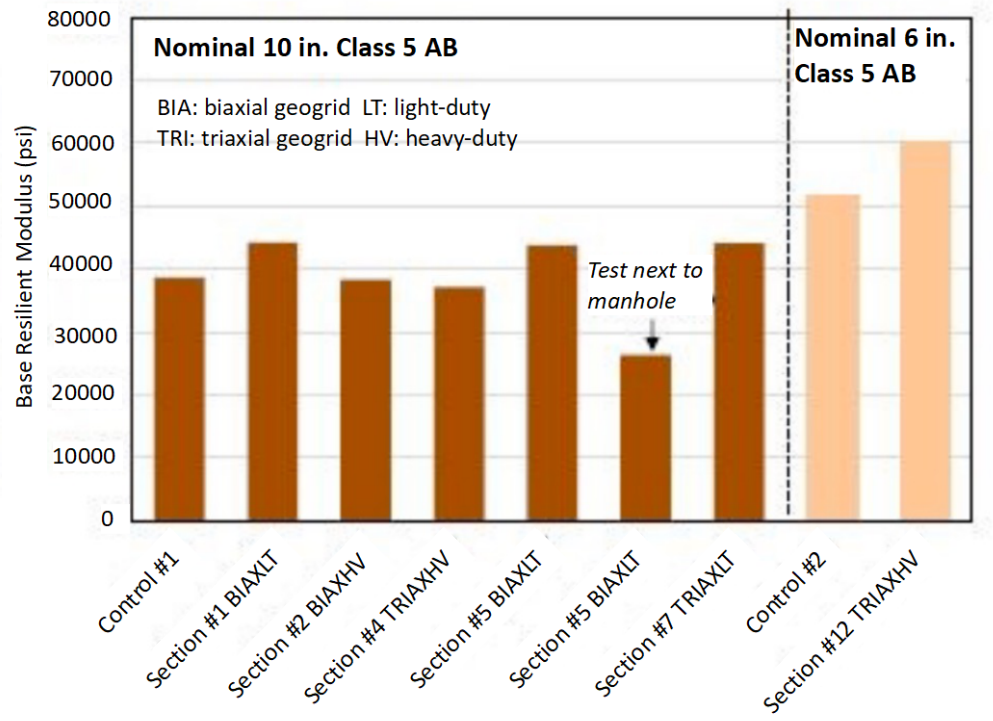

Figure 15. Measured resilient modulus for 10-in. and 6-in. reinforced and unreinforced granular base layers (Alimohammdi et al., 2021)

2.5.2 Pavement Mechanical Responses

Stress and strain are critical mechanical responses that could predict long-term pavement performance such as rutting accumulation for flexible pavement (Chow et al., 2014a; Erlingsson, 2012) and cracking for rigid pavement (Selezneva et al., 2004). Varying aggregate base/subbase thickness could affect the pavement responses at the critical locations, which are directly linked to pavement distress.

As depicted in Figure 16, Shaban et al. (2020) investigated the effect of aggregate base/subbase thickness on the bending stresses in concrete slabs. Varying the thickness of the aggregate base from 150 mm (6 in.) to 500 mm (20 in.) does not substantially influence the bending stresses, while increasing the thickness of the subbase drastically reduced the tensile bending stresses. Additionally, they concluded that increasing the thickness of the subbase did not change the compressive stresses. Thus, subbase thickness is much more critical than aggregate base thickness in terms of the effects on bending stresses in concrete slabs.

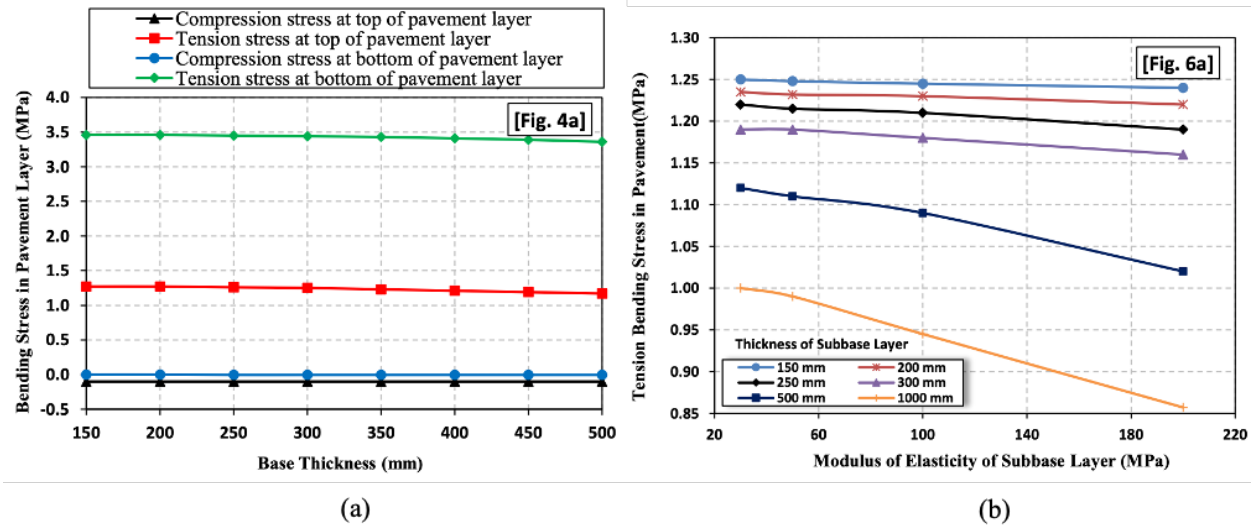

Figure 16. Effect of base and subbase thicknesses on bending stress in concrete slab (Shaban et al., 2020)

On the other hand, for flexible pavements, granular layers play an important role in sustaining and distributing loads. Hadi and Al-Sherrawi (2021) found the stresses on the top of the aggregate base and subbase layers were reduced when the thickness of the aggregate base layer changed from 10 cm to 30 cm in an FEM pavement model. Gopalakrishnan and Tompson (2008) observed from field heavy weight deflectometer (HWD) tests that increasing the thickness of the granular subbase could reduce surface deflections. Then, ILLI-PAVE, an FEM pavement analysis software, was utilized to predict the rutting performance of the field test sections with different subbase thicknesses. As shown in Figure 17, subgrade deviator stresses and strains decrease with increasing subbase thickness. It can be inferred that increasing aggregate base/subbase thickness can relieve the stresses and strains in flexible pavement foundations.

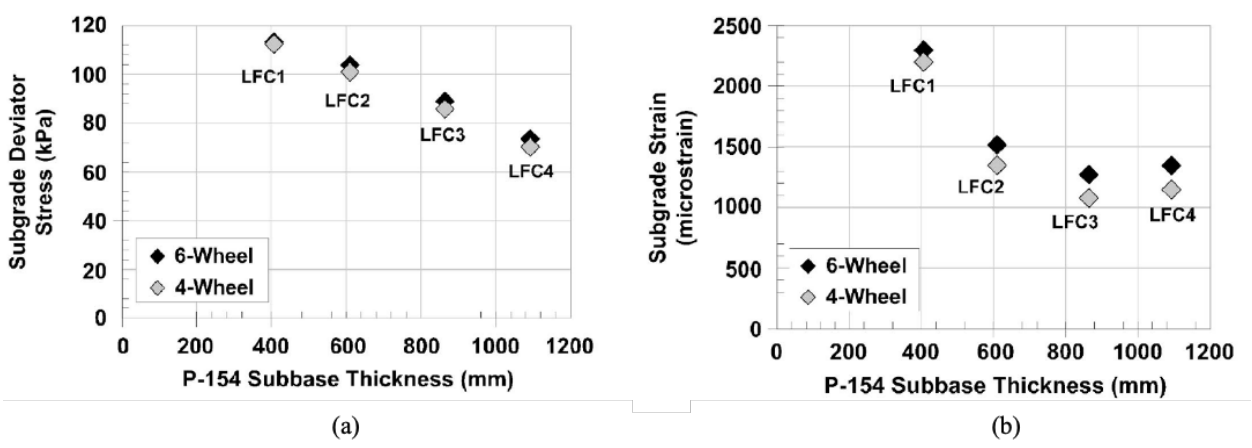

Figure 17. Effect of subbase thickness on subgrade stress and strain in flexible pavement (Gopalakrishnan & Thompson, 2008)

2.5.3 Pavement Distress and Service Life

As mentioned previously, pavement distresses such as rutting, fatigue and cracking are commonly used to predict a pavement's service life. Varying aggregate base/subbase thickness influences pavement structural responses and changes pavement service life.

Rutting and fatigue cracking are major distresses for flexible pavements. Velasquez et al. (2009) studied the effect of layer thickness and materials on distresses of flexible and rigid pavements in Minnesota using the MEPDG models for total rutting, longitudinal cracking, transverse cracking, and alligator cracking. The sensitivity summary of the considered variables is compiled in Table 6 and Table 7 for 1 million and 10 million ESALs, respectively. AC thickness was more sensitive to pavement performance, while aggregate base and subbase thickness had non to low sensitivity to pavement distresses in both traffic scenarios.

Table 6. Sensitivity summary for flexible pavements under 1 million ESALs

Parameter	L. Cracking	T. Cracking	A. Cracking	T. Rutting
Climate	LS	HS	LS	LS
AC thickness	HS	LS	HS	HS
Binder	LS	HS	LS	LS
Gradation	LS	IS	LS	LS
Subbase thickness	LS	IS	LS	LS
Soil	HS	HS	HS	LS

IS = insensitive; LS = low sensitivity; HS = high sensitivity

Table 7. Sensitivity summary for flexible pavements under 10 million ESALs

Parameter	L. Cracking	T. Cracking	A. Cracking	T. Rutting
Climate	IS	HS	LS	LS
AC thickness	HS	HS	HS	HS
Binder	LS	HS	LS	LS
Gradation	LS	IS	LS	LS
Base thickness	IS	IS	IS	IS
Subbase thickness	LS	IS	LS	LS
Soil	HS	HS	HS	LS

IS = insensitive; LS = low sensitivity; HS = high sensitivity

Xiao and Tutumluer (2012) studied the effects of aggregate base/subbase material quality and thickness on fatigue and rutting behaviors of flexible pavements in Minnesota. As shown in Figure 18, using a low-quality aggregate base and a high-quality subbase does not make a significant difference from the use of a high-quality aggregate base and a low-quality subbase. They also found that when low-quality aggregate base materials are used, increasing aggregate base thickness does not improve fatigue life but can significantly extend rutting life. Interestingly, they found that increasing subbase thickness could significantly improve both rutting and fatigue performances. More importantly, rutting performance can benefit more from an increase in subbase thickness than aggregate base thickness. Haider and Chatti

(2009) conducted statistical analysis on field data collected from the long-term performance pavement (LTPP) program and concluded that fatigue cracking was insensitive to aggregate base thickness. The same trend that aggregate base thickness has more impact on rutting than fatigue cracking was also observed by Behiry (2012). Aggregate base reinforcement allows a reduction in aggregate base thickness without sacrificing rutting performances. For example, placing a geogrid at the interface of a 10-in. base and the underlying subgrade layer decreases the required aggregate base thickness by more than 3 in. (Alimohammdi et al., 2021). Note that the benefits from reinforcement such as permanent deformation reduction could be reduced when aggregate base thickness increases (Leng & Gabr, 2002).

For concrete pavements, granular base/subbase course primarily provides uniform support to the concrete slabs. Accordingly, cracking, and joint faulting in the concrete surface are commonly considered for pavement design. According to Velasquez et al.'s study (2009), when the aggregate base thickness in rigid pavements was varied from 6 in. to 48 in., as shown in Figure 19, all cases satisfied the MnDOT's design requirements on cracking and faulting (faulting < 0.25 in.). The other parameters are summarized at the bottom of Figure 19. Note that most variables are near the minimum requirements, such as slab thickness and aggregate base material class, which indicates that the thickness of the aggregate base layer in rigid pavements is not the most critical factor on performance and life span. Tutumluer et al. (2015) investigated the impact of aggregate base material and thickness on rigid pavement distresses in Minnesota as shown in Figure 20. It can be observed that varying aggregate base thickness from 4 in. to 10 in. does not substantially affect the rigid pavement performances including IRI, transverse cracking and joint faulting.

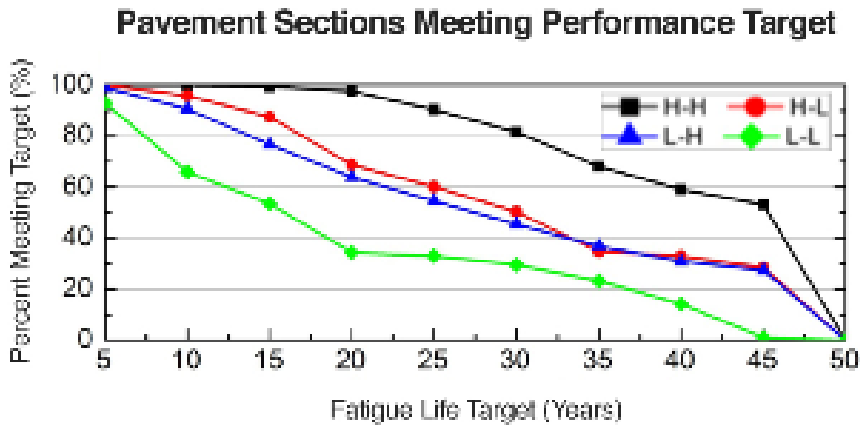

Figure 18. Effect of aggregate base and subbase material quality on fatigue life for Beltrami County, Minnesota, under 1.5 million ESALs (Xiao and Tutumluer, 2012). H-H represents high-quality aggregate base and high-quality subbase; H-L represents high-quality aggregate base and low-quality subbase; L-H represents low-quality aggregate base and high-quality subbase; and L-L represents low-quality aggregate base and low-quality subbase.

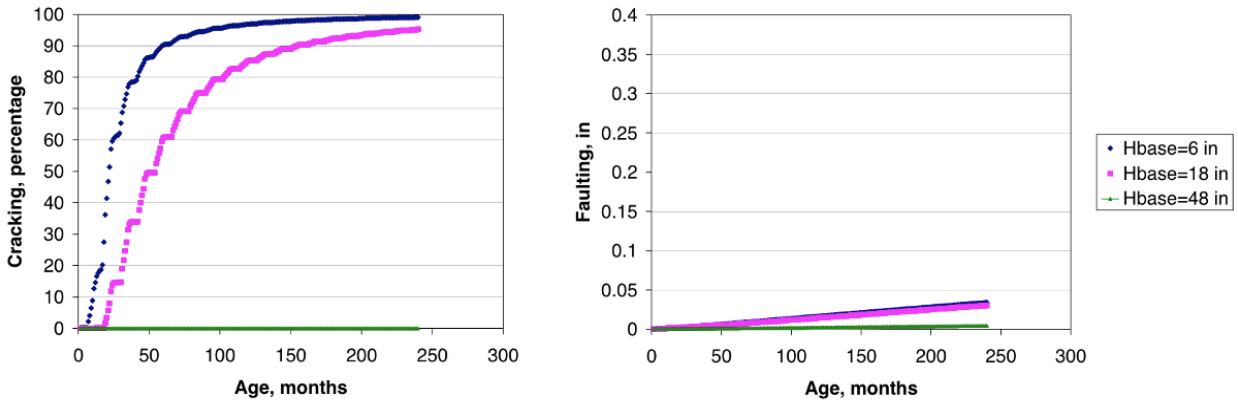

Slab thickness	6 in.	**Base class**	5
Location	Rochester	**Subgrade class**	A-6
AADTT	500	**Joint spacing**	15
Shoulders	Asphalt	**Lane width**	12

Figure 19. Effect of aggregate base thickness on cracking and faulting performances (Velasquez et al., 2009)

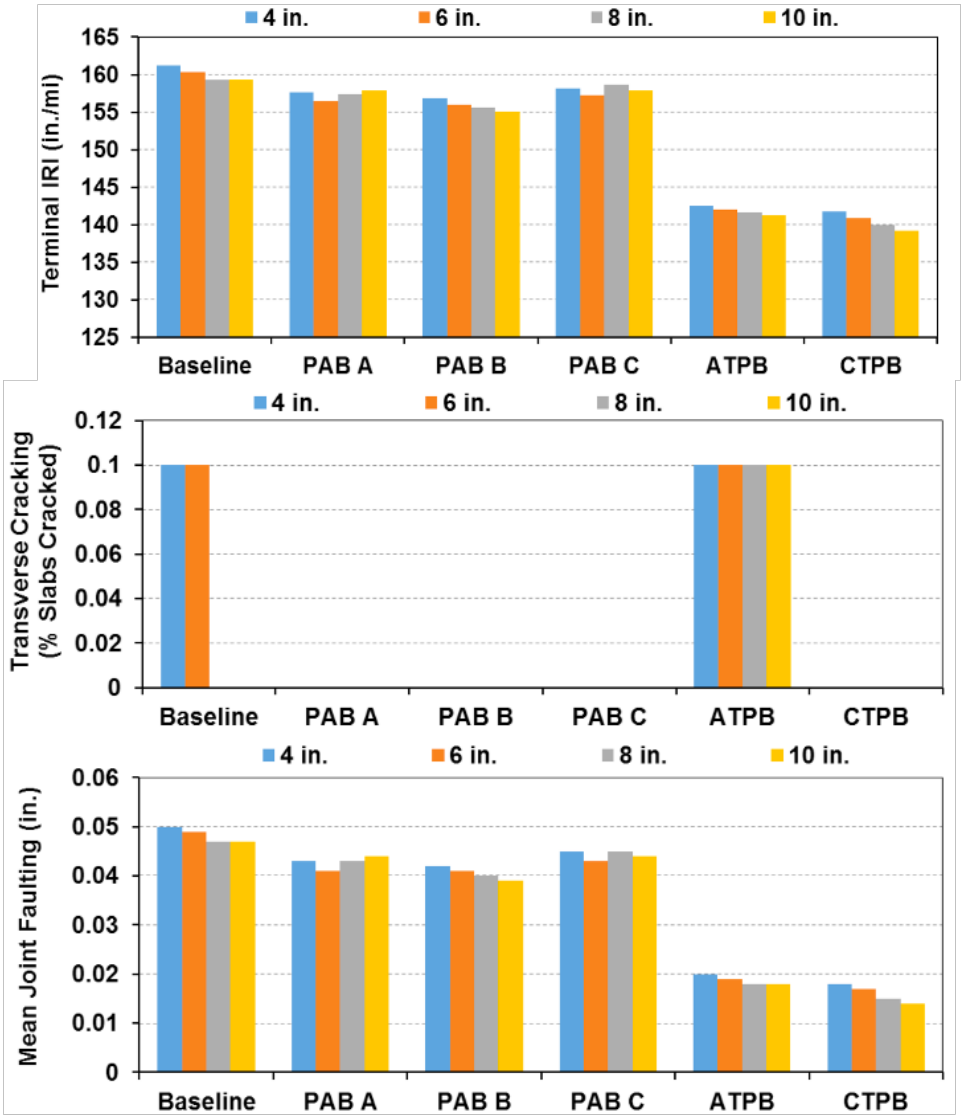

Figure 20. Effect of aggregate base material and thickness on international roughness index (IRI), transverse cracking and joint faulting for rigid pavements (Tutumluer et al., 2015)

2.5.4 Drainage

In the 1993 AASHTO design manual (AASHTO 1993), the empirical design equations considered the drainage effect and increased aggregate base/base thickness for poor drainage conditions. The drainage capacity of granular bases is linked to geometric properties such as aggregate base thickness and slope in the theoretical equations used for estimating time to drain (Barber & Sawyer, 1952; Casagrande & Shannon, 1952; Haider et al., 2014; McEnroe, 1994). These equations indicate the time to drain to 50% moisture decreases when the aggregate base thickness increases. However, Dan et al. (2017) found the layer thickness did not significantly affect the time to drain compared to layer slope and hydraulic

conductivity. As shown in Figure 21, Rabab'ah (2007) simulated drainage of permeable aggregate base layer over time and claimed that the thickness of the permeable aggregate base layer did not impact the drainage efficiency. On the other hand, the drainage performance was sensitive to the material hydraulic properties such as hydraulic conductivity. This observation also aligns with the AASHTO and MnDOT design manuals where only a fixed thickness is recommended for drainable aggregate base layers.

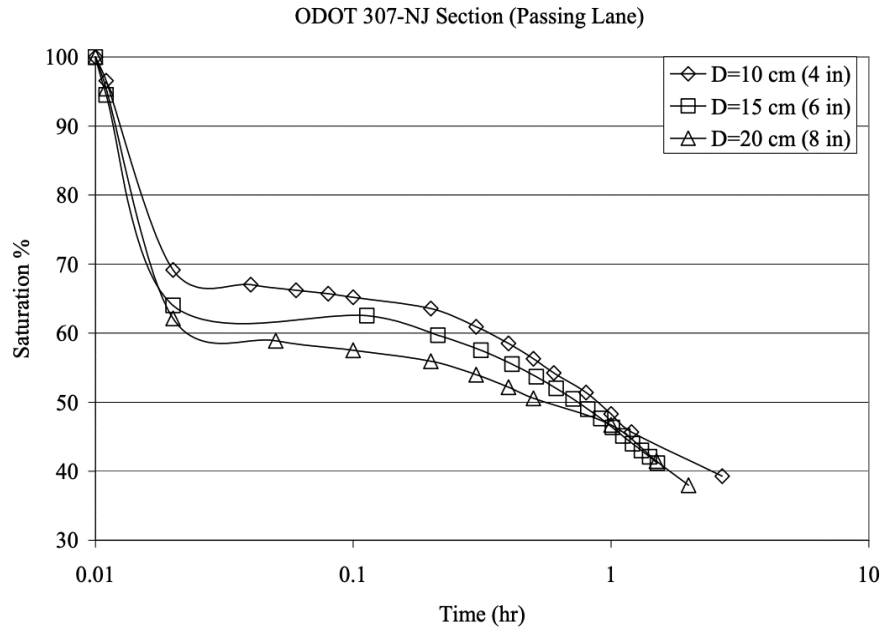

Figure 21. Effect of thickness of permeable base layer on drainage (Rabab'ah, 2007)

2.5.5 Frost Action

Increasing the aggregate's layer thickness theoretically lengthens the path for frost traveling towards the level of water table and mitigates frost heave by preventing moisture from freezing due to frost penetration. Bly et al. (2009) performed statistical analysis on frost heaving data collected from the Minnesota Road Test Research Facility (MnROAD) test sections. The sections were divided into two groups based on total pavement structural thickness (surface course + base + subbase): (1) thinner pavement structures with thicknesses less than 17 in., and (2) thicker pavement structures with thicknesses more than 26 in. It was found that thicker pavements experienced significantly lower magnitudes of frost heave. However, no significant effect of the pavement thickness on uniformity of frost heave was found. Similar results were observed in Oman et al.'s study (2018), in which the change in the IRI from summer to winter of pavements in Minnesota was investigated. The researchers noticed that the pavement performance was improved when the pavement's thickness exceeded 25 in. This might be attributed to the fact that most pavements thinner than 25 in. did not contain a subbase layers, whereas 71% of the thicker pavements (> 25 in.) had a subbase layer. It was recommended to determine the required pavement thickness based on the silt content in the subgrade, as shown in

Figure 22, where the percent frost depth protection is defined as the percentage of required minimum pavement thickness over the predicted frost depth.

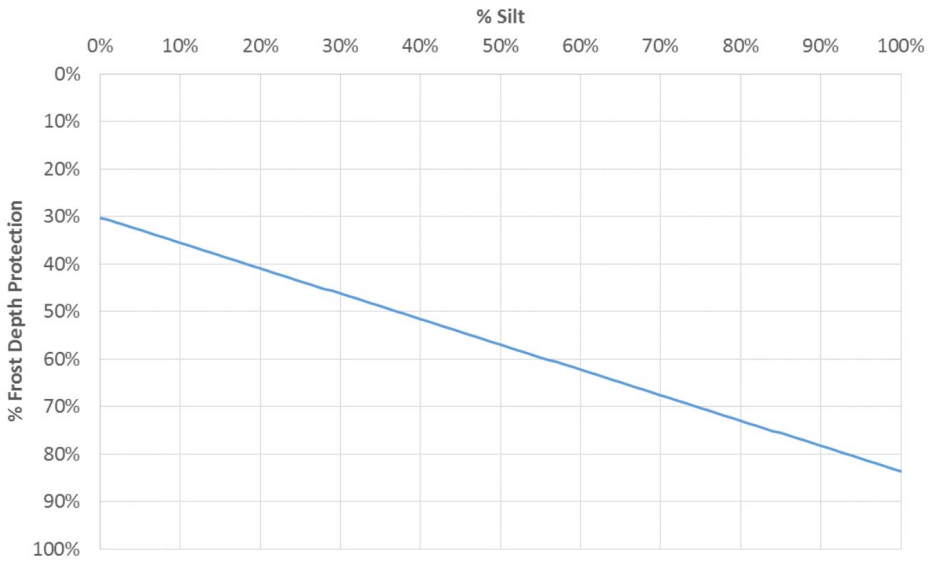

Figure 22. Minimum frost depth treatment based on silt content in subgrade (Oman et al., 2018)

2.6 Summary

This chapter presented a thorough review of national and international literature to evaluate aggregate quality indicators and their impact on pavement performance. Unbound aggregate materials used in aggregate base and subbase layers of flexible and rigid pavements were discussed in relation to how their physical, chemical, and mechanical properties influence structural integrity, durability, drainage, and resistance to traffic and environmental loadings.

This literature review chapter outlined the roles of pavement foundation layers—aggregate base, subbase, and subgrade—and their performance requirements, including load-carrying capacity, permeability, frost resistance, and resistance to pumping as a first phase. It highlighted key aggregate properties such as gradation, fines content, angularity, mineralogy, moisture content, and degree of compaction, linking each to observed pavement distresses like rutting, fatigue cracking, faulting, and frost heave. A detailed discussion of aggregate quality indicators emphasized the importance of shear strength, stiffness, and resilient modulus in maintaining pavement performance. The review further addressed shape and degradation resistance using advanced laboratory and imaging methods, including particle morphology characterization and abrasion testing (e.g., Los Angeles and Micro-Deval tests).

The reviewed literature also connects aggregate properties to performance indicators in both flexible and rigid pavements. For flexible pavements, the focus is on fatigue cracking and rutting, while for rigid pavements, emphasis is placed on cracking, pumping, and faulting. The chapter summarized how aggregate-related parameters like fines type, permeability, and support uniformity critically affect these distresses.

In this chapter we also reviewed existing pavement design methodologies, ranging from empirical (AASHTO 1993) to mechanistic-empirical models (e.g., AASHTOWare Pavement ME), and discussed how design inputs account for aggregate properties. Several state-specific and international design tools were also evaluated, including MnPAVE, EverPave, and FPS21.

Finally, we evaluated the influence of aggregate base and subbase layer thickness on resilient modulus, pavement responses, service life, drainage, and frost protection. Research findings suggest that thicker subbase layers improve performance more significantly than aggregate base layers, especially under harsh environmental conditions. The chapter also highlighted strategies for long-life pavement design in cold regions, emphasizing the importance of drainage systems, insulation, and geosynthetics in mitigating freeze-thaw damage and enhancing structural longevity.

Chapter 3: Establishing Aggregate Index Properties

The main objective of this chapter is to update the existing aggregate database with materials/sources added since 2012 and additional aggregate resource considerations. This chapter categorizes the types, sources, and properties of locally available aggregates. The index property database established in this chapter potentially supports the linkages between aggregate index properties and resilient modulus or strength of the aggregate materials presented in later chapters.

The index database was constructed based on two databases MnDOT provided to the research team at the University of Illinois Urbana-Champaign (UIUC) and Iowa State University (ISU), namely the aggregate source information system (ASIS) and the laboratory information management system (LIMS). An exploratory data analysis was first conducted to determine the needs for refining and processing the data in these two databases. A series of data processing and cleaning activities were performed to construct the aggregate index property (AIP) database. This chapter mainly introduces the procedure adopted in the development of the AIP database.

3.1 Exploratory Analyses of Received Databases

The ASIS and LIMS databases provided by MnDOT were primarily used to develop the AIP database for this project. In this section, a brief overview of the ASIS and LIMS datasets is presented. Observations from the exploratory data analyses conducted on the two databases are introduced, which indicates the need for data processing and cleaning.

3.1.1 ASIS Database

ASIS is a database developed by the MnDOT Office of Materials for storing and retrieving information related to gravel pits, rock quarries, and commercial aggregate sources. It is primarily used by the Aggregate Unit at the Maplewood Lab and by District Materials personnel as a resource for recommending aggregate sources for construction projects. In the ASIS database, each aggregate source is assigned a unique source number with which other information including status classification, material class and quantity, aggregate source properties, and Universal Transverse Mercator (UTM) coordinates, etc. is associated. Table 8 lists part of the aggregate source properties stored in the ASIS database; and a snapshot of the ASIS database in Microsoft Access is shown in Figure 23. In total, there are 8,475 rows in the ASIS database, each corresponding to a unique material source. However, according to the status code as described in Table 9, a total of 2,078 material sources, having status code “I”, are not actively providing materials (the status codes are explained in Table 9). The inactive material sources were not considered in the development of the AIP database. Therefore, data cleaning was needed to remove the inactive sources.

SOURCENUM	STATUS	STATUS2	COUNTY	SEC	TWN	RNG	RDIR	PM	UTM_X	UTM_Y
18144	C		Crow Wing	34	046	29	W	4	424180	5141838
18145	C		Crow Wing	20	138	26	W	5	423970	5178370
18146	C		Crow Wing	19	043	19	W	4	409772	5116624
18147	C		Crow Wing	27	138	28	W	5	407070	5176487
18148	C		Crow Wing	12	045	30	W	4	417177	5138839
19001	C		Dakota	35	115	20	W	5	484944	4952490
19002	C		Dakota	27	115	20	W	5	483977	4953597
19004	C		Dakota	06	114	19	W	5	488400	4950400
19005	C		Dakota	22	115	20	W	5	483986	4955210
19006	I	C	Dakota				W	4		
19007	C		Dakota	35	115	17	W	5	514245	4952099
19008	C		Dakota	26	114	21	W	5	477349	4944178
19009	C		Dakota	36	115	17	W	5	515098	4952751
19010	O		Dakota	05	113	18	W	5	499983	4940365
19011	O		Dakota	20	114	19	W	4	490734	4945926
19012	O		Dakota	29	114	20	W	4	481480	4944094

Record: 35 of 8475 Unfiltered Search

Figure 23. A snapshot of the ASIS database in Microsoft Access

Table 8. Illustrative examples of aggregate source properties stored in the ASIS database

Field Name	Description
PASS3QTR	Percent passing ¾ in. sieve
PASSNUM4	Percent passing # 4 U.S. sieve
PASSNUM10	Percent passing # 10 U.S. sieve
PASSNUM40	Percent passing # 40 U.S. sieve
PASSNUM200	Percent passing # 200 U.S. sieve
SH4LO	Lowest value for % shale @ minus 4 mesh
SH4HI	Highest value for % shale @ minus 4 mesh
MINUS4AVG	Average value for % shale @ minus 4 mesh
MINUS4OF	Number of shale @ minus 4 mesh samples
MS3_2TO1	Magnesium Sulfate (Soundness), Size range 1-1/2 in. to 1 in.
LARLO	Lowest Los Angeles Rattler value
LARHI	Highest Los Angeles Rattler value
LARAVG	Average Los Angeles Rattler value
LAROF	Number of Los Angeles Rattler tests
PCTLIMESTO	Percent limestone
PCTSANDSTO	Percent sandstone
PCTSOFTROC	Percent soft rock
PCTHARDROC	Percent hard rock
TOTALSHALE	Percent total shale by mass
TOTALSPALL	Percent total spall by mass
UCHERT	Percentage of unsound chert
UCHERTOF	Number of unsound chert tests
IOXIDE	Percent iron oxide
IOXIDEOF	Number of iron oxide tests

Table 9. Description of status code

Status	Description
C	Commercial aggregate source
I	Inactive aggregate source
M	Aggregate source owned or managed by MnDOT
P	Pit that was prospected or leased by MnDOT
O	Other aggregate pit
Q	Bedrock quarry
MRC	Former MnDOT aggregate pit that has been reconveyed
MRW	MnDOT owned aggregate pit that is located a highway Right-of-Way

3.1.2 LIMS Database

LIMS database is composed of laboratory test results of one or multiple material samples obtained from some of the material sources. It includes laboratory tests on aggregate gradation, density, chemical composition, shape properties, abrasion, etc. Figure 24 illustrates a part of the LIMS database in Microsoft Access. The material source number, i.e., “pit #”, and “sample id” indicate which material source and sample were used to conduct a specific material test, respectively. The “pit #” is identical to the “SOURCENUM” in the ASIS database, and both are material source identification numbers. Column “descr” describes individual laboratory test results, and Column “test result” registers the corresponding quantities. In total, the LIMS dataset has 2,429,952 rows. Note that the LIMS dataset has more detailed gradation with sieve sizes of 3 in., 2 in., 2.5 in., ¾ in., 5/8 in., 3/8 in., #8, #80, #100, and #200, while the ASIS database considers sieve sizes of ¾ in., #4, #10, #40, and #200 only. Moreover, the sample and test dates were registered in the LIMS database, while the updated dates on the gradation data in the ASIS database are unknown and might be outdated. Therefore, the LIMS database could provide more detailed gradation information compared to the ASIS database.

sample id	result name	descr	test result	field id	pit #	date sample	date received
MT-CA05-1414	gapp_16m	Avg % Pass 5/8"	86	39A 3/4-	19001	7/27/2005	7/28/2005
MT-CA05-1414	gapp_19m	Avg % Pass 3/4"	97	39A 3/4-	19001	7/27/2005	7/28/2005
MT-CA05-1414	gapp_25m	Avg % Pass 1"	100	39A 3/4-	19001	7/27/2005	7/28/2005
MT-CA05-1308	gapp_600	Avg % Pass #30	46	36A=7Q	19001	7/19/2005	7/20/2005
MT-CA05-1308	gapp1_18	Avg % Pass #16	71	36A=7Q	19001	7/19/2005	7/20/2005
MT-CA05-1308	gapp_150	Avg % Pass #100	3	36A=7Q	19001	7/19/2005	7/20/2005
CO-CA05-0472	gapp4_75	Avg % Pass #4	97	36A = 7Q	19001	7/19/2005	7/20/2005
CO-CA05-0503	gapp_600	Avg % Pass #30	50	PROGRESS	19001	7/27/2005	7/28/2005
CO-CA05-0502	gapp_19m	Avg % Pass 3/4"	98	PROGRESS	19001	7/27/2005	7/28/2005
CO-CA05-0502	gapp_25m	Avg % Pass 1"	100	PROGRESS	19001	7/27/2005	7/28/2005
CO-CA05-0502	gapp31_5	Avg % Pass 1-1/4"	100	PROGRESS	19001	7/27/2005	7/28/2005
CO-CA05-0502	gapp4_75	Avg % Pass #4	9	PROGRESS	19001	7/27/2005	7/28/2005
CO-CA05-0502	gapp_9_5	Avg % Pass 3/8"	46	PROGRESS	19001	7/27/2005	7/28/2005
CO-CA05-0502	gapp12_5	Avg % Pass 1/2"	68	PROGRESS	19001	7/27/2005	7/28/2005
MT-CA98-0377	gfinemod	Fineness Modulus	2.9311905176104	5C	19001	4/20/1998	4/21/1998
MT-CA98-0377	gapp_9_5	Avg % Pass 3/8"	100	5C	19001	4/20/1998	4/21/1998
MT-CA05-1247	gapp_075	Avg % Pass #200	0.6	35A	19001	7/13/2005	7/14/2005
CO-CA05-0472	gapp_9_5	Avg % Pass 3/8"	100	36A = 7Q	19001	7/19/2005	7/20/2005
CO-CA05-0538	gpironox	WA Pct Iron Oxide	0.2	9	19001	8/8/2005	8/9/2005
CO-CA05-0472	gapp2_36	Avg % Pass #8	86	36A = 7Q	19001	7/19/2005	7/20/2005
CO-CA05-0472	gapp_2mm	Avg % Pass #10	83	36A = 7Q	19001	7/19/2005	7/20/2005
CO-CA05-0472	gapp1_18	Avg % Pass #16	70	36A = 7Q	19001	7/19/2005	7/20/2005

Record: 1419245 of 2429952 No Filter Search

Figure 24. A snapshot of the LIMS database in Microsoft Access

To develop the AIP database for this chapter, data cleaning and processing were required due to the following observations from the LIMS database:

1. 53% of the rows have empty “pit #.” In addition, some “pit #” values are not valid identification numbers, e.g., “CRANE”. As a result, the material sources of these rows could not be identified.
2. Each row only registers one individual result in a test. For a test with multiple metrics, multiple rows are used to store them. For example, if a gradation test was performed using ten different sieves, ten rows will be used in the LIMS database to store the results for the tested sample. Apparently, the data is not stored efficiently for the development of the AIP database, and some preprocessing activities were required.
3. For a material source, there could be multiple samples evaluated in the laboratory, and those samples could be collected at different times. For example, as highlighted in Figure 24, the material source with “pit #” of 19001 has two samples with “sample id” of “MT-CA98-0377” and “CO-CA05-0472”. The gradation tests for these two samples were conducted in 1998 and 2005, respectively.

The proposed approach to address the issues is as follows:

1. Rows without “pit #” were removed.
2. To better organize the results in the developed AIP database, the LIMS database was pivoted to combine all results of a sample in one row. An example is presented in the next section to show the pivoted table.
3. Because the aggregate gradation from a quarry or a pit might change over time and vary by sampling location, only the three most recent samples based on sampling dates were considered. This approach ensures that up-to-date and accurate information is collected for the developed AIP database.

3.2 Methodology

A similar methodology to the 2012 MnDOT project, titled *Best Value Granular Material for Road Foundations*, was adopted in this project. Figure 25 visualizes the data pipelines adopted in the 2012 and current projects. The 2012 AIP database was developed by merging reliable gradation and UTM data, which were separately provided by MnDOT in 2012 with the ASIS dataset. In this project, the reliable gradations of materials will also be combined with the ASIS dataset, however, they had to be extracted from the LIMS database instead. The provided ASIS dataset already includes UTM data, so no extra UTM dataset was used in this project. In contrast, the current project obtained reliable gradations for 1,118 material sources, whereas the 2012 project included reliable gradations for 118 material sources.

Python, a popular programming language for data processing and analysis, was leveraged in this study. The step-by-step data processing methods to build the AIP database from the ASIS and LIMS databases are presented in this section. The provided raw ASIS and LIMS databases are saved in a ".MDB" format file, which could not be properly accessed using Python. Thus, the two databases were first exported as comma-separated value (.CSV) files using Microsoft Access (a database management software for MDB files) before all data processing.

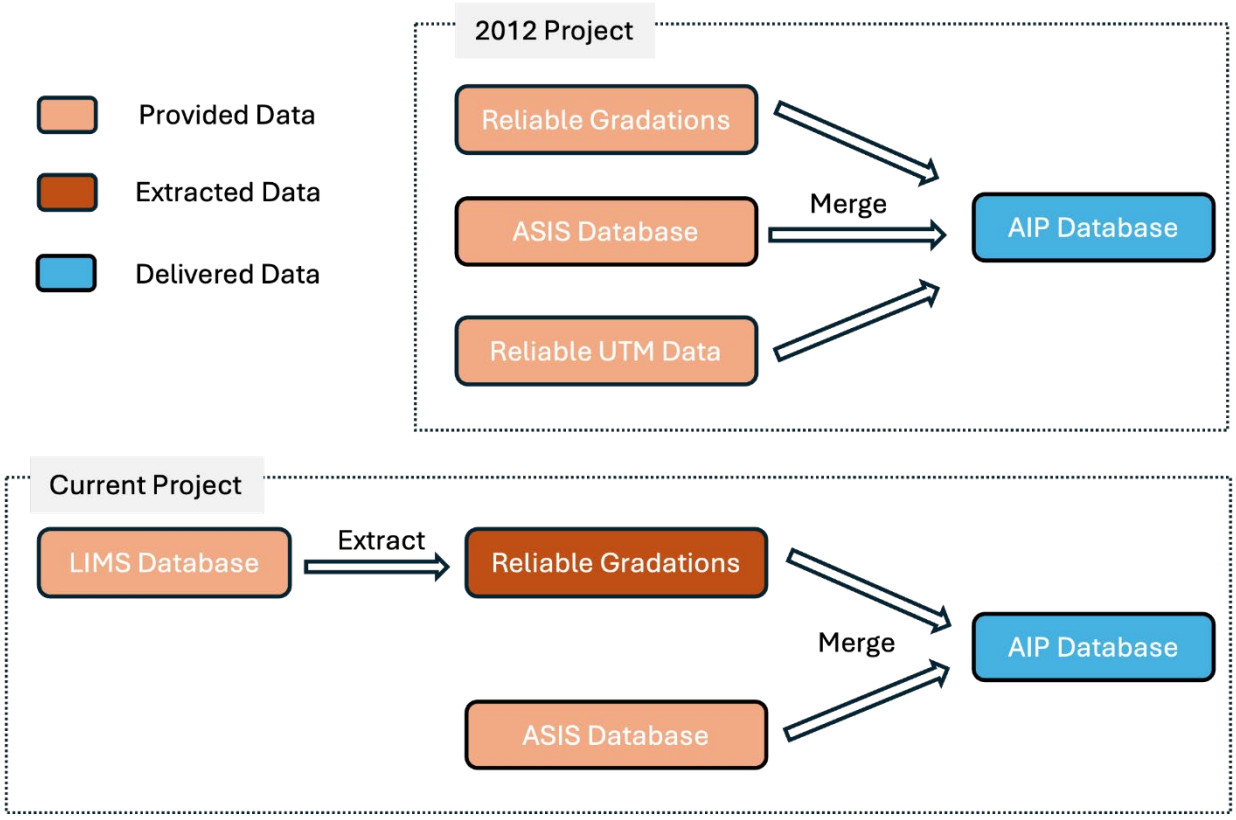

Figure 25. Data pipelines involved in the 2012 study effort and the current project

3.2.1 Step 1: Remove Rows with Empty Material Source Entries in LIMS

As previously mentioned, over half of the rows in the LIMS dataset have empty material source numbers, “pit #”, and thus their corresponding material sources could not be identified. Therefore, in this step, all rows without material source numbers were manually removed in Microsoft Excel. This process was straightforward and easy to perform using the “sort” function in Microsoft Excel. After the removal, 1,023,964 rows with non-empty material source entries remained. This intermediate database includes results for 106,841 unique tested samples from 1,844 unique material sources. Figure 26 shows part of the database after concluding Step 1. Note that some rows still have invalid material source numbers in the column of “pit #”, and they were cleaned in a later step.

	pit #	sample id	date sampled	date received	descr	test result
2	19001	CO-CA09-0290	6/1/09 00:00	6/9/09 00:00	Avg % Pass 3/8"	100
3	19001	CO-CA09-0290	6/1/09 00:00	6/9/09 00:00	Avg % Pass #4	99
4	19001	CO-CA09-0290	6/1/09 00:00	6/9/09 00:00	Avg % Pass #8	92
5	19001	CO-CA09-0290	6/1/09 00:00	6/9/09 00:00	Avg % Pass #10	90
6	19001	CO-CA09-0290	6/1/09 00:00	6/9/09 00:00	Avg % Pass #16	79
7	AMRL	07-BA08-0080	9/1/08 00:00	9/15/08 00:00	Avg % Pass #100	
8	AMRL	07-BA08-0080	9/1/08 00:00	9/15/08 00:00	Percent -#200 Lab	4.08831455
9	AMRL	07-BA08-0080	9/1/08 00:00	9/15/08 00:00	Avg % Pass #200	
10	AMRL	07-BA08-0080	9/1/08 00:00	9/15/08 00:00	Avg % Pass #8	
11	AMRL	07-BA08-0080	9/1/08 00:00	9/15/08 00:00	Avg % Pass 1/2"	63
12	AMRL	07-BA08-0080	9/1/08 00:00	9/15/08 00:00	Avg % Pass 1/4"	
13	AMRL	07-GS00-0072	10/1/00 00:00	10/15/00 00:00	Avg % Pass #4	0
14	AMRL	07-GS00-0073	10/1/00 00:00	10/15/00 00:00	Avg % Pass 3/8"	11
15	AMRL	07-GS00-0073	10/1/00 00:00	10/15/00 00:00	Pct Absorption- Avg	0.23950444
16	AMRL	07-GS00-0073	10/1/00 00:00	10/15/00 00:00	LAR B - Pct Loss	20.7
17	AMRL	07-GS00-0073	10/1/00 00:00	10/15/00 00:00	Pct Lost 3/4" - 1/2"	0.69162532

Figure 26. A snapshot of the reduced LIMS database after Step 1

3.2.2 Step 2: Construct Laboratory Test Results Database

As shown in Figure 26, each row of the database corresponds to only an individual metric of a test. To better organize the results, the database was pivoted to add columns for all test metrics in “descr” such that all the test results of a sample could be combined in one row. As shown in Figure 27, new columns such as “Avg % Pass 3/8” were added from Column “descry.” In this manner, all information for a sample of a material source only occupies one row. After Step 2, the number of rows was reduced to 16,850 rows.

	pit #	sample id	date sampled	date received	Avg % Pass 3"	Avg % Pass 2-1/2"	Avg % Pass 2"	Avg % Pass 1-1/2"	Avg % Pass 1-1/4"	Avg % Pass 1"	Avg % Pass 3/4"	Avg % Pass 5/8"	Avg % Pass 1/2"	Avg % Pass 3/8"
2	19001	CO-CA09-0289	6/1/09 00:00	6/9/09 00:00					100	100	95	83	60	37
3	19001	CO-CA09-0290	6/1/09 00:00	6/9/09 00:00										100
4	19001	CO-CA09-0328	6/16/09 00:00	6/17/09 00:00										100
5	19001	CO-CA09-0336	6/16/09 00:00	6/19/09 00:00					100	100	97	85	64	42
6	19001	CO-CA09-0363	6/19/09 00:00	6/23/09 00:00						100	100	100	100	100
7	19001	CO-CA09-0364	6/19/09 00:00	6/23/09 00:00						100	100	100	100	100
8	19001	CO-CA09-0367	6/23/09 00:00	6/24/09 00:00			100	100	82	47	15	5	3	3
9	19001	CO-CA09-0368	6/23/09 00:00	6/24/09 00:00					100	100	94	80	57	34
10	19001	CO-CA09-0420	7/1/09 00:00	7/9/09 00:00					100	100	97	82	56	34
11	19001	CO-CA09-0421	7/1/09 00:00	7/9/09 00:00										100
12	19001	CO-CA09-0499	7/23/09 00:00	7/27/09 00:00					100	100	96	86	64	41
13	19001	CO-CA09-0719	9/3/09 00:00	9/8/09 00:00			100	99	80	43	10		3	2
14	19001	CO-CA09-0720	9/3/09 00:00	9/8/09 00:00			100	100	100	100	100	100	100	100
15	19001	CO-CA09-0721	9/3/09 00:00	9/8/09 00:00			100	100	100	100	94	81	51	27
16	19001	CO-CA09-0722	9/3/09 00:00	9/8/09 00:00			100	100	100	100	100	100	100	100
17	19001	CO-CA09-0764	9/11/09 00:00	9/15/09 00:00			100	98	83	46	10		2	1

Figure 27. A snapshot of the pivoted database after concluding Step 2

3.2.3 Step 3: Clean Up and Filter Data

In this step, three filters were sequentially applied to remove rows with (1) invalid dates, (2) missing gradation data, and (3) invalid pit numbers. The material sampling dates in the database ranged from 1997 to 2023. As mentioned earlier, the final AIP database would include the three latest gradation test results for a material source, so it is necessary to clean the rows without valid dates. Specifically, rows with sampling and receiving dates later than February 2023 were filtered out. It was found that some rows did not record any gradation data for all the sieve sizes. Since aggregate gradation is the key index property considered in this project, the rows without any gradation data were also removed. In addition, the invalid pit number, for example “AMRL” shown in Figure 26, was handled. According to the ASIS database, the valid material source numbers are integers greater than 1,000. Therefore, only rows with integer numbers greater than 1,000 were collected in this step. The number of remaining rows after each filter is summarized in Table 10.

Table 10. Number of rows after data cleaning

Process	Number of rows after process
Before filtering	106,850
Invalid dates	100,432
Missing gradation data	91,460
Invalid pit number	90,828

3.2.4 Step 4: Retrieve the Three Most Recent Results for Each Material Source

The AIP database is expected to have reliable and up-to-date gradation data. The materials from a source were sampled and tested in a large time window from 1997 to 2023. The gradation might not be consistent over time. In addition, the sample gradation is dependent on the sampling location and methods in a pit or quarry. To guarantee the AIP database has representative and up-to-date gradation information, up to the three most recent results for each material source were collected. Figure 28 illustrates part of the database after Step 4. Among the materials displayed, Material 1036 and Material 1092 have results from only one sample, while the others have results from three samples. This is because only one sample was recorded in LIMS database for Materials 1036 and 1092. Table 11 tabulates the number of material sources having results from three, two and one samples after this step was concluded.

	pit #	sample id	date sampled	date received	Avg % Pass 3"	Avg % Pass 2-1/2"	Avg % Pass 2"	Avg % Pass 1-1/2"	Avg % Pass 1-1/4"	Avg % Pass 1"	Avg % Pass 3/4"	Avg % Pass 5/8"	Avg % Pass 1/2"
2	1013	01-GS09-0085	6/23/09	6/26/09				100	98.7	95.7	93.5	91.1	88.3
3	1013	01-GS07-0179	10/9/07	10/10/07						100	92.7	88.1	81.6
4	1013	01-GS07-0180	10/9/07	10/10/07						100	95	90.3	84
5	1036	3A-GS13-0001	3/29/13	4/23/13						100	97	94	91
6	1039	01-GS09-0172	8/5/09	8/12/09						100	94.1	88.6	80.3
7	1039	01-GS09-0161	8/4/09	8/5/09									
8	1039	01-GS05-0080	7/12/05	7/12/05			100	97.6	96.1	94.6	93	91.3	88.9
9	1092	01-GS05-0207	9/20/05	9/23/05						100	99.3	96.6	92.5
10	1115	01-GS09-0164	8/8/09	8/10/09						100	97	92	83
11	1115	01-GS09-0166	8/8/09	8/10/09					100	100	97	93	85
12	1115	01-GS09-0188	8/8/09	8/14/09				100	99	98.6	93.6	88.8	80.7
13	1136	CO-CA13-0001	12/12/12	1/4/13									
14	1136	3A-CA12-0063	7/31/12	8/7/12									
15	1136	3A-CA12-0038	7/2/12	7/3/12									

Figure 28. A snapshot of the database after Step 4

Table 11. Number of rows after data cleaning

Material source	Frequency
With 3 samples	578
With 2 samples	175
With 1 sample	365
Total	**1,118**

3.2.5 Step 5: Merge Gradation Data into ASIS Database

The inactive materials in the ASIS database were assigned a status code “I.” The rows for inactive materials were first removed from the ASIS database before adding the gradation information obtained from the previous steps. Then, the reliable gradation data of 1,118 material sources were joined into the ASIS database based on the material source number to produce the final AIP database. Figure 29 shows part of the developed AIP database. To distinguish the reliable gradation data from the LIMS database from the original gradations in the ASIS database, a prefix of “LIMS-” was added to the column names of the joined gradation data from the LIMS database. The Column “SAM_ID” represents the sample identification number assigned in the LIMS database. The materials that do not have gradation test records in the LIMS database have empty “SAM_ID” and LIMS gradation.

All Aggregate Sources - Aggregate Sources

SOURCENUM	SAM_ID	STATUS	STATUS2	COUNTY	LIMS-Avg % Pass 3"	LIMS-Avg % Pass 2-1/2"	LIMS-Avg % Pass 2"	LIMS-Avg % Pass 1-1/2"	LIMS-Avg % Pass 1-1/4"	LIMS-Avg % Pass 1"	LIMS-Avg % Pass 3/4"	LIMS-Avg % Pass 5/8"	LIMS-Avg % Pass 1/2"	LIMS-Avg % Pass 3/8"
3082	02-CA08-0002	C	P	Becker						100	90	80	65	46
4120	02-CA14-0051	C	P	Beltrami						100	95	84	62	46
4120	04-CA14-0114	C	P	Beltrami						100	96	83	65	47
4120	04-CA14-0115	C	P	Beltrami										100
4134	02-GS05-0019	C	P	Beltrami						100				
4134	02-GS05-0021	C	P	Beltrami						100	99.8	97.9	91.8	82.3
4134	02-GS05-0041	C	P	Beltrami							100	99.7	96.6	92
5012	3A-GS13-0039	C	P	Benton						100	98.1			80.8
6037	04-GS02-0065	C	P	Big Stone						100	100	97	89	81
6037	04-GS02-0067	C	P	Big Stone							100	99	95	89
6037	04-GS11-0067	C	P	Big Stone						100	99.9	97.8	90.4	83.4
14010	04-GS11-0020	C	P	Clay						100	100	100	100	99.6
14010	04-GS11-0021	C	P	Clay						100	96.3	92.3	85.6	79.3
14010	04-GS12-0002	C	P	Clay							100	98.8	93.6	88
26065	04-GS06-0002	C	P	Grant						100	99.4	97.9	94.1	89
29015	3A-BA07-0213	C	P	Hubbard							100		81	
45070	02-GS11-0068	C	P	Marshall						100	94.2	90	85	80
49104	3A-GS06-0003	C	P	Morrison						100	96	92	88	84
49104	3A-GS10-0005	C	P	Morrison						100	96.5	92.4	87.5	82.7
57048	02-GS11-0102	C	P	Pennington							100	98.6	94.8	90.9
16069	01-PS06-0012	P		Cook		100	93	90	87	84	82	80	78	76
16069	01-PS06-0013	P		Cook	100	95	95	93	92	90	88	86	84	81
16069	01-PS06-0014	P		Cook	86	86	77	71	67	64	60	58	56	53
17075	8A-BA14-0099	Q		Cottonwood									100	100
17075	8A-BA14-0102	Q		Cottonwood									100	100
17075	8A-BA14-0104	Q		Cottonwood									100	100
17077	07-GS10-0027	O		Cottonwood			100		98.8	98.5	96.8	96	94.4	92.4
18002	3A-CA98-0038	C		Crow Wing						100	96.19834711	83.71900826	66.90082645	45.82644628
18002	3A-CA98-0046	C		Crow Wing						100	95.59378934	73.89844734	42.25765841	16.86949224
18061	3A-BA13-0065	P		Crow Wing							100	100	58	8
18099	3B-PS10-0029	M		Crow Wing			100	98	97	96	92	89	86	82
18099	3B-PS10-0030	M		Crow Wing	95	95	95	94	93	91	89	88	86	84
18099	3B-PS10-0031	M		Crow Wing						100	100	100	99	99
18104	3A-PS12-0023	M		Crow Wing		100	98	95	92	91	89	85	80	75
18104	3A-PS12-0024	M		Crow Wing			100	99	98	97	96	94	93	91
18104	3A-PS12-0025	M		Crow Wing		100	97	94	92	89	86	83	79	74
18119	3A-CA11-0015	C		Crow Wing										100
18126	3A-CA05-0063	C		Crow Wing				100	93	45	3	1	1	1
18126	3A-CA05-0064	C		Crow Wing						100	86	67	46	28
18126	3A-GS08-0002	C		Crow Wing						100	92.9	87.3	81.1	74.7
18128	3A-GS12-0037	C		Crow Wing						100	98	93	87.5	82.6
18128	3A-GS12-0038	C		Crow Wing				100	99.3	98.8	93	86.5	79.3	73.1

Figure 29. A snapshot of the AIP database

3.3 Summary

An AIP database was established based on the provided ASIS and the LIMS databases. According to the initial data exploratory analysis on ASIS and LIMS databases, the need for data cleaning and preprocessing was identified as follows:

- ASIS database includes inactive material sources that would not be considered in the AIP database.
- LIMS database has a large amount of missing and invalid material identification numbers, which prevented the testing results from being linked to material sources. Invalid sampling and testing dates occur in some rows. In addition, the data is stored inefficiently in the LIMS database.

After necessary processing, the AIP database was developed by merging the three latest gradations of 1,118 material sources with the ASIS database. The AIP database is intended for linking the aggregate index properties with the pavement analysis and design inputs, e.g., resilient modulus and strength properties, in the next chapter.

Chapter 4: Establishing Linkages between Aggregate Properties and Pavement Design Inputs Using Aggregate Property Data

The main objectives of this chapter are to improve the previously developed relationships between aggregate properties and pavement design inputs, and to develop a new prediction model that will achieve better accuracy and suitability for use with the up-to-date AIP database compiled in Chapter 3. The developed model will support the evaluation and selection of materials for later chapters, which will investigate the effects of pavement design inputs on pavement performance. This chapter also compiles and updates the cost information for aggregate materials in Minnesota to supplement the aggregate source database.

To achieve the chapter objectives, the resilient modulus (M_R) and strength characteristics of the aggregates will need to be evaluated using the prediction model established based on the linkages between source properties and pavement design inputs. A multilinear regression (MLR) model was first developed by incorporating many of the identified aggregate properties in the new database. An artificial neural network (ANN) model was then developed and coded in Python language to enhance the accuracy of the statistically derived model. As a result of its superior performance, the ANN model was then used to predict the resilient modulus and strength characteristics of the aggregates given in the AIP database for different qualities of aggregates represented by material properties. Additionally, the AIP database listed aggregate materials were further evaluated for their permeability and water-retention characteristics.

4.1 Cost Information of Local Materials

Historical bidding information was received by the research team to estimate the costs of aggregate materials produced from across Minnesota. The historical bid prices database includes item descriptions, project numbers (SP numbers), letting dates, quantities, awarded prices, construction locations, contract IDs, construction counties, and construction districts, covering the past five years until June 12, 2024. Due to the lack of precise information on the locations of aggregate sources from which the aggregate materials were transported from to the construction sites, all locally available aggregates were assumed to be sourced from the same county where the construction took place. Because the awarded bid price combines raw-material, hauling, placement, and contractor overhead costs, it provides only an indirect proxy for the true unit cost of each aggregate quality tier.

Figure 30a summarizes the construction costs for subbase materials (Class 3 and Class 4) while Figure 30b and Figure 30c summarize the construction costs for Class 5 and Class 6 aggregate base materials, respectively. Please note that these costs include material and transportation costs. Therefore, for Class 5 aggregate base aggregate costs, even though Sibley County and Nicollet County are geologically close, the material costs in these counties differ.

Figure 30 Aggregate cost information obtained from MnDOT (MnDOT, 2024) related to a) Class 3/4 and Class 3/4 modified aggregates, b) Class 5 and Class 5 modified aggregates and c) Class 6 and Class 6 modified aggregates

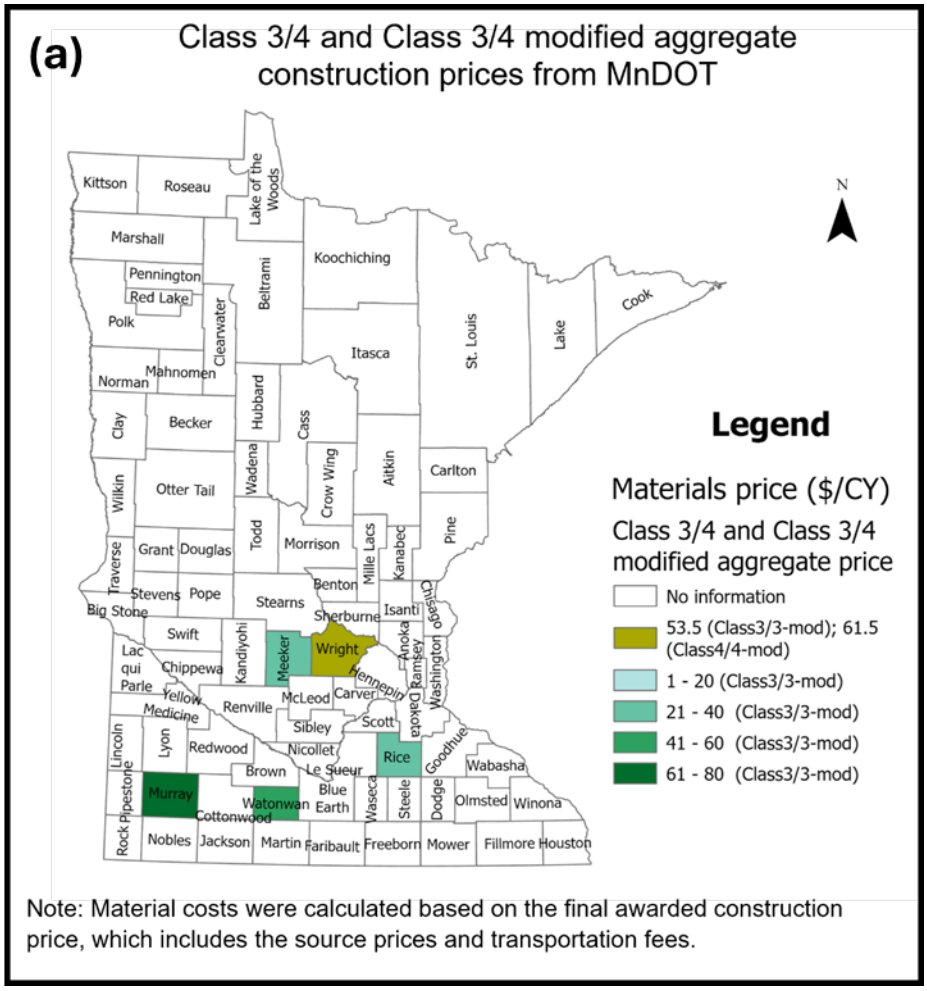

Note: Material costs were calculated based on the final awarded construction price, which includes the source prices and transportation fees.

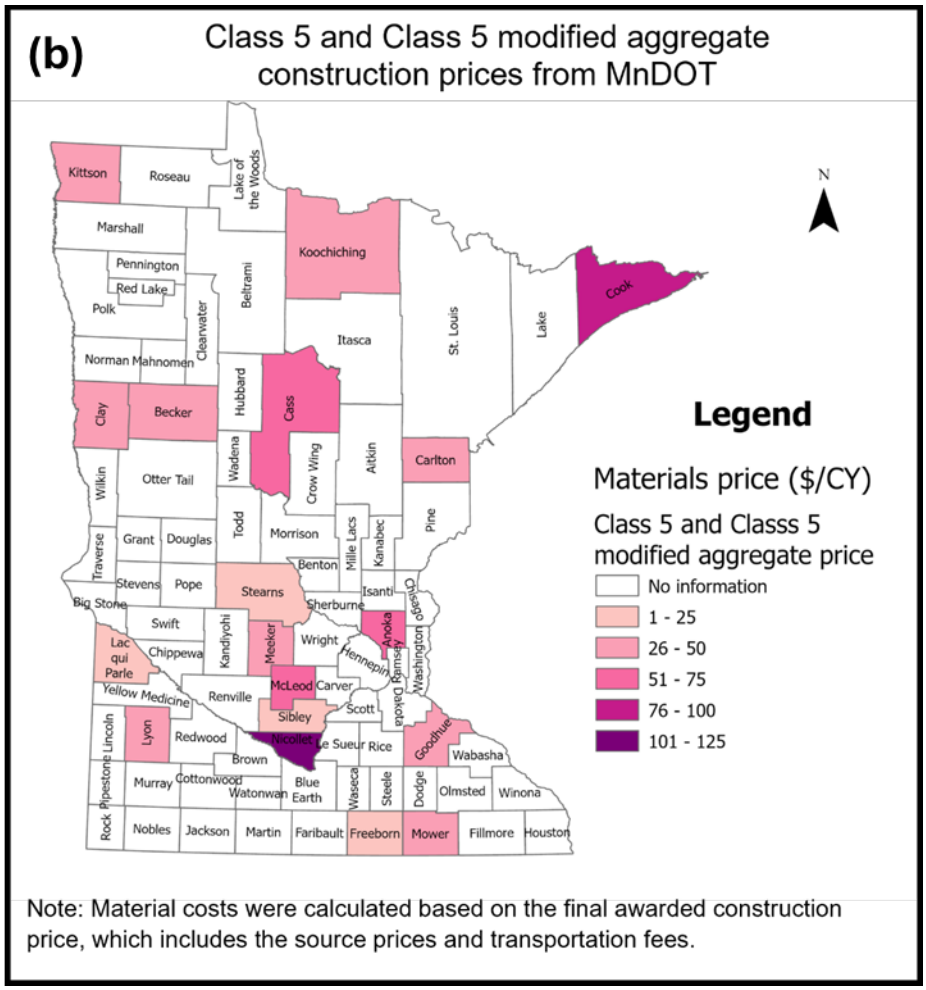

Note: Material costs were calculated based on the final awarded construction price, which includes the source prices and transportation fees.

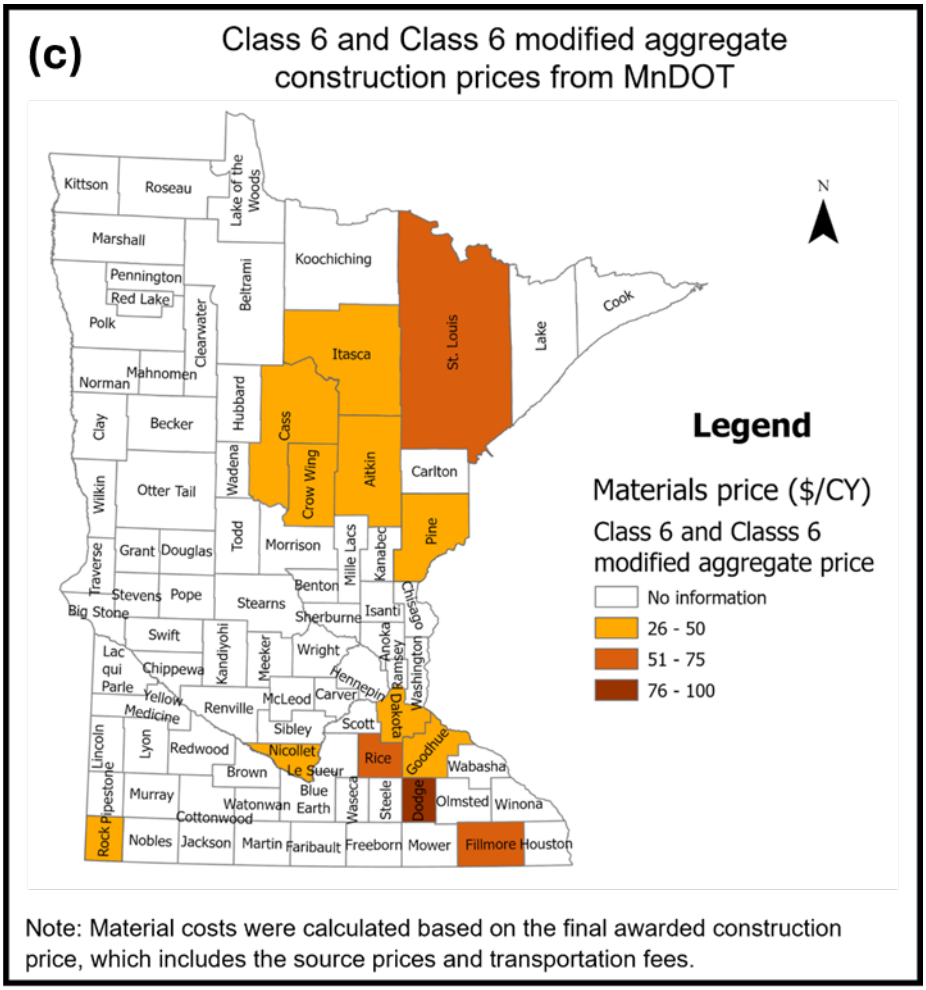

Note: Material costs were calculated based on the final awarded construction price, which includes the source prices and transportation fees.

4.2 Establishing Linkages Between AIPs and Pavement Design Inputs

To evaluate different pavement design alternatives associated with critical pavement responses, it is essential to obtain design inputs based on reliable relationships established between aggregate properties and constructed aggregate layer strength and modulus characteristics. This section aims to enhance the existing regression correlation between aggregate source properties and aggregate mechanical characteristics, as established in the MN/RC 2012-01 project (Xiao & Tutumluer, 2012). Additionally, a new ANN model is developed to provide a more accurate and effective means to account for aggregate qualities influencing pavement design and performance through MnPAVE analyses.

4.2.1 Existing Aggregate M_R Database

The database used for the model development included aggregate source properties, along with their corresponding aggregate M_R and shear strength characteristics collected from the previous MN/RC 2012-01 project (Xiao & Tutumluer, 2012) and MnDOT. This was due to the lack of additional M_R testing completed and added to the MnROAD mechanical property database since 2011. In accordance, the research efforts were limited to those aggregate sources for which strength and modulus data existed.

The database contained 376 aggregate specimens of unbound aggregate base and subbase materials from Classes 3, 4, 5, and 6. Note that Class 7 and unclassified materials were not included in the established new database.

The previous MN/RC 2012-01 project found aggregate shape properties, in addition to aggregate sizes or gradations, as important factors influencing the M_R and permanent deformation behavior of aggregates (Pan et al., 2005a-b; Tutumluer & Pan, 2008). To account for this, nine aggregate samples received from Minnesota were scanned to determine three shape indices—F&E ratio, Angularity Index (AI), and Surface Texture (ST)—using the University of Illinois Aggregate Image Analyzer (UIAIA) (Tutumluer et al., 2000; Rao, 2001). The determined shape properties were then assigned to 91 samples from consistent sources, based on the MN/RC 2012-01 project's assumption that the tested samples adequately represented those aggregate sources from which they were sampled. Additionally, to further enrich the database with other aggregate shape properties, 65 cases extracted from the Illinois DOT ICT R27-1 (Tutumluer et al., 2009) project's M_R database were included in the statistical model development.

4.2.2 AIP Database

The AIP database was updated in Chapter 3 by combining the ASIS and the LIMS databases. The updated AIP database provides more detailed information about gradation and categorizes the source, type, and properties of locally available aggregates since 2012. This enhanced database includes 475 samples of subbase materials (Class 3 and Class 4) and 1,668 samples of aggregate base materials (Class 5 and Class 6).

4.2.3 Summary of Datasets

The existing aggregate database with complete M_R and strength characteristics was divided into 80% for establishing and 20% for validating prediction models investigated between aggregate source properties and laboratory-measured mechanical behavior trends. The developed models were then employed to predict the M_R along with shear strength for the materials in the updated AIP database. Specifically, the databases used in this project were organized as follows:

1. **Model Development and Validation Dataset (Dataset No. 1)**
   This dataset consists of 376 cases of aggregate source properties without shape properties, along with the corresponding M_R and shear strength data, from the MN/RC 2012-01 project.
2. **Model Development and Validation Dataset (Dataset No. 2)**
   This dataset consists of 156 cases of aggregate source properties with known morphological shape properties:
   - 91 cases from the MN/RC 2012-01 project, including shape properties and corresponding M_R data from 9 samples within the 376 cases.
   - 65 cases extracted from the Illinois DOT ICT R27-1 (Tutumluer et al., 2009) project M_R database.
3. **Model Application Dataset:**
   This dataset consists of 475 subbase material samples and 1,668 aggregate base material

samples obtained from the enhanced AIP database. No mechanical characteristics, such as resilient modulus and strength, were available for these materials.

4.2.4 Development of Statistical Regression and ANN Models

Table 12 presents a summary of the aggregate properties that were tested as well as the calculated parameters in Dataset No. 1. The regression model previously developed in the MN/RC 2012-01 project is presented below with MEPDG M_R constitutive model includes three regression model parameters, k_1, k_2, and k_3, as expressed in Equation 1 below. Scatter plots and correlation coefficients were generated using this model to identify key predictor variables for k_1, k_2, and k_3, using a first-order regression approach, achieving reasonable accuracy (Equations 2, 3, and 4 show the k_1, k_2, and k_3 equations, respectively). However, the coefficients of determination (R^2 and adjusted R^2) and the root mean squared errors (RMSE) of the predictions, especially for k_1 prediction, indicated that there was certainly room for improvement.

$$M_R = k_1 P_a \left(\frac{\theta}{P_a}\right)^{k_2} \left(\frac{\tau_{oct}}{P_a} + 1\right)^{k_3} \quad (1)$$

$$k_1 = 10^{\left(1.379 - 0.041\omega_{opt} - 0.005\gamma_{dry} - 0.294\frac{\omega}{\omega_{opt}} + 0.001FSAND\right)} \quad (2)$$

(R^2 = 0.14; Adjusted R^2 = 0.13; RMSE = 0.16)

$$k_2 = 1.606 - 0.012\omega + 0.006\gamma_d - 0.0002\frac{\gamma_{MAX}^2}{P_{40}} - 0.004C_u - 0.427C_c - 0.011PP\_19MM \quad (3)$$

(R^2 = 0.32; Adjusted R^2 = 0.31; RMSE = 0.16)

$$k_3 = -9.867 + 0.001\frac{\gamma_{MAX}^2}{P_{40}} + 0.007C_u + 0.067PP\_50MM + 0.015PP\_19MM + 0.009PP\_425UM \quad (4)$$

(R2 = 0.39; Adjusted R2 = 0.39; RMSE = 0.42)

where M_R=resilient modulus,

θ=bulk stress =$\sigma_1+\sigma_2+\sigma_3$,

σ_1=major principal stress,

σ_2=intermediate principal stress = σ_3 for M_R test on cylindrical specimen,

σ_3=minor principal stress or confining pressure in triaxial tests,

σ_d=deviator stress = $\sigma_1-\sigma_2= \sigma_1-\sigma_3$,

τ_{oct}=octahedral shear stress $\tau_{oct}=\frac{1}{3}\sqrt{(\sigma_1-\sigma_2)^2+(\sigma_1-\sigma_3)^2+(\sigma_2-\sigma_3)^2}$, and

Pa=normalizing stress (atmospheric pressure =100 kPa=14.7 psi).

Table 12. Aggregate property abbreviation list

Predictor abbreviation	Description
OPT_MOIST	Optimum Moisture Content (ω_{opt})
MAX_DENS	Maximum Dry Density (γ_{MAX})
ACT_MOIST	Achieved Moisture Content (ω)
ACT_DRY_DENSITY	Achieved Dry Density (γ)
D10	Sieve size (mm) through which 10% passes
D60	Sieve size (mm) through which 60% passes
PP_63MM	Percent Passing the 63mm Sieve
PP_50MM	Percent Passing the 50mm Sieve
PP_37_5MM	Percent Passing the 37.5mm Sieve
PP_31_5MM	Percent Passing the 31.5mm Sieve
PP_25MM	Percent Passing the 25mm Sieve
PP_19MM	Percent Passing the 19mm Sieve
PP_16MM	Percent Passing the 16mm Sieve
PP_12_5MM	Percent Passing the 12.5mm Sieve
PP_9_5MM	Percent Passing the 9.5mm Sieve
PP_4_75MM	Percent Passing the 4.75mm Sieve
PP_2_36MM	Percent Passing the 2.36mm Sieve
PP_2MM	Percent Passing the 2mm Sieve
PP_1_18MM	Percent Passing the 1.18mm Sieve
PP_600UM	Percent Passing the 600um Sieve
PP_425UM	Percent Passing the 425um Sieve
PP_300UM	Percent Passing the 300um Sieve
PP_150UM	Percent Passing the 150um Sieve
PP_075UM	Percent Passing the 75um Sieve
Fsand	Percent of fine sand (0.42 to 0.075mm))
Csand	Percent of Coarse sand (2 to 0.42mm)
Gravel	Percent Gravel (75 to 2 mm)
Cu	Coefficient of Uniformity
Cc	Coefficient of Curvature
P200/logCu	Calculated parameter PP_0.75um/logCu
w/wopt	Calculated parameter ω/ω_{opt}
rdry/rmax	Calculated parameter γ/γ_{MAX}
r2/p40	Calculated parameter γ_{MAX}/PP_425UM

Based on the preliminary analyses, additional variables were sought out to improve the prediction accuracy and to enhance the selection of aggregate properties for model improvement and development. Note that the additional properties as variables using Dataset No. 1 did not include aggregate morphological shape properties. An ANN model was also developed for this project to further improve the prediction accuracy using Dataset No. 1. Both the improved regression model and the newly developed ANN model will be presented in the next sections and evaluated using Dataset No. 2, which includes aggregate morphological shape properties.

4.2.5 Procedures for Establishing Linkages

4.2.5.1 Step 1: Selection of Aggregate Prediction Variables

To understand the interrelationships among prementioned aggregate property variables shown in Table 12, a Pearson's correlation chart was analyzed, as shown in Figure 31. This analysis was based on 376 cases from the MN/RC 2012-01 project dataset, excluding shape factors. The significant correlations with MEPDG M_R model with three model parameters, (i.e., k_1, k_2, and k_3) are summarized in Table 13, with the top 10 correlated items having a Pearson correlation coefficient above 0.2. These parameters are utilized in the development of enhanced and new models.

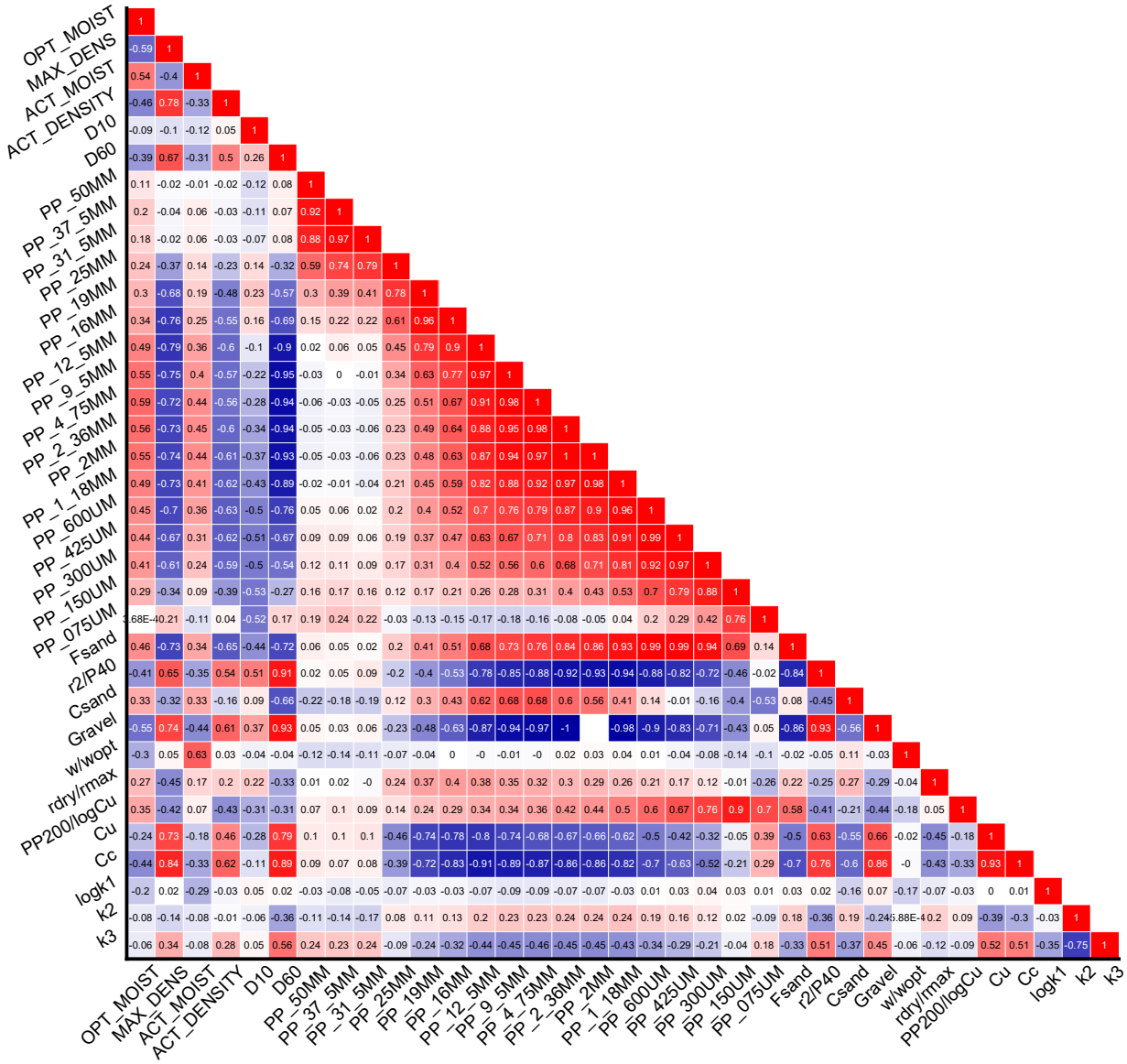

Figure 31. Pearson's correlation between aggregate properties and resilient modulus parameters.

Table 13. Significant aggregate index properties for the dataset without shape properties (Dataset No. 1)

Response variables	Aggregate index properties that play a significant role in prediction
k_1	OPT_MOIST, Cs and, w/wopt
k_2	D60, PP_9_5MM, Gravel, r2/p40, rdry/rmax, Cu, Cc
k_3	MAX_DENS, D60, r2/P40, Gravel, Cu, Cc, PP_50MM, PP_19MM, PP_4_75MM, PP_425UM

Please note that not all aggregate variables influencing the k-parameters are listed. Many aggregate property terms defined do not differ significantly from each other. These correlated variables are summarized in Table 14. Aggregate property variables were analyzed using ANOVA in OriginLab software with a significance level set at $\alpha = 0.05$. The null ($H_0 = \mu_1 = \mu_2 = \ldots\mu_n$) and alternative ($H_a$) hypotheses, which is at least one category needs to differ from the rest, for this analysis were also defined.

The purpose of this ANOVA analysis is to determine whether there is a statistically significant difference between the correlated variables. While Pearson's correlation highlights the relationships between variables, it does not provide information on the confidence level for eliminating variables in the multilinear regression model. The ANOVA results, specifically the q-values and Prob-values, provide this confidence. In Table 14, the MeanDiff represents the difference between the means of two groups being compared. The q-value and the Prob value are related to Tukey's test. A lower q-value indicates a weaker correlation between groups. A higher Prob value (typically more than α value = 0.05) suggests that the observed difference between groups is not statistically significant. Therefore, Table 14 lists the aggregate index properties, which are not significantly different, indicating that aggregate index properties are correlated with each other.

Table 14. Correlated independent variables

Independent variables 1	Independent variables 2	MeanDiff	q-value	Prob
ACT_MOIST	OPT_MOIST	-1.426	0.405	1.0
ACT_DENSITY	MAX_DENS	0.101	0.029	1.0
PP_37_5MM	PP_50MM	-0.160	0.045	1.0
PP_31_5MM	PP_50MM	-0.303	0.086	1.0
PP_31_5MM	PP_37_5MM	-0.144	0.041	1.0
PP_25MM	PP_50MM	-1.018	0.289	1.0
PP_25MM	PP_37_5MM	-0.858	0.244	1.0
PP_25MM	PP_31_5MM	-0.714	0.203	1.0
PP_19MM	PP_50MM	-4.170	1.186	1.0
PP_19MM	PP_37_5MM	-4.011	1.140	1.0
PP_19MM	PP_31_5MM	-3.867	1.100	1.0
PP_19MM	PP_25MM	-3.153	0.895	1.0
PP_16MM	PP_50MM	-7.673	2.182	1.0
PP_16MM	PP_37_5MM	-7.513	2.136	1.0

Independent variables 1	Independent variables 2	MeanDiff	q-value	Prob
PP_16MM	PP_31_5MM	-7.370	2.095	1.0
PP_16MM	PP_25MM	-6.655	1.890	1.0
PP_16MM	PP_19MM	-3.503	0.996	1.0
PP_12_5MM	PP_50MM	-13.934	3.962	0.6
PP_12_5MM	PP_37_5MM	-13.774	3.916	0.6
PP_12_5MM	PP_31_5MM	-13.630	3.876	0.7
PP_12_5MM	PP_25MM	-12.916	3.668	0.8
PP_12_5MM	PP_19MM	-9.763	2.776	1.0
PP_12_5MM	PP_16MM	-6.261	1.780	1.0
PP_9_5MM	PP_25MM	-18.876	5.360	0.1
PP_9_5MM	PP_19MM	-15.723	4.471	0.3
PP_9_5MM	PP_16MM	-12.221	3.475	0.9
PP_9_5MM	PP_12_5MM	-5.960	1.695	1.0
PP_4_75MM	PP_12_5MM	-18.434	5.241	0.1
PP_4_75MM	PP_9_5MM	-12.473	3.547	0.8
PP_2_36MM	PP_4_75MM	-9.734	2.768	1.0
PP_2MM	PP_4_75MM	-12.051	3.426	0.9
PP_2MM	PP_2_36MM	-2.316	0.659	1.0
PP_1_18MM	PP_2_36MM	-9.835	2.796	1.0
PP_1_18MM	PP_2MM	-7.519	2.138	1.0
PP_600UM	PP_2MM	-18.931	5.383	0.1
PP_600UM	PP_1_18MM	-11.412	3.245	0.9
PP_425UM	PP_1_18MM	-17.880	5.084	0.1
PP_425UM	PP_600UM	-6.468	1.839	1.0
PP_300UM	OPT_MOIST	13.800	3.924	0.6
PP_300UM	ACT_MOIST	15.226	4.329	0.4
PP_300UM	D60	18.254	5.190	0.1
PP_300UM	PP_600UM	-13.963	3.970	0.6
PP_300UM	PP_425UM	-7.495	2.131	1.0
PP_150UM	OPT_MOIST	3.074	0.874	1.0
PP_150UM	ACT_MOIST	4.500	1.279	1.0
PP_150UM	D10	11.510	3.273	0.9
PP_150UM	D60	7.528	2.140	1.0
PP_150UM	PP_425UM	-18.221	5.181	0.1
PP_150UM	PP_300UM	-10.726	3.050	1.0
PP_075UM	OPT_MOIST	-1.626	0.462	1.0
PP_075UM	ACT_MOIST	-0.199	0.057	1.0
PP_075UM	D10	6.811	1.937	1.0
PP_075UM	D60	2.829	0.804	1.0
PP_075UM	PP_300UM	-15.425	4.386	0.4
PP_075UM	PP_150UM	-4.699	1.336	1.0

4.2.5.2 Step 2: Improving the Existing MLR Model and Developing the ANN Model

Improving the Existing MLR model

To enhance the accuracy of the MLR model developed in the previous MN/RC 2012-01 project for predicting the three regression model parameters, k_1, k_2, and k_3, additional significant variables identified in Step 1 were carefully selected and incorporated into the regression model based on the Pearson's correlation in Figure 31. Note that 80% of the 376 cases without shape properties were used to develop the models, while the remaining 20% were used for model validation. During the model evaluation stage, R^2 and RMSE were used to assess model accuracy. Higher R^2 and lower RMSE indicate a more accurate model. Adjusted R^2, another criterion for quantifying regression accuracy, was accounted for the number of variables used in the model. The standard error (SE) reflected the error associated with each variable. Aggregate variables were considered statistically significant when the p-value was less than 0.05.

In the Pearson correlation chart as shown in Figure 31, the Pearson correlation coefficient for k_1 is generally below 0.2, which may suggest a nonlinear relationship between the response variable k_1 and the aggregate property variables. As listed in Table 13, factors such as optimum moisture content (OPT_MOIST), coarse sand percentage (Csand), and ω/ω_{opt} (w/wopt) have Pearson correlation coefficients greater than 0.2. These variables were therefore added to those used in the MN/RC 2012-01 project, as given in Tables 15 through 17. T-test was performed for each coefficient in a multilinear regression model. The Prob > |t| values indicate the probability that the relationship between each predictor and the response variable is due to random variation. Specifically, smaller Prob-values (e.g., <0.1) suggest that the predictor significantly contributes to the model, while larger values may indicate less statistical certainty about the predictor's importance. As a result, the R^2 value has improved to 0.18 when to compared to 0.14 for the previous MN/RC 2012-01 project although that is still a low coefficient of determination (R^2).

Table 15. Comparison between MN/RC 2012-01 MLR model and the improved MLR model for log(k_1)

Log(k_1)	MN/RC 2012-01 MLR		Improved MLR (This Project)		
	Estimated value	Prob>|t|	Estimated value	SE	Prob>|t|
Intercept	1.379	<0.0001	1.996	0.323	<0.0001
OPT_MOIST	-0.041	<0.0001	-0.046	0.009	<0.0001
ACT_DENSITY	-0.005	0.004	-0.004	0.002	<0.0001
Fsand	0.001	0.044	-0.0002	0.001	<0.0001
Csand	-	-	-0.004	0.001	0.004
w/wopt	-0.294	<0.0001	-0.298	0.066	<0.0001

	MN/RC 2012-01 MLR	Improved MLR (This Project)
R^2	0.14	0.18
Adjusted R^2	0.13	0.16
RMSE	0.16	0.16

Similarly, D60, γ/γ_{max} (rdry/rmax), and gravel percentage (Gravel) were identified as highly correlated parameters for k_2. Therefore, these factors were also taken into consideration in the model, along with achieved moisture content (ACT_MOIST), achieved dry density (ACT_DENSITY), r2/P40, Cu, Cc, and percentage passing 19 mm (PP_19MM) which were considered in the previous MN/RC 2012-01 project. It is important to note that PP_9.5MM has a high correlation with PP_19MM, as shown in Table 14. As a result, PP_19MM were used in the model instead of percentage passing 9.5 mm (PP_9.5MM), even though PP_9.5MM was identified as one of the significant aggregate properties affecting performance.

Table 16. Comparison between MN/RC 2012-01 MLR model and improved MLR model for k_2

k_2	MN/RC 2012-01 MLR		Improved MLR (This Project)		
	Estimated value	Prob>|t|	Estimated value	SE	Prob>|t|
Intercept	1.606	<0.0001	1.474	0.413	<0.001
ACT_MOIST	-0.012	0.031	-0.008	0.006	0.017
ACT _DENSITY	0.006	0.002	0.007	0.003	0.022
r2/p40	-0.0002	<0.0001	-0.001	0.000	<0.001
Gravel	-	-	0.008	0.002	0.001
rdry/rmax	-	-	-0.312	0.406	0.044
Cu	-0.004	<0.0001	-0.001	0.001	0.031
Cc	-0.427	0.01	-0.225	0.163	0.017
PP_19MM	-0.011	<0.0001	-0.009	0.003	0.001
D60	-	-	0.004	0.011	0.072
k_2	**MN/RC 2012-01 MLR**		**Improved MLR (This Project)**		
R2	0.32		0.38		
Adjusted R2	0.31		0.36		
RMSE	0.16		0.16		

In addition to the prediction variables used in the MN/RC 2012-01 project, Pearson correlation analyses suggested maximum dry density (MAX_DENS), D60, percentage passing 4.75 mm (PP_4_75MM), percentage of gravel (Gravel), and Cc as significant influencing factors for k_3. Incorporating these variables, along with those from the previous model-r2/P40, Cu, percentage passing 50 mm (PP_50MM), percentage passing 19 mm (PP_19MM), and percentage passing 425 μm (PP_425UM)-improved the prediction model, resulting in an R^2 value of 0.44.

Table 17. Comparison between MN/RC 2012-01 MLR model and improved MLR model for k_3

k_3	MN/RC 2012-01 MLR		Improved MLR (This Project)		
	Estimated Value	Prob>|t|	Estimated Value	SE	Prob>|t|
Intercept	-9.867	<0.0001	0.291	0.858	0.073
MAX_DENS			0.009	0.003	0.010
D60			0.019	0.018	0.028

k_3	MN/RC 2012-01 MLR		Improved MLR (This Project)		
	Estimated Value	Prob>|t|	Estimated Value	SE	Prob>|t|
PP_50MM	0.067	0.002	0.001	0.009	0.087
PP_19MM	0.015	0.06	-0.010	0.004	0.008
PP_4_75MM			0.006	0.003	0.077
PP_425UM	0.009	0.009	0.001	0.001	0.035
r2/P40	0.001	<0.0001	-6.2E-4	1.4E-4	<0.001
Gravel			0.014	0.004	<0.001
Cu	0.007	<0.0001	-0.002	0.001	0.017
Cc			-0.281	0.168	0.010

k_3	MN/RC 2012-01 MLR	Improved MLR (This Project)
R^2	0.39	0.44
Adj. R^2	0.39	0.42
RMSE	0.42	0.40

Based on the above analyses, the improved regression models without shape properties for the k-parameters are given by Equations 5, 6, 7, and 8 as follows:

$$M_R=k_1 P_a \left(\frac{\theta}{P_a}\right)^{k_2} \left(\frac{\tau_{oct}}{P_a}+1\right)^{k_3} \quad (5)$$

$$k_1=10^{\left(1.996-0.046\omega_{opt}-0.004\gamma_{dry}-0.0002FSAND-0.004CSAND-0.298\frac{\omega}{\omega_{opt}}\right)} \quad (6)$$

R^2=0.18; Adj R^2=0.16; RMSE=0.16

$$k_2=1.474-0.008\omega+0.007\gamma_d-0.001\frac{\gamma_{MAX}^2}{P_{40}}+0.008Gravel$$
$$-0.312\frac{\gamma}{\gamma_{MAX}}-0.001C_u-0.225C_c-0.009PP\_19MM+0.004D60 \quad (7)$$

R^2=0.38; Adj R^2=0.36; RMSE=0.16

$$k_3=0.291+0.009\gamma_{MAX}+0.019D60+0.001PP_{50MM}-0.01PP\_19MM$$
$$+0.006PP\_4\_75MM+0.001PP\_425UM-0.0006\frac{\gamma_{MAX}^2}{P_{40}}+0.014Gravel-0.002C_u-0.281C_c \quad (8)$$

R^2=0.44; Adj R^2=0.42; RMSE=0.40

Where:

M_R=resilient modulus,
θ=bulk stress =$\sigma_1+\sigma_2+\sigma_3$,
σ_1=major principal stress,
σ_2=intermediate principal stress = σ_3 for M_R test on cylindrical specimen,
σ_3=minor principal stress or confining pressure in triaxial tests,
σ_d=deviator stress = $\sigma_1-\sigma_2=\sigma_1-\sigma_3$,

τ_{oct}=octahedral shear stress $\tau_{oct}=\frac{1}{3}\sqrt{(\sigma_1-\sigma_2)^2+(\sigma_1-\sigma_3)^2+(\sigma_2-\sigma_3)^2}$, and

Pa=normalizing stress (atmospheric pressure =100 kPa=14.7 psi).

Although there was an improvement in prediction accuracy over the previous the MN/RC 2012-01 project findings, the R^2 values and the goodness of prediction is in general not as high as when shape properties were considered. Having said that imaging based quantitative aggregate shape indices are not readily available in practice when using these equations in field implementation projects. Therefore, the research team further concentrated efforts in artificial intelligence-based modeling of mechanical properties to improve model accuracy while maintaining aggregate property inputs based on the information available in the current AIP aggregate source property database.

ANN model

The MLR model has been updated and improved by incorporating the significant variables detailed in the previous section; however, the improvement in R^2 was not substantial. This led to the development of a new model-the ANN model. After fine-tuning the hyperparameters, including a batch size of four and a hidden layer configuration of 29-25-12-3 (20 input variables, 25 and 12 hidden neurons in two layers, and three k-parameter outputs), the ANN model achieved the lowest RMSE for predicting M_R. Compared to the improved MLR model (Figure 32), the ANN model (Figure 33) significantly enhances k_1 prediction, as shown in Figure 33(a), due to the nonlinear relationship properly captured between aggregate properties and k_1. Although the MLR method attempted logarithmic scale regression, k_1 prediction with the MLR method remains the least accurate among the three M_R parameter predictions, as shown in Figure 32(a). Having said that, a jump in the R^2 value from 0.18 to 0.67 is truly remarkable as achieved in the developed ANN model. Similarly, the prediction of k_2 improved from an R^2 of 0.38 to 0.47, and the prediction of k_3 also presented a significant improvement, with the R^2 increasing from 0.44 to 0.63 using the ANN model.

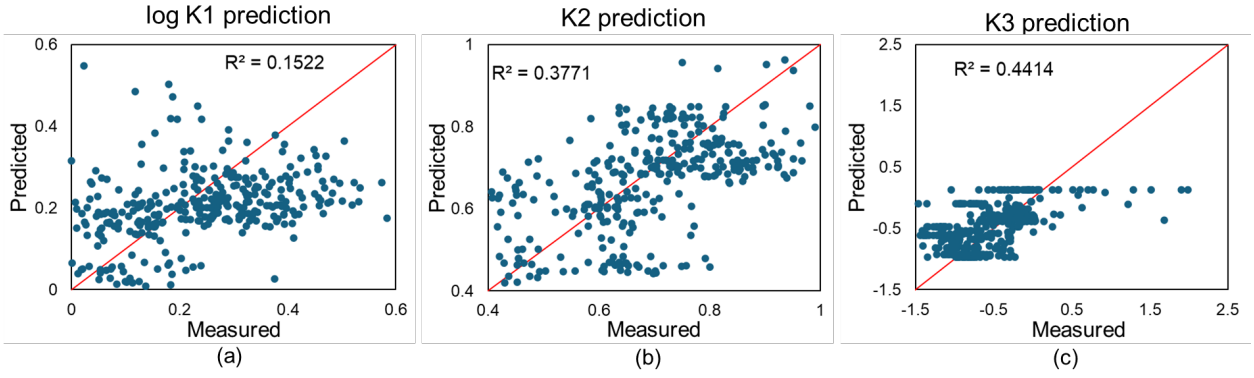

Figure 32. Measured vs. predicted values for k_1, k_2, and k_3 using the MLR model

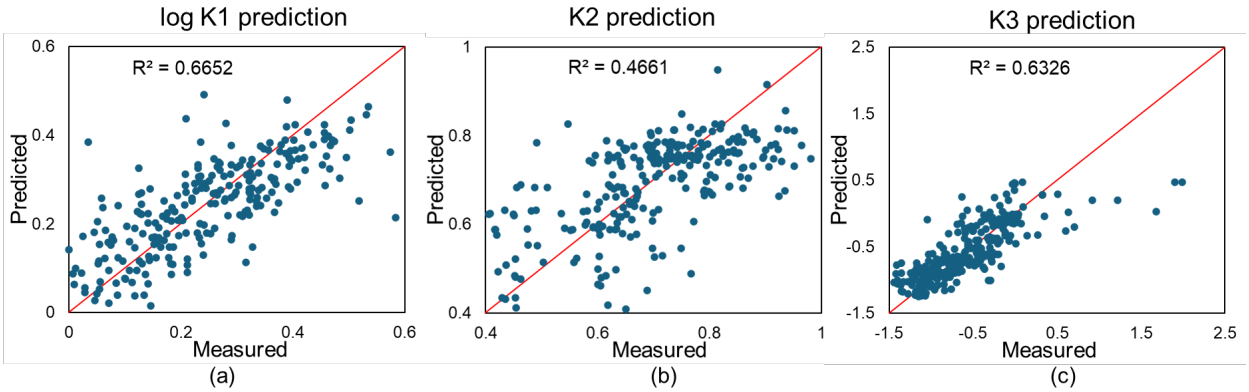

Figure 33. Measured vs. predicted values for k_1, k_2, and k_3 using the ANN model

Model validation using 20% of the 376 cases of Dataset No. 1

Note that 20% of the cases in Dataset No. 1 were used to validate the improved and the new models, and the results are summarized in Figures 34 and 35. Overall, the ANN model significantly outperformed the improved MLR model, particularly in enhancing k_1 prediction, as shown in Figure 35(a).

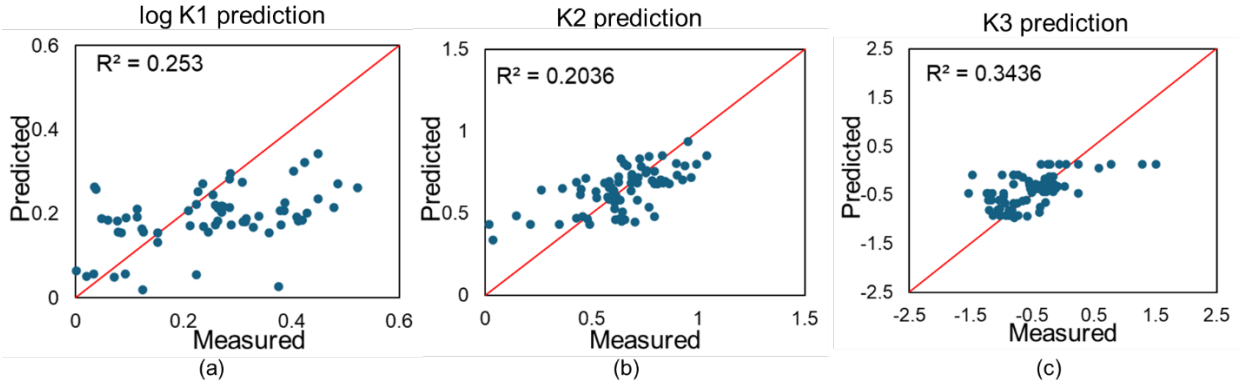

Figure 34. The improved MLR model validation

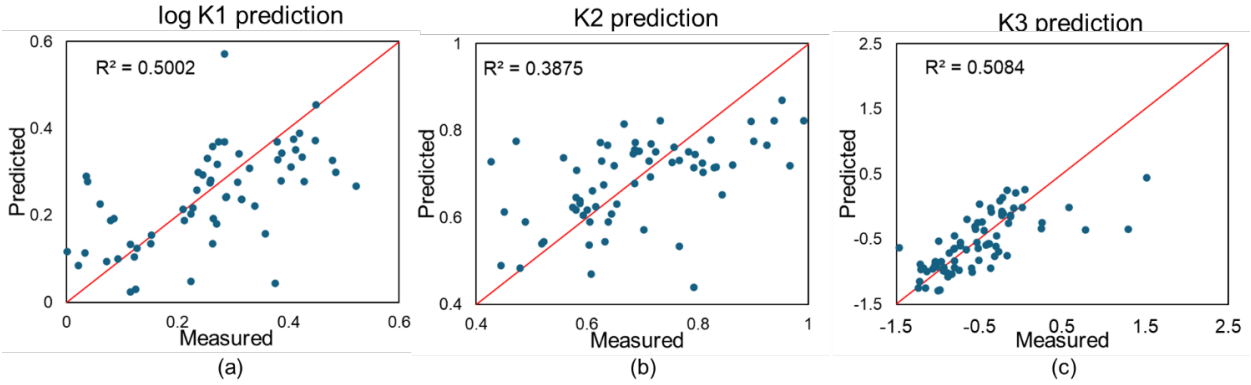

Figure 35. The newly developed ANN model validation

AASHTO T 307 test procedure is the most used test for determining M_R of unbound materials. In the AASHTO T 307 procedure, the primary testing after specimen conditioning is conducted at certain confining and deviator stresses, resulting in 15 applied stress states, as listed in Table 18. For the M_R prediction, the RMSE were calculated for the improved MLR model, and the ANN model also developed in this chapter and compared with the RMSE value of the previous MN/RC 2012-01 project model, as presented in Figure 36. Note that the ANN model demonstrated the best prediction ability compared to both the improved MLR model and the original MN/RC 2012-01 MLR model. The differences in the RMSE values between the MN/RC 2012-01 model and the improved MLR model are significant, which may be attributed to the different training and validation dataset combinations used.

Table 18. 15 stress states according to the AASHTO T307 M_R test procedure

AASHTO T307 Applied Stress Sequence	Confining Pressure (psi)	Deviator Stress (psi)
1	3	3
2	3	6
3	3	9
4	5	5
5	5	10
6	5	15
7	10	10
8	10	20
9	10	30
10	15	15
11	15	15
12	15	30
13	20	10
14	20	15
15	20	30

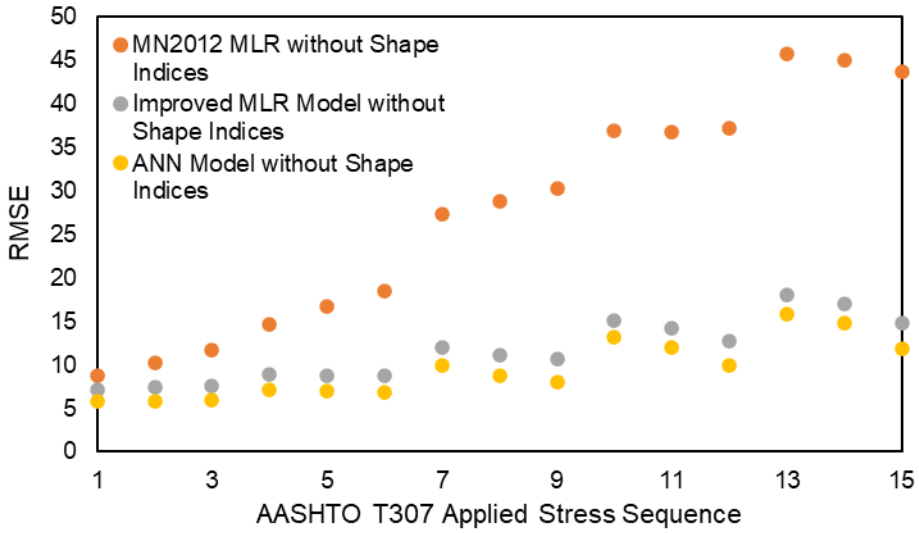

Figure 36. RMSE comparisons for MR considering the 15 AASHTO T 307 stress states among the MN/RC 2012-01 model and the MLR and ANN models

ANN Model with Shape Factors

To further enhance the prediction accuracy, aggregate shape indices were also included in the development of the ANN model. The dataset used (Dataset No. 2) consists of combined ICT R27-1 and MN/RC 2012-01 data and comprises a total of 124 cases for training and 32 cases for validation. The optimal ANN configuration was found to be 20-25-12-3 (20 input variables, 25 and 12 hidden neurons in two layers, and three k-parameter outputs). As indicated in Table 19, both ANN models (with and without morphological shape properties) achieved similar accuracy to the MLR model for predicting the modulus characterization model parameters (k_1, k_2 and k_3) with slight improvements. The model that incorporates shape indices into the ANN model improved the R^2 value, but there was only a slight difference in performance between the models with and without the shape indices, likely due to the complexity of the neural network architecture and its superior prediction ability.

Table 19. Comparisons of ANN models with and without shape indices

Model	MLR with Shape Properties		ANN without Shape Properties		ANN with Shape Properties	
Response variables	R^2	RMSE	R^2	RMSE	R^2	RMSE
k_1	0.5523	0.12157	0.5745	0.12258	0.5945	0.11967
k_2	0.5062	0.12422	0.5213	0.11229	0.5501	0.10886
k_3	0.6633	0.28858	0.6724	0.25047	0.6747	0.24956

4.2.5.3 Step 3: Material Quality Selection Criteria

To investigate the effects of unbound aggregate layer mechanical characterization on pavement performance to be studied by MnPAVE pavement analysis and design program, this step aims to characterize and categorize aggregate materials in the updated AIP dataset based on their aggregate base/subbase layer mechanical behavior characteristics.

The criteria for classifying different quality aggregates depend on their M_R and permanent deformation characteristics. Permanent deformation behavior is highly correlated with shear strength. As a result, both M_R and shear strength properties were predicted using the ANN model without morphological shape properties developed in Step 2.

Provided that the AIP database does not include aggregate shape properties, and that the ANN model generally presented better prediction accuracy, the ANN model without shape properties was used to obtain the aggregate mechanical properties. In the AIP database, there are 475 cases of Class 3 and 4 aggregates (subbase materials), and 1,668 cases of Class 5 and 6 aggregates (aggregate base materials). Two common stress levels for aggregate base and subbase field conditions, as presented in Table 20, were applied for computing the M_R, as depicted in Figure 37. Figure 37 presents the M_R values at the applied stress states, represented by MR_1 and MR_2 for all the materials in the AIP database and their average levels considered.

Table 20. Common stress states for base and subbase assumed in field constructed pavement layers

Parameter	Stress state 1 (MR_1) for Aggregate Base materials	Stress state 2 (MR_2) for Aggregate Base materials	Stress state 1 (MR_1) for Subbase materials	Stress state 2 (MR_2) for Subbase materials
Confining Pressure σ_3 (psi)	10	5	5	3.5
Deviator Stress σ_d (psi)	30	15	10	5

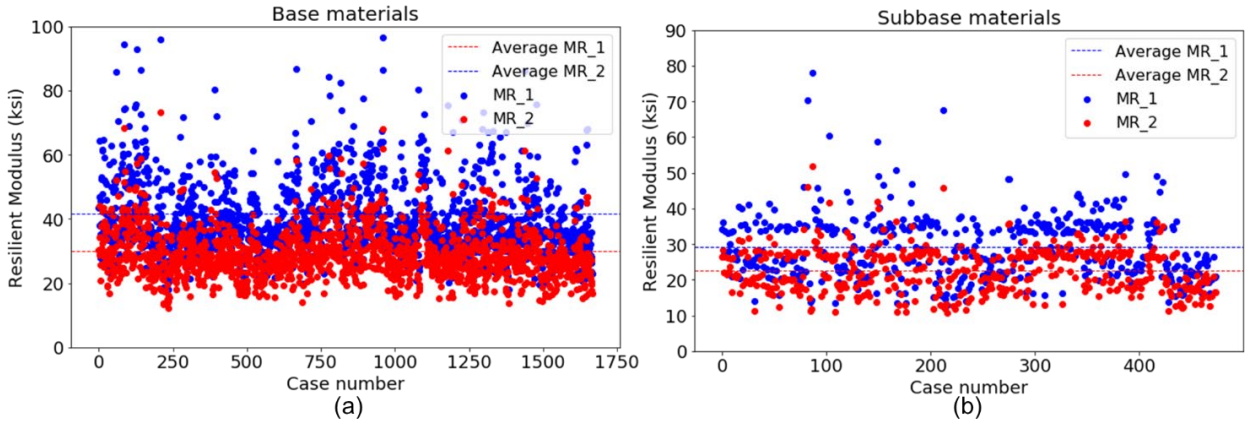

Figure 37. Computed M_R using the AIP database granular (a) aggregate base and (b) subbase aggregate materials (1 psi = 6.89 kPa)

A comparison of the M_R values predicted at the two, MR_1 and MR_2, stress states using the current AIP dataset and the MN/RC 2012-01 project dataset is presented in Table 21. The modulus behavior has been adequately characterized for the nonlinear stress-dependent behavior of aggregates. If the combination of k_1, k_2, and k_3 results in a higher M_R value at any given stress state, the materials corresponding to these parameter combinations are likely to exhibit better resilient behavior performance. Based on the M_R values computed at each stress state, the subbase and aggregate base materials can be categorized into low, medium, and high-quality groups. The ranges established for these quality groups are given in Table 21.

Please note that the M_R values determined for the three quality levels using the AIP database were based on the predictions of the ANN model without morphological shape properties, whereas the k_1, k_2, and k_3 parameters in the MN/RC 2012-01 database were based on experimental M_R data. The adequacy of the predicted k_1, k_2, and k_3 parameters to generate representative moduli for pavement analysis will be evaluated in later chapters. Having said that, the three quality levels for both databases are similar, as indicated in Table 21, suggesting that representative materials from the AIP database can be selected from the MN/RC 2012-01 project dataset.

Table 21. M_R linked to quality levels for the AIP and the MN/RC 2012-01 project databases

		Aggregate Base material M_R at stress state 1 (MR_1) [ksi]		Aggregate Base material M_R at stress state 2 (MR_2) [ksi]		Subbase material M_R at stress state 1 (MR_1) [ksi]		Subbase material M_R at stress state 2 (MR_2) [ksi]	
Predictions	**Quality Group**	**Lower limit**	**Upper limit**	**Lower limit**	**Upper limit**	**Lower limit**	**Upper limit**	**Lower limit**	**Upper limit**
Prediction based on the AIP dataset	**Low**	17.959	44.16	12.196	32.561	12.874	34.626	10.7	24.377
	Medium	44.16	70.361	32.561	52.926	34.626	56.379	24.377	38.055
	High	70.361	96.562	52.926	73.292	56.379	78.131	38.055	51.733
Prediction based on the previous MN/RC 2012-01 database	**Low**	21.012	42.66	13.094	32.178	11.722	31.799	8.022	23.88
	Medium	42.66	64.308	32.178	51.261	31.799	51.876	23.88	39.737
	High	64.308	85.955	51.261	70.345	51.876	71.953	39.737	55.594

Moreover, the aggregate materials from the AIP database and the MN/RC 2012-01 project were combined into an integrated dataset because the M_R values were similar across the three quality levels. The ANN model, excluding shape properties, was then used to predict the M_R for the integrated dataset at the two stress states designated for aggregate base and subbase materials. This combination resulted in an expanded range of the integrated dataset, accommodating more qualified materials. The results are presented in Table 22.

Table 22. M_R linked to quality levels for the combined AIP and MN/RC 2012-01 databases

AIP and MN/RC 2012-01 combined databases / quality groups	Aggregate Base materials M_R at stress state 1 (MR_1) [ksi]		Aggregate Base materials M_R at stress state 2 (MR_2) [ksi]		Subbase materials M_R at stress state 1 (MR_1) [ksi]		Subbase materials M_R at stress state 2 (MR_2) [ksi]	
	Lower limit	**Upper limit**	**Lower limit**	**Upper limit**	**Lower limit**	**Upper limit**	**Lower limit**	**Upper limit**
Low	17.603	44.193	11.955	32.729	12.992	33.719	10.826	23.367
Medium	44.193	70.782	32.729	53.502	33.719	54.446	23.367	35.908
High	70.782	97.372	53.502	74.276	54.446	75.174	35.908	48.448

It is crucial to account for shear strength when determining aggregate qualities because strength governs permanent deformation. Like it was done for predicting M_R, another ANN model could facilitate characterizing the aggregate materials from a strength perspective. For the strength prediction ANN model, the optimal layer configuration was found to be 25-20-10-1 (25 input variables, 20 and 10 hidden neurons in two layers, and 1 strength output). The training dataset comprised 80% of the 109 cases from the previous MN/RC 2012-01 project. In the MN/RC 2012-01 project, after completing the M_R tests, the specimens were loaded to failure at constant confining pressures ranging from 4 to 10 psi, using a constant loading rate of 0.03 in./s to determine the peak deviator stress values. The peak deviator stress data at 4 psi confining pressure were collected as an indicator of the aggregate material's shear strength

for use in the training datasets. This approach taken was in line with what Tutumluer & Pan (2008) found a strong correlation between the failure deviator stress at a given confining pressure and permanent strain accumulation in unbound aggregate materials. Figure 38(a) presents the actual versus predicted peak deviator stresses of the training dataset at a 4-psi confining pressure. Note that this model did not take certain aggregate properties, such as optimum moisture content (OPT_MOIST), maximum dry density (MAX_DENS), achieved moisture content (ACT_MOIST), and achieved density (ACT_DRY_DENSITY), into consideration because these parameters were not available in the AIP database. Therefore, for the validation dataset, the prediction accuracy decreased as shown in Figure 38(b). It can be observed that multiple points are predicted to have similar strength, likely because the model does not account for these critical variables.

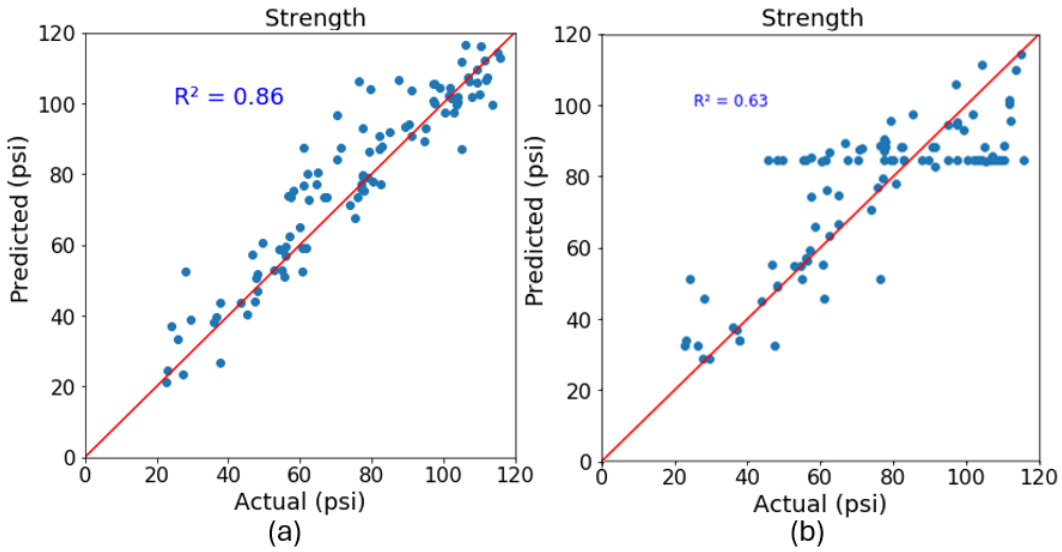

Figure 38. Strength predictions using the ANN model for (a) the training dataset and (b) the validation dataset

Table 23 presents the predicted peak deviator stresses for the aggregate base and subbase materials at 4-psi confining pressure. The ANN strength model was used to estimate the peak deviator stress at failure for materials in the AIP database. Consistent with observations from the experimental strength results, high-quality crushed aggregates, such as Class 5 and Class 6, generally exhibit higher shear strength compared to Class 3 and Class 4 aggregates. The predicted peak deviator stress at failure is generally higher than the experimental strength from the MN/RC 2012-01 project. This suggests that the model might have overestimated the peak deviator stress at failure. There are two possible reasons for this discrepancy: 1) the training dataset for the strength prediction model is limited to 109 cases, whereas the training dataset for resilient modulus prediction model consists of 376 cases; and 2) the training dataset for strength prediction includes variations in achieved moisture content and achieved dry density, which affect the measured strength, but were not considered in the AIP database.

Table 23. Peak deviator stress at failure determined at 4-psi confining pressure

Datasets	Quality Groups	Classes 3 and 4		Classes 5 and 6	
		Lower limit (psi)	Upper Limit (psi)	Lower limit (psi)	Upper limit (psi)
MnDOT experimental peak deviator stress at 4-psi confining pressure	Low	22.623	40.234	24.050	54.635
	Medium	40.234	57.845	54.635	85.220
	High	57.845	75.456	85.220	115.805
ANN model predictions based on the AIP dataset for peak deviator stress at 4-psi confining pressure	Low	10.527	88.035	4.722	94.057
	Medium	88.035	165.543	94.057	183.390
	High	165.543	243.051	183.392	272.727

Therefore, based on both M_R and peak deviator stress at failure criteria, materials can be classified into three quality levels. The permeability and water-retention characteristics of aggregate sources were also evaluated using the approach from Oh et al. (2022), resulting in the classifications of excellent, marginal, or poor. The representative samples for each quality level are listed in Table 24. Note that the overall ratings reflect a combination of saturated hydraulic conductivity and the minimum saturation criteria. If either of these is poor or the other one is designated as marginal, the final quality is rated as M-P.

Table 24. Modulus and drainability characteristics for the AIP and MN/RC 2012-01 combined database

Materials Property	Aggregate Base materials			Subbase materials		
MEPDG M_R Model Parameters	High	Medium	Low	High	Medium	Low
k_1	4.716	1.817	0.62	3.195	1.621	0.724
k_2	1.042	0.924	1.022	0.711	0.624	0.795
k_3	-1.855	-0.959	-0.895	-1.226	-0.593	-0.289
R^2	0.740	0.830	0.972	0.606	0.943	0.993
Peak deviator stress at 4 psi confining pressure	115	81	56	61	47	37
Achieved dry density (pcf)	135.3	130.2	130.6	119.3	125.4	129
Max. dry density (pcf)	133.0	127.4	131.1	124.3	126.2	127.7
Saturated hydraulic conductivity (cm/s)	0.070	0.099	0.084	0.026	0.017	0.092
Min. Saturation	0.331	0.890	0.407	0.186	0.197	0.725
Qualitative drainability	M-P	M-P	M-P	Marginal	M-P	M-P

4.3 Summary

This chapter summarized the cost information for aggregates used in aggregate base and subbase construction across Minnesota, providing additional context to the aggregate source information previously presented in Chapter 3.

The relationship between aggregate source properties and mechanical properties was enhanced for the existing MLR model by identifying and incorporating the most significant impacting variables (i.e., aggregate properties) into the prediction model developed. This included a new ANN-based model which was also developed in this chapter. Both the improved MLR model and the ANN model increased the M_R prediction accuracy for the 376 aggregate cases in the database. Notably, the R^2 of the M_R model parameter k_1 was significantly improved from 0.18 to 0.67 Although incorporating shape properties generally improved the MLR model predictions, the favorable impact on the ANN model predictions was not as significant.

Following the development of the ANN models for predicting M_R and strength characteristics of the aggregate materials, both M_R and permanent deformation behavior trends were estimated for all materials listed in the AIP database. In accordance, selection criteria were established based on both the M_R and permanent deformation (or strength) behavior trends to identify representative materials to be studied in Chapter 5 within three predetermined quality ranges (low-, medium-, and high-quality materials). Additionally, the drainability properties of selected aggregate base and subbase materials across these quality levels were evaluated.

Chapter 5: Evaluating Design Alternatives and Determining Granular Equivalency Factors

The main objectives of Chapter 5 are to investigate the effect of pavement inputs, particularly (1) HMA, aggregate base, and subbase layer thicknesses, (2) aggregate base and subbase quality, and (3) subgrade conditions on pavement designs. This chapter also calculates granular equivalency (GE) to quantify the combined effects of aggregate qualities and thicknesses on aggregate base and subbase layer performance. The GE outcomes will support Chapter 6 in developing optimized pavement designs that can reduce material costs while maintaining desired service life.

For flexible pavement performance, a detailed sensitivity analysis matrix was developed with various scenarios incorporating pavement structure and climate factors. The matrix was analyzed using MnPAVE, enabling the evaluation of different layer thicknesses, climatic conditions, traffic/load levels, and subgrade conditions within Minnesota, and proposing an approach for optimizing pavement design alternatives in Chapter 6.

5.1 Sensitivity Analysis Matrix

To evaluate how varying design features and site conditions affect pavement performance, a full factorial sensitivity analysis matrix was designed for use in MnPAVE analysis.

5.1.1 Climatic Zones

Because climatic zones significantly affect flexible pavement performance, four counties, i.e., Beltrami (north zone), Todd (central zone), Redwood (south zone), and Olmsted (southeast zone), were selected based on MnDOT's seasonal load limit zone divisions (Ovik et al., 2000). These locations, shown in Figure 39, were chosen to capture key climate differences in Minnesota. Table 25 shows that when examining the transition from Beltrami in the north to Olmsted in the south, winter days become shorter, summer days become longer, and both winter and summer temperatures increase. Because Redwood and Olmsted counties are geographically close, their seasonal differences are minimal.

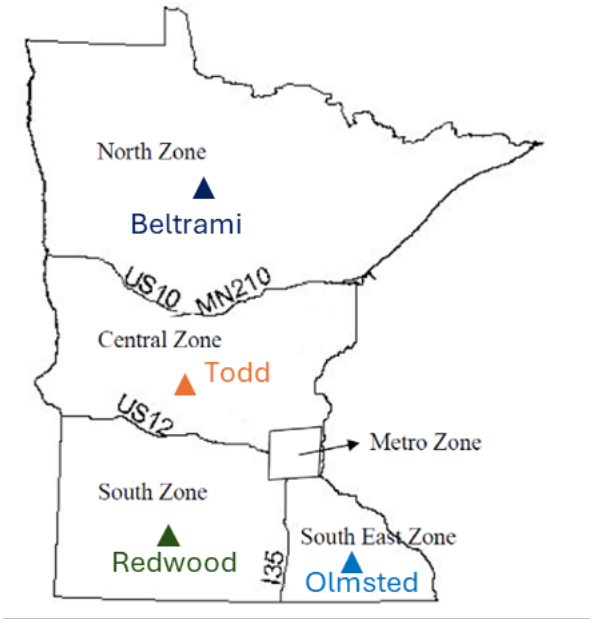

Figure 39. County selections based on climate differences (Source: Ovik et al., 2000)

Table 25. The four selected zones and their seasonal variations

County	Seasonal Variations	Fall	Winter	Early Spring	Late Spring	Summer
Beltrami	Days	90	123	14	62	76
	Pavement Surface Temp. (°F)	49	16	36	59	79
Todd	Days	90	107	14	58	96
	Pavement Surface Temp. (°F)	48	20	38	59	81
Redwood	Days	89	100	14	56	106
	Pavement Surface Temp. (°F)	48	22	38	59	83
Olmsted	Days	93	95	14	58	105
	Pavement Surface Temp. (°F)	48	23	38	59	82

5.1.2 Pavement Structures

In MnPAVE, HMA, aggregate base, subbase, and subgrade layers are assigned seasonal elastic moduli through default multipliers, reflecting moisture susceptibility and freezing/thawing states. An 18 in. early Spring thaw depth was assumed in all pavement sections based on Local Road Material Properties and Calibration for MnPAVE Summary Report (MnDOT, 2008). Because the goal of this chapter is to analyze the influences of unbound aggregate quality and layer thickness, no designs deemed 'unrealistic' were excluded from the test matrix.

The asphalt concrete layer used in this study is PG 58H-34, commonly used for new construction and wearing courses supporting fewer than 10 million ESALs over 20 years of service life (MnDOT, 2015). In

MnPAVE, asphalt materials are modeled as linearly elastic with seasonally varying moduli. County-specific asphalt moduli are used by MnPAVE even when the same asphalt binder type is selected.

Chapter 4 selected three representative aggregate materials with high, medium, and low unbound layer moduli obtained from the AIP database received from MnDOT and MN/RC 2012-01 combined database. The k_1-k_2-k_3, i.e., MEPDG M_R model parameters, assigned to the aggregate materials and the peak deviator stresses at failure are shown in Table 26.

Table 26. Material characterizations and properties for the AIP and MN/RC 2012-01 combined database

Material Characterization / Property		Aggregate Base Materials			Subbase Materials		
		High	Medium	Low	High	Medium	Low
MEPDG M_R Model Parameters	**k_1**	4.716	1.817	0.62	3.195	1.621	0.724
	k_2	1.042	0.924	1.022	0.711	0.624	0.795
	k_3	-1.855	-0.959	-0.895	-1.226	-0.593	-0.289
	R^2	0.740	0.830	0.972	0.606	0.943	0.993
Peak Deviator Stress at 4 psi Confining Pressure (psi)		115	81	56	61	47	37

In previous MN/RC 2012-01 project (Xiao & Tutumluer, 2012), the GT-PAVE nonlinear finite element (FE) program was used to predict aggregate base and subbase layer moduli distributions using the MEPDG M_R model parameters k_1, k_2, and k_3. The Uzan models were adopted in this project (Xiao & Tutumluer, 2012) for the GT-PAVE analysis to characterize the unbound aggregate base and granular subbase layers. The FE mesh used in GT-PAVE comprised 780 isoparametric eight-node quadrilateral elements for analyzing each pavement section. Figure 40 illustrates the FE mesh and representative distributions of the stress-dependent moduli in the aggregate base and granular subbase layers for one of the 2,592 pavement sections analyzed. A single wheel load of 9 kip was modeled as a uniform pressure of 80 psi applied over a circular contact area with a radius of 6 in. Poisson's ratios were assumed to be 0.3 for asphalt concrete, 0.4 for the unbound aggregate base and granular subbase, and 0.45 for both engineered and natural subgrade soils. The asphalt concrete layer (PG 58-34) was assigned an elastic modulus of 490 ksi, corresponding to MnPAVE's default value for the Fall season. The equivalent single M_R values for the aggregate base/granular subbase to be used in subsequent linear elastic MnPAVE analyses were obtained by averaging moduli throughout each layer depth from the elements located at the load axis. Because the representative materials selected from each quality level in Chapter 4 were consistent with the database for the selected materials in the MN/RC 2012-01 project, the current project conveniently adopted the equivalent M_R associated with each quality level from the MN/RC 2012-01 project. The results of fall season equivalent M_R values linked to high, medium, and low aggregate quality levels are shown in Figure 41. The engineered subgrade was simplified to a constant M_R, while the natural subgrade was modeled at 50% of the engineered subgrade M_R in accordance with the assumptions for MnPAVE analyses.

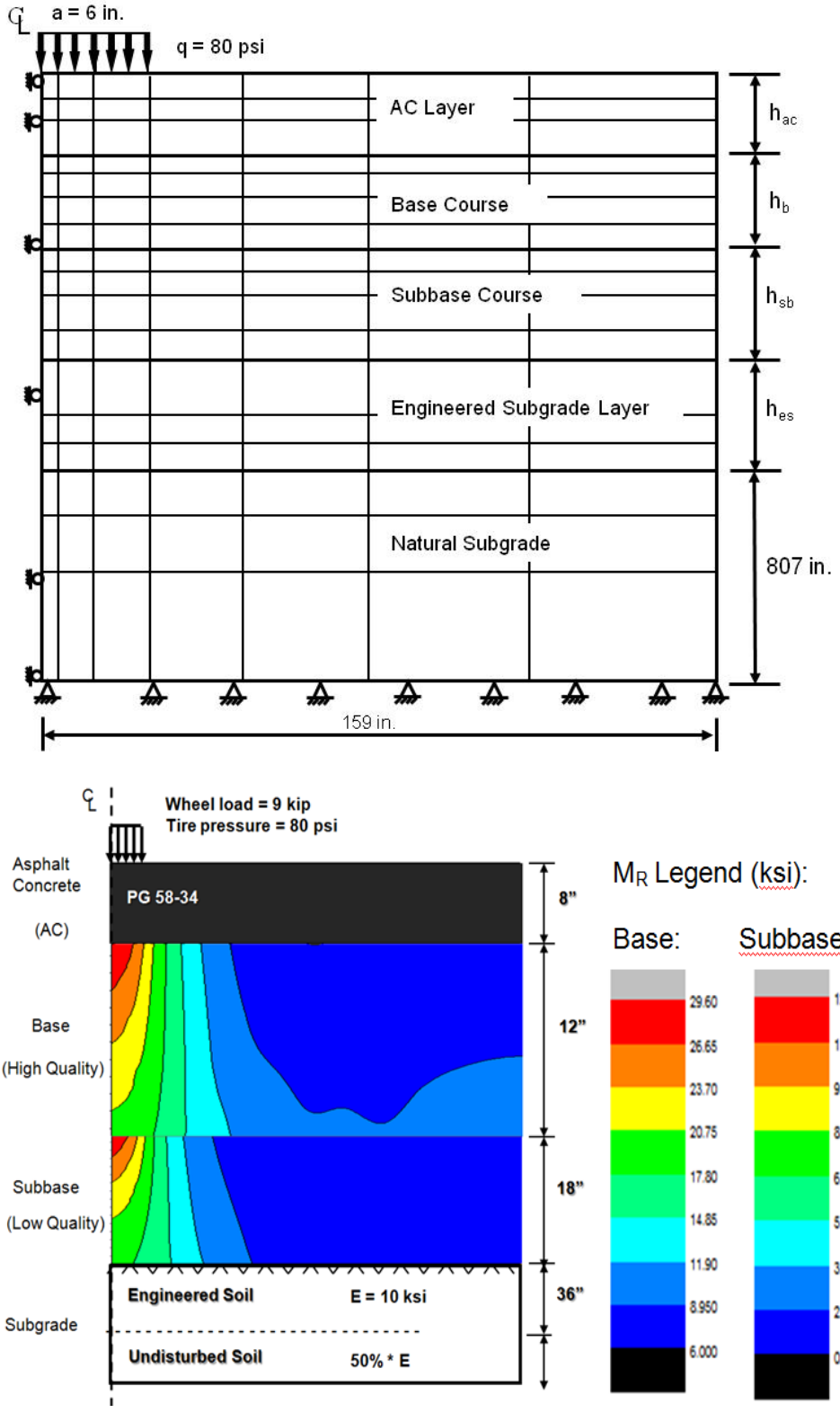

Figure 40. GT-PAVE finite element model (top) and corresponding analysis results showing stress-dependent modulus distributions in the unbound aggregate base and granular subbase layers (bottom) (Xiao & Tutumluer, 2012).

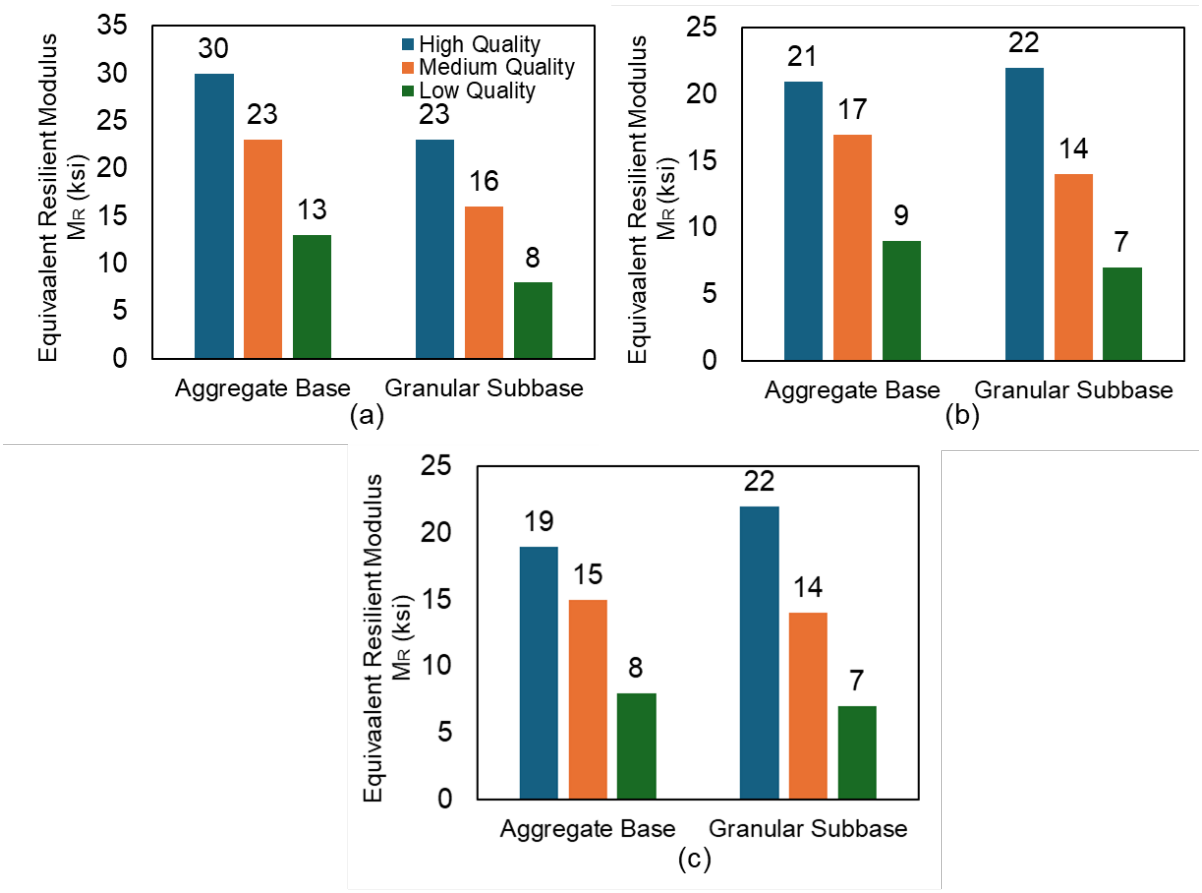

Figure 41. Equivalent fall season M_R values linked to aggregate quality for (a) 4-in., (b) 6-in., and (c) 8-in. asphalt surface thicknesses.

Variables considered in the full factorial sensitivity matrix are listed in Table 27. A MnPAVE batch-run script, formulated for the test matrix pavement structural analyses and provided expertly by Mr. Bruce Tanquist of MnDOT, was used to facilitate running individual cases, a total of 41,472 pavement section combinations. An Excel spreadsheet file listing input information and major damage indicators, including fatigue life, rutting life, fatigue damage ratio, and rutting damage ratio, were generated. In this section, pavement performance trends, mainly related to rutting life and fatigue life, were analyzed based on the test matrix.

5.2 Sensitivity Analysis Results and Discussion

Figure 42 shows fatigue and rutting life predictions for 0.2, 0.6, 1.5, and 6 million ESALs for a pavement structure consisting of 4 in. of HMA over 12 in. of aggregate base and 12 in. of subbase on a 12 in. of engineered subgrade. For traffic levels below 1.5 million ESALs, all material quality levels achieved the 20-year service life with only 4 in. of HMA, implying that use of locally available, lower-quality aggregates may be cost-effective for low-volume roads. Moving through Minnesota counties North to

South, pavement service lives tended to decrease, likely due to shorter winters, longer summers, and higher temperatures.

Table 27. Pavement design inputs for sensitivity analysis

Input Category	Number of Variables	Input Variables
Climate Zones	4	Beltrami, Todd, Redwood, Olmsted
Design Traffic Volume	4	0.2, 0.6, 1.5 and 6 million ESALs
Asphalt PG 58H-34	3	One Elastic Modulus per Each County
		Thickness (in.): 4, 6, 8
		Poisson's Ratio: 0.3
Aggregate Base	4 *3	3 Level-Quality
		Thickness (in.): 3, 6, 9, 12
		Poisson's Ratio: 0.4
Subbase	3* 3	3 Level-Quality
		Thickness (in.): 6, 12, 18
		Poisson's Ratio: 0.4
Engineered Subgrade	4*2	Elastic Modulus: 2, 4, 7, 10 ksi
		Thickness (in.): 12, 24
		Poisson's Ratio: 0.45
Undisturbed Subgrade	1	Elastic Modulus
		50% of Engineered subgrade
		Poisson's Ratio: 0.45

Total Cases: 41,472

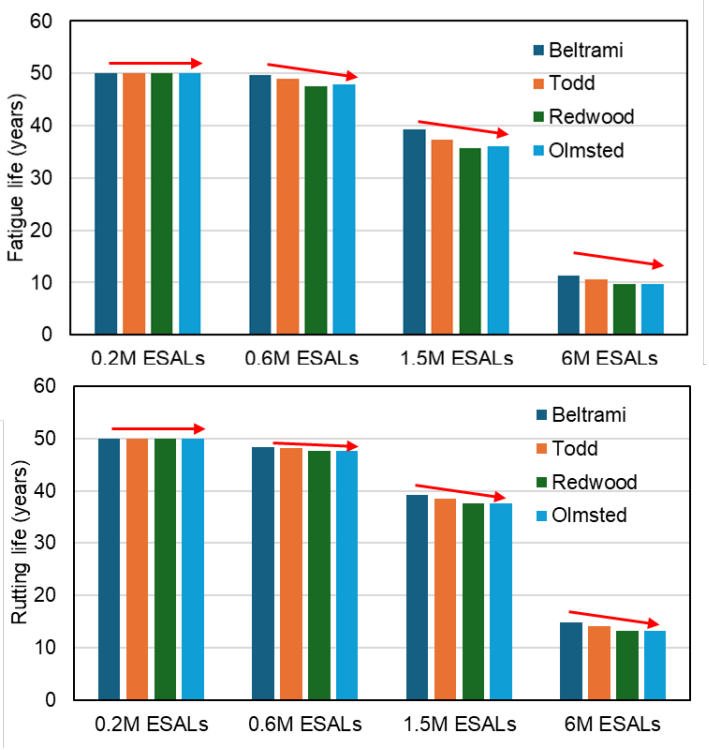

Figure 42. Fatigue life (above) and rutting life (below) predictions via MnPAVE analyses for different counties and traffic levels.

5.2.1 Effect of HMA Layer Thickness on Performance

The effect of HMA layer thickness on pavement fatigue life for Beltrami County is presented in Figure 43. The standard pavement structure consisted of 12-in. aggregate base and 12-in. subbase over a 12-in. engineered subgrade (modulus = 2 ksi). Note that all levels of qualities were averaged for drawing a more generalized conclusion in this session. Figure 43 shows the percentages of pavement sections (y-axis) having service lives greater than a given target fatigue life (x-axis). The results indicate that HMA layer thickness becomes increasingly critical for traffic levels exceeding 0.6 million ESALs. In terms of rutting life predictions shown in Figure 44, HMA layer thickness indicates a higher impact on rutting life with increasing traffic. Comparing trends presented in Figures 43 and 44 for design traffic levels below 0.6 million ESALs, layer thickness has a more pronounced effect on rutting life than fatigue life. For design traffic levels exceeding 0.6 million ESALs, while layer thickness still has a significant influence on rutting life, its impact on fatigue life becomes more evident. This is due to increased traffic loads and repetitions that result in higher tensile strain predictions within the HMA layers, especially for the 4-in. HMA, making fatigue performance more critical.

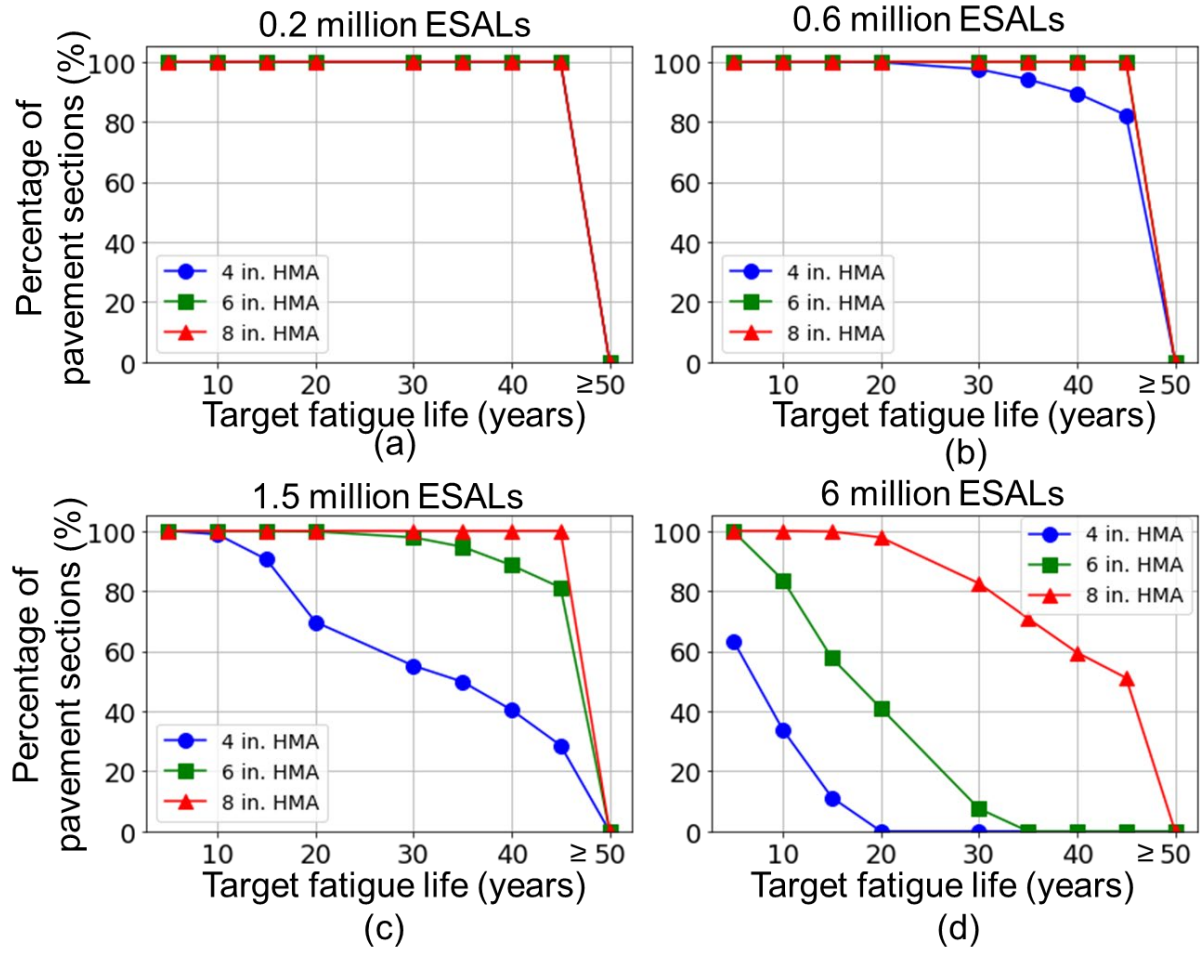

Figure 43. HMA layer thickness affecting fatigue life for (a) 0.2 million ESALs, (b) 0.6 million ESALs, (c) 1.5 million ESALs, and (d) 6 million ESALs.

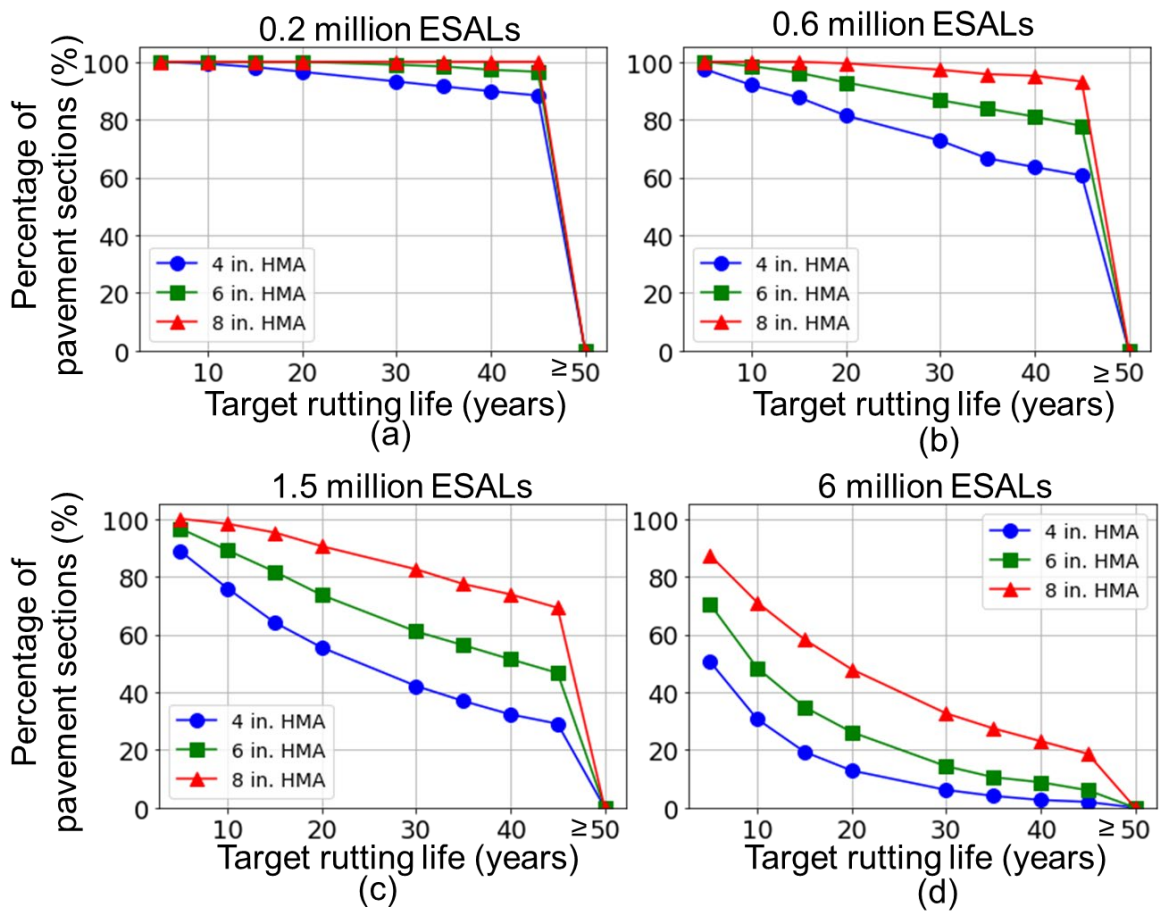

Figure 44. HMA layer thickness affecting rutting life for (a) 0.2 million ESALs, (b) 0.6 million ESALs, (c) 1.5 million ESALs, and (d) 6 million ESALs.

5.2.2 Effect of Aggregate Base Layer Thickness on Performance

Figures 45 and 46 show how aggregate base layer thickness (varying from 4 in. to 12 in.) affects fatigue and rutting lives, respectively, in a standard structure with a 4-in. thick HMA, a 12-in. subbase, and a 12-in. engineered subgrade (modulus = 2 ksi). Although the impact of thickness on fatigue life is not as significant as that of the HMA layer, it still has a notable effect, particularly for target service lives exceeding 0.6 million ESALs. Comparing Figures 45 and 46, aggregate base layer thickness plays a more critical role in controlling rutting than fatigue cracking across all traffic levels. This indicates that, for an aggregate base layer of given quality, increasing thickness could protect the subgrade from rutting damage and extend pavement rutting life.

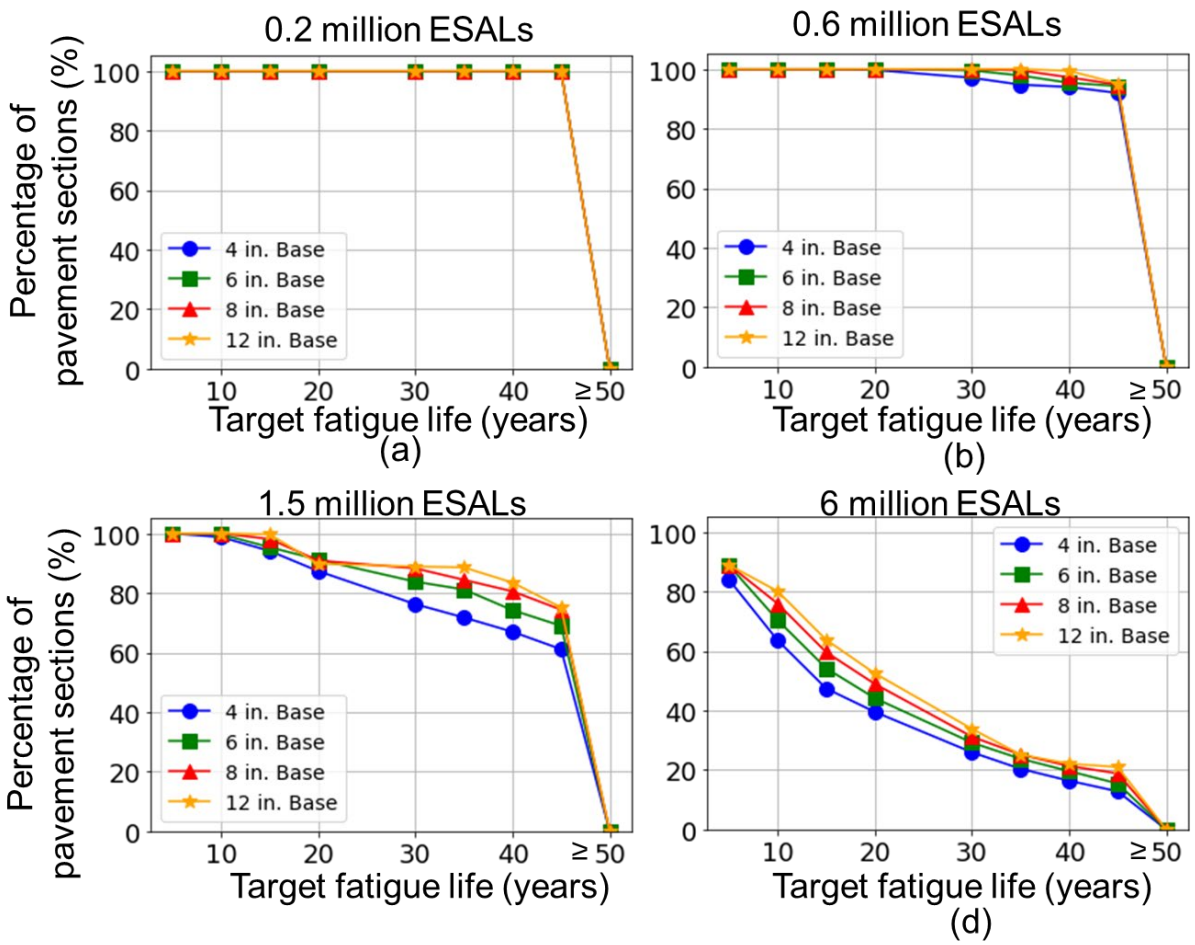

Figure 45. Effect of aggregate base layer thickness on fatigue life for (a) 0.2 million ESALs, (b) 0.6 million ESALs, (c) 1.5 million ESALs, and (d) 6 million ESALs.

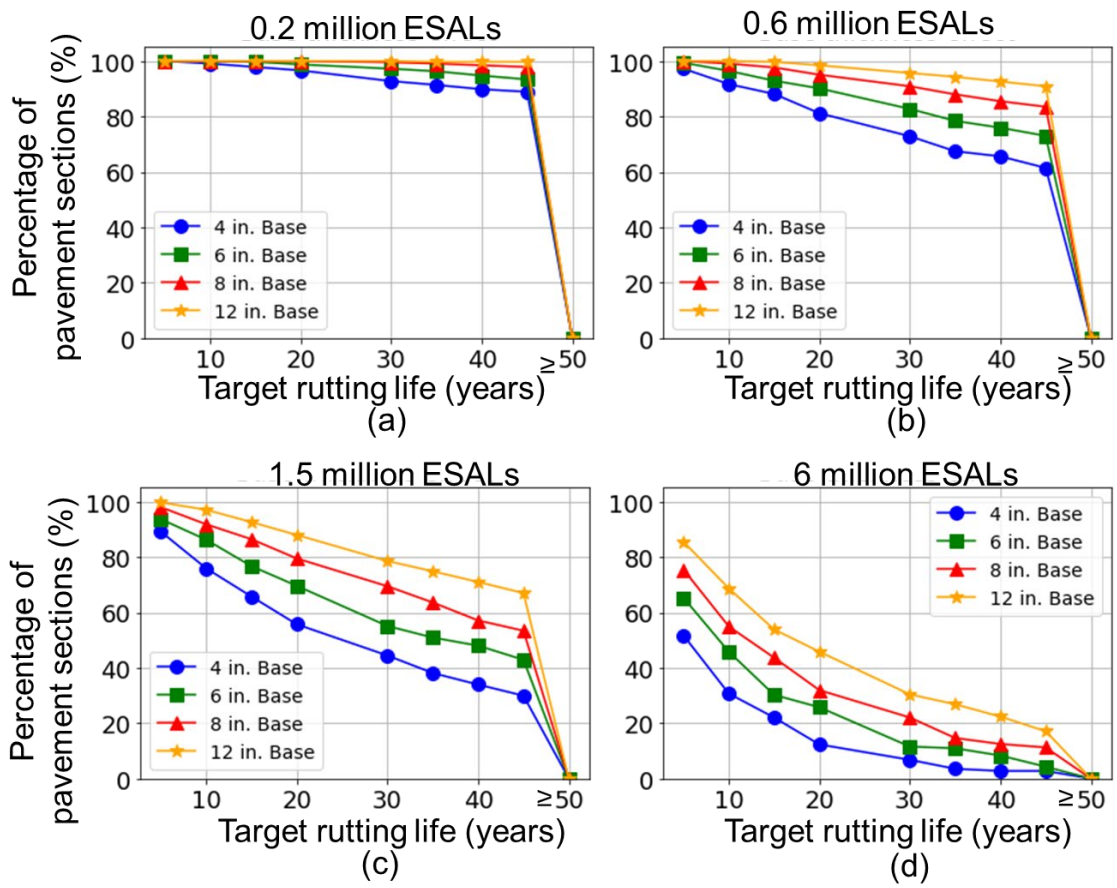

Figure 46. Aggregate Base layer thickness effect on rutting life for (a) 0.2 million ESALs, (b) 0.6 million ESALs, (c) 1.5 million ESALs, and (d) 6 million ESALs.

5.2.3 Effect of Subbase Layer Thickness on Performance

Figures 47 and 48 illustrate the effect of subbase layer thickness on pavement performance. The standard structure consists of a 4-in. HMA layer underlain by a 12-in. aggregate base, a subbase with varying layer thicknesses (6, 12, and 18 in.), and a 12-in. engineered subgrade (modulus = 2 ksi). Like the sensitivity analysis results for the case of varying aggregate base layer thicknesses, Figures 47 and 48 clearly indicate that the subbase layer thickness has a more pronounced impact on rutting life than fatigue life.

A comparison of the effects of aggregate base and subbase layer thicknesses on pavement service life for both fatigue and rutting, as shown in Figures 45 and 47 and Figures 46 and 48, respectively, reveals that aggregate base and subbase layer thicknesses contribute similarly to fatigue and rutting performance trends. It can be concluded that supplementing the aggregate base layer with a thick subbase layer can achieve a comparable service life expectancy, offering flexibility in pavement design to optimize material use and performance.

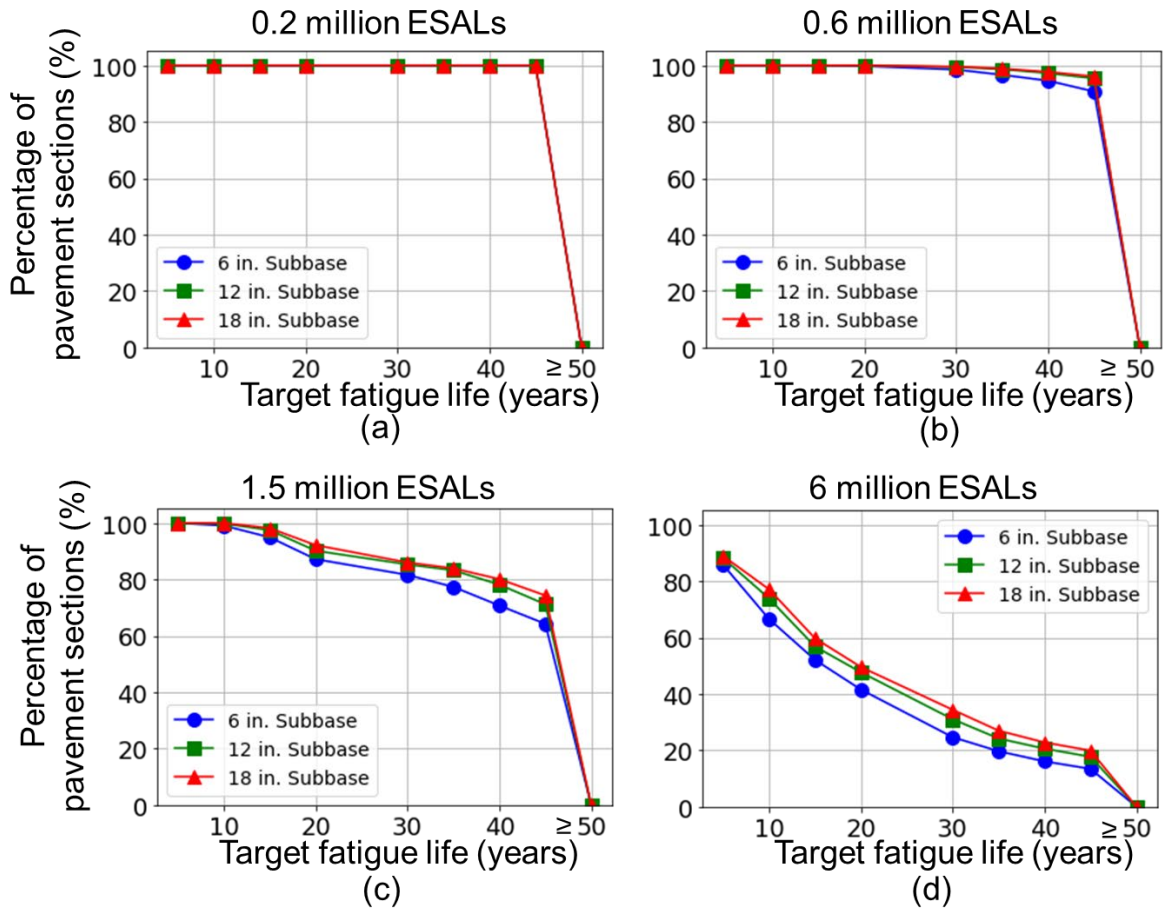

Figure 47. Effect of subbase layer thickness on fatigue life for (a) 0.2 million ESALs, (b) 0.6 million ESALs, (c) 1.5 million ESALs, and (d) 6 million ESALs.

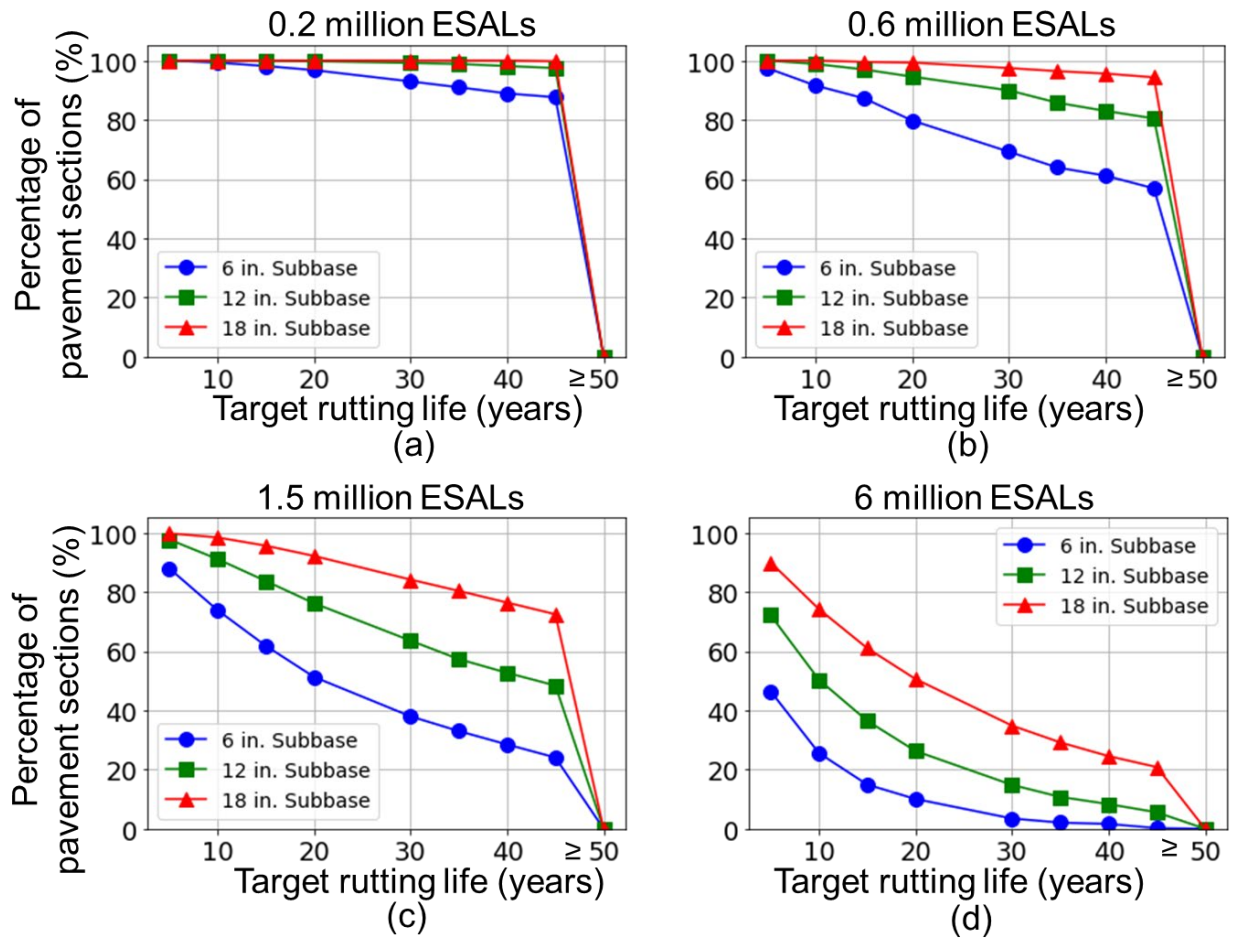

Figure 48. Effect of subbase layer thickness on rutting life for (a) 0.2 million ESALs, (b) 0.6 million ESALs, (c) 1.5 million ESALs, and (d) 6 million ESALs.

5.2.4 Effect of Unbound Granular Material Quality on Performance

The effect of unbound aggregate quality on the aggregate base and subbase combination on pavement fatigue life prediction is illustrated in Figure 49. The standard pavement structure again consisted of 4-in. HMA over a 12-in. aggregate base and a 12-in. subbase over a 12-in. engineered subgrade (modulus = 2 ksi). In Figure 49, the first letter in the legend refers to the aggregate base layer quality: high (H), medium (M), or low (L), while the second letter refers to the subbase layer quality, also ranging from high (H), medium (M), to low (L). Figure 49 demonstrates that both aggregate base and subbase layer quality aspects significantly influence fatigue life. For design traffic levels below 0.6 million ESALs, all material quality combinations in the aggregate base and subbase could achieve a 20-year fatigue life, suggesting that material costs for low-volume roads could be reduced by using lower-quality aggregate base and subbase materials without any premature pavement failure, thereby achieving the targeted design service life. For traffic levels higher than 0.6 million ESALs, however, changes in subbase quality from high (H) to low (L) have a less significant effect on fatigue life than changes in aggregate base layer quality, highlighting the critical role of base layer quality in determining fatigue life expectancy.

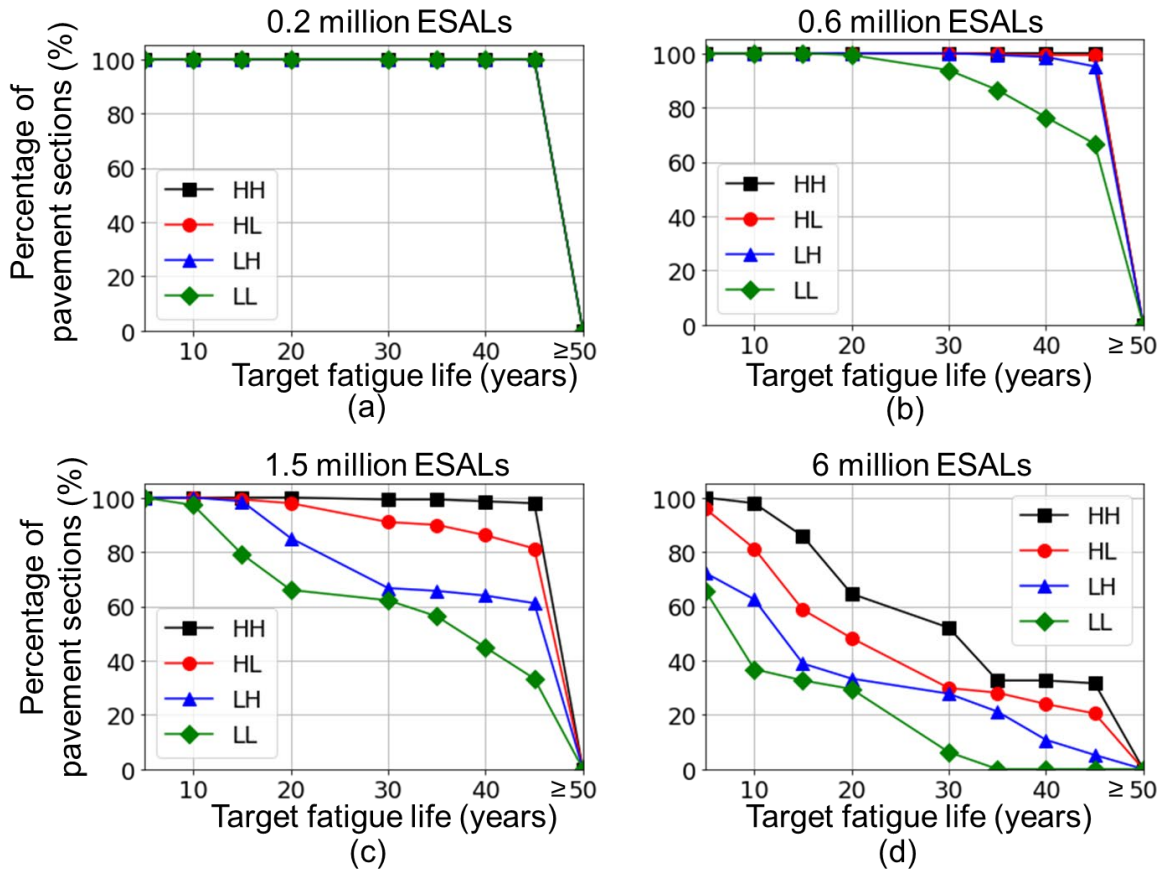

Figure 49. Unbound granular material quality in the aggregate base and subbase influencing fatigue life for (a) 0.2 million ESALs, (b) 0.6 million ESALs, (c) 1.5 million ESALs, and (d) 6 million ESALs. HH refers to a high-quality aggregate base and high-quality subbase, HL refers to a high-quality aggregate base and low-quality subbase, LH refers to a low-quality aggregate base and high-quality subbase, and LL refers to a low-quality aggregate base and low-quality subbase.

The effect of unbound aggregate quality on pavement rutting life prediction is illustrated in Figure 50. The standard pavement structure consists of a 4-in. HMA over a 12-in. aggregate base and a 12-in. subbase, placed on a 12-in. engineered subgrade (modulus = 2 ksi). The results show that pavement rutting life decreases as the granular material quality in the aggregate base and subbase layers decreases from high (H) to low (L) across all traffic levels, particularly for the 4-in. HMA, indicating that stiffer and better quality aggregate layers are essential for protecting the subgrade layer from rutting damage. The reduction in aggregate base layer quality from high (H) to low (L) has a less siginificant effect on rutting life compared to the reduction in subbase layer quality. This finding is in agreement with the recommendations of project MN/RC 2012-01 and suggests that subbase layer quality plays a more critical role in determining rutting performance. Low-quality aggregate base layer and high-quality subbase layer (LH) combinations performs similarly to, and slightly better than, high-quality aggregate base layer and low-quality subbase (HL) combinations, highlighting the compensatory effect of a high-quality subbase in protecting the subgrade and mitigating the negative impacts of a low-quality aggregate base layer.

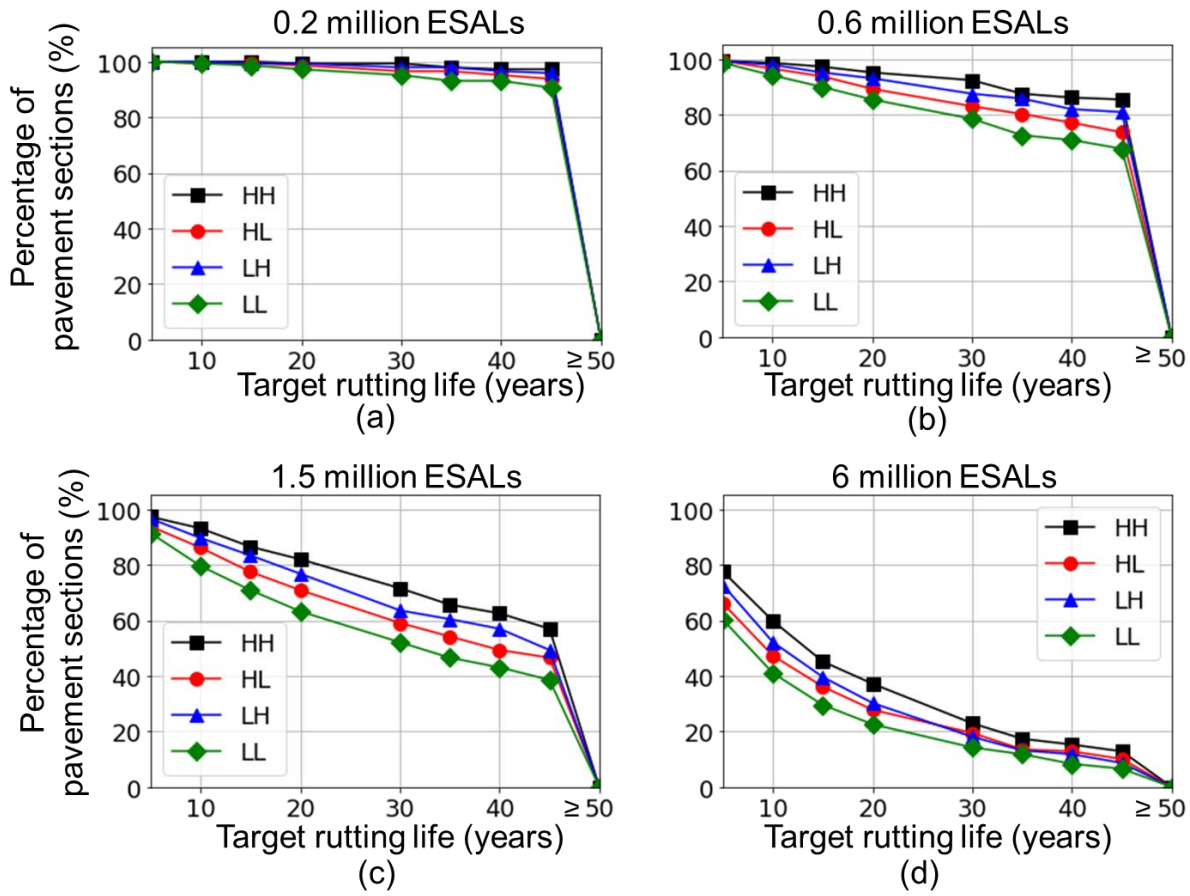

Figure 50. Unbound granular material quality in the aggregate base and subbase influencing rutting life for (a) 0.2 million ESALs, (b) 0.6 million ESALs, (c) 1.5 million ESALs, and (d) 6 million ESALs. HH refers to a high-quality aggregate base and high-quality subbase, HL refers to a high-quality aggregate base and low-quality subbase, LH refers to a low-quality aggregate base and high-quality subbase, and LL refers to a low-quality aggregate base and low-quality subbase.

5.2.5 Combined Effects of Thickness and Quality on Performance

From the above discussion, both unbound aggregate layer thicknesses and aggregate material qualities exhibit important influences on pavement performance trends making it somewhat difficult to single out and distinguish the individual aggregate base and subbase layer contribution to the pavement structure in flexible pavement design and analysis. Minnesota pavement design methodology for low volume roads commonly incorporates a GE factor based on the AASHTO flexible pavement design method (AASHTO, 1993) to quantify each layer's contribution to the entire pavement structure. The GE factors reflect the different pavement material contributions to pavement structural adequacy by taking the MnDOT's Class 5 aggregate base as a standard (Jibon et al., 2024). Jibon et al. (2024) mentioned GE factor estimated the material's contribution to pavement strength compared to Class 5/Class 6 materials, so it is reasonable to use the combined dataset of Class 5 and Class 6 to obtain the reference value for GE computation.

5.2.5.1 Estimation of Granular Equivalency

Because the GE factors estimate the materials contribution to pavement strength compared to Class 5 and Class 6 materials, it was critical to determine the M_R of Class 5 and Class 6 materials as a reference. Chapter 4 generated a combined aggregate materials database that included the most recent AIP database and MN/RC 2012-01 aggregate property database. The average M_R of Class 5 and Class 6 materials in this database was assumed to be the reference in this project. In accordance, Figure 51 presents the M_R of all 1,668 sample materials (Class 5 and Class 6 aggregates) from the combined database with values estimated at a typical stress state (confining pressure = 5 psi, deviator stress = 15 psi). The average M_R was found to be 30 ksi for the Class 5 and Class 6 reference modulus in GE estimation. Table 28 lists the GE factors for aggregate base and subbase materials at high, medium, and low aggregate quality levels.

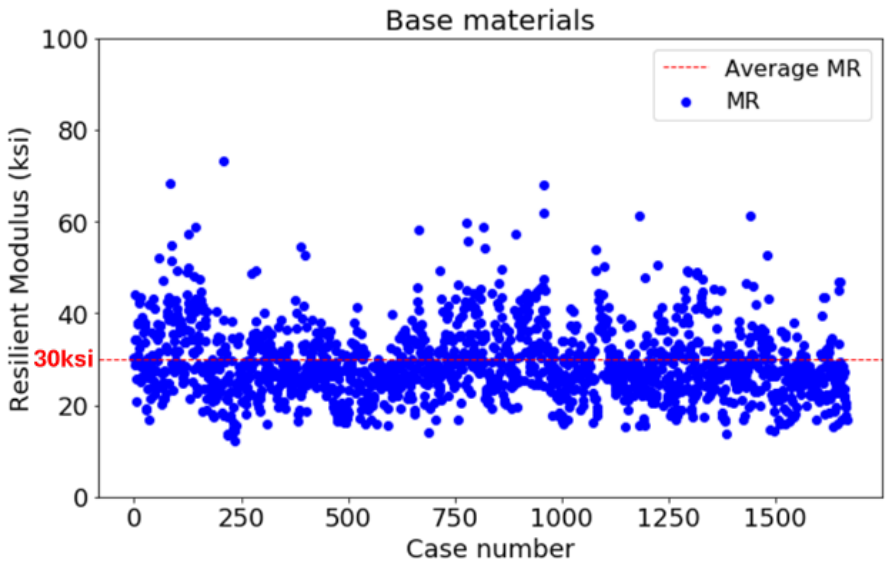

Figure 51. Average aggregate base material resilient modulus.

Table 28. Granular equivalency factors for aggregate base and subbase aggregate materials

Layer	Parameter	Aggregate Base Materials			Subbase Aggregate Materials		
	Materials level of Quality	High	Medium	Low	High	Medium	Low
4-in. HMA	M_R (ksi)	30	23	13	23	16	8
	GE Factor	1.0	0.8	0.4	0.8	0.5	0.3
6-in. HMA	M_R (ksi)	21	17	9	22	14	7
	GE Factor	0.7	0.6	0.3	0.7	0.5	0.2
8-in. HMA	M_R (ksi)	19	15	8	22	14	7
	GE Factor	0.6	0.5	0.3	0.7	0.5	0.2

For local agencies/counties in Minnesota, design procedure uses GE thickness to define pavement structural adequacy. The GE thickness is defined by Equation 9 as follows (Fredrickson et al., 1970):

$$GE = a_1D_1+a_2D_2+a_3D_3+\ldots \quad (9)$$

Where:

GE = granular equivalency thickness for a designed pavement section, in inches,
a_1, a_2, a_3, ... = granular equivalency factor of the given layer material, and
D_1, D_2, D_3… = thickness of individual layers, in inches.

In this chapter, for better quantification of the effect of contribution of aggregate base and subbase layers on pavement performance trends, GE thicknesses for aggregate base and subbase layers were defined as stated in Equations 10 and 11, based on the GE thickness concept.

$$GEbase = GEf\text{-}base \times Dbase \quad (10)$$

$$GE_{subbase} = GE_{f\text{-}subbase} \times D_{subbase} \quad (11)$$

where

GE_{base},$GE_{subbase}$ = granular equivalency thicknesses for aggregate base and subbase layers, in inches,
$GE_{f\text{-}base}$, $GE_{f\text{-}subbase}$ = granular equivalency factor for a given aggregate base and subbase material, and
$D_{base,}$ $D_{subbase}$ = thickness of aggregate base and subbase layers, in inches.

5.2.5.2 Effect of Granular Equivalency Thickness for Aggregate Base and Subbase Layers on Performance

Figures 52 through 55 show the effects of GE thicknesses of aggregate base and subbase on pavement performance trends for 0.2 million, 0.6 million, 1.5 million and 6 million ESALs. The standard pavement structure consists of a 4-in. HMA layer and with various quality and thickness considerations of aggregate base and subbase layers over a 12-in. subgrade (modulus = 2 ksi). Pavement service lives tend to increase with increasing GE thickness values. Assume that 20 years of service life is the target service life in this study. For less than 1.5 million ESALs, rutting might be more critical than fatigue because almost all quality combinations could achieve targeted fatigue service lives, although there exist cases for the LL quality combination with 4 in. HMA layer that might need improvement to achieve target service life for 0.6 million ESALs as shown in Figure 53. If the design fatigue life has been achieved and needs to reach design rutting service life, employing a LL quality combination of aggregate base and subbase might be a more economic option because GE_{base}+$GE_{subbase}$ for LL quality was lower than that of other quality combinations. That confirms that locally available and marginal materials could be used to economically construct low volume roads.

For traffic volumes of 1.5 million ESALs and higher, fatigue life depends more on aggregate base layer quality. Specifically, at 1.5 million ESALs, pavement structures exhibit two distinct plateaus in fatigue life based on low and combined medium/high quality aggregate base layers. At 6 million ESALs, fatigue life exhibits three plateaus corresponding to low, medium, and high-quality aggregate base layers. That means when a certain quality of materials has been used in the aggregate base, increasing GE values by increasing layer thickness does not improve fatigue life because there is not enough support under HMA to minimize bending under wheel loading. Additionally, as shown in Figure 54, the drops in fatigue life for the LH combination at the plateau region occur because the low-quality aggregate base has a

modulus of 13 ksi, significantly lower than the high-quality subbase (23 ksi). In these cases, increasing GE by adding more aggregate base thickness does not effectively enhance fatigue life, though it does improve rutting resistance. Therefore, when the aggregate base quality is lower than the subbase quality, fatigue life improvements reach a limit beyond a certain GE value. Simply increasing aggregate base thickness beyond this point is not an efficient strategy for enhancing fatigue life.

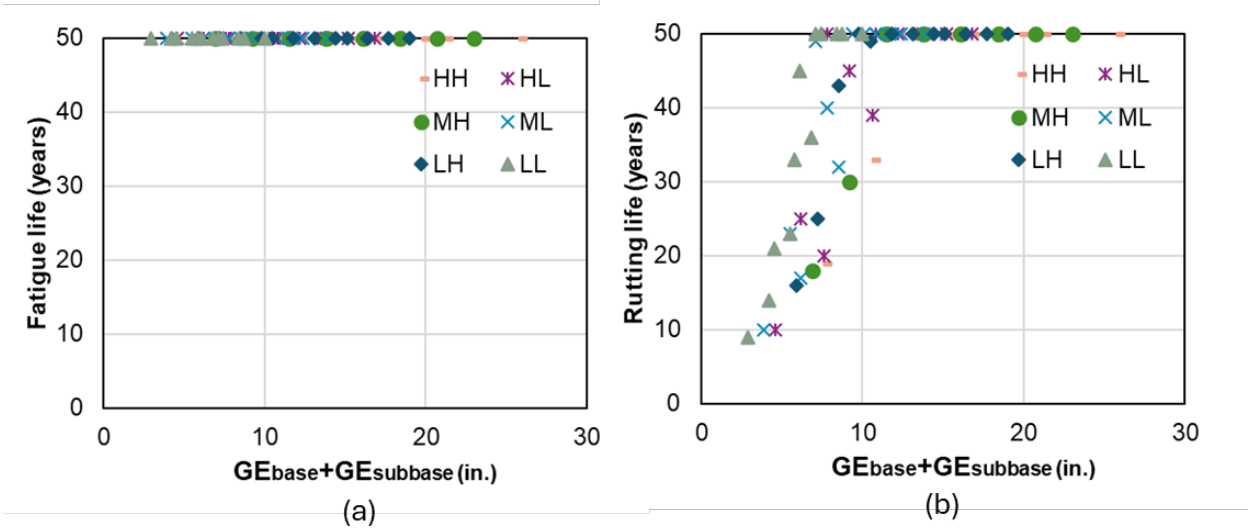

Figure 52. Effect of granular equivalency thickness for aggregate base and subbase layers on pavement performance for 0.2 million ESALs. HH refers to a high-quality aggregate base and high-quality subbase, HL refers to a high-quality aggregate base and low-quality subbase, MH refers to a medium-quality aggregate base and high-quality subbase, and ML refers to a medium-quality aggregate base and low-quality subbase, LH refers to a low-quality aggregate base and high-quality subbase, and LL refers to a low-quality aggregate base and low-quality subbase. (a) Fatigue life (years) and (b) Rutting life (years)

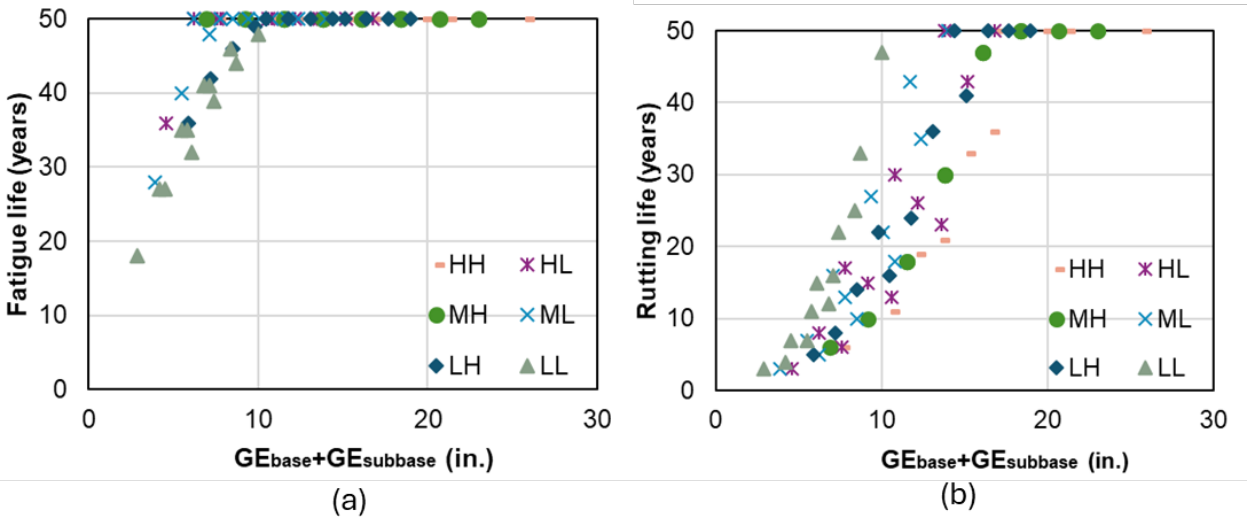

Figure 53. Effect of granular equivalency thickness for aggregate base and subbase layers on pavement performance for 0.6 million ESALs. HH refers to a high-quality aggregate base and high-quality subbase, HL refers to a high-quality aggregate base and low-quality subbase, MH refers to a medium-quality aggregate base and

high-quality subbase, and ML refers to a medium-quality aggregate base and low-quality subbase, LH refers to a low-quality aggregate base and high-quality subbase, and LL refers to a low-quality aggregate base and low-quality subbase. (a) Fatigue life (years) and (b) Rutting life (years)

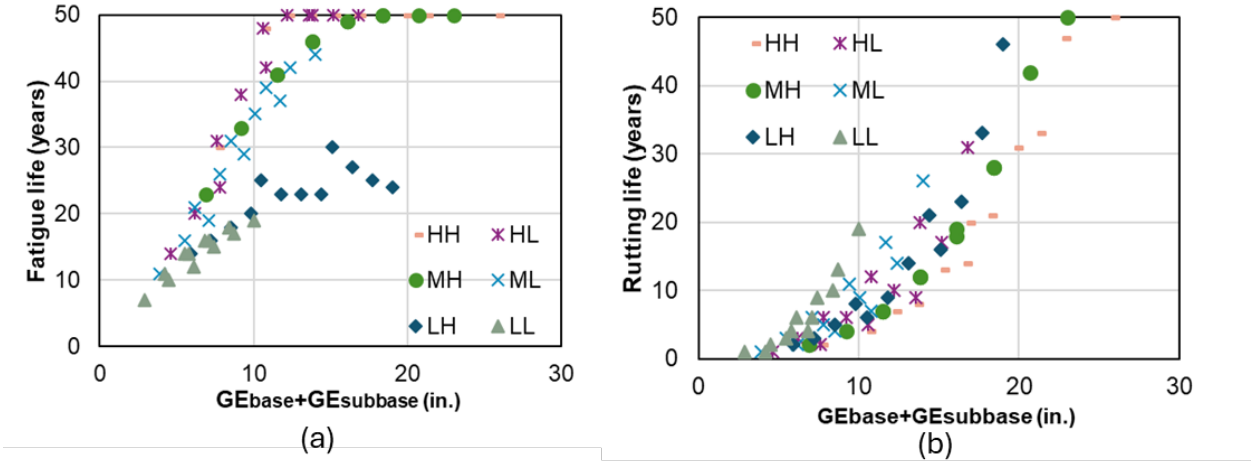

Figure 54. Effect of granular equivalency thickness for aggregate base and subbase layers on pavement performance for 1.5 million ESALs. HH refers to a high-quality aggregate base and high-quality subbase, HL refers to a high-quality aggregate base and low-quality subbase, MH refers to a medium-quality aggregate base and high-quality subbase, and ML refers to a medium-quality aggregate base and low-quality subbase, LH refers to a low-quality aggregate base and high-quality subbase, and LL refers to a low-quality aggregate base and low-quality subbase. (a) Fatigue life (years) and (b) Rutting life (years)

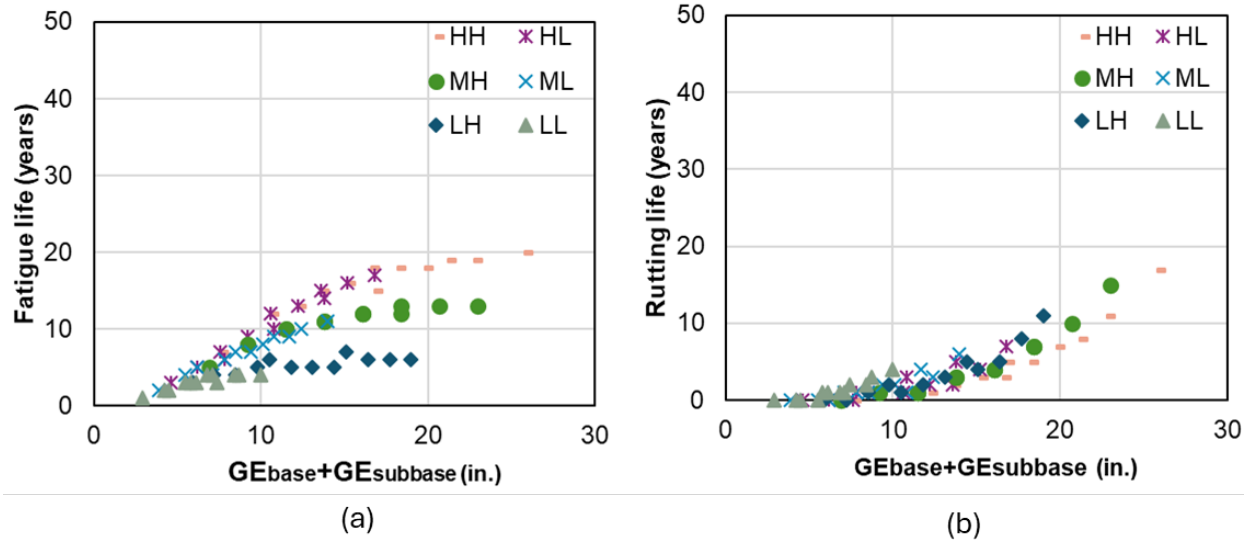

Figure 55. Effect of granular equivalency thickness for aggregate base and subbase layers on pavement performance for 6 million ESALs. HH refers to a high-quality aggregate base and high-quality subbase, HL refers to a high-quality aggregate base and low-quality subbase, MH refers to a medium-quality aggregate base and high-quality subbase, and ML refers to a medium-quality aggregate base and low-quality subbase, LH refers to a low-quality aggregate base and high-quality subbase, and LL refers to a low-quality aggregate base and low-quality subbase. (a) Fatigue life (years) and (b) Rutting life (years)

5.2.6 Effect of Subgrade on Performance

The effects of subgrade modulus on fatigue and rutting performance trends are illustrated in Figures 56 and 57, respectively. The standard pavement structure used for this analysis consisted of a 4-in. asphalt concrete surfacing over a 12-in. aggregate base and a 12-in. subbase, placed over a 12-in. engineered subgrade. The subgrade modulus values considered were 2 ksi, 4 ksi, 7 ksi, and 10 ksi. Comparison of Figure 56 and Figure 57 reveals that the subgrade modulus has a limited impact on fatigue performance but significantly influences rutting performance. This is because, in MnPAVE analysis, rutting is primarily governed by the vertical strain on top of the subgrade. For traffic levels below 0.6 million ESALs, the subgrade condition has a negligible influence on pavement fatigue. These findings suggest that, for low-volume roads, the design life for fatigue performance is more dependent on the granular material qualities and layer thicknesses of the HMA, aggregate base, and subbase layers than on the subgrade modulus.

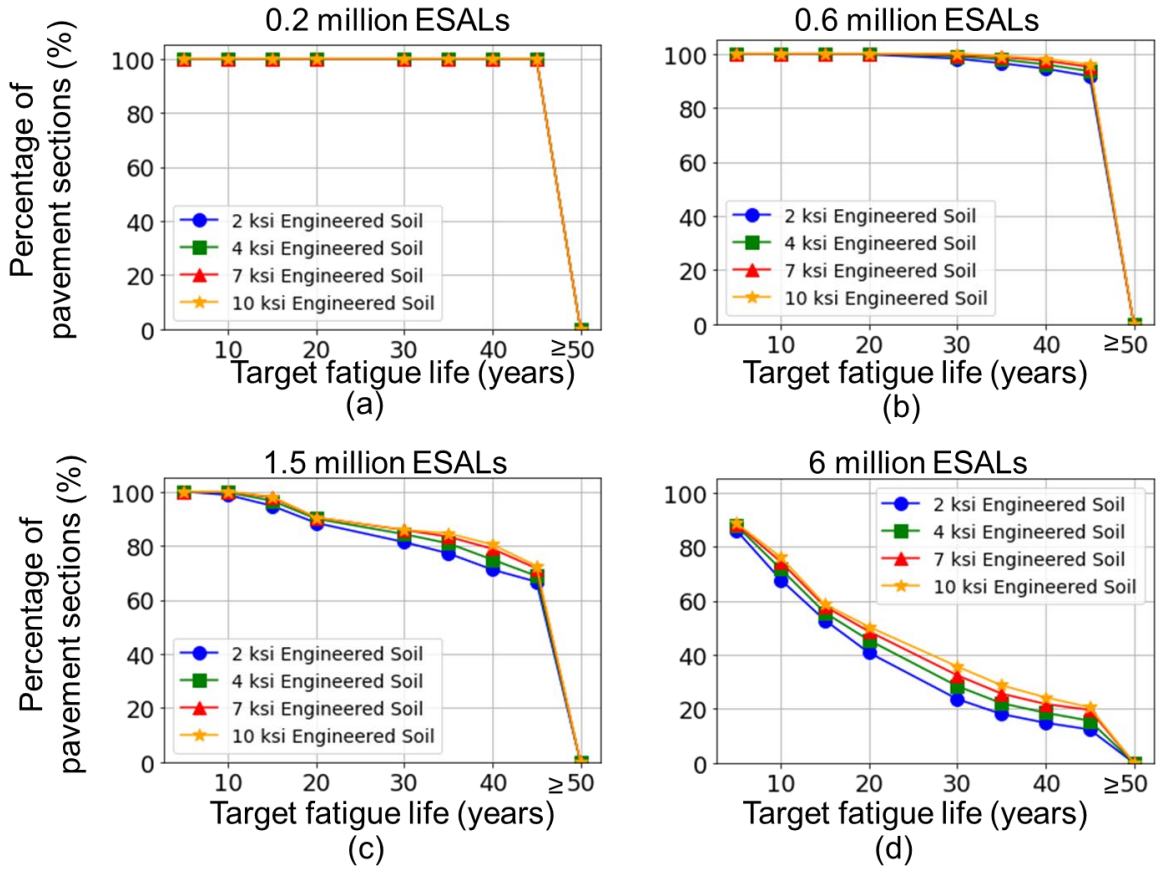

Figure 56. Effect of subgrade elastic modulus on fatigue for (a) 0.2 million ESALs, (b) 0.6 million ESALs, (c) 1.5 million ESALs, and (d) 6 million ESALs.

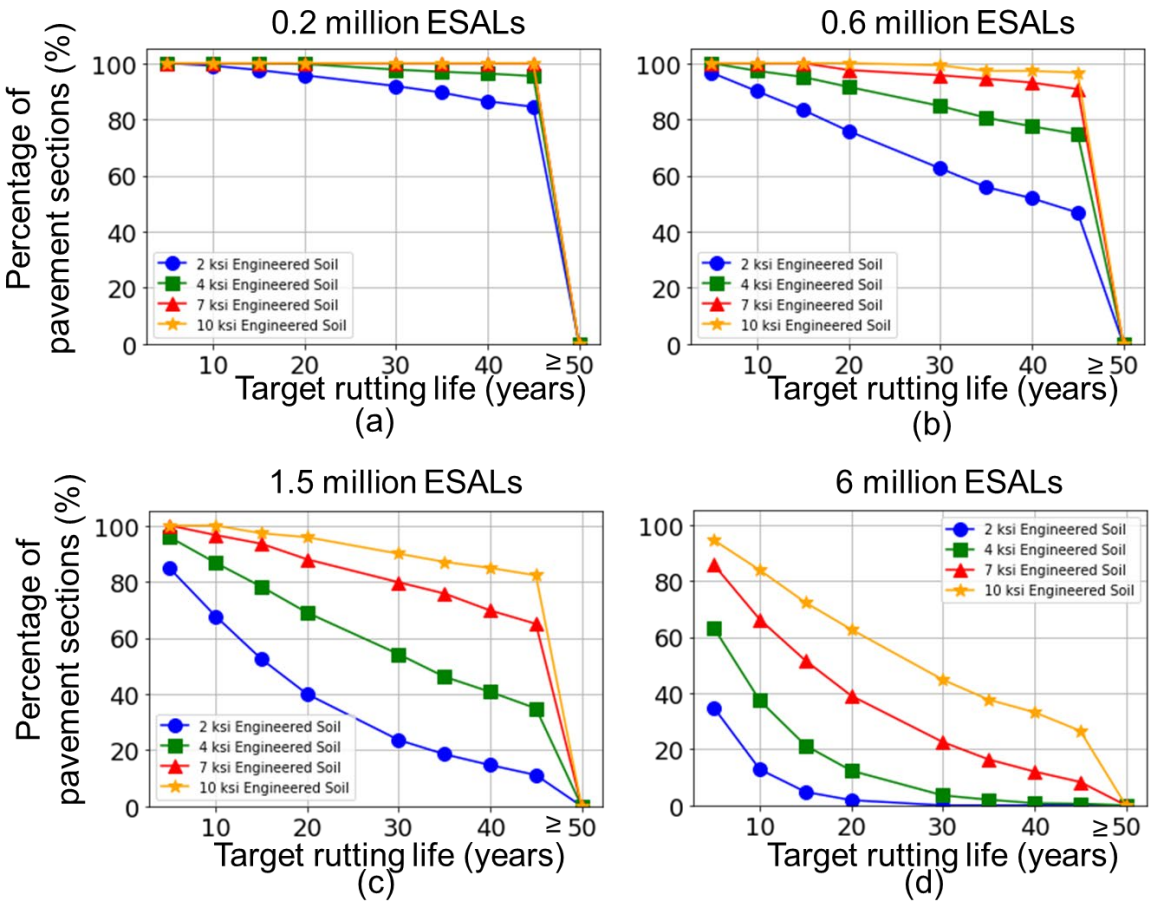

Figure 57. Effect of subgrade elastic modulus on rutting for (a) 0.2 million ESALs, (b) 0.6 million ESALs, (c) 1.5 million ESALs, and (d) 6 million ESALs.

5.3 Summary

A comprehensive matrix of conventional flexible pavement sections was analyzed using MnPAVE to evaluate key design factors, including climatic conditions, HMA/aggregate base/subbase thicknesses, aggregate quality, and subgrade conditions. The analysis results are summarized in this chapter for important pavement performance trends influenced by the design factors studied. In accordance, the key findings presented herein provide important design considerations for Chapter 6, which is about the aggregate base and subbase thickness optimizations when high-quality materials are in limited supply.

The findings of this chapter regarding the aggregate base and subbase layer properties, thickness requirements and quality aspects are as:

- Four counties from different climate zones (Beltrami, Todd, Redwood, and Olmsted) were selected to reflect varying temperature and seasonal freeze-thaw conditions. Results showed that moving from North to South generally decreases pavement service life due to shorter winters, longer summers, and higher seasonal temperatures.

- Increasing HMA thickness substantially enhances fatigue life for traffic levels beyond 0.6 million ESALs, while at lower traffic volumes, HMA thickness plays a more prominent role in rutting resistance rather than fatigue performance. When traffic demands exceed 1.5 million ESALs, a thin HMA layer (e.g., 4 in.) cannot be fully compensated for by a thicker aggregate base or subbase layer alone.
- While both aggregate base and subbase layers influence fatigue and rutting performance trends, their thicknesses are particularly critical for controlling permanent deformation (i.e., rutting). For design traffic levels below 0.6 million ESALs, relatively thin aggregate base/subbase sections can still achieve 20-year performance lives. Beyond 0.6 million ESALs, thicker or higher-quality aggregate base layers become more essential for preventing fatigue cracking, while a higher subbase thickness most directly protects against rutting damage.
- Low-quality (L) aggregate layers with specific thicknesses can suffice for low-volume roads, enabling 20-year fatigue and rutting lives at or below 0.6 million ESALs. However, once traffic exceeds 1.5 million ESALs, higher aggregate base quality is particularly critical to meet satisfactory fatigue performance requirements. Conversely, subbase quality exerts a stronger influence on rutting life, meaning a high-quality subbase layer can partially offset a lower-quality aggregate base layer if the traffic level remains moderate (e.g., around 1.5 million ESALs).
- For local agencies/counties, design uses GE factors to quantify how much each aggregate layer contributes to the overall structural capacity, with MnDOT Class 5 and Class 6 used as a reference. In this study, GE values were determined by considering the moduli and thicknesses of selected aggregate materials (low, medium, and high quality). GE-based analyses highlighted that while at lower traffic levels, most combinations of aggregate layer quality and thickness can achieve the target service life under different HMA thicknesses. However, for higher traffic levels (greater than or equal to 1.5 million ESALs), insufficient aggregate base quality cannot be compensated solely by increasing the thickness of low-quality aggregate layers, underscoring the need to enhance the aggregate base layer quality.
- Subgrade moduli ranging from 2 to 10 ksi often reflected a minor impact on fatigue life through the MnPAVE analyses, however, exhibited significant influences on rutting performance by changing vertical stresses and strains on the top of the subgrade. For low-volume roads, subgrade conditions can be less of a concern than aggregate thickness and quality, but at higher traffic levels, improved subgrade properties (e.g., engineered subgrade) can prolong rutting life.

Aggregate base and subbase thicknesses are generally more important for controlling rutting, while HMA thickness is more critical for fatigue once traffic demand increases. Local available, lower-quality aggregate materials can be used effectively for low-volume roads (up to 0.6 million ESALs) to achieve 20-year service life. At higher traffic levels, aggregate base-layer quality largely determines fatigue performance, while subbase quality strongly affects rutting.

Chapter 6: Cost-Benefit Analyses of Various Design Alternatives

In Chapter 6, the objectives are to evaluate and compare the various proposed designs entailing different aggregate base/subbase layer thicknesses and material qualities for their potential costs and benefits. The different designs will be rated in terms of benefit-to-cost ratios to determine the top design recommendations for scenarios where a thicker subbase is utilized when high-quality aggregate materials are in short supply. This chapter will recommend potential pavement designs to MnDOT and local agencies after defining cut-off limits for subbase thickness and minimum aggregate quality requirements to ensure that the designs are cost-effective and beneficial.

This chapter outlines an approach for optimizing pavement design. Various design alternatives, featuring different combinations of aggregate base and subbase aggregate layer thicknesses and granular material qualities, assessed by M_R values, will be compared to identify the most cost-effective solutions. Recommendations for pavement designs will be provided to MnDOT and local agencies seeking to ensure cost savings and sustained performance.

Two primary steps have been undertaken in this chapter. First, the most cost-effective aggregate base and subbase quality combinations have been determined by comparing material costs against projected performance. Next, a flowchart-based iterative process has been employed to refine aggregate base and subbase thicknesses until an optimized design is identified.

6.1 Method for Determining Optimized Design

6.1.1 Optimization Scope

The impacts of various pavement design factors, including layer thickness, aggregate base and subbase quality, and subgrade condition, on pavement fatigue and rutting performance trends were thoroughly investigated in Chapter 5, producing findings indicating that aggregate base and subbase layer thicknesses, along with aggregate base and subbase materials quality assessed by M_R values, could result in cost-effective design combinations under specific scenarios. Since these scenarios depend on factors such as traffic levels, HMA layer thickness, and subgrade conditions, this chapter aims to determine optimized aggregate base and subbase designs for each identified scenario.

The optimization process is comprised of two distinct phases:

1. The first step, highlighted in Table 29, involves the evaluation of various design cases to assess the benefit-cost relationships, with the objective of identifying the optimal quality combination for aggregate base and subbase materials.

2. Following the selection of an optimal quality combination, the second step focuses on refining the thickness requirements of unbound aggregate base and subbase courses. This iterative process continues until an optimized design is achieved for each scenario under consideration.

The optimization scope is listed in Table 29. Based on the 48 cases identified in Table 29, this chapter develops a systematic methodology to assist practitioners in determining the most cost-effective designs with respect to quality and thickness selection for the aggregate base and subbase layers.

Table 29. Optimization scope

Input Category	Number of Variables	Input Variables
Design Traffic Volume	4	0.2, 0.6, 1.5 and 6 million ESALs
Asphalt PG 58H-34	3	Resilient Modulus: 526 ksi for Fall Season
		Thickness (in.): 4, 6, 8
		Poisson's Ratio: 0.3
Engineered Subgrade	4	Resilient Modulus: 2, 4, 7, 10 ksi
		Thickness (in.): 12
		Poisson's Ratio: 0.45
Undisturbed Subgrade	1	Resilient Modulus: 50% of Engineered Subgrade
		Poisson's Ratio: 0.45

Total Cases: 48

6.1.2 Cost Estimation Approach

The material cost estimation was conducted based on historical bid price data obtained from the MnDOT (2024). Table 30 shows a small portion of the database, showing prices awarded for Class 3, Class 4, Class 5 and Class 6 aggregate materials, along with their corresponding project information.

Table 30. A snapshot of historical bid price database for aggregates

Item Description	Quarter	Contract ID	County	Sp No.	Units	Quantity	Awarded Price	Engineers Estimate	Class
AGGREGATE BASE (CV) CLASS 3	2022Q1	220071	WRIGHT	8680-191	C Y	535.00	53.50	38.00	Class 3+ Class 3 modified
AGGREGATE BASE (CV) CLASS 3	2020Q4	200121	RICE	6605-37	C Y	2966.00	25.73	34.97	Class 3+ Class 3 modified
AGGREGATE BASE (CV) CLASS 3	2024Q1	240003	WATONWAN	8302-48	C Y	73.00	41.00	38.08	Class 3+ Class 3 modified
AGGREGATE BASE (CV) CLASS 3	2022Q1	220071	WRIGHT	8680-191	C Y	535.00	53.50	38.00	Class 3+ Class 3 modified
AGGREGATE BASE (CV) CLASS 3	2020Q4	200121	RICE	6605-37	C Y	2966.00	25.73	34.97	Class 3+ Class 3 modified
AGGREGATE BASE (CV) CLASS 3	2019Q1	190040	MEEKER	4704-89	C Y	3416.00	20.50	36.69	Class 3+ Class 3 modified
AGGREGATE BASE (CV) CLASS 3 MODIFIED	2019Q1	190015	MURRAY	5107-14	C Y	139.00	75.00	42.00	Class 3+ Class 3 modified
AGGREGATE BASE (CV) CLASS 3	2019Q1	190040	MEEKER	4704-89	C Y	3416.00	20.50	36.69	Class 3+ Class 3 modified
AGGREGATE BASE (CV) CLASS 4	2022Q1	220071	WRIGHT	8680-191	C Y	912.00	61.50	47.00	Class 4

The awarded prices for aggregates were categorized into two groups: Class 3 and Class 4 and Class 3 Modified and Class 4 Modified, and Class 5 and Class 6 and Class 5 Modified and Class 6 Modified. Within each group, maximum and minimum prices were assumed to represent the unit costs of high-quality and low-quality materials, respectively. The average of the maximum and minimum prices was calculated to estimate the unit cost for typical medium-quality aggregates, with the resultant unit cost estimations presented in Table 31. For comparative analysis of various design alternatives in this chapter, it was assumed that the total material cost was based on a one-mile, two-lane road configuration. Table 31 provides the estimated costs of aggregate base materials (Class 5 and Class 6 and Class 5 Modified and Class 6 Modified) and subbase materials (Class 3 and Class 4 and Class 3 Modified and Class 4 Modified) per inch of layer thickness.

Table 31. Estimated unit costs of aggregate base and subbase materials for pavement design alternatives

	Min awarded price ($/CY)	Medium awarded price ($/CY)	Max awarded price ($/CY)
Class 5 and Class 6+ Class 5 mod. and Class 6 mod.	23.2	65.0	114.0
Class 3 and Class 4 + Class 3 mod. and Class 4 mod.	20.5	47.8	75.0

	Low quality cost ($ per inch thickness)	Medium quality cost ($ per inch thickness)	Max quality cost ($ per inch thickness)
Aggregate Base cost (Class 5 and Class 6+ Class 5 mod. and Class 6 mod.)	11,317.1	31,680.0	70,183.4
Subbase cost (Class3 and Class 4+ Class 3 mod. and Class 4 mod.)	9,991.4	23,272.6	36,553.9

6.1.3 Step 1: Determination of Minimum Quality Combination

This initial step determines the minimum required qualities for both aggregate base and subbase course materials by evaluating the costs and benefits associated with various design options, including different aggregate layer thicknesses and material qualities. While Chapter 5 established the relationship among pavement fatigue and rutting performance trends and required structural configurations and properties, it did not account for cost considerations, so this step incorporates aggregate base and subbase design options from Chapter 5 to calculate material costs and assess their cost-benefit relationships.

In Table 29, the critical scenario is defined as a pavement structure with a 4-in. HMA layer and a 2-ksi engineered subgrade. This pavement structure serves as the reference case for quality selection of aggregate base and subbase materials across different traffic levels. Figure 58 illustrates performance

trends and total material costs for a traffic level of 1.5 million ESALs in this scenario, using various combinations of aggregate base and subbase thicknesses. The results shown in Figure 58(a) indicate that fatigue life generally increases with a higher pavement structural adequacy; with sufficient structural thickness, all quality combinations can achieve a 20-year fatigue life. Figure 58(b) identifies the LL quality combination for aggregate base-subbase materials to be the most cost-effective, hence meeting the 20-year rutting life requirement. This finding infers that the LL quality combination provides the most economical solution for achieving a 20-year service life when the pavement structure includes an HMA layer thicker than 4 in., a subgrade stiffer than 2 ksi, and traffic volumes below 1.5 million ESALs.

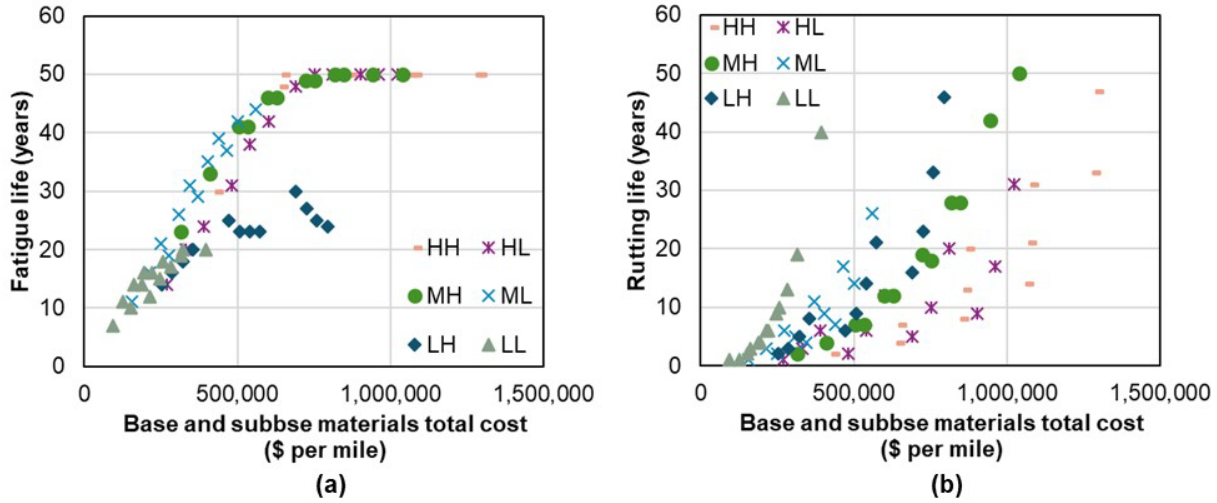

Figure 58. (a) Fatigue and (b) rutting performance trends with total material costs for a pavement structure with 1.5 million ESALs and a 4-in. HMA layer

For pavement structures with a 2-ksi engineered subgrade subjected to a traffic level of 6 million ESALs, specific scenarios were analyzed based on varying HMA layer thicknesses (4, 6, and 8 in.). Figure 59 illustrates a pavement structure scenario designed for 6 million ESALs, consisting of a 4-in. HMA layer and a 2-ksi engineered subgrade. The results show that fatigue life is predominantly influenced by aggregate base layer quality. Notably, pavement structures with low or medium quality aggregate base materials cannot achieve the target service life. Although high-high (HH) quality combinations of aggregate base and subbase materials may partially meet the target service life, it would necessitate excessively thick aggregate base and subbase layers. This analysis highlights that, in this scenario, aggregate base and subbase quality improvements alone cannot offset the inadequacies of an under-designed pavement structure. To meet the target service life, increasing the thickness of the HMA layer would be a more effective approach.

For a pavement structure subjected to 6 million ESALs, consisting of a 6-in. HMA layer and a 2-ksi engineered subgrade, the corresponding fatigue life along with material costs were determined, as illustrated in Figure 60. Figure 60(a) shows that a low-quality aggregate base achieves approximately 15 years of fatigue life, while medium and high-quality bases provide fatigue lives exceeding 20 years. With respect to rutting performance, highlighted in Figure 60(b), all quality combinations with sufficient

aggregate base and subbase thickness can achieve a 20-year service life. Among cost-based optimized design alternatives, the combination of medium-quality aggregate base and low-quality subbase (ML) is the most economical choice while meeting both fatigue and rutting life expectations.

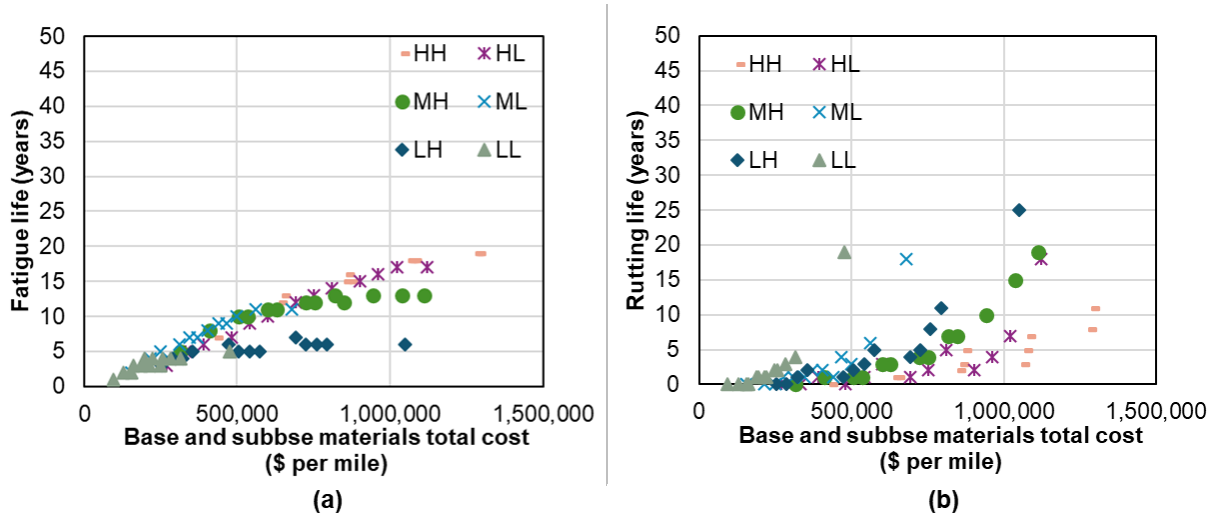

Figure 59. (a) Fatigue and (b) rutting performance trends with total material costs for a pavement structure with 6 million ESALs and a 4-in. HMA layer

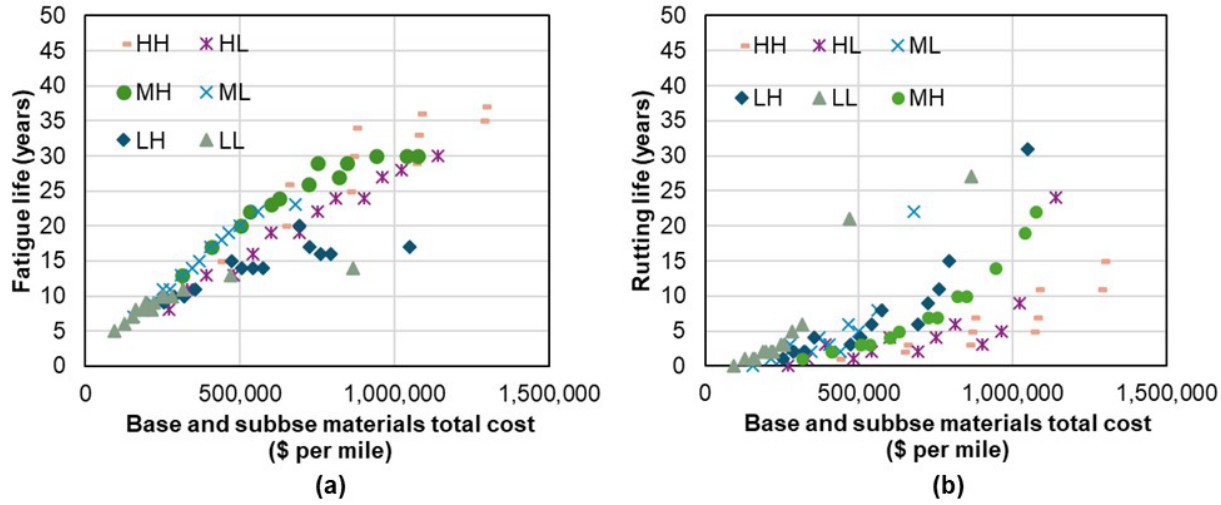

Figure 60. (a) Fatigue and (b) rutting performance trends with total material costs for a pavement structure with 6 million ESALs and a 6-in. HMA layer

With 6 million ESALs of traffic, for a pavement structure with an 8-in. HMA layer and a 2-ksi engineered subgrade, all quality combinations of aggregate base and subbase materials meet the target fatigue. For rutting life, some cases with LL material qualities meet rutting criteria if sufficient thickness was provided. In this case, the LL quality combination is the most cost-effective, as shown in Figure 61.

Based on similar principles, the recommended quality combinations for various scenarios are summarized in Table 32. It is important to note that some cases are labeled as over-designed, meaning that all aggregate base and subbase configurations exceed a 20-year service life. Such over-designed cases fall outside the scope of this study and have not been considered for optimization. Generally, LL quality and ML quality combinations are sufficient to meet the target service lives across all scenarios in this chapter. The LL quality combination is applicable to traffic levels up to and including 1.5 million ESALs, while the ML quality combination is suitable for 6 million ESALs with a structure consisting of 6 in. of HMA. For pavements with an 8 in. HMA, the LL quality combination is sufficient for traffic levels up to 6 million ESALs. In these cases, the use of high-quality aggregate base and subbase materials are not required.

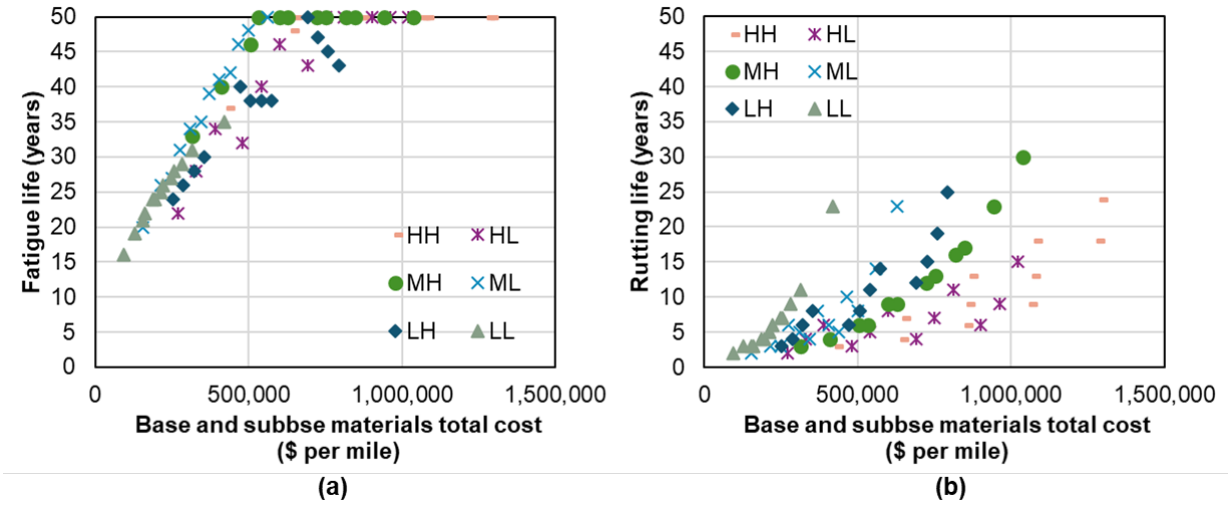

Figure 61. (a) Fatigue and (b) rutting performance trends with total material costs for a pavement structure with 8-in. HMA layer and 2-ksi engineered subgrade when subjected to 6 million ESALs.

Table 32. Quality combination recommendations for various scenarios in Chapter 5

** — Refers to the optimized thickness of aggregate base and subbase that will be determined in Step 2.*
OD— refers to over-designed cases, in which all designs could achieve or exceed target service life.
UD — refers to under-designed cases, in which no designs could achieve target service life by only optimizing aggregate base and subbase.
TO — refers to design cases, in which further optimization of base and subbase thickness is needed.

For engineered subgrade modulus 2 ksi

HMA layer		4 in. HMA				6 in. HMA				8 in. HMA			
Traffic (MESALs)		0.2	0.6	1.5	6	0.2	0.6	1.5	6	0.2	0.6	1.5	6
Optimized design	Design evaluation	TO	TO	TO	UD	OD	TO	TO	TO	OD	OD	TO	TO
	Aggregate quality	LL	LL	LL	-	-	LL	LL	ML	-	-	LL	LL
	Base thickness (in.)	*	*	*	-	-	*	*	*	-	-	*	*
	Subbase thickness (in.)	*	*	*	-	-	*	*	*	-	-	*	*

For engineered subgrade modulus 4 ksi

HMA layer		4 in. HMA				6 in. HMA				8 in. HMA			
Traffic (MESALs)		0.2	0.6	1.5	6	0.2	0.6	1.5	6	0.2	0.6	1.5	6
Optimized design	Design evaluation	OD	TO	TO	UD	OD	OD	TO	TO	OD	OD	OD	TO
	Aggregate quality	-	LL	LL	-	-	-	LL	ML	-	-	-	LL
	Base thickness (in.)	-	*	*	-	-	-	*	*	-	-	-	*
	Subbase thickness (in.)	-	*	*	-	-	-	*	*	-	-	-	*

For engineered subgrade modulus 7 ksi

HMA layer		4 in. HMA				6 in. HMA				8 in. HMA			
Traffic (MESALs)		0.2	0.6	1.5	6	0.2	0.6	1.5	6	0.2	0.6	1.5	6
Optimized design	Design evaluation	OD	OD	TO	UD	OD	OD	OD	TO	OD	OD	OD	TO

HMA layer		4 in. HMA				6 in. HMA				8 in. HMA			
	Aggregate quality	-	-	LL	-	-	-	-	ML	-	-	-	LL
	Base thickness (in.)	-	-	*	-	-	-	-	*	-	-	-	*
	Subbase thickness (in.)	-	-	*	-	-	-	-	*	-	-	-	*

For engineered subgrade modulus 10 ksi

HMA layer		4 in. HMA				6 in. HMA				8 in. HMA			
Traffic (MESALs)		0.2	0.6	1.5	6	0.2	0.6	1.5	6	0.2	0.6	1.5	6
Optimized design	**Design evaluation**	OD	OD	TO	UD	OD	OD	OD	TO	OD	OD	OD	OD
	Aggregate quality	-	-	LL	-	-	-	-	ML	-	-	-	-
	Base thickness (in.)	-	-	*	-	-	-	-	*	-	-	-	-
	Subbase thickness (in.)	-	-	*	-	-	-	-	*	-	-	-	-

6.1.4 Step 2: Determination of The Optimal Thicknesses for Base and Subbase

6.1.4.1 Minimum Thickness Requirement

Using the minimum quality combination of aggregate base and subbase determined in Step 1, Step 2 optimizes the thicknesses of aggregate base and subbase courses until cost-effective designs are selected for each scenario. For optimizing thickness, minimum aggregate base and subbase thicknesses are required, and per MnDOT pavement design manual Chapter 4 (2019b), a 6-in. minimum aggregate base layer thickness is required. Although the MnDOT Pavement Design Manual specifies a minimum total pavement structure thickness (i.e., pavement, aggregate base, and subbase) of 30 in. for 20-year traffic levels $\leq$ 7 million BESALs, a 4-in. minimum thickness was adopted herein because it has been commonly used in conventional flexible pavements based on Unified Facilities Criteria (US Army Corps of Engineers standard, 2004) and Illinois DOT Chapter 44 Pavement Design (2018).

6.1.4.2 Aggregate Base and Subbase Layer Thickness Determination Flowchart

A flowchart was developed in this step to optimize the aggregate base and subbase layer thicknesses for various pavement design scenarios. The process involves two iterative stages. The first stage focuses on

adjusting the aggregate base and subbase thicknesses to meet the fatigue life criteria. Once the aggregate base layer thickness has been finalized in this step, the second stage adjusts only the subbase thickness to meet rutting life expectations. Such a sequential approach is reasonable because fatigue performance is primarily influenced by the aggregate base layer, while rutting performance is governed by both the aggregate base and subbase layers, so by first determining the aggregate base layer thickness, the rutting life can be optimized by modifying the subbase thickness alone. The flowchart serves as a decision-making tool applicable to all cases, providing guidance on determining the appropriate thicknesses of the aggregate base and subbase layers. This step will be detailed through two examples to clearly explain the use of this flowchart.

Example 1:

For pavements designed to support 0.2 million ESALs and 0.6 million ESALs with 4 in. of HMA and engineered subgrade having a modulus of 2 ksi, as indicated in Step 1, a LL quality combination of aggregate base and subbase materials was selected as the minimum quality. Using this quality combination, the effect of aggregate base and subbase thickness on fatigue and rutting life expectations for both traffic levels are presented in Figure 62 and Figure 63.

By applying the flowchart shown in Figure 64, the minimum aggregate base thickness (6 in.) and minimum subbase thickness (4 in.) were found to meet the target fatigue life. This result was validated by Figures 62(a) and 63(a), that demonstrated that all design cases satisfied or exceeded the target fatigue life, even with the assigned minimum aggregate base thickness and minimum subbase thickness. Given the limited availability of aggregate base materials, the selection of a 6 in. aggregate base thickness achieves savings on material costs while satisfying performance requirements.

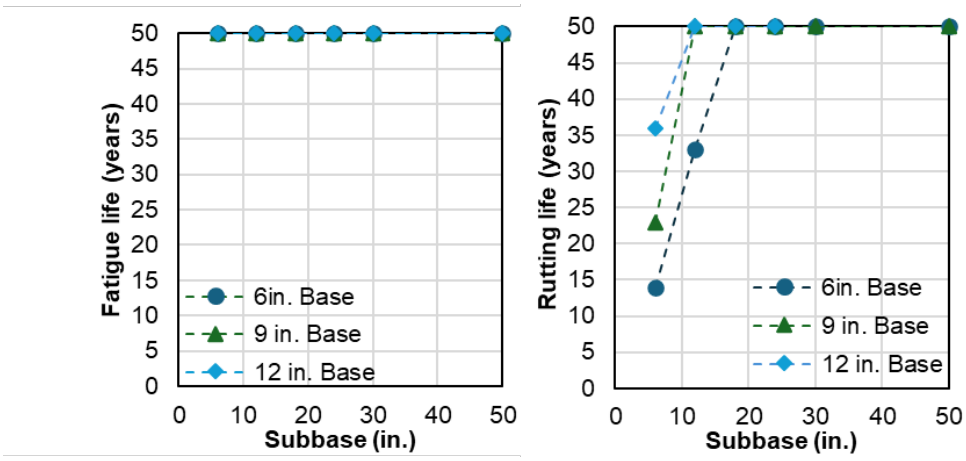

Figure 62. The effects of aggregate base and subbase thicknesses on (a) fatigue and (b) rutting lives for 0.2 million ESALs

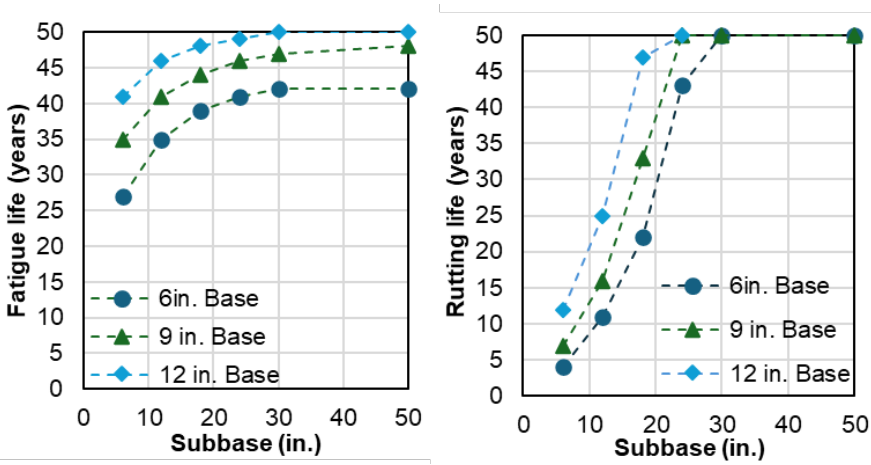

Figure 63. The effects of aggregate base and subbase thicknesses on (a) fatigue and (b) rutting lives for 0.6 million ESALs

To address the rutting issue, the flowchart further guided adjustments to the subbase thickness as highlighted by the red dash lines in Figure 64. It should be noted that MnPAVE was needed for using the flowchart to determine the thickness of aggregate base and subbase. For 0.2 million ESALs, the subbase thickness had to be increased to 9 in. to meet the target rutting life, while for 0.6 million ESALs, the subbase thickness required an increase to 17 in. to satisfy the rutting life criterion. These adjustments ensure that the pavement design adheres to the needed performance requirements under varying traffic loads while allowing local material use and achieving cost effectiveness.

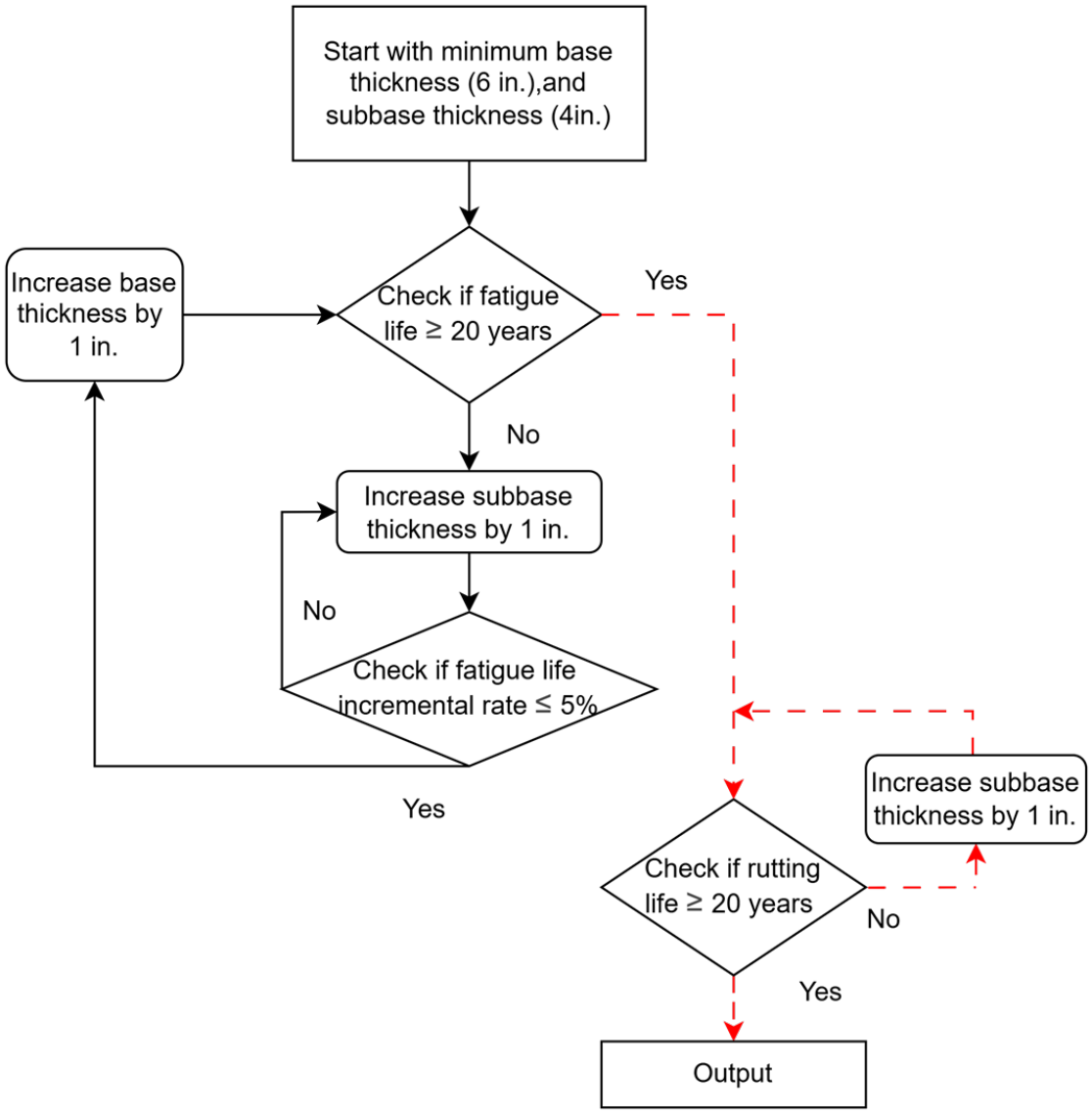

Figure 64. Flowchart for aggregate base and subbase thickness determination (Example 1 follows the red dash lines)

Note that within the selected quality combination, there may be multiple aggregate base-subbase thickness combinations that can achieve the required service life for a given scenario. As emphasized in Table 33, for 0.6 million ESALs, a pavement with a 4 in. of HMA and an engineered subgrade with a modulus of 2 ksi and LL quality combination of aggregate base and subbase materials was chosen. Within this combination, multiple pavement structure options (design alternatives) could achieve a 20-year service life. Although the combination with the lowest material costs could be identified, the total material cost depends on the assumed unit costs of the aggregate base and subbase layers, meaning that variance of these unit cost assumptions would alter the selection of the lowest-cost designs, making it challenging to draw a consistent conclusion about achieving the lowest cost by balancing aggregate base and subbase thicknesses. While there is thus no consistent conclusion about how to achieve the

lowest cost by balancing thickness among aggregate base and subbase, to optimize resource efficiency, the flowchart recommends prioritizing structures with the lowest aggregate base thickness while maintaining the required service life, since aggregate base materials are typically in limited supply.

Table 33. Potential cases achieving target service life of a pavement with a 4 in. of HMA and an engineered subgrade with a modulus of 2 ksi with 0.6 million ESALs.

Case No.	Aggregate Base thickness (in.)	Subbase thickness (in.)	Aggregate Base unit cost ($ per mile)	Subbase aggregate unit cost ($ per mile)	Cost ($ per mile)	Fatigue life (years)	Rutting life (years)
1	6	17.0	11,317.1	9,991.4	237,756.0	38	20
2	7	16.0	11,317.1	9,991.4	239,081.6	40	20
3	8	14.8	11,317.1	9,991.4	237,909.5	41	20
4	9	13.5	11,317.1	9,991.4	236,737.3	42	20
5	10	12.5	11,317.1	9,991.4	238,063.0	43	20
6	12	10.3	11,317.1	9,991.4	238,216.5	44	20
7	15	7.0	11,317.1	9,991.4	239,695.8	46	20

Example 2:

For a pavement consisting of 4 in. of HMA and engineered subgrade with a modulus of 2 ksi subjected to a traffic level of 1.5 million ESALs, the LL quality combination of aggregate base and subbase materials in Step 1 was selected. Step 2 was to determine the thickness of aggregate base and subbase layers. The effects of aggregate base and subbase thicknesses on fatigue and rutting lives for 1.5 million ESALs are illustrated in Figure 65. Using the flowchart outlined in Figure 66, the thickness determination process began by evaluating the minimum aggregate base (6 in.) and subbase (4 in.) thicknesses. However, this initial combination failed to achieve the target fatigue life.

Then, following the flowchart in Figure 66, the aggregate base layer thickness was fixed at 6 in., while the subbase thickness was incrementally increased by 1 in. per each step to assess fatigue life. However, until the fatigue incremental improvement rate fell below 5%, increase of subbase thickness could not improve fatigue life to the target. This limitation is evident in Figure 65(a), which highlights that each aggregate base layer thickness has a fatigue life limit. After approaching this fatigue life limit, increasing the subbase thickness offers negligible benefits.

To further improve fatigue life, the aggregate base layer thickness was increased by 1 in., while the subbase thickness was reset to its minimum value (4 in.) and again incrementally increased to improve fatigue life. These iterations, illustrated in the flowchart and highlighted in red, ultimately determined the optimal thickness for aggregate base and subbase layer. The finalized pavement structure includes a 12 in. low-quality aggregate base layer and a 26 in. low-quality subbase layer (LL). This configuration

successfully met the target fatigue life while also satisfying the rutting target life. The selected design represents a cost-effective solution, providing adequate performance while optimizing material usage.

Similarly, by following the procedures outlined in Step 1 and Step 2, optimized designs were determined for all other scenarios with the results summarized in Table 34.

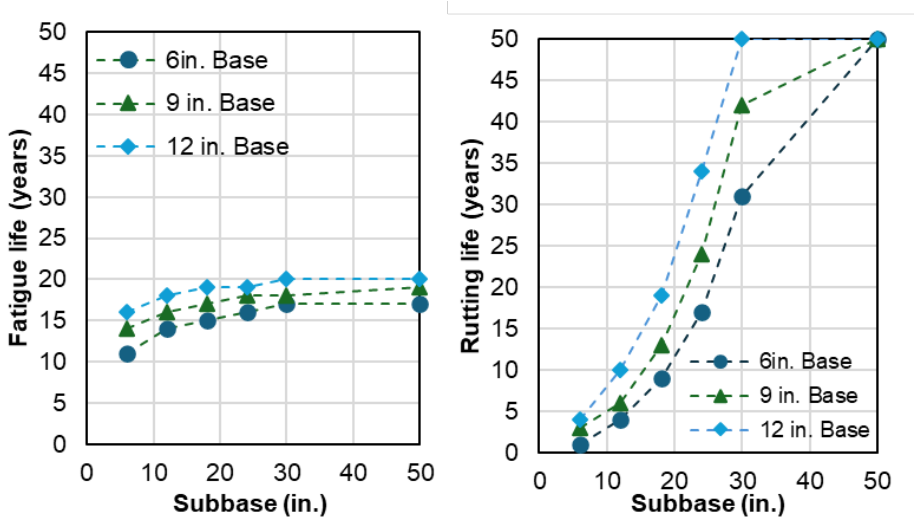

Figure 65. The effects of aggregate base and subbase thicknesses on (a) fatigue and (b) rutting life for 1.5 million ESALs

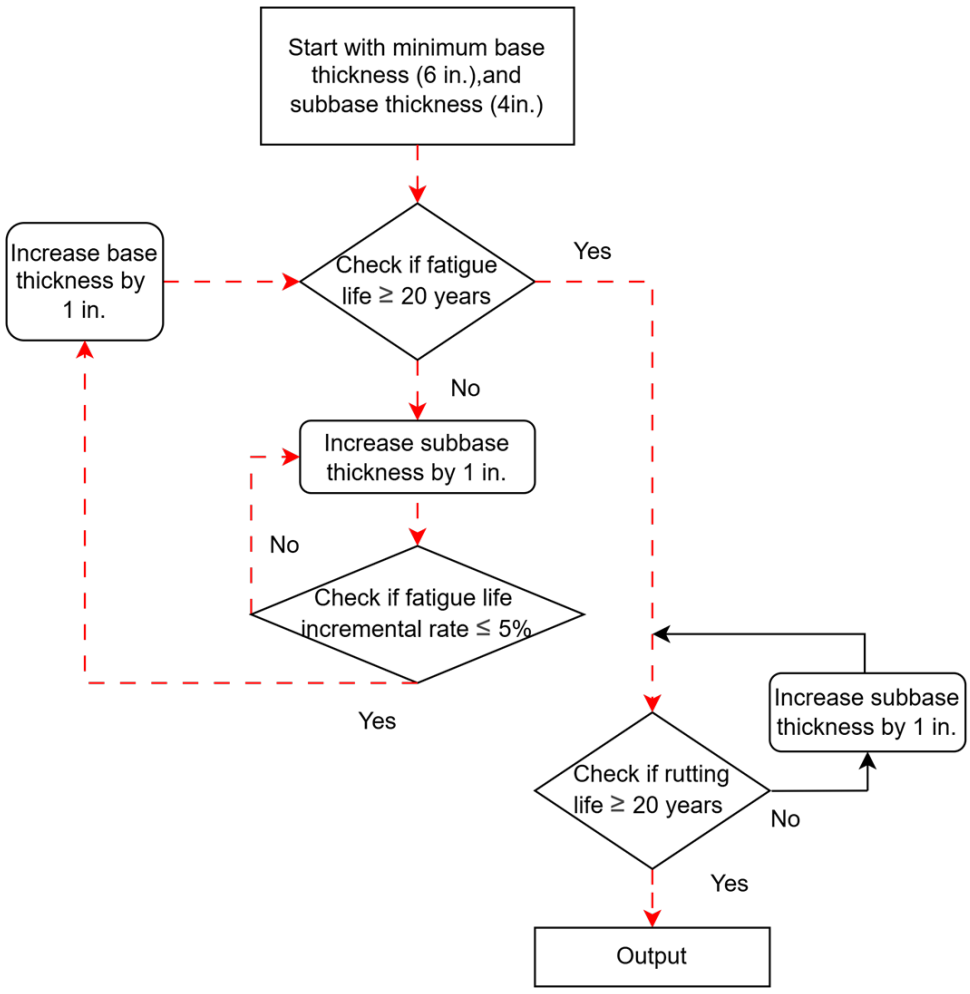

Figure 66. Flowchart for base and subbase thickness determination (Example 2 follows the red dash lines)

Table 34. Optimized pavement designs for scenarios considered in Beltrami County

OD refers to over-designed cases, in which all designs could achieve or exceed target service life
UD refers to under-designed cases, in which no designs could achieve target service life by only optimizing base and subbase.
DO refers to design-optimized, in which the design has been optimized and meets the target service life without being under- or over- built.

For engineered subgrade modulus 2 ksi

		HMA layer											
		4 in. HMA				6 in. HMA				8 in. HMA			
Traffic (MESALs)		0.2	0.6	1.5	6	0.2	0.6	1.5	6	0.2	0.6	1.5	6
Optimized design	**Design evaluation**	DO	DO	DO	UD	OD	DO	DO	DO	OD	OD	DO	DO
	Aggregate quality	LL	LL	ML	-	-	LL	LL	ML	-	-	LL	LL
	Base thickness (in.)	6	6	6	-	-	6	6	9	-	-	6	6
	Subbase thickness (in.)	9	18	24	-	-	12	22	33	-	-	14	33

For engineered subgrade modulus 4 ksi

		HMA layer											
		4 in. HMA				6 in. HMA				8 in. HMA			
Traffic (MESALs)		0.2	0.6	1.5	6	0.2	0.6	1.5	6	0.2	0.6	1.5	6
Optimized design	**Design evaluation**	OD	DO	DO	UD	OD	OD	DO	DO	OD	OD	OD	DO
	Aggregate quality	-	LL	ML	-	-	-	LL	ML	-	-	-	LL
	Base thickness (in.)	-	6	6	-	-	-	6	9	-	-	-	6
	Subbase thickness (in.)	-	11	17	-	-	-	13	28	-	-	-	21

For engineered subgrade modulus 7 ksi

		HMA layer											
		4 in. HMA				6 in. HMA				8 in. HMA			
Traffic (MESALs)		0.2	0.6	1.5	6	0.2	0.6	1.5	6	0.2	0.6	1.5	6
Optimized design	**Design evaluation**	OD	OD	DO	UD	OD	OD	OD	DO	OD	OD	OD	DO
	Aggregate quality	-	-	ML	-	-	-	-	ML	-	-	-	LL
	Base thickness (in.)	-	-	6	-	-	-	-	9	-	-	-	6
	Subbase thickness (in.)	-	-	10	-	-	-	-	18	-	-	-	10

For engineered subgrade modulus 10 ksi

		HMA layer											
		4 in. HMA				6 in. HMA				8 in. HMA			
Traffic (MESALs)		0.2	0.6	1.5	6	0.2	0.6	1.5	6	0.2	0.6	1.5	6
Optimized design	**Design evaluation**	OD	OD	DO	UD	OD	OD	OD	DO	OD	OD	OD	OD
	Aggregate quality	-	-	ML	-	-	-	-	ML	-	-	-	-
	Base thickness (in.)	-	-	6	-	-	-	-	9	-	-	-	-
	Subbase thickness (in.)	-	-	6	-	-	-	-	8	-	-	-	-

Additionally, optimized base and subbase layer thicknesses for flexible pavement sections in other three counties (i.e., Todd, Redwood, and Olmsted Counties) are also derived and provided in Tables 35 through 37, offering practitioners reference values that align with their specific pavement design needs.

Table 35. Optimized pavement designs for scenarios considered in Todd County

OD — refers to over-designed cases, in which all designs could achieve or exceed target service life
UD — refers to under-designed cases, in which no designs could achieve target service life by only optimizing base and subbase.
DO — refers to design-optimized, in which the design has been optimized and meets the target service life without being under- or over- built.

For engineered subgrade modulus 2 ksi

		HMA layer											
		4 in. HMA				6 in. HMA				8 in. HMA			
Traffic (MESALs)		0.2	0.6	1.5	6	0.2	0.6	1.5	6	0.2	0.6	1.5	6
Optimized design	**Design evaluation**	DO	DO	DO	UD	OD	DO	DO	DO	OD	OD	DO	DO
	Aggregate quality	LL	LL	ML	-	-	LL	LL	ML	-	-	LL	LL
	Base thickness (in.)	6	6	6	-	-	6	6	13	-	-	6	6
	Subbase thickness (in.)	9	18	25	-	-	13	23	28	-	-	16	34

For engineered subgrade modulus 4 ksi

		HMA layer											
		4 in. HMA				6 in. HMA				8 in. HMA			
Traffic (MESALs)		0.2	0.6	1.5	6	0.2	0.6	1.5	6	0.2	0.6	1.5	6
Optimized design	**Design evaluation**	OD	DO	DO	UD	OD	OD	DO	DO	OD	OD	OD	DO
	Aggregate quality	-	LL	ML	-	-	-	LL	ML	-	-	-	LL
	Base thickness (in.)	-	6	6	-	-	-	6	13	-	-	-	6
	Subbase thickness (in.)	-	12	18	-	-	-	14	25	-	-	-	23

For engineered subgrade modulus 7 ksi

		HMA layer											
		4 in. HMA				6 in. HMA				8 in. HMA			
Traffic (MESALs)		0.2	0.6	1.5	6	0.2	0.6	1.5	6	0.2	0.6	1.5	6
Optimized design	**Design evaluation**	OD	OD	DO	UD	OD	OD	OD	DO	OD	OD	OD	DO
	Aggregate quality	-	-	ML	-	-	-	-	ML	-	-	-	LL
	Base thickness (in.)	-	-	6	-	-	-	-	13	-	-	-	6
	Subbase thickness (in.)	-	-	11	-	-	-	-	18	-	-	-	12

For engineered subgrade modulus 10 ksi

		HMA layer											
		4 in. HMA				6 in. HMA				8 in. HMA			
Traffic (MESALs)		0.2	0.6	1.5	6	0.2	0.6	1.5	6	0.2	0.6	1.5	6
Optimized design	**Design evaluation**	OD	OD	DO	UD	OD	OD	OD	DO	OD	OD	OD	OD
	Aggregate quality	-	-	ML	-	-	-	-	ML	-	-	-	-
	Base thickness (in.)	-	-	6	-	-	-	-	13	-	-	-	-
	Subbase thickness (in.)	-	-	6	-	-	-	-	4	-	-	-	-

Table 36. Optimized pavement designs for scenarios considered in Redwood County

OD — refers to over-designed cases, in which all designs could achieve or exceed target service life
UD — refers to under-designed cases, in which no designs could achieve target service life by only optimizing base and subbase.
DO — refers to design-optimized, in which the design has been optimized and meets the target service life without being under- or over- built.

For engineered subgrade modulus 2 ksi

		HMA layer											
		4 in. HMA				6 in. HMA				8 in. HMA			
Traffic (MESALs)		0.2	0.6	1.5	6	0.2	0.6	1.5	6	0.2	0.6	1.5	6
Optimized design	**Design evaluation**	DO	DO	DO	UD	OD	DO	DO	DO	OD	OD	DO	DO
	Aggregate quality	LL	LL	ML	-	-	LL	LL	ML	-	-	LL	LL
	Base thickness (in.)	6	6	6	-	-	6	6	18	-	-	6	6
	Subbase thickness (in.)	10	19	25	-	-	14	23	28	-	-	17	35

For engineered subgrade modulus 4 ksi

		HMA layer											
		4 in. HMA				6 in. HMA				8 in. HMA			
Traffic (MESALs)		0.2	0.6	1.5	6	0.2	0.6	1.5	6	0.2	0.6	1.5	6
Optimized design	**Design evaluation**	OD	DO	DO	UD	OD	OD	DO	DO	OD	OD	OD	DO
	Aggregate quality	-	LL	ML	-	-	-	LL	ML	-	-	-	LL
	Base thickness (in.)	-	6	6	-	-	-	6	18	-	-	-	6
	Subbase thickness (in.)	-	12	10	-	-	-	15	20	-	-	-	24

For engineered subgrade modulus 7 ksi

		HMA layer											
		4 in. HMA				6 in. HMA				8 in. HMA			
Traffic (MESALs)		0.2	0.6	1.5	6	0.2	0.6	1.5	6	0.2	0.6	1.5	6
Optimized design	**Design evaluation**	OD	OD	DO	UD	OD	OD	OD	DO	OD	OD	OD	DO
	Aggregate quality	-	-	ML	-	-	-	-	ML	-	-	-	LL
	Base thickness (in.)	-	-	6	-	-	-	-	19	-	-	-	6
	Subbase thickness (in.)	-	-	11	-	-	-	-	10	-	-	-	13

For engineered subgrade modulus 10 ksi

		HMA layer											
		4 in. HMA				6 in. HMA				8 in. HMA			
Traffic (MESALs)		0.2	0.6	1.5	6	0.2	0.6	1.5	6	0.2	0.6	1.5	6
Optimized design	**Design evaluation**	OD	OD	DO	UD	OD	OD	OD	DO	OD	OD	OD	OD
	Aggregate quality	-	-	ML	-	-	-	-	ML	-	-	-	-
	Base thickness (in.)	-	-	6	-	-	-	-	19	-	-	-	-
	Subbase thickness (in.)	-	-	7	-	-	-	-	4	-	-	-	-

Table 37. Optimized pavement designs for scenarios considered in Olmsted County

OD — refers to over-designed cases, in which all designs could achieve or exceed target service life
UD — refers to under-designed cases, in which no designs could achieve target service life by only optimizing base and subbase.
DO — refers to design-optimized, in which the design has been optimized and meets the target service life without being under- or over- built.

For engineered subgrade modulus 2 ksi

		HMA layer											
		4 in. HMA				6 in. HMA				8 in. HMA			
Traffic (MESALs)		0.2	0.6	1.5	6	0.2	0.6	1.5	6	0.2	0.6	1.5	6
Optimized design	**Design evaluation**	DO	DO	DO	UD	OD	DO	DO	DO	OD	OD	DO	DO
	Aggregate quality	LL	LL	ML	-	-	LL	LL	ML	-	-	LL	LL
	Base thickness (in.)	6	6	6	-	-	6	6	16	-	-	6	6
	Subbase thickness (in.)	10	19	26	-	-	14	23	26	-	-	16	35

For engineered subgrade modulus 4 ksi

		HMA layer											
		4 in. HMA				6 in. HMA				8 in. HMA			
Traffic (MESALs)		0.2	0.6	1.5	6	0.2	0.6	1.5	6	0.2	0.6	1.5	6
Optimized design	**Design evaluation**	OD	DO	DO	UD	OD	OD	DO	DO	OD	OD	OD	DO
	Aggregate quality	-	LL	ML	-	-	-	LL	ML	-	-	-	LL
	Base thickness (in.)	-	6	6	-	-	-	6	16	-	-	-	6
	Subbase thickness (in.)	-	12	18	-	-	-	14	16	-	-	-	24

For engineered subgrade modulus 7 ksi

		HMA layer											
		4 in. HMA				6 in. HMA				8 in. HMA			
Traffic (MESALs)		0.2	0.6	1.5	6	0.2	0.6	1.5	6	0.2	0.6	1.5	6
Optimized design	**Design evaluation**	OD	OD	DO	UD	OD	OD	OD	DO	OD	OD	OD	DO
	Aggregate quality	-	-	ML	-	-	-	-	ML	-	-	-	LL
	Base thickness (in.)	-	-	6	-	-	-	-	16	-	-	-	6
	Subbase thickness (in.)	-	-	11	-	-	-	-	12	-	-	-	13

For engineered subgrade modulus 10 ksi

		HMA layer											
		4 in. HMA				6 in. HMA				8 in. HMA			
Traffic (MESALs)		0.2	0.6	1.5	6	0.2	0.6	1.5	6	0.2	0.6	1.5	6
Optimized design	**Design evaluation**	OD	OD	DO	UD	OD	OD	OD	DO	OD	OD	OD	OD
	Aggregate quality	-	-	ML	-	-	-	-	ML	-	-	-	-
	Base thickness (in.)	-	-	6	-	-	-	-	16	-	-	-	-
	Subbase thickness (in.)	-	-	7	-	-	-	-	4	-	-	-	-

6.2 Summary

This chapter focused on identifying cost-effective pavement designs by integrating the performance findings from Chapter 5 with a cost-benefit analysis approach. This chapter employed two main steps: (1) determining the minimum required quality combination of aggregate base and subbase, and (2)

refining the aggregate base and subbase layer thicknesses to achieve an optimal design under various scenarios. Key highlights from Chapter 6 include:

- A statewide database of historical MnDOT bid prices was analyzed to estimate the unit costs of different quality aggregates. High-quality materials were assumed to correspond to maximum awarded prices, low-quality materials to minimum awarded prices, and medium-quality materials to an average of the two extremes. These unit cost estimates were applied on a per-inch-thickness and per-mile-of-pavement basis, enabling direct comparisons of the total material cost for each different design alternatives.
- In Step 1, drawing on Chapter 5's performance data, aggregate base and subbase materials were grouped into low (L), medium (M), and high (H) quality categories. For each scenario of traffic level (0.2, 0.6, 1.5, and 6 million ESALs), HMA thickness (4, 6, 8 in.) and engineered subgrade modulus (2, 4, 7, 10 ksi), cost and performance outcomes were evaluated.
- By evaluating material costs and benefits of various design options, the minimum required qualities for both aggregate base and subbase layers for different scenarios were selected and summarized. The findings indicate that LL quality and ML quality aggregate base and subbase combinations are generally sufficient to meet the target service life across all scenarios considered in this chapter. This step also indicated potential design alternatives to be used when high-quality aggregate materials are in short supply.
- In Step 2, a flowchart to determine the thicknesses of the aggregate base and subbase courses was developed. Using the selected quality combination, the flowchart helps determine the optimal thicknesses for both layers, ensuring that the minimum required thicknesses are chosen while maintaining performance.
- A two-stage flowchart to systematically determining layer thicknesses was introduced. First, fatigue life requirements were satisfied by adjusting both aggregate base and subbase thicknesses. Once the aggregate base thickness was finalized (often near the minimum required to achieve the target fatigue life), only the subbase thickness was further adjusted to meet rutting life requirements.

Chapter 7: Research Benefits and Implementation Steps

This chapter outlines the key technical and practical benefits of the research and proposes steps for implementing the findings within MnDOT and local agency practices. By translating the study's analytical results and performance evaluations into design guidance, the implementation framework aims to support more sustainable, cost-effective, and locally optimized pavement designs.

7.1 Research Benefits

The findings of this research project provide substantial benefits to the MnDOT and local transportation agencies by offering a comprehensive framework for optimizing pavement foundation design using locally available aggregate materials. These benefits extend to technical, economic, and environmental dimensions, and support MnDOT's strategic goals in innovation, asset management, and sustainability.

First, the development of an updated AIP database enables engineers and researchers to evaluate locally available aggregate sources more effectively. By integrating recent data from MnDOT's ASIS and LIMS systems and categorizing materials by gradation, mineralogy, and other properties, the AIP database serves as a centralized resource for identifying suitable materials for aggregate base and subbase applications.

Second, the enhanced predictive models established in this study, including improved MLR and ANN models, offer greater accuracy in estimating critical pavement design inputs such as resilient modulus and strength characteristics. These models allow for performance-based material selection and facilitate the use of lower-quality or marginal materials where appropriate, thereby expanding the viable resource pool and enabling cost-effective design solutions.

Third, the research calculated and evaluated GE factors based on aggregate quality levels and material behavior under varying stress conditions. These GE values provide a more rational basis for evaluating the structural contribution of aggregate base and subbase layers, helping to ensure that pavement sections are neither over- nor under-designed. This is particularly beneficial in scenarios where high-quality materials are limited or unavailable.

Lastly, through all the studies conducted in each chapter, multiple design alternatives were investigated to account for different combinations of unbound layer thicknesses and varying aggregate quality classifications (low, medium, or high). These alternatives were evaluated under a range of traffic demands (0.2 to 6 million ESALs), HMA layer thicknesses, and subgrade stiffness levels (2 ksi to 10 ksi), using cost data derived from historical MnDOT bid prices. The primary advantage of this structured approach is that it helps engineers and local agencies select the most suitable combination of aggregate quality and thickness in a cost-effective manner as follows:

- Lower-quality aggregates can be used safely on low-volume roads (< 1.5 million ESALs) as long as the base or subbase thickness is adjusted to meet 20-year design requirements. This finding significantly reduces material costs and alleviates dependence on scarce high-quality sources. For high-volume roads (e.g., 6 million ESALs), medium or high aggregate quality layers and/or thicker HMA layers are recommended.

- By calculating GE factors and layer thicknesses systematically, engineers and local agencies can see exactly how different combinations of aggregate base and subbase materials and thicknesses contribute to the flexible pavement's overall structural capacity, making it easier to incorporate cost-benefit trade-offs.

- Iterative flowchart-based method was introduced to optimize aggregate base and subbase thicknesses. Agencies can thus incrementally adjust either layer to achieve targeted fatigue and rutting lives, reducing the likelihood of under- or over-design.

Overall, these design alternatives provide more detailed guidance on unbound layer thickness and quality optimizations, allowing agencies easily and confidently select local, lower-cost materials where feasible and higher-quality materials only were needed. The following sub-sections provide detailed explanations of the analysis parameters, key assumptions, and the advantages of design optimization in enhancing pavement design effectiveness and reducing material costs.

7.1.1 Analysis Parameters and Key Assumptions

The following parameters and assumptions were used for the calculation of flexible pavement performance, cost estimation, and subsequent design recommendations:

- Aggregate Quality Definitions
    - Low (L), medium (M), high (H) qualities: Chapters 4 and 5 used an updated AIP database to classify aggregates based on MR and shear strength. Quality thresholds were set to ensure a consistent distinction among the three classes.
    - Class 5 and Class 6 aggregates from historical MnDOT data served as baselines to determine granular equivalency factors.
- Analysis Conditions
    - Design optimization was conducted using a comprehensive analysis matrix, including varying HMA thicknesses (4, 6, 8 in.), engineered subgrade moduli (2, 4, 7, and 10 ksi), and traffic levels (0.2, 0.6, 1.5, and 6 million ESALs).
    - Four climatic zones (i.e., Beltrami, Todd, Redwood, and Olmsted Counties) were included in analysis to capture Minnesota's north-to-south climatic temperature differentials, influencing pavement life outcomes in MnPAVE.
- Cost Estimation Method
    - Awarded bid data over the past five years were compiled for Class 3/4 and Class 5/6 materials. Minimum, maximum, and average values were taken to represent low-, high-, and medium-quality aggregates.

    - Material costs were normalized to a one-mile, two-lane road configuration, allowing direct comparisons across thickness and quality choices.
- Performance Criteria
    - A 20-year design life was set as the criterion for both fatigue cracking and rutting. Chapter 5's MnPAVE outputs were used to check whether each design combination exceeded or fell short of these thresholds.
- Design Flowchart
    - An iterative method was employed to (1) fix the HMA thickness, (2) increase aggregate base thickness and subbase thickness to meet fatigue life, and (3) further adjust the subbase layer for rutting resistance—only once the fatigue cracking criteria had been satisfied.

These modeling assumptions and parameters ensure that the recommended design alternatives are both technically sound and practically implementable.

7.1.2 Pavement Design Effectiveness and Material Cost Savings

By systematically matching optimized qualities, preferably from local sources, and thicknesses of unbound aggregate layers to actual traffic demands, agencies can reliably achieve 20-year flexible pavement performance against both fatigue cracking and rutting. For example, an L-L quality combination is applicable to traffic levels up to and including 1.5 million ESALs, an M-L combination can handle 6 million ESALs when used with a 6 in. HMA layer, and even an L-L combination remains sufficient for up to 6 million ESALs if using 8 in. of HMA and adequately thick unbound aggregate layers. These findings indicate that high-quality aggregate base and subbase materials are not always necessary, if layer thickness, especially subbase thickness, is properly designed. Such measures can significantly lower material costs, particularly when locally available marginal aggregates are utilized.

The flowchart developed in Chapter 6 revealed multiple scenarios where modest increases in unbound aggregate thicknesses negate the need for high-quality materials, helping agencies avoid premium prices from statewide or out-of-county sources. Because aggregate base layer materials are usually more expensive with higher quality and unit cost than subbase materials, having the flexibility in flexible pavement design by balancing qualities and thicknesses of aggregate base and subbase can yield material savings. By following the Chapter 6 flowcharts, engineers can select the quality combination that best aligns with local cost structures and resource availability while adjusting unbound aggregate thicknesses to reflect varied HMA thicknesses and subgrade strengths. Even for high-volume roads, selecting an M-L quality design can balance initial construction and maintenance costs, provided HMA and subgrade conditions are adequately addressed. Note that the current version of MnPAVE assumes that each layer is linear-elastic and assigns a single modulus to the HMA for each season. As a result, MnPAVE does not simulate true viscoelastic relaxation or rate-of-loading effects in the HMA layer. This simplification, combined with the model's layered-elastic formulation, may place disproportionate emphasis on HMA thickness when predicting fatigue life. Also, MnPAVE simplifies the stress-dependent and nonlinear behaviors of unbound aggregate layers. Consequently, while increases in HMA thickness can significantly improve fatigue life predictions within MnPAVE, the role of high-quality aggregate base

or subbase materials may be underrepresented in some configurations. This modeling bias should be considered when interpreting cost-benefit outcomes, especially in scenarios where structural performance enhancements could be more cost-effectively achieved through improved aggregate quality rather than solely through increased HMA thickness.

In summary, these recommended design alternatives enable agencies to tailor flexible pavement structures to actual traffic demands, HMA thicknesses, and subgrade conditions without routinely resorting to higher-cost aggregates. This approach leads to more cost-effective pavement designs, from low-volume roads to high-traffic scenarios.

7.2 Implementation Steps

To ensure effective implementation of the research findings, the following steps are recommended for MnDOT and local agencies:

1. **Integration of the AIP Database into Design Tools**
   The updated AIP database would be beneficial to be integrated into MnDOT's internal systems and used as a reference in pavement design projects. Materials classified by quality level, modulus, and strength can help designers make informed decisions about the suitability of local aggregates.

2. **Incorporation of Predictive Models into Design Tools**
   The ANN models predicting resilient modulus and strength could be incorporated into design tools (e.g., MnPAVE) or complementary decision-support tools. This would enable practitioners to estimate design inputs for materials not directly tested, using known index properties from the AIP database.

3. **Development of Design Aids and Flowcharts**
   The flowchart developed in Chapter 6 for determining optimal aggregate base and subbase thicknesses under varying traffic and subgrade conditions can be formalized into a design aid. This flowchart can be used by local agencies during the pavement design phase to evaluate alternatives and select cost-effective configurations.

4. **Updates to MnDOT Pavement Design Guidelines**
   MnDOT's Pavement Design Manual can be updated to reflect the findings from this study, including guidance on selecting aggregate base/subbase material quality levels, evaluating GE values, and using optimized thickness combinations based on cost and performance criteria.

Through these implementation steps, MnDOT and local agencies will be better understanding how to make informed, performance-based decisions in pavement design and material selection, enhancing durability, reducing costs, and promoting the efficient use of regional resources.

Chapter 8: Conclusions and Recommendations for Future Research

This chapter summarizes the key findings of the study and provides recommendations for future research to further enhance the performance-driven and cost-effective use of aggregate materials in pavement foundation design. The conclusions draw on a comprehensive literature review, robust database development, predictive modeling, pavement performance analysis, and cost-benefit analyses. The recommendations aim to extend the utility and practical impact of the research outcomes for MnDOT, local agencies, and the broader pavement engineering community.

8.1 Conclusions

This study was initiated to address the growing need for sustainable and cost-effective pavement design practices in Minnesota, particularly under constraints posed by limited availability of high-quality aggregate materials. The findings of the study demonstrate how to design cost-effective, durable flexible pavements by systematically linking an AIP database to critical pavement design inputs, investigating performance trends under a combination of pavement structures, traffic inputs, and climatic conditions, and identifying optimal combinations of aggregate base and subbase quality and thicknesses. Key contents include the creation of an updated AIP database, improvements in pavement design modeling through ANN models, and extensive cost-benefit analyses using MnPAVE pavement analyses, as detailed below:

- **Establishing Aggregate Index Properties**
  MnDOT's aggregate material database was updated with newly added sources and additional aggregate resource considerations. The main purpose of this task was to create an aggregate index property (AIP) database that will support linking various aggregate index properties, including gradation, chemical composition, and strength, to important pavement design parameters like resilient modulus. The AIP database has been updated using two primary databases: (i) aggregate source information system (ASIS) containing broad information on gravel pits, quarries, and baseline aggregate properties and (ii) laboratory information management system (LIMS) containing detailed laboratory test results (e.g., gradation, abrasion, shape properties) for various samples drawn from these sources over time.

  An initial exploratory analysis found that the ASIS database holds 8,475 rows of information (each representing a unique material source) but includes inactive sources (status code "I"), which needed to be filtered out. Meanwhile, the LIMS database contains over two million test rows, many without valid source identifiers or valid sampling dates, posing a significant data-cleaning challenge. Following a methodology consistent with a 2012 MnDOT project on best-value granular material (Xiao & Tutumluer, 2012), this study developed a systematic data-cleaning and merging pipeline using Python. After necessary processing, the AIP database was developed by merging the three latest gradations of 1,118 material sources with the ASIS

database. The AIP database is intended for linking the aggregate index properties with the pavement analysis and design inputs (e.g., resilient modulus and strength properties).

- **Methodology for Linking Aggregate Properties to Pavement Inputs**
  The research team substantially refined the existing relationships between AIP and critical pavement design parameters, notably the resilient modulus (M_R) and shear strength. Building on the updated AIP database from Chapter 3, Chapter 4 examined historical bid information to integrate cost data, allowing a more practical approach to selecting aggregates for aggregate base and subbase layers across Minnesota. The researchers improved on an earlier regression-based model by incorporating additional relevant properties, such as gradation indices and optimum moisture content, which increased prediction accuracy for M_R but still fell short of capturing the full complexity of aggregate behavior. To address this limitation, artificial neural network (ANN) models were developed to demonstrate much higher prediction accuracy for M_R, particularly for the k_1 parameter, thereby highlighting the significance of nonlinear relationships in aggregate characterization. Although incorporating morphological shape indices into the ANN offered modest further improvement, the developed models without shape data still performed robustly and are more readily applicable in practice, given that shape information is not always available. This task also created a secondary ANN model for predicting shear strength, which is critical for understanding permanent deformation, and used both M_R and shear strength outputs to categorize aggregates into low-, medium-, or high-quality classes. As a result, the ANN-based approach for strength estimation enabled a systematic selection of representative materials to be studied in Chapter 5 within three quality ranges based on strength and M_R trends.

- **MnPAVE Design Evaluations and Granular Equivalency (GE) Factors**
  The research team investigated how flexible pavement performance responds to changes in aggregate base and subbase thickness and quality. Using MnPAVE, a comprehensive set of simulations was conducted across four representative Minnesota climate zones, including Beltrami, Todd, Redwood, and Olmsted, chosen to capture the seasonal variations and temperatures typical of northern through southern parts of the state. The MnPAVE analysis also focused on how varying degrees of traffic loading (from 0.2 to 6 million ESALs) and different aggregate properties (high-, medium-, or low-quality) affected fatigue cracking and rutting over the service life of pavement systems.
  The analysis results indicated that, for lower traffic volumes up to around 0.6 million ESALs, even thin HMA layers (4 in.) and locally available, low-quality aggregate layers can still meet design life goals for both fatigue and rutting. As traffic demands grow beyond 1.5 million ESALs, HMA thickness becomes far more decisive in preventing fatigue cracking, while subbase quality more strongly controls rutting. In other words, at higher traffic levels, no amount of added thickness to a poor-quality aggregate base layer alone can fully compensate for the lower stiffness needed to curb fatigue-related damage, whereas improvements in the subbase provide crucial resistance against rutting. The study also incorporated subgrade moduli ranging from 2 ksi to 10 ksi and found that a stronger subgrade had a limited effect on fatigue but significantly

reduced rutting by limiting vertical strain at the top of the subgrade.
The team further computed granular equivalency (GE) factors to translate material stiffness properties and thicknesses into design coefficients, with MnDOT Class 5 and Class 6 used as baseline. This allowed a deeper examination of how each combination of aggregate base and subbase quality and thickness contributed to overall pavement life. Through these runs, it became evident that local agencies can use locally available and marginal materials for the aggregate base or subbase on lower-volume roads without compromising the 20-year service life, yet thicker or higher-quality layers become essential once traffic demands rise above 1.5 million ESALs. These findings set the stage for Chapter 6, where the project used the insights gained from this extensive MnPAVE analysis to develop optimized, cost-effective pavement designs that balance material availability, performance, and service-life requirements.

- **Cost-Benefit Analyses of Design Alternatives**
  Cost-benefit analysis was conducted in Chapter 6 to provide recommendations for designing base and subbase layers in flexible pavements. The goal was to identify optimal combinations of layer thickness and aggregate quality, which classified as low (L), medium (M), or high (H) qualities from Chapter 5, such that pavement systems met 20-year fatigue and rutting life requirements for different traffic levels and subgrade conditions, all while minimizing material costs.

  Drawing on a Minnesota-wide database of historical awarded bid prices, representative unit costs for Class 3/4 (subbase) and Class 5/6 (base) materials were established. Low-quality materials were assigned to lowest-cost bids, high-quality materials to the highest-cost bids, and medium quality to average-cost bids. This cost-per-inch-thickness approach allowed quick comparisons of total material expenses for each design scenario. Using performance trends (fatigue cracking and rutting life) from Chapter 5, the research team initially investigated the least expensive acceptable quality levels. In many low- to moderate-traffic cases (up to 1.5 million ESALs), a low-low (L-L) quality combination of aggregate base and subbase materials was sufficient to achieve 20-year service life when having enough thicknesses. For higher traffic levels (6 million ESALs) or thinner HMA layers, better aggregate base, and subbase qualities (e.g., M-L) or thicker HMA was needed to meet the target. This stage helped rule out unnecessarily high-quality (and more expensive) aggregates in situations where local, marginal materials need to be used. Having established the optimal quality, an iterative flowchart was developed to incrementally adjust the thicknesses of aggregate base and subbase.

8.2 Recommendations for Future Research

While the current study addressed key aspects of aggregate performance and design optimization, several areas merit further investigation to enhance implementation and expand the applicability of the findings. Recommended topics for future research include:

1. **Field Validation of Optimized Designs**
   To validate the practical effectiveness of the optimized pavement design configurations identified in this study, future work needs to include pilot test sections constructed across various regions of Minnesota. These sections need to be instrumented and monitored over time to collect field performance data (i.e., rutting and fatigue cracking) under actual traffic and climatic conditions. Emphases should be placed on designs that incorporate different quality aggregate materials and thicknesses of unbound aggregate layers to confirm that these alternatives achieve the predicted service lives. Comparisons between measured field performance and MnPAVE-based predictions would allow calibration of performance models, refinement of GE factors, and update on design optimization procedures, ultimately increasing confidence in their adoption by practitioners.

2. **Expansion of Mechanical Property Database**
   Although the prediction models developed in this study were based on existing laboratory and field datasets, many aggregate sources in Minnesota still lack direct mechanical property measurements such as M_R and shear strength. A statewide testing program focused on collecting high-quality laboratory and in-situ mechanical data—including FWD, DCP, and repeated load triaxial tests—would greatly enhance the robustness of the predictive framework. Prioritizing material sources currently underrepresented in the database will increase model generalizability. Additionally, testing materials across a broader range of moisture contents, densities, and seasonal conditions will support more comprehensive performance modeling and improve the reliability of ANN- and MLR-based predictions.

3. **Advanced Mechanistic Analysis for Unbound Aggregate and Fine-Grained Soil Layers**
   While MnPAVE's linear elastic multilayer analysis provided valuable insights into pavement responses and service lives, it did not fully capture the nonlinear and stress-dependent behavior trends of unbound granular materials and fine-grained subgrades. Future research should apply advanced mechanistic analysis tools—such as finite element analysis (FEA)—that incorporate nonlinear constitutive models (e.g., k-θ, Uzan, or MEPDG models) and consider isotropic/anisotropic properties, especially under repeated traffic loading and environmental effects (e.g., freeze-thaw, saturation). The use of advanced computational models will enhance the mechanistic understanding of how aggregate properties and layer configurations influence pavement performance and support more refined design practices.

4. **Model Integration into Design Software**
   To ensure that the updated database, predictive models, and design optimization procedures developed in this project are readily accessible to practitioners, future work should focus on integrating these tools into MnDOT's existing design platforms such as MnPAVE and MnDOT's design manuals. This integration may include (i) embedding the ANN and MLR models for modulus and strength prediction within MnPAVE's input interface, (ii) creating a module for importing and querying the AIP database based on project location and material class, and (iii) automating the optimization post-processing for sustainable and economic pavement system

design. Developing a user-friendly interface or plugin that connects the models to MnPAVE or other pavement analysis and design software will streamline the design process.

5. **Evaluation of Stabilized Aggregate or Geosynthetic-Stabilization Options**
   In addition to evaluating unbound aggregates, future studies should investigate the mechanical and economic benefits of chemically stabilized aggregates (e.g., cement-, lime-, or asphalt-treated) and geosynthetic-stabilized pavement systems (e.g., geogrids, geotextiles) in aggregate base and subbase applications, correlating with qualities and thicknesses of unbound aggregate layers. Stabilization (chemical or mechanical) can improve stiffness and extend service life, particularly where low-quality materials are used. Experimental studies—both in laboratory and field demonstration projects—should examine how stabilization would affect resilient modulus, permanent deformation, drainage, and frost resistance to enhance the design optimization methodologies suggested in this study.

By pursuing these research directions, MnDOT and LRRB can continue to enhance the performance, sustainability, and cost-efficiency of Minnesota's pavement infrastructure, while promoting the sustainable use of local materials and advanced analysis methods.

References

AASHTO. (1993). G*uide for design of pavement structures.* Washington, DC: American Association of State Highway and Transportation & Officials.

AASHTO (2020). *Mechanistical-empirical pavement design guide: A manual of practice (3rd edition).* Washington, DC: American Association of State Highway and Transportation & Officials.

Ahmed, I., Thom, N., Zaidi, S. B. A., Ahmed, N., Carvajal-Munoz, J. S., Rahman, T., & Ahmad, N. (2021). A mechanistic approach to evaluate the fatigue life of inverted pavements. *Construction and Building Materials*, 311, 125288. https://doi.org/10.1016/j.conbuildmat.2021.125288.

Alavi, S., Merport, T., Wilson, T., Groeger, J., & Lopez Jr, A. (1997). *LTPP materials characterization program: Resilient modulus of unbound materials (LTPP Protocol P46) laboratory startup and quality control procedure*. Washington, DC: Federal Highway Administration.

Alimohammdi, H., Schaefer, V. R., Zheng, J., Jahren, C. T., Zheng, G., & White, D. (2021). *Effectiveness of geotextiles/geogrids in roadway construction; determine a granular equivalent (GE) factor.* St. Paul, MN: Minnesota. Department of Transportation. https://hdl.handle.net/20.500.14153/mndot.3269

Allen, J. J. (1973). *The effects of non-constant lateral pressures on the resilient response of granular materials*. Urbana-Champaign, IL: University of Illinois at Urbana-Champaign.

Allen, J. J., & Thompson, M. R. (1974). Resilient response of granular materials subjected to time-dependent lateral stresses. *Transportation Research Record*, 510.

Andersland, O. B., & Anderson, D. M. (1978). *Geotechnical engineering for cold regions.* New York, NY: McGraw-Hill.

Armaghani, J., & Schmitt, R. (2006). Long-life concrete pavements-the Florida perspective. Paper presented at the *International Conference on Long-Life Concrete Pavements*, Chicago, Illinois, October 25-27.

Barber, E. S., & Sawyer, C. L. (1952). Highway subdrainage. *Highway Research Board Proceedings*, 31. https://trid.trb.org/view/127663

Barksdale, R. D. (1972). Laboratory evaluation of rutting in base course materials. Paper presented at the *Third International Conference on the Structural Design of Asphalt Pavements*, Grosvenor House, Park Lane, London, England, Sept. 11-15, 1972.

Barskale, R. D., & Itani, S. Y. (1989). Influence of aggregate shape on base behavior. *Transportation Research Record,* 1227.

Behiry, A. E. A. E.-M. (2012). Fatigue and rutting lives in flexible pavement. *Ain Shams Engineering Journal*, 3(4), 367–374. https://doi.org/10.1016/j.asej.2012.04.008.

Bilodeau, J.-P., Cloutier, J.-P., & Doré, G. (2017). Experimental damage assessment of flexible pavements during freeze-up. *Journal of Cold Regions Engineering*, 31(4), 04017014. https://doi.org/10.1061/(ASCE)CR.1943-5495.0000140.

Bly, P., Shamim, A., Khazanovich, L., Barnes, R., & Worel, B. (2009). Effects of pavement design on frost heave at MnROAD. *TRB 88th Annual Meeting Compendium of Papers* [DVD].

Brown, S., & Chan, F. (1996). Reduced rutting in unbound granular pavement layers through improved Grading Design. *Proceedings of the Institution of Civil Engineers-Transport*, 117(1), 40–49.

Browne, C., Rauch, A., Haas, C., & Kim, H. (2001). Comparison tests of automated equipment for analyzing aggregate gradation. *Proceedings of the 9th Annual Symposium of the International Center for Aggregates Research: Aggregates — Concrete, Bases and Fines* (CD-ROM). Austin, TX: International Center for Aggregates Research.

Caestecker, C. (2006). The motorway E40 (formerly E5) from Brussels to Liege. *Proceedings of the International Conference on Long-Life Concrete Pavements,* Chicago, IL, October 25-27.

Caltrans. (2020). *California highway design manual.* Retrieved from https://dot.ca.gov/programs/maintenance/pavement/concrete-pavement-and-pavement-foundations/manuals-and-bulletins.

Casagrande, A., & Shannon, W. L. (1952). Base course drainage for airport pavements. *Transactions of the American Society of Civil Engineers*, 117(1), 792–814. https://doi.org/10.1061/TACEAT.0006654.

Ceylan, H., Cable, J., & Gopalakrishnan. (2006). Defining the attributes of well-performing, long-lasting jointed Portland cement concrete pavements. *Proceedings of the International Conference on Long-Life Concrete Pavements*, Chicago, IL, October 25-27.

Chavan, H. L. (2012). *Field investigation of subgrade non-uniformity effects on concrete pavement* (Master's thesis). Urbana, IL: University of Illinois at Urbana-Champaign.

Chen, Y., & Lytton, R. L. (2019). Development of a new faulting model in jointed concrete pavement using LTPP data. *Transportation Research Record*, 2673(5), 407–417. https://doi.org/10.1177/0361198119838988.

Chow, L. C., Mishra, D., & Tutumluer, E. (2014a). *Aggregate base course material testing and rutting model development*. Raleigh, NC: North Carolina Department of Transportation.

Chow, L. C., Mishra, D., & Tutumluer, E. (2014b). Framework for development of an improved unbound aggregate base rutting model for mechanistic–empirical pavement design. *Transportation Research Record,* 2401(1), 11–21.

Cook, C. S., Tanyu, B. F., & Yavuz, A. B. (2017). Effect of particle shape on durability and performance of unbound aggregate base. *Journal of Materials in Civil Engineering*, 29(2), 04016221.

Cooley Jr, L. A., & James, R. S. (2003). Micro-Deval testing of aggregates in the southeast. *Transportation Research Record*, 1837(1), 73–79.

Currey, J. (2016). H2Ri *Wicking fabric experimental feature final report Dalton highway MP 197–209 Rehabilitation* (Final Project Report). Juneau, AK: Alaska Department of Transportation & Public Facilities, Research, Development & Technology Transfer.

Dan, H.-C., Zhang, Z., Liu, X., & Chen, J. (2017). Transient unsaturated flow in the drainage layer of a highway: Solution and drainage performance. *Road Materials and Pavement Design*, 20, 1–26. https://doi.org/10.1080/14680629.2017.1397049

Darter, M. I., LaCoursiere, S. A., & Smiley, S. A. (1979). Structural distress mechanisms in continuously reinforced concrete pavement. *Transportation Research Record*, 715, 1–7.

Dawson, A., Thom, N., & Paute, J. (1996). *Mechanical characteristics of unbound granular materials as a function of condition.* Gomes Correia, Balkema, Rotterdam, 35–44.

Delatte, N. (2018). *Concrete pavement design, construction, and performance*. Boca Raton, FL: CRC Press.

Dempsey, B. J. (1981). Laboratory and field studies of channeling and pumping. *Transportation Research Record*, 849, 1–12.

Dunford, A. (2013). *Friction and the texture of aggregate particles used in the road surface course* [PhD thesis]. Nottingham, UK: University of Nottingham.

Erichsen, E., Ulvik, A., & Sævik, K. (2011). Mechanical degradation of aggregate by the Los Angeles-, the micro-Deval-and the Nordic test methods. *Rock Mechanics and Rock Engineering*, 44, 333–337.

Erlingsson, S. (2012). Rutting development in a flexible pavement structure. *Road Materials and Pavement Design*, 13(2), 218–234. https://doi.org/10.1080/14680629.2012.682383.

Esch, D. C. (1995). Long-term evaluations of insulated roads and airfields in *Alaska. Transportation Research Record*, 1481, 56–62.

Fredrickson, F. C., Diethelm, P. J., & Zwiers, D. M. (1970). Minnesota Department of Highways Flexible Pavement Design-1969. *Highway Research Record*, 329, 55-64.

Galinmoghadam, J., Liu, J., Zhang, X., Lin, C., & Guo, Y. (2022). Mitigating pumping in pavement shoulder using wicking geotextile: An experimental study. *Transportation Research Record,* 2676(11), 145–159. https://doi.org/10.1177/03611981221091730.

Gopalakrishnan, K., & Thompson, M. R. (2008). Effect of granular subbase thickness on airfield pavement structural response. *Journal of Materials in Civil Engineering*, 20(5), 331–342. https://doi.org/10.1061/(ASCE)0899-1561(2008)20:5(331).

Hadi, M. A. S., & Al-Sherrawi, M. H. (2021). The Influence of base layer thickness in flexible pavements. *Engineering, Technology & Applied Science Research*, 11(6), 7904–7909, https://doi.org/10.48084/etasr.4573.

Haider, Kaya, Z., Cetin, A., Hatipoglu, M., Cetin, B., & Aydilek, A. H. (2014). Drainage and mechanical behavior of highway base materials. *Journal of Irrigation and Drainage Engineering,* 140(6), 04014012. https://doi.org/10.1061/(ASCE)IR.1943-4774.0000708.

Haider, S. W., & Chatti, K. (2009). Effect of design and site factors on fatigue cracking of new flexible pavements in the LTPP SPS-1 experiment. *International Journal of Pavement Engineering*, 10(2), 133–147. https://doi.org/10.1080/10298430802169390.

Hall, K. T. (2007). *Long-life concrete pavements in Europe and Canada (FHWA-PL-07-027)*. Washington, DC: Federal Highway Administration, U.S. Department of Transportation.

Hanna, A. N. (2003). Aggregate tests for Portland cement concrete pavements: Review and recommendations. *NCHRP Research Results Digest,* 281.

Holtz, R. (1990). *Compaction Concepts. State of the art report. Guide to earthwork construction*. Transportation Research Board. National Research Council. Washington, DC.

Hossain, S., & Elfino, M. (2006). Impact of construction on the life of a jointed plain concrete pavement in Virginia. Paper presented at the International Conference on Long-life Concrete Pavements, Chicago, Illinois, October 25-27.

Huang, H., Luo, J., Tutumluer, E., Hart, J. M., & Qamhia, I. (2020). *Size and shape determination of riprap and large-sized aggregates using field imaging (FHWA-ICT-20-002)*. Rantoul, IL: Illinois Center for Transportation/Illinois Department of Transportation.

Huang, H., Tutumluer, E., Luo, J., Ding, K., Qamhia, I., & Hart, J. M. (2022). *3D image analysis using deep learning for size and shape characterization of stockpile riprap aggregates—Phase 2*. Springfield, IL: Illinois. Department of Transportation.

Huang, Y. H. (2004). *Pavement design and analysis (2. ed)*. Upper Saddle River, NJ: Pearson Prentice Hall.

IDOT. (2018). Chapter 44. In *Pavement design, Bureau of local roads and street manual*. Springfield, IL: Illinois Department of Transportation.

Jameel, A. K., & Yousif, R. A. (2021). Pavement Structural Analysis [Lecture notes]. University of Mustansiriyah, Faculty of Engineering, Highway and Transportation Engineering Department.

Jiang, X., Zhang, M., Xiao, R., Polaczyk, P., Bai, Y., & Huang, B. (2021). An investigation of structural responses of inverted pavements by numerical approaches considering nonlinear stress-dependent properties of unbound aggregate layer. *Construction and Building Materials*, 303, 124505. https://doi.org/10.1016/j.conbuildmat.2021.124505

Jibon, M., Mahedi, M., Yang, B., Ceylan, H., Rutherford, C. J., Cetin, B., & White, D. (2024). *Base stabilization additives–effect on granular equivalency (GE) (No. MN 2024-15)*. St. Paul, MN: Minnesota Department of Transportation. https://hdl.handle.net/20.500.14153/mndot.16613

Johnson, A. (2012). *Freeze-thaw performance of pavement foundation materials.* Retrieved from https://dr.lib.iastate.edu/handle/20.500.12876/27013

Jorenby, B. N., & Hicks, R. G. (1986). Base course contamination limits. *Transportation Research Record*, 1095, 86–101.

Jung, Y. S., & Zollinger, D. G. (2011). New laboratory-based mechanistic–empirical model for faulting in jointed concrete pavement. *Transportation Research Record,* 2226(1), 60–70. https://doi.org/10.3141/2226-07

Kamal, M., Dawson, A., Farouki, O., Hughes, D., & Sha'at, A. (1993). Field and laboratory evaluation of the mechanical behavior of unbound granular materials in pavements. *Transportation Research Record*, 1406, 88–97.

Kazmee, H., Tutumluer, E., & Qamhia, I. (2019). Strength properties of large sized virgin and recycled aggregates influencing rutting performances of pavement working platforms and low volume roads. *Proceedings of the XVI Pan-American Conference on Soil Mechanics and Geotechnical Engineering*, Cancún, Mexico, 17–20 November 2019, pp. 1667–1674, Amsterdam, Netherlands: IOS Press.

Khawaja, H., & Tanveer, A. (2018). Review of low-temperature crack (LTC) developments in asphalt pavements. *The International Journal of Multiphysics*, 12(2). https://doi.org/10.21152/1750-9548.12.2.169

Khazanovich, L., Celauro, C., Chadbourn, B., Zollars, J., & Dai, S. (2006). Evaluation of subgrade resilient modulus predictive model for use in mechanistic–empirical pavement design guide. *Transportation Research Record*, 1947(1), 155–166. https://doi.org/10.1177/0361198106194700115.

Kwon, J., & Tutumluer, E. (2009). Geogrid base reinforcement with aggregate interlock and modeling of associated stiffness enhancement in mechanistic pavement analysis. *Transportation Research Record*, 2116(1), 85–95.

Lekarp, F., Isacsson, U., & Dawson, A. (2000). State of the art. I: Resilient response of unbound aggregates. *Journal of Transportation Engineering*, 126(1), 66–75.

Leng, J., & Gabr, M. A. (2002). Characteristics of geogrid-reinforced aggregate under cyclic load. *Transportation Research Record,* 1786(1), 29–35.

Li, N., & Haas, R. (1996). Design and construction for asphalt pavements in permafrost areas: Case study of Qinghai-Tibet highway. *Proceedings of the 8th International Conference on Cold Regions Engineering*, Fairbanks, AK, August 12–16, 1996, pp. 866–877, New York, NY: American Society of Civil Engineers.

Luo, J., Ding, K., Huang, H., Hart, J.M., Qamhia, I.I., Tutumluer, E., Thompson, H. and Sussmann, T.R. (2023). Toward automated field ballast condition evaluation: Development of a ballast scanning vehicle. *Transportation Research Record*, 2678(3), 24-36.

MacKay, M. H., Hein, D. K., & Emery, J. J. (1992). Evaluation of frost action mitigation procedures for highly frost-susceptible soils. *Transportation Research Record*, 1362.

Maerz, N. H., & Zhou, W. (1999). Flat and elongated: Advances using digital image analysis. Paper presented at the *Center for Aggregates Research (ICAR) Seventh Annual Symp.*, Austin, TX, April 19–21.

Mahedi, M., Rajewski, D., Kim, S., Ceylan, H., Cho, I.-H., & Takle, E. S. (2022). *Effect of warmer Minnesota winters on freeze-thaw cycles (MN 2022-04)*. (Article MN 2022-04). Retrieved from https://trid.trb.org/view/2078728

Masad, E. (2003). *The development of a computer-controlled image analysis system for measuring aggregate shape properties (NCHRP-IDEA Project 77 Final Report).* Washington, DC: Transportation Research Board, National Research Council.

Masad, E. (2007). *Test methods for characterizing aggregate shape, texture, and angularity* (Vol. 555). Washington, DC: Transportation Research Board.

McEnroe, B. M. (1994). *Drainability of granular bases for highway pavements.* Lawrence, KS: Department of Civil Engineering, University of Kansas for Kansas Department. https://onlinepubs.trb.org/Onlinepubs/trr/1994/1434/1434.pdf#page=29

MnDOT [Jonquist, B]. (2008). *Local road material properties and calibration for MnPAVE summary report (Report 2008-56)*. Minnesota Department of Transportation: St. Paul, MN https://hdl.handle.net/20.500.14153/mndot.2764

MnDOT (2012). Best value granular material for road foundations. Minnesota Department of Transportation: St. Paul, MN. https://hdl.handle.net/20.500.14153/mndot.2873

MnDOT. (2015). MnDOT PG binder guidelines-MSCR. Retrieved from https://www.dot.state.mn.us/materials/bituminousdocs/bituminous-design/pg-mscr-guidelines-final.pdf

MnDOT. (2019a). MnDOT standard specifications for pavement design. Retrieved from https://www.dot.state.mn.us/materials/pvmtdesign/manual.html

MnDOT. (2019b). Chapter 4. In *HMA, MnDOT pavement design manual.* Retrieved from https://www.dot.state.mn.us/materials/pvmtdesign/manual.html

MnDOT. (2024). Historical bid price – Past five years. Retrieved from https://www.dot.state.mn.us/pre-letting/cost-estimating/index.html

Moaveni, M. (2015). *Advanced image analysis and techniques for degradation characterization of aggregates* [Text, University of Illinois at Urbana-Champaign]. Retrieved from https://hdl.handle.net/2142/78734

Muench, S., Pierce, L., Uhlmeyer, J., & Anderson, K. (2006). The evolution of long life concrete Pavements in Washington state. *Proceedings of the International Conference on Long-Life Concrete Pavements,* Chicago, IL, October 25–27, 2006, pp. 19–35.

Nazarian, S., & Yuan, D. (2008). Variation in moduli of base and subgrade with moisture. *GeoCongress* 2008, 570–577. https://doi.org/10.1061/40971(310)71

Oh, H., Likos, W. J., & Edil, T. B. (2022). Qualitative rating system for drainability of roadway base materials. *Transportation Research Record,* 2676(4), 683-696.

Oman, M. S., Lund, N. G., & Braun Intertec. (2018). *Designing base and subbase to resist environmental effects on pavements (MN/RC 2018-06)*. Retrieved from https://rosap.ntl.bts.gov/view/dot/35388

Ovik, J. M., Siekmeier, J. A., & Van Deusen, D. A. (2000). *Improved spring load restriction guidelines using mechanistic analysis (Report No. MN/RC-2000-18)*. St. Paul, MN: Minnesota Department of Transportation. https://hdl.handle.net/20.500.14153/mndot.2398

Pan, T. & Tutumluer, E. (2005). Imaging based evaluation of coarse aggregate size and shape properties affecting pavement performance. *Advances In Pavement Engineering,* 130.

Pan, T., Tutumluer, E., & Carpenter, S.H. (2005). Effect of coarse aggregate morphology on resilient modulus of hot-mix asphalt. *Transportation Research Record*, 1929, 1-9.

Pereira, P., & Pais, J. (2017). Main flexible pavement and mix design methods in Europe and challenges for the development of an European method. *Journal of Traffic and Transportation Engineering*, 4(4), 316–346.

Rabab'ah, S. R. (2007). *Integrated assessment of free draining base and subbase materials under flexible pavement.* Akron, OH: University of Akron. https://etd.ohiolink.edu/acprod/odb_etd/etd/r/1501/10?clear=10&p10_accession_num=akron1189128048

Rajaei, P., & Baladi, G. Y. (2015). Frost depth: General prediction model. T*ransportation Research Record*, 2510(1), 74–80.

Rao, C. B. (2001). *Development of three-dimensional image analysis techniques to determine shape and size properties of coarse aggregate*. Urbana-Champaign, IL: University of Illinois at Urbana-Champaign.

Rao, C., Darter, M., & Pyle, T. (2006). Extended service life of continuously reinforced concrete pavement in California. *Proceedings of the international conference on long-life concrete pavements*, Chicago, IL, October 25–27, 2006, pp. 61–78.

Rao, C., Tutumluer, E., & Kim, I. T. (2002). Quantification of coarse aggregate angularity based on image analysis. *Transportation Research Record*, 1787(1), 117–124. https://doi.org/10.3141/1787-13

Roesler, J. R., Chavan, H., King, D., & Brand, A. S. (2016). Concrete slab analyses with field-assigned non-uniform support conditions. *International Journal of Pavement Engineering*, 17(7), 578–589. https://doi.org/10.1080/10298436.2015.1007231

Rokade, S., Agarwal, P. K., & Shrivastava, R. (2012). Drainage and flexible pavement performance. *International Journal of Engineering Science and Technology*, 4.

Saeed, A. (2008). *Performance-related tests of recycled aggregates for use in unbound pavement layers* (p. 23108). Washington, DC: Transportation Research Board. https://doi.org/10.17226/23108

Saeed, A., Hall, J. W., & Barker, W. R. (2001). *Performance-related tests of aggregates for use in unbound pavement layers*. Washington, DC: National Academy Press, Transportation Research Board, National Research Council.

Selezneva, O., Rao, C., Darter, M. I., Zollinger, D., & Khazanovich, L. (2004). Development of a mechanistic-empirical structural design procedure for continuously reinforced concrete pavements. *Transportation Research Record*, 1896(1), 46–56. https://doi.org/10.3141/1896-05.

Shaban, A. M., Alsabbagh, A., Wtaife, S., & Suksawang, N. (2020). Effect of pavement foundation materials on rigid pavement response. *IOP Conference Series: Materials Science and Engineering*, 671(1), 012085. https://doi.org/10.1088/1757-899X/671/1/012085.

Shoop, S. A., & Henry, K. S. (1991). Effect of a geotextile on water migration and frost heave in a large-scale test basin. *Transportation Research Record,* 1307.

Simonsen, E., & Isacsson, U. (1999). Thaw weakening of pavement structures in cold regions. *Cold Regions Science and Technology*, 29(2), 135–151. https://doi.org/10.1016/S0165-232X(99)00020-8.

Skok, E. L., Timm, D. H., Brown, M., Clyne, T. R., & Johnson, E. N. (2003). *Best practices for the design and construction of low volume roads: Revised (Report No. MN/RC-2002-17)*. St. Paul, MN: Minnesota Department of Transportation. https://hdl.handle.net/20.500.14153/mndot.2455

Smith, B. S. (2006). *Design and construction of pavements in cold regions: State of the practice.* Provo, UT: Brigham Young University.

Tanyu, B. F., Benson, C. H., Edil, T. B., & Kim, W.-H. (2004). Equivalency of crushed rock and three industrial by-products used for working platforms during pavement construction. *Transportation Research Record,* 1874(1), 59–69. https://doi.org/10.3141/1874-07

Thom, N., & Brown, S. (1988). The effect of grading and density on the mechanical properties of a crushed dolomitic limestone. *Proceedings of the 14th ARRB Conference*, Part 7, 94-100.

Thom, N., & Brown, S. F. (1987). Effect of moisture on the structural performance of a crushed-limestone road base. *Transportation Research Record*, 1121, 50–56.

Thompson, M. R., & Robnett, Q. L. (1979). Resilient properties of subgrade soils. *Transportation Engineering Journal of ASCE,* 105(1), 71–89.

Tolppanen, P. (2001). *3-D characterization and degradation analysis of rock aggregates* [PhD thesis]. Stockholm, Sweden: Royal Institute of Technology.

Tutumluer, E., & Barksdale, R. D. (1995). Inverted flexible pavement response and performance. *Transportation Research Record*, 1482, 102–110.

Tutumluer, E., Mishra, D., & Butt, A. A. (2009). *Characterization of Illinois aggregates for subgrade replacement and subbase (ICT-09-060 UILU-ENG-2009-2042)*. Urbana, IL: Department of Civil and Environmental Engineering, University of Illinois at Urbana-Champaign.

Tutumluer, E., Moaveni, M., & Qamhia, I. I. A., (2018) *Aggregate quality requirements for pavements*. (NCHRP Synthesis 524) Washington, DC: The National Academies Press. https://doi.org/10.17226/25205.

Tutumluer, E. (2013). *Practices for unbound aggregate pavement layers (NCHRP Synthesis 445)* (p. 22469). Washington, DC: The National Academies Press. https://doi.org/10.17226/22469

Tutumluer, E. & Pan, T. (2008). Aggregate morphology affecting strength and permanent deformation behavior of unbound aggregate materials. *Journal of Materials in Civil Engineering*, 20(9), 617-627.

Tutumluer, E., Pan, T., & Carpenter, S. H. (2005). *Investigation of aggregate shape effects on hot mix performance using an image analysis approach (UILU-ENG-2005-2003)*. Urbana, IL: Department of Civil and Environmental Engineering, University of Illinois at Urbana-Champaign.

Tutumluer, E., Rao, C., & Stefanski, J. A. (2000). *Video image analysis of aggregates (Final Project Report, FHWA-IL-UI-278, Civil Engineering Studies UILU-ENG-2000-2015).* Urbana-Champaign: University of Illinois Urbana-Champaign.

Tutumluer, E., Xiao, Y., & Wilde, W. J. (2015). *Cost-effective base type and thickness for long-life concrete pavements (MN/RC 2015-42)*. St. Paul, MN: Minnesota Department of Transportation.

Tyler, W. (2001). *Particle size and shape analyzers (CPA)*. [Product brochure.] Mentor, OH: W. S. Tyler.

US Army Corps of Engineers. (2004). *Pavement design for roads, streets, walks, and open storage areas (UFC 3-250-01FA).* Washington, DC: US Army Corps of Engineers.

Velasquez, R., Hoegh, K., Yut, I., Funk, N., Cochran, G., Marasteanu, M., & Khazanovich, L. (2009). *Implementation of the MEPDG for new and rehabilitated pavement structures for design of concrete and asphalt pavements in Minnesota* [Report]. St. Paul, MN: Minnesota Department of Transportation. http://conservancy.umn.edu/handle/11299/150992

Vorobieff, G., & Moss, J. (2006). Australia's experience with long-life, heavy-duty concrete pavements. Paper presented at the *International Conference on Long-Life Concrete Pavements*, Chicago, Illinois, October 25-27.

Wang, F., Han, J., Zhang, X., & Guo, J. (2017). Laboratory tests to evaluate effectiveness of wicking geotextile in soil moisture reduction. *Geotextiles and Geomembranes*, 45(1), 8–13.

White, D. J., Vennapusa, P., Eichner, D., Gieselman, H., Zhao, L., & Jahren, C. (2010). *Rapid, self-contained in-situ permeameter for field QA/QC of pavement base/subbase materials.* Ames, IA: Iowa State University.

White, D. J., Vennapusa, P., & Jahren, C. T. (2004). *Determination of the optimum base characteristics for pavements (Iowa DOT Project TR-482, CTRE Project 02-119)*. Ames, IA: Center for Transportation Research and Education, Iowa State University.

Winkelman, T. (2006). Design and construction of extended life concrete pavements in Illinois. Paper presented at the *International Conference on Long-Life Concrete Pavements*, Chicago, IL, October 25-27.

Won, M., Kim, D., Cho, Y., & Medina-Chavez, C. (2006). Long-term performance of continuously reinforced concrete pavement in Texas. *Proceedings of the International Conference on Long-Life Concrete Pavements*, pp. 25-27.

Woolf, D. O. (1953). *Results of physical tests of road-building aggregate*. Washington, DC: U.S. Government Printing Office, Bureau of Public Roads.

Wu, Y., Parker, F., & Kandhal, P. S. (1998). Aggregate toughness/abrasion resistance and durability/soundness tests related to asphalt concrete performance in pavements. *Transportation Research Record*, 1638(1), 85–93.

Xiao, Y., & Tutumluer, E. (2012). *Best value granular material for road foundations (MN/RC 2012-01)*. St. Paul, MN: Minnesota Department of Transportation. https://hdl.handle.net/20.500.14153/mndot.2873

Xiao, Y., Tutumluer, E., & Siekmeier, J. (2011). Mechanistic–empirical evaluation of aggregate base and granular subbase quality affecting flexible pavement performance in Minnesota. *Transportation Research Record*, 2227(1), 97–106. https://doi.org/10.3141/2227-11

Zeiada, W., Hamad, K., Omar, M., Underwood, B. S., Khalil, M. A., & Karzad, A. S. (2019). Investigation and modelling of asphalt pavement performance in cold regions. *International Journal of Pavement Engineering*, 20(8), 986–997.

Zhang, Y., White, D. J., Vennapusa, P. K. R., Johnson, A. E., & Prokudin, M. M. (2018). Investigating frost heave deterioration at pavement joint locations. *Journal of Performance of Constructed Facilities,* 32(2), 04018001. https://doi.org/10.1061/(ASCE)CF.1943-5509.0001143

Zornberg, J., & Gupta, R. (2009). Reinforcement of pavements over expansive clay subgrades. *Proceedings of the 17th International Conference on Soil Mechanics and Geotechnical Engineering,* pp. 765–768.

Zubeck, H. K., & Doré, G. (2009). Introduction to cold regions pavement engineering. In *Cold regions engineering 2009: Cold regions impacts on research, design, and construction* (pp. 337-345). Reston, VA: American Society of Civil Engineers.

Appendix A: Applications of Design Optimization Procedure for Implementation

Example Applications of the Proposed Design Procedure for Implementation

This appendix provides a step-by-step illustration of how to apply the proposed design procedure for a specific pavement section in Beltrami, Todd, Redwood, and Olmsted Counties that can represent four different climatic zones in Minnesota. These examples demonstrate each stage of the process, from selecting proper quality combination of aggregate base and subbase layers as well as optimizing thickness requirements using the iterative design flowchart. Note that, if users would like to use the updated aggregate index property (AIP) database or any laboratory and field data for pavement design, they may use the ANN models developed in Chapter 4 of the final report to derive aggregate properties (e.g., resilient modulus [M_R] and shear strength) and classify aggregates as low-, medium-, or high-quality prior to determining the optimal design, as demonstrated in each case study.

Case 1. Pavement Design for Beltrami County

The design inputs for Beltrami County are provided in Table A.1. Below is a recommended design procedure from start to end, incorporating methodologies established in Chapter 6 of the final report.

Table A.1. Design inputs for a conventional flexible pavement section design in Beltrami County (*Traffic volume – 1.5 million ESALs)*

Type	Design Input Values
Asphalt Concrete	PG Grade: PG58H-34
	Thickness (in.): 6
	Poisson's Ratio: 0.3
Base	To be determined
Subbase	To be determined
Engineered Subgrade	Elastic Modulus (ksi): 7
	Thickness (in.): 12
	Poisson's Ratio: 0.45
Undisturbed Subgrade	Elastic Modulus (ksi): 3.5 (50% of Engineered Subgrade)
	Thickness (in.): ∞
	Poisson's Ratio: 0.45

Type	Design Input: Seasonal Elastic Moduli (ksi)*				
	Fall	Winter	Early Spring	Late Spring	Summer
Asphalt Concrete	551	1,415	808	365	145

**Applied default seasonal elastic moduli for PG 58H-34 as provided in MnPAVE 7.1.*

Step 1. Match the Aggregate Quality Combinations with the Optimized Pavement Design Scenarios

According to Table 32 in Chapter 6, the pavement design consisting of 6 in. of HMA, an undisturbed subgrade modulus of 3.5 ksi (i.e., 50% of engineered subgrade modulus presented in Table 32 in Chapter 6), and 1.5 million ESALs was determined to be over-designed. It means that according to these HMA

thickness, subgrade modulus, and traffic conditions, all design variations—regardless of aggregate base and subbase thickness—are anticipated to exceed the target service life. Therefore, a more efficient design alternative is to reduce the HMA thickness to 4 in. while maintaining the existing subgrade modulus (traffic level remains unchanged). Under these conditions, an M-L quality aggregate base-subbase combination is recommended for the pavement structure as suggested in Table 32 in Chapter 6. The next step is to conduct the thickness optimization as outlined in step 2.

Step 2. Determine Optimal Design Using the Iterative Design Flowchart

Table 34 in Chapter 6 provided the optimized combinations of aggregate base and subbase materials in Beltrami County. In accordance, when HMA thickness decreased to 4 in. with a subgrade modulus of 3.5 ksi (i.e., an engineered subgrade modulus of 7 ksi) and a traffic condition of 1.5 million ESALs, M-L quality combination of aggregate base and subbase with recommended thicknesses of 6 in. and 10 in., respectively, would be sufficient for meeting both the rutting and fatigue cracking life expectations.

Step 3. Cost Comparison Implications

In the Beltrami case, where M-L quality materials are used for the aggregate base and subbase layers, the design is controlled by the rutting criterion, which is primarily influenced by the subbase layer's quality and thickness. As a result, reducing the subbase would not satisfy the rutting requirement. Also, the minimum aggregate base layer should be at least 6 in., which is align with the optimized aggregate base layer thickness. Therefore, a cost comparison step is not necessary for this design case.

Case 2. Pavement Design for Todd County

The design inputs for Todd County are presented in Table A.2. Below is a recommended design procedure from start to end, incorporating methodologies established in Chapter 6 of the final report.

Table A.2. Design inputs for a conventional flexible pavement section design in Todd County. (Traffic volume: 1.5 million ESALs)

Type	Design Input Values
Asphalt Concrete	PG Grade: PG58H-34
	Thickness (in.): 4
	Poisson's Ratio: 0.3
Base	To be determined
Subbase	To be determined
Engineered Subgrade	Elastic Modulus (ksi): 10
	Thickness (in.): 12
	Poisson's Ratio: 0.45
Undisturbed Subgrade	Elastic Modulus (ksi): 5 (50% of Engineered Subgrade)
	Thickness (in.): ∞
	Poisson's Ratio: 0.45

Type	Design Input: Seasonal Elastic Moduli (ksi)*				
	Fall	Winter	Early Spring	Late Spring	Summer
Asphalt Concrete	538	1,570	836	367	154

**Applied default seasonal elastic moduli for PG 58H-34 as provided in MnPAVE 7.1.*

Step 1. Match the Aggregate Quality Combinations with the Optimized Pavement Design Scenarios

Based on the conclusions of Chapter 6, an M-L quality combination is suggested in Table 35 in Chapter 6 for the pavement structure comprising 4 in. of HMA, an undisturbed subgrade modulus of 5 ksi (i.e., an engineered subgrade modulus of 10 ksi), and a traffic condition of 1.5 million ESALs.

Step 2. Determine Optimal Design Using the Iterative Design Flowchart

A flowchart was introduced to determine the layer thickness as shown in Figure A.1. The process began with an aggregate base thickness of 6 in. and a subbase thickness of 4 in., along with the design parameters listed in Table A.2. Upon performing analysis using MnPAVE, this pavement structure with 6 in. and 6 in. of base and subbase layer thickness, respectively, was found to satisfy both fatigue and rutting performance criteria.

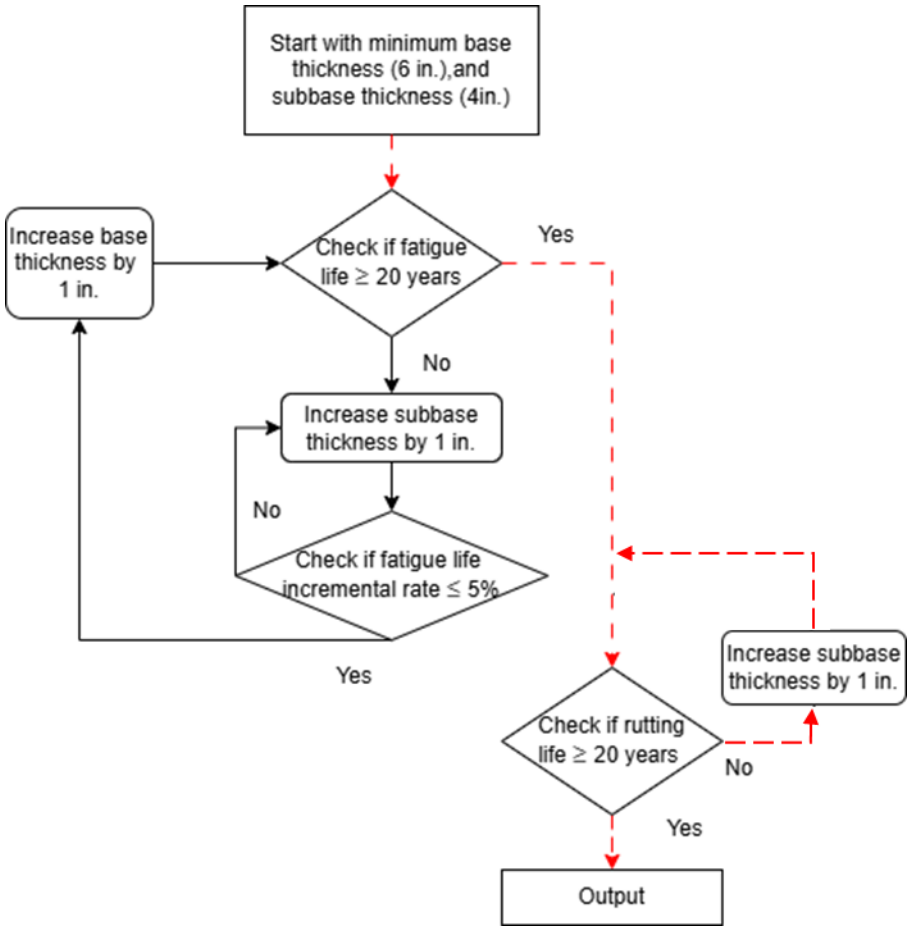

Figure A.1. Flowchart for aggregate base and subbase thickness determination (Case 2 follows red dash lines)

Step 3. Cost Comparison Implications

In the Todd County case, where M-L quality materials are used for the aggregate base and subbase layers, the design is controlled by the rutting criterion, as similar as Beltrami County case, which is primarily influenced by the subbase layer's quality and thickness. As a result, reducing the subbase

would not satisfy the rutting requirement. Also, the minimum aggregate base layer should be at least 6 in., which is align with the optimized aggregate base layer thickness. Therefore, a cost comparison step is not necessary for this design case.

Case 3. Pavement Design for Redwood County

For Redwood County, the design inputs are provided in Table A.3, and the recommended design procedure is outlined below.

Table A.3. Design inputs for a conventional flexible pavement section design in Redwood County (Traffic volume: 6 million ESALs)

Type	Design Input Values
Asphalt Concrete	PG Grade: PG58H-34
	Thickness (in.): 4
	Poisson's Ratio: 0.3
Base	To be determined
Subbase	To be determined
Engineered Subgrade	Elastic Modulus (ksi): 10
	Thickness (in.): 12
	Poisson's Ratio: 0.45
Undisturbed Subgrade	Elastic Modulus (ksi): 5 (50% of Engineered Subgrade)
	Thickness (in.): ∞
	Poisson's Ratio: 0.45

Type	Design Input: Seasonal Elastic Moduli (ksi)*				
	Fall	Winter	Early Spring	Late Spring	Summer
Asphalt Concrete	551	1415	808	365	145

**Applied default seasonal elastic moduli for PG 58H-34 as provided in MnPAVE 7.1.*

Step 1. Match the Aggregate Quality Combinations with the Optimized Pavement Design Scenarios

According to the analysis results from MnPAVE, the initial pavement structure, with any combination of aggregate base and subbase layer thickness and qualities, was determined to be under-designed, as the pavement structure could not meet the required fatigue and rutting performance criteria by only optimizing aggregate base and subbase layers. To address this, a thicker HMA layer (6 in.) was recommended. Based on the findings in the quality selection Table 32 in Chapter 6, an M-L quality combination of aggregate base and subbase layers was identified as a suitable option to satisfy performance requirements while optimizing material usage.

Step 2. Determine Optimal Design Using the Iterative Design Flowchart

A flowchart was introduced to determine the layer thickness as shown in Figure A.2. The process began with a minimum aggregate base thickness of 6 in. and a subbase thickness of 4 in. Following the flowchart steps, the aggregate base layer thickness was iteratively increased until a thickness of 19 in.

was found to meet the required fatigue life. The subbase layer remained at the minimum thickness of 4 in., which was sufficient to meet the 20-year rutting life requirement.

The final design was confirmed as 6 in. of HMA, 19 in. of base, and 4 in. of subbase, meeting both fatigue and rutting performance criteria.

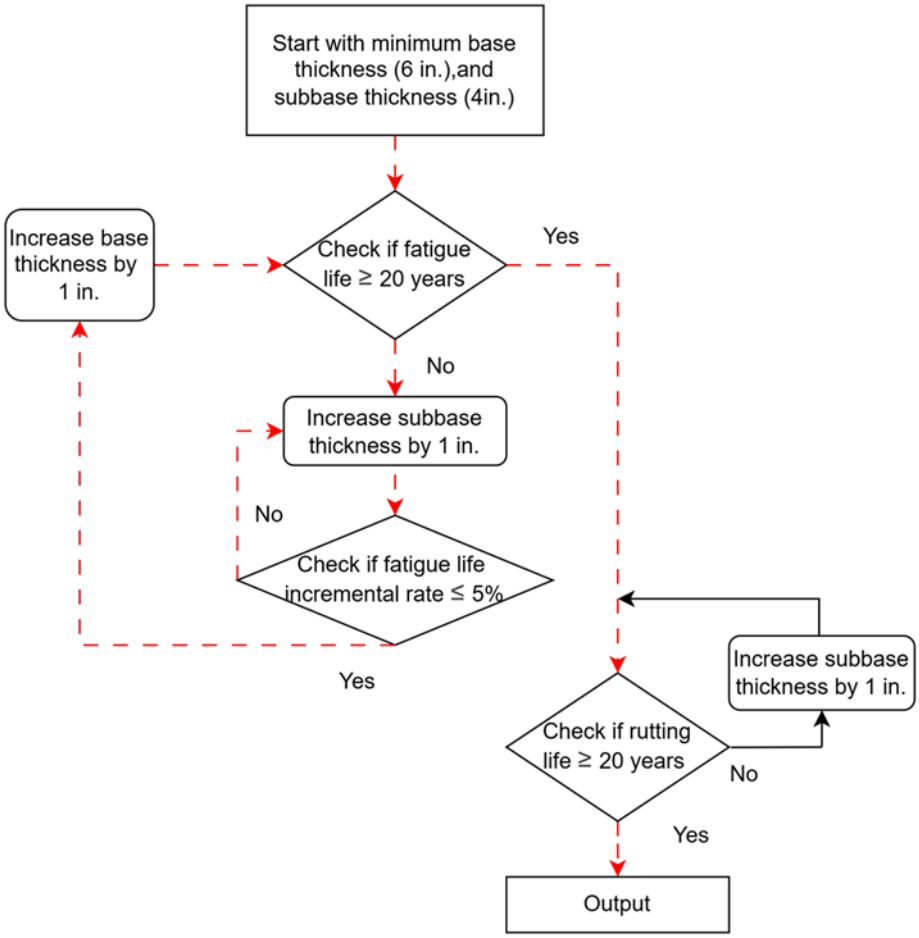

Figure A.2. Flowchart for aggregate base and subbase thickness determination (Case 3 follows red dash lines)

Step 3. Cost Comparison Implications

Table A.4 presents design alternatives that reduce aggregate base layer thickness while increasing subbase layer thickness. To satisfy both fatigue and rutting criteria, the aggregate base layer may be reduced to 18 in. or 17 in., with corresponding subbase layer thicknesses of 10 in. and 25 in., respectively. As shown in Table A.4, the cost comparison among these alternatives indicates that total material cost per mile increases as the base layer thickness decreases and the subbase layer thickness increases, until both performance criteria are met. These findings support the design optimization approach proposed in this study. However, practitioners should recognize that cost differences among design alternatives are highly influenced by the unit costs of aggregate base and subbase materials, and the pavement design and construction costs can be significantly affected by the quality and associated costs of locally available aggregate materials.

Table A.4. Design alternative cost comparison for Redwood County design case

Alternatives	Aggregate Base thickness (in.)	Subbase thickness (in.)	Aggregate Base unit cost ($ per mile)	Subbase aggregate unit cost ($ per mile)	Cost ($ per mile)	Fatigue life (years)	Rutting life (years)
1	19	4	31,680.0	9,991.4	641,885.6	20	20
2	18	10	31,680.0	9,991.4	670,154.0	20	33
3	17	25	31,680.0	9,991.4	788,345.0	20	>50

Case 4. Pavement Design for Olmsted County

The design inputs for Olmsted County are provided in Table A.5. The following discussion presents the results based on the recommended design procedure in Chapter 6 of the final report.

Step 1. Match the Aggregate Quality Combinations with the Optimized Pavement Design Scenarios

As shown in Table 32 of Chapter 6, the recommended aggregate quality combination for this pavement structure is L-L. The optimal layer thicknesses will be determined in Step 2 using the iterative design flowchart.

Table A.5. Design inputs for a conventional flexible pavement section design in Olmsted County (Traffic volume 1.5 million ESALs)

Type	Design Input Values
Asphalt Concrete	PG Grade: PG58H-34
	Thickness (in.): 8
	Poisson's Ratio: 0.3
Base	To be determined
Subbase	To be determined
Engineered Subgrade	Elastic Modulus (ksi): 2
	Thickness (in.): 12
	Poisson's Ratio: 0.45
Undisturbed Subgrade	Elastic Modulus (ksi): 1 (50% of Engineered Subgrade)
	Thickness (in.): ∞
	Poisson's Ratio: 0.45

Type	Design Input: Seasonal Elastic Moduli (ksi)*				
	Fall	Winter	Early Spring	Late Spring	Summer
Asphalt Concrete	544	1,370	811	367	150

**Applied default seasonal elastic moduli for PG 58H-34 as provided in MnPAVE 7.1.*

Step 2. Determine Optimal Design Using the Iterative Design Flowchart

As shown in Figure A.3, starting with a 6-in. thick base layer, the structure satisfied the fatigue life requirement. To conserve aggregate base material, the aggregate base thickness was held constant per

the flowchart guidance, and the subbase thickness was adjusted iteratively to meet the rutting life criteria. Based on iterative MnPAVE analysis and results, the subbase layer was increased to 35 in. Therefore, the optimized pavement structure consists of an 8-in thick HMA layer, a 6-in. thick Low-quality aggregate base, and a 35-in. thick Low-quality subbase.

Step 3. Cost Comparison Implications

Since the optimized base layer thickness equals the minimum required thickness, a cost comparison with alternative designs is unnecessary.

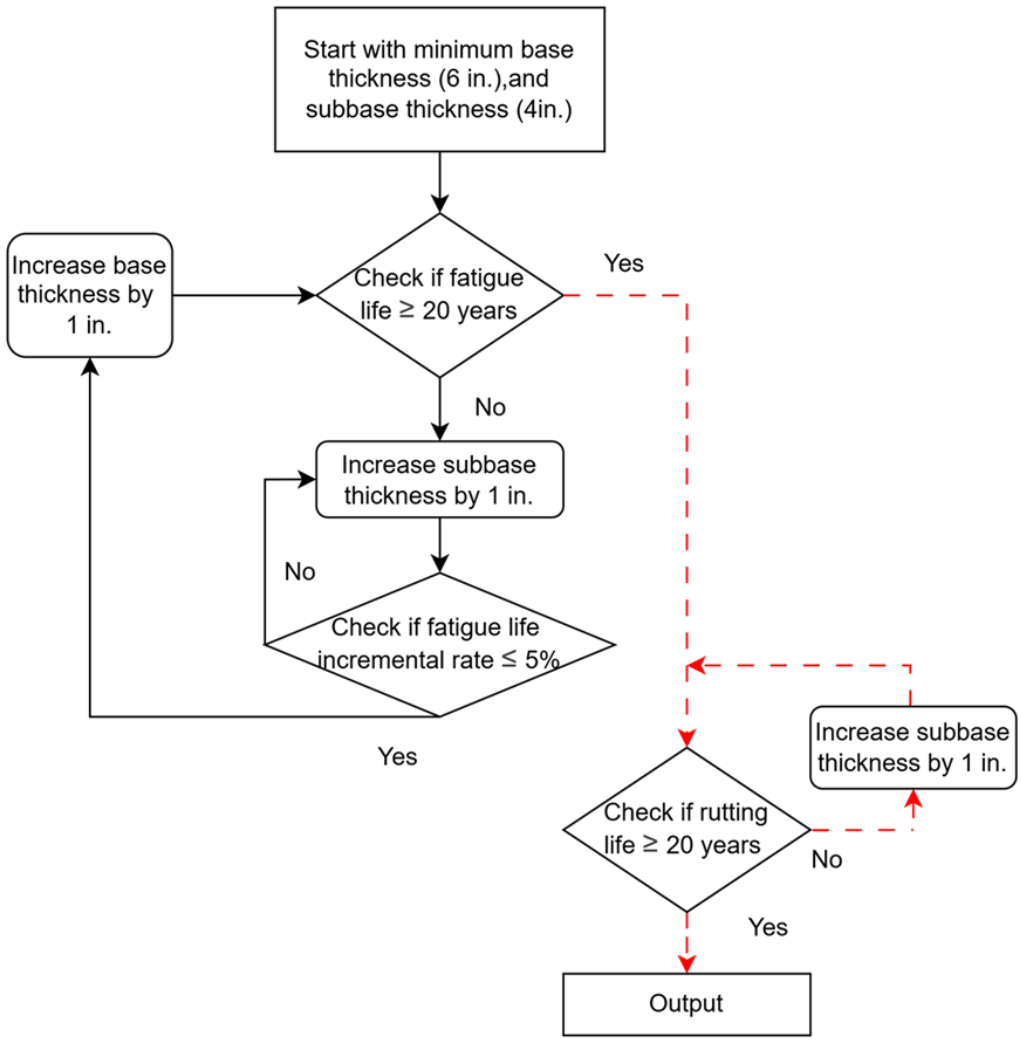

Figure A.3. Flowchart aggregate for base and subbase thickness determination (Case 4 follows red dash lines)